



**HAL**  
open science

# Encres Polymères pour l'Électronique Imprimée : Synthèse, Formulation et Impression

Alizée Glasser

► **To cite this version:**

Alizée Glasser. Encres Polymères pour l'Électronique Imprimée : Synthèse, Formulation et Impression. Polymers. Université de Bordeaux, 2019. English. NNT : 2019BORD0381 . tel-03264173

**HAL Id: tel-03264173**

**<https://theses.hal.science/tel-03264173>**

Submitted on 18 Jun 2021

**HAL** is a multi-disciplinary open access archive for the deposit and dissemination of scientific research documents, whether they are published or not. The documents may come from teaching and research institutions in France or abroad, or from public or private research centers.

L'archive ouverte pluridisciplinaire **HAL**, est destinée au dépôt et à la diffusion de documents scientifiques de niveau recherche, publiés ou non, émanant des établissements d'enseignement et de recherche français ou étrangers, des laboratoires publics ou privés.

THÈSE PRÉSENTÉE  
POUR OBTENIR LE GRADE DE

**DOCTEUR DE  
L'UNIVERSITÉ DE BORDEAUX**

ÉCOLE DOCTORALE DES SCIENCES CHIMIQUES

Spécialité : Polymères

Par Alizée GLASSER

---

**POLYMER ELECTRONIC INKS: SYNTHESIS, FORMULATION AND  
PROCESSING**

—  
ENCRES POLYMÈRES POUR L'ÉLECTRONIQUE IMPRIMÉE:  
SYNTHÈSE, FORMULATION ET IMPRESSION

---

Sous la direction de : Éric CLOUTET

co-directeurs : Hamid KELLAY et Georges HADZIIOANNOU

Soutenue le 17/12/2019

Membres du jury :

Dr. Jean-Baptiste SALMON	Directeur de Recherche	CNRS	Président du jury
Prof. Pascal PANIZZA	Professeur	Université de Rennes 1	Rapporteur
Prof. Jean-Charles MAJESTÉ	Professeur	Université de Saint Étienne	Rapporteur
Dr. Sylvie TENCÉ-GIRAULT	Ingénieure de Recherche	Arts et Métiers ParisTech, Arkema	Examinatrice
Prof. Jean-François TASSIN	Professeur	Université Le Mans	Examineur
Prof. Natalie STINGELIN	Professeure	Georgia Institute of Technology	Invitée
Dr. Éric CLOUTET	Directeur de Recherche	CNRS	Directeur de Thèse
Prof. Hamid KELLAY	Professeur	Université de Bordeaux	Directeur de Thèse
Prof. Georges HADZIIOANNOU	Professeur	Université de Bordeaux	Directeur de Thèse



« Une image vaut mille mots. »

Confucius



# Remerciements

Je voudrais tout d'abord remercier les six membres du jury, Jean-Baptiste SALMON, Pascal PANIZZA, Jean-Charles MAJESTÉ, Sylvie TENCÉ-GIRAULT, Jean-François TASSIN et Natalie STINGELIN, qui ont accepté d'évaluer mes travaux de thèse. Merci pour votre présence, même par visio-conférence, et pour la discussion très enrichissante à l'issue de ma présentation.

Merci aux directeurs du LCPO, Sébastien LECOMMANDOUX, et du LOMA Jean-Pierre DELVILLE puis Fabio PISTOLESI, de m'avoir accueillie au sein de vos laboratoires.

Merci à mes directeurs de thèse, Hamid KELLAY, Georges HADZIIOANNOU et Éric CLOUTET, de m'avoir fait confiance pour travailler sur ce sujet interdisciplinaire, qui m'a permis d'apprendre tant de techniques, de la synthèse à la caractérisation avec des appareils de pointe. Merci pour les discussions qui ont fait avancer ce travail. Merci aussi Hamid pour l'aide lors de la rédaction en anglais de ce manuscrit et de la publication.

Je remercie la région Nouvelle-Aquitaine et le LabexAMADEus pour le financement.

Mes remerciements également à Aude, Annie, Dominique, Suzanne, Bernadette et Mme ROUDIER qui m'ont aidée dans les démarches administratives. Merci à Muthas et Mélanie pour l'aide lors des synthèses. Merci au service technique du LOMA pour la réalisation de pièces, et à William pour la récupération de données perdues !

Merci aux experts qui m'ont aidée dans les manip ou leurs interprétations : Gilles pour l'AFM, Anne-Laure pour la RMN, Cédric pour la DSC, Mélanie pour la SEC, Sabrina LACOMME et Etienne GONTIER du BIC pour la formation au TEM, Isabelle SVAHN du BIC et Philippe LEGROS de PLACAMAT pour les mesures de cryo-MEB, Wiljan et Sokha pour l'aide sur un grand nombre d'appareils de la plateforme ELORPrintTec, Manuel Hidalgo de Piezotech pour les discussions que nous avons eues. Je remercie également Rémi DUBOIS et Pierre JAIS du Liryx (IHU de Bordeaux) pour l'opportunité du projet « sweat heart ».

Merci enfin à tous mes collègues et amis pour tous les moments partagés : du B8 et du LCPO – Lauriane, Cindy, Nicoletta, Rim, Solène, Konstantinos, Naser, Emin, Lorenzo, Yanid, Florian, Florent, Geoffrey, Cian, Ariana, Silvia, Olga, Alberto, Nils, Daniele, Antoine, Eunkyung, Micah, Benjamin, Tommaso, Shekhar, Alexander, Guillaume, Eleni, Gilles, Cyril, Camille, Mélanie, Marina, Béatrice, Anirudh, Fiona, Christopher, Erwan, Quentin, Michèle, Coralie, Esra, Beste, Martin, Evangelos, Nicolas, Jérémy, etc. – et du LOMA – Marion, Paul, Raphaël, Goce, Julie, Quentin, Nina, Mikaël, Marcela, Juho, Benjamin, Hernando, Hugo, Houssein, Stefano, Maxime, Kaili, Christine, Alexandre, etc. Ces trois ans n'auraient pas été aussi agréables sans vous, entre les sorties, les

verres après le travail, le yoga, les discussions, les repas, etc. Merci en particulier à Lauriane pour tes succulents et magnifiques gâteaux et tous les bons moments passés ensemble, à Rim pour ton soutien moral et les bons thés à la menthe et à mes nombreux « co-bureaux » de toutes nationalités – française, italienne, grecque, iranienne, turque, colombienne et chinoise – qui ont égaillé mes journées et ont accepté gentiment mon jardin ambulancier un peu envahissant !

De façon plus générale, je voudrais remercier toutes les personnes rencontrées au sein du LCPO et du LOMA pendant ces 3 années, permanents, post-doctorants et thésards.

Merci également à ma famille et à Hubert pour le soutien permanent !

Merci à vous tous.

# Contents

Résumé en français .....	3
List of Abbreviations.....	15
List of Symbols and Physical Constants.....	17
General Introduction.....	19
1 Organics electronics and printing technologies .....	23
1.1 Organic electronics .....	24
1.1.1 Poly(3,4-ethylenedioxythiophene) (PEDOT): a semiconducting polymer .....	24
1.1.2 Poly(vinylidene fluoride- <i>co</i> -trifluoroethylene) P(VDF-TrFE): a piezoelectric polymers .....	41
1.2 Printing technologies.....	50
1.2.1 Printing processes overview .....	50
1.2.2 The rheological behavior of inks.....	57
1.3 Conclusion.....	59
2 PEDOT:PSTFSI inks for various deposition processes.....	67
2.1 Introduction.....	68
2.2 Materials & Methods .....	70
2.3 PEDOT:PSTFSI inks characterization.....	79
2.4 PEDOT:PSTFSI inks processing: inkjet printing, doctor blading, screen-printing, and soft-blading.....	91
2.5 Film characterization.....	95
2.6 Conclusion.....	104

---

3	P(VDF-TrFE) inks for screen-printing.....	109
3.1	Introduction.....	110
3.2	Materials & Methods.....	113
3.3	Characterization of the neat polymer .....	115
3.4	P(VDF-TrFE) solutions with a gelifying agent .....	119
3.5	P(VDF-TrFE) solutions in a mixture of a good and a bad solvent.....	134
3.6	Conclusion.....	140
4	Piezoelectric devices .....	145
4.1	Introduction.....	146
4.2	Materials & Methods.....	148
4.3	Thermal evaporated metal electrodes & spin coated or doctor bladed P(VDF-TrFE) layer .....	152
4.4	Printed PEDOT:PSTFSI electrodes & doctor blading of P(VDF-TrFE) solutions .....	156
4.5	Screen-printed and stencil-printed commercial PEDOT:PSS electrodes & new P(VDF-TrFE) formulations.....	159
4.6	Conclusion.....	164
	General conclusion and perspectives .....	167
	Appendices .....	171

# Résumé en français

Introduction.....	3
Électronique organique et procédés d'impression.....	6
Encre PEDOT:PSTFSI formulée pour différents procédés d'impression.....	6
Encres P(VDF-TrFE) formulées pour la sérigraphie.....	9
Capteurs de pression.....	11
Conclusion .....	13

## Introduction

Les polymères sont connus pour être des isolants. Cependant, en fonction de leur composition chimique et de leur conformation structurale, certains polymères peuvent avoir des propriétés électriques allant de complètement isolant à semi-conducteur en passant par les diélectriques. Le polyacétylène est le premier polymère semi-conducteur à l'état dopé, découvert en 1977. Sa conductivité vient de la présence d'une chaîne carbonée conjuguée (*i.e.* alternance de simple et double liaisons), et peut être augmentée en améliorant l'empilement des chaînes ainsi qu'en dopant le polymère. Le polymère semi-conducteur le plus représentatif et étudié est actuellement le poly(3,4-éthylène dioxythiophène) (PEDOT). Il est commercialisé sous la forme d'encres aqueuses PEDOT:PSS où le PSS (poly(4-styrenesulfonate)) est un polyanion qui stabilise le PEDOT dans l'eau.

D'autres polymères ont des propriétés diélectriques et peuvent donc être polarisés sous l'action d'un champ électrique. Parmi eux, le polyfluorure de vinylidène (PVDF) est beaucoup étudié. Il peut cristalliser sous différentes formes et devient alors polarisable. La polarisation est maintenue après suppression du champ électrique : le matériau est alors piézoélectrique. Un de ces copolymères, le poly(fluorure de vinylidène-*co*-trifluoroéthylène) (P(VDF-TrFE)), cristallise plus facilement en une conformation complètement « trans », ce qui se traduit par une meilleure polarisation. Il a été découvert au début des années 1980.

Ces deux types de polymères, semi-conducteur et piézoélectrique, sont utilisés en électronique imprimée. Un avantage important des polymères sur les matériaux inorganiques ayant des propriétés électriques est la possibilité de les déposer avec des techniques d'impression déjà bien étudiées dans l'industrie de la communication imprimée. De fortes pressions et

températures ne sont pas nécessaires, contrairement au cas des céramiques, d'où le récent développement de l'électronique imprimée.

Il existe de nombreuses applications pour les polymères en électronique imprimée. Parmi elles, les diodes électroluminescentes organiques (OLED), les transistors organiques à effet de champ (OEFT) et les cellules photovoltaïques organiques (OSC), sont bien connues. D'autres applications, tels des dispositifs implantables pour l'administration de médicaments, des affichages électrochromiques, des dispositifs thermoélectriques, des actionneurs, des capteurs de pression, des dispositifs acoustiques, etc. Chaque dispositif est composé de plusieurs couches ayant des propriétés différentes. Chaque couche nécessite une épaisseur, un motif, et des conditions expérimentales (température, atmosphère inerte, etc.) spécifiques. Des dispositifs flexibles peuvent être conçus, ouvrant la voie à une grande variété d'applications.

Pour obtenir ces dispositifs, les solutions de polymères peuvent être déposées en utilisant différentes techniques dont de nombreux procédés d'impression. Principalement employés pour la communication imprimée, ces derniers ont été développés depuis les premières presses au milieu du 15<sup>ème</sup> siècle. Chaque type de dépôt a des avantages et inconvénients en matière d'épaisseur, de résolution, de motifs, d'homogénéité, etc... et nécessite des encres avec des caractéristiques, notamment rhéologiques, spécifiques. En fonction du procédé de dépôt, des interactions capillaires peuvent avoir lieu entre l'encre et les mailles d'un écran, une buse, une lame, etc. Les propriétés de mouillage des encres sur différents substrats jouent également un rôle important. Dans tous les cas, les propriétés capillaires et de mouillage des encres doivent être ajustées. En effet, pour former des dispositifs en électronique imprimée, un nombre important de couches, composées de différents matériaux, sont déposées les unes sur les autres. La formulation de l'encre doit donc être optimisée en fonction de la couche inférieure qui devient son substrat. Outre les propriétés capillaires et de mouillage, les propriétés rhéologiques des encres doivent être ajustées en fonction du procédé de déposition : une encre très fluide est nécessaire pour des impressions utilisant des buses, comme le jet d'encre, alors que des solutions plus visqueuses permettent des dépôts homogènes en utilisant une lame. Le comportement rhéologique des solutions de polymères est alors essentiel pour permettre leur dépôt en utilisant différents procédés.

Dans ce travail, deux types d'encres électroniques organiques ont été étudiées : elles contiennent respectivement un polymère semi-conducteur et un polymère piézoélectrique.

La première encre est composée d'un complexe entre le polymère semi-conducteur, le poly(3,4-éthylène dioxythiophène) (PEDOT), et un polyanion isolant, le poly(4-styrène

trifluorométhyl (bissulfonylimide)) (PSTFSI), qui stabilise le PEDOT dans l'eau. La structure de l'encre, son comportement rhéologique, ainsi que les propriétés des films séchés déposés par jet d'encre, lame rigide (doctor blade), sérigraphie et lame souple ont été étudiés. L'effet de la concentration du complexe PEDOT:PSTFSI dans l'eau sur les propriétés rhéologiques de l'encre a été examiné.

Le deuxième type de polymère étudié est composé d'un copolymère piézoélectrique, le poly(fluorure de vinylidène-*co*-trifluoroéthylène) (P(VDF-TrFE)), dans des solvants organiques. En raison de la structure du polymère, des moments dipolaires sont créés dans la chaîne carbonée. Ceux-ci peuvent être orientés sous l'action d'un champ électrique. La présence de dipôles dans le matériau est utilisée dans des dispositifs piézoélectriques pour obtenir un déplacement lorsqu'une tension est appliquée, ou pour obtenir une tension lors d'un déplacement du matériau. Dans ce cas, le polymère piézoélectrique doit être encapsulé entre deux électrodes. La réponse du dispositif est augmentée avec l'épaisseur de la couche active. Parmi les techniques d'impression, le motif le plus épais peut être obtenu en sérigraphie. Cette technique requiert une encre très visqueuse et rhéofluidifiante. Des encres P(VDF-TrFE) ont été formulées pour devenir rhéofluidifiantes en utilisant un agent gélifiant. Une étude plus complexe utilisant un bon et un mauvais solvant du polymère a aussi été réalisée.

Finalement, les encres formulées ont été utilisées pour créer des dispositifs piézoélectriques. Les encres PEDOT ont permis de former les électrodes, et les encres P(VDF-TrFE) ont permis de former la couche piézoélectrique. Deux objectifs étaient ciblés. Le premier était de développer une matrice de capteurs de pression flexibles. Ces dispositifs devaient notamment permettre la localisation précise ainsi que la mesure de la force appliquée à l'intérieur d'un cœur imprimé en 3D. Cela sera utilisé comme simulateur pour exercer des étudiants en chirurgie cardiovasculaire. Le second objectif était de comparer les propriétés des capteurs de pression utilisant les différentes formulations des encres P(VDF-TrFE).

Le premier chapitre de ce manuscrit rappelle les connaissances nécessaires sur les polymères ayant des propriétés électroniques et les techniques d'impression à même de les mettre en œuvre. Dans un second chapitre, les propriétés des encres PEDOT:PSTFSI sont analysées en fonction de divers procédés d'impression. Les propriétés des encres P(VDF-TrFE) formulées pour la sérigraphie sont détaillées au chapitre trois. Et dans un dernier chapitre, les propriétés de dispositifs piézoélectriques imprimés en utilisant les encres formulées précédemment sont examinées.

## Électronique organique et procédés d'impression

Dans le premier chapitre un état de l'art sur l'électronique organique et les procédés d'impression est réalisé. Dans un premier temps, les polymères conducteurs et piézoélectriques sont présentés : synthèses, structures, formulations, fabrications de films solides et optimisations des propriétés des films, mécanismes attribués aux propriétés électroniques, optiques et thermiques des polymères, applications possibles dans des dispositifs. Dans un second temps, les procédés d'impression utilisés en électronique imprimée sont décrits, ainsi que les propriétés rhéologiques et physico-chimiques des encres requises en fonction des techniques d'impression.

## Encre PEDOT:PSTFSI formulée pour différents procédés d'impression

Dans le cas des encres de PEDOT:PSTFSI, le monomère STFSI ainsi que le polyanion PSTFSI ont été synthétisés. Des études structurales du complexe PEDOT:PSTFSI en solution au moyen de DLS, d'AFM liquide et de cryo-MEB ont montré que les polymères forment un réseau dans l'eau. Les dimensions du polyanion qui forme le réseau sont de l'ordre de quelques nanomètres d'épaisseur et d'un demi-micromètre de long. Le polymère conducteur, le PEDOT, forme de petits nano-objets de 5 – 15 nm le long du polyanion. Une étude systématique du comportement rhéologique des encres PEDOT:PSTFSI en fonction de la concentration a montré que l'encre a un comportement Newtonien aux faibles concentrations, puis devient rhéofluidifiante avec des propriétés de gel aux plus fortes concentrations.

L'étude de ce comportement rhéologique en fonction de la concentration, ainsi que les paramètres des lois de Herschel-Bulkley et puissance sont récapitulés en Figure R.1.

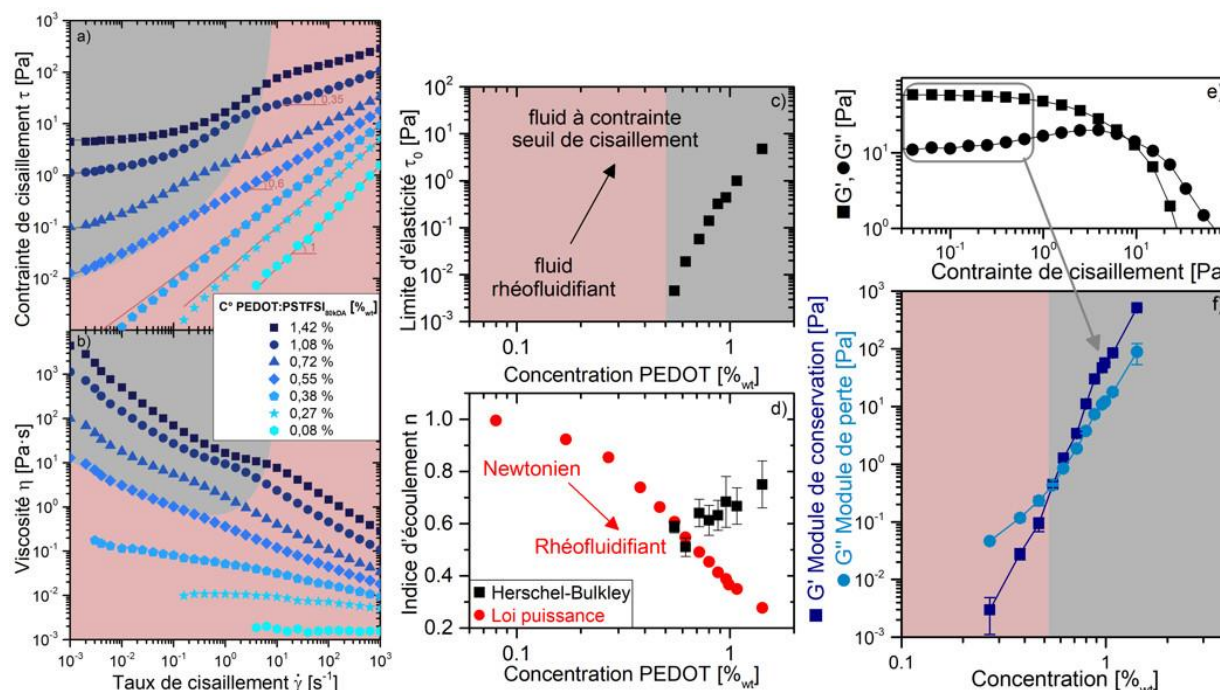


Figure R.1 : Propriétés rhéologiques d'une encre PEDOT:PSTFSI 80 kDa mesurée avec un rhéomètre en cisaillement (géométrie cône-plan : diamètre de 50 mm et angle de 1°) : a) contrainte de cisaillement  $\tau$ , et b) viscosité  $\eta$  en fonction du taux de cisaillement pour des rampes de cisaillement appliquées à 18°C ; c) et d) paramètres des modèles de Herschel-Buckley (région grise) et de la loi puissance (région rouge) appliqués aux courbes de cisaillement présentées en a) : limite d'élasticité  $\tau_0$  et indice d'écoulement  $n$  ; e) module de conservation  $G'$  et module de perte  $G''$  obtenus à une fréquence de 1 Hz à 18°C, pour une encre PEDOT:PSTFSI 80 kDa concentrée à 0,99 %wt dans l'eau, en fonction de la contrainte de cisaillement ; f) Moyenne des valeurs de  $G'$  et  $G''$  dans la zone linéaire de viscoélasticité (c'est-à-dire sur le plateau de la figure e)) en fonction de la concentration.

La mise en forme ou « processabilité » de ces encres est contrôlée par leur viscosité et leurs propriétés rhéologiques qui peuvent être adaptées simplement en modifiant la concentration du complexe ou de la masse molaire du polyanion. Des tensioactifs ont été ajoutés dans les formulations pour diminuer la tension de surface des encres et pour ainsi les rendre compatibles avec des substrats à faible énergie de surface. Des solvants à haut point d'ébullition tels le diméthylsulfoxyde (DMSO) ou l'éthylène glycol (EG) ont également été utilisés pour augmenter la conductivité et la résistance à l'eau des films séchés.

Quatre procédés de dépôt différents ont été utilisés avec les encres PEDOT:PSTFSI : la lame rigide (doctor blade), le jet d'encre, la sérigraphie, et une lame souple. La Figure R.2 rassemble les schémas des quatre types de dépôts utilisés ainsi que les photos des dépôts obtenus (homogènes dans les deux premiers cas, inhomogène en sérigraphie, et fines lignes dans le dernier cas), et certaines mesures de conductivité en AFM conductrice.

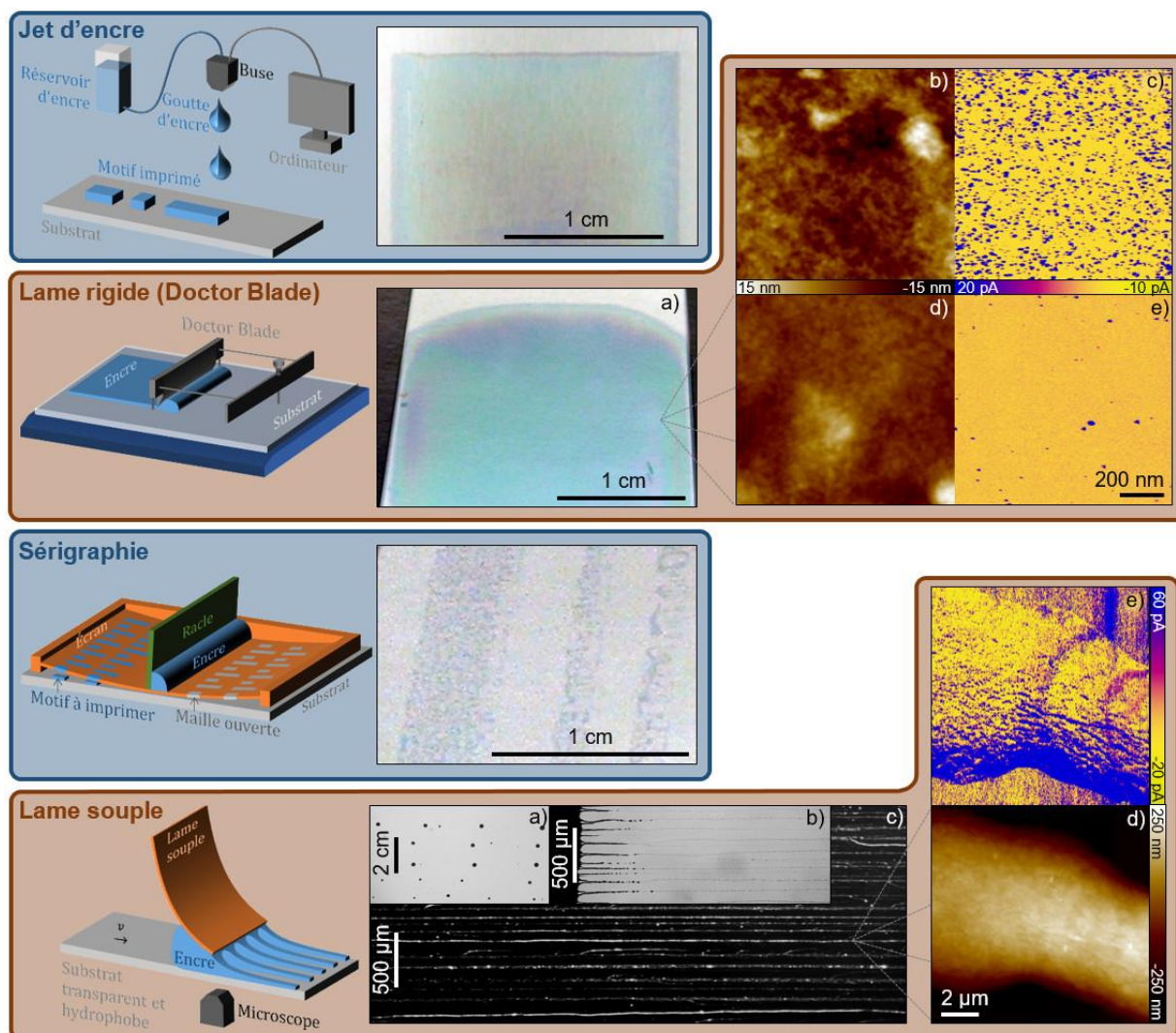


Figure R.2 : Schémas des quatre types de dépôts utilisés : jet d'encre, lame rigide (doctor blade), sérigraphie, lame souple. Photo des dépôts correspondants, et images d'AFM (topologie) et d'AFM conductrice dans le cas des dépôts aux lames rigide et souple. Dans le cas de la lame rigide : a) photo du dépôt, b) et c) AFM et AFM conductrice d'un dépôt obtenu avec une encre de PEDOT:PSTFSI<sub>80 kDa</sub> contenant du DMSO, d) et e) AFM et AFM conductrice d'un dépôt obtenu avec une encre de PEDOT:PSTFSI<sub>80 kDa</sub> ne contenant pas de DMSO. Dans le cas de la lame souple : a), b) et c) photo de dépôts obtenus respectivement avec une encre PEDOT:PSTFSI<sub>80 kDa</sub> à 1 %<sub>wt</sub> (a), et l'encre 0,3 %<sub>wt</sub> PEDOT:PSTFSI<sub>80 kDa</sub> + 5000 ppm PEO<sub>8000 kDa</sub> (b : lors du dépôt, c : après séchage en contraste de phase), d) AFM et e) AFM conductrice de la dernière encre.

Des films homogènes ont été obtenus en utilisant la lame rigide ou le jet d'encre avec des solutions de PEDOT:PSTFSI concentrées respectivement à 1 %<sub>wt</sub> et 0,5 %<sub>wt</sub>. Les transmittances (72 – 93 %), les rugosités et les conductivités (230 – 380 S/cm) mesurées sont comparables à celles obtenues avec l'encre commerciale PEDOT:PSS de même formulation similaire. Des figures de mérite prometteuses jusqu'à 31 ont été atteintes, ce qui est proche du minimum nécessaire dans l'industrie des électrodes transparentes. Pour la sérigraphie, des films inhomogènes ont été obtenus. Cela est principalement dû aux interactions capillaires entre l'encre et le maillage de l'écran. Une étude systématique utilisant différents types d'écrans et différents surfactants doit être menée pour obtenir une meilleure formulation de l'encre PEDOT:PSTFSI pour la sérigraphie.

Pour la lame souple, des lignes de PEDOT ont été obtenues en ajoutant un polymère à haute masse molaire dans la formulation pour augmenter l'élasticité de l'encre. Le dépôt a été réalisé sur du verre silanisé, du PET, ou de l'or traité avec de l'octane-thiol. Les lignes, bien définies, ont une épaisseur proche de 700 nm, et une largeur de 20 – 25 nm. L'AFM conductrice a montré que ces lignes sont conductrices et que les polymères s'alignent dans la direction du dépôt. Une étude plus systématique sur la conductivité des lignes de PEDOT devrait être réalisée en utilisant différents types de pointe conductrice pour mieux mesurer et comprendre la conductivité des lignes.

Il a ainsi été possible de formuler simplement les encres PEDOT:PSTFSI en jouant sur leur concentration. Les propriétés optoélectroniques des films obtenus sont comparables de celles obtenues avec les encres commerciales, quel que soit le procédé d'impression.

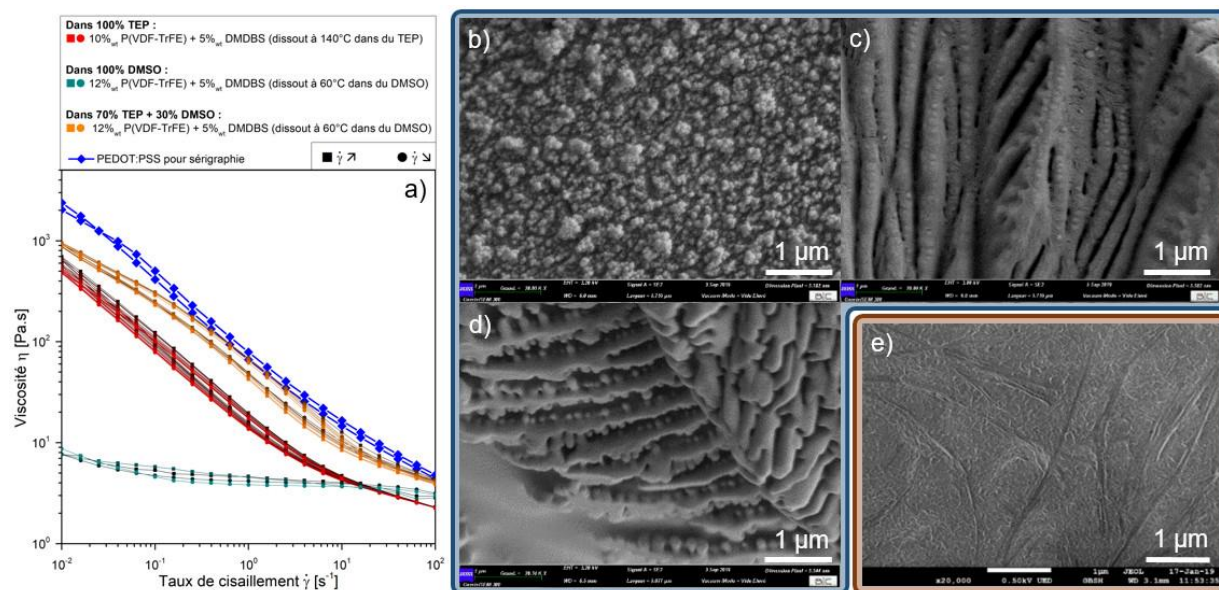
## Encres P(VDF-TrFE) formulées pour la sérigraphie

Pour les encres P(VDF-TrFE), deux lots de polymères ont été étudiés, contenant 79.4 %<sub>wt</sub> d'unités de VDF et 20.6 %<sub>wt</sub> d'unités de TrFE, avec des masses molaires moyennes respectivement de 238 et 278 kDa. Une étude systématique de la dépendance des comportements rhéologiques de l'encre en fonction de la concentration a montré que le P(VDF-TrFE) dans du gamma-butyrolactone (GBL) est Newtonien pour toutes les concentrations à faible cisaillement, et devient faiblement rhéofluidifiant à très fortes concentrations et très forts taux de cisaillements.

Pour modifier ce comportement et rendre les solutions rhéofluidifiantes pour des applications en sérigraphie, deux pistes ont été explorées.

Premièrement un agent gélifiant, le 1,3:2,4-bis(3,4-diméthylbenzylidène) sorbitol (DMDBS), a été ajouté dans un ou deux bons solvants du P(VDF-TrFE) : le triéthylphosphate (TEP), présent dans l'encre commerciale, et le DMSO. L'ajout de cet agent permet l'obtention d'un comportement rhéofluidifiant adéquat avec une viscosité et une élasticité suffisamment élevées. Ceci a été expliqué par la structure de l'encre sous forme de billes de polymère lors de l'absence d'agent gélifiant, et sous forme de billes alignées lors de la présence de celui-ci comme montré dans les images en cryo-MEB Figure R.3-b-c-d. Le désavantage de cette formulation est la nécessité d'utiliser des fortes températures, 130 – 140°C, pour dissoudre l'agent gélifiant dans le TEP. Pour réduire cette température, le DMDBS peut être dissous au préalable à 60°C dans du DMSO, qui est un bon solvant du DMDBS. Le même comportement rhéofluidifiant est obtenu pour des encres utilisant 30 %<sub>vol</sub> de DMSO et 70 %<sub>vol</sub> de TEP [Figure R.3-a]. Cependant, cette quantité de DMSO dans la formulation est incompatible avec le masque de l'écran sérigraphique testé. En effet, le masque a été partiellement dissous par cette formulation. Une étude avec différents masques pour

écrans sérigraphiques et leur compatibilité avec le DMSO devrait être réalisée, ainsi qu'une étude utilisant d'autres agents gélifiants compatibles avec le P(VDF-TrFE) et pouvant être dissous à faible température. Il a toutefois été possible d'imprimer ces deux encres en utilisant la lame rigide, un écran sérigraphique dans le cas de la formulation sans DMSO, et un pochoir avec lame rigide (stencil printing) pour la formulation avec DMSO. Les films obtenus étaient plutôt homogènes [Figure R.3-e]. D'autres caractérisations de ces films ont montré que l'agent gélifiant n'affectait pas la taille des cristaux de P(VDF-TrFE). L'utilisation de l'agent gélifiant est ainsi prometteuse dans la formulation d'encres P(VDF-TrFE) sérigraphiques en vue du dépôt de couches piézoélectriques.



Le deuxième type d'encre P(VDF-TrFE) a été formulé en utilisant un bon solvant du polymère, le GBL, et un mauvais solvant, l'alcool benzylique (BzOH). Une nano-émulsion est formée par les deux solvants, et l'ajout du P(VDF-TrFE) fait augmenter la taille des domaines de GBL [Figure R.4-b-c]. À température ambiante, le comportement rhéologique de l'encre est fortement dépendant de son histoire en cisaillement, particulièrement pour des températures proches d'une température critique qui est elle-même reliée à la concentration en mauvais solvant et en polymère.

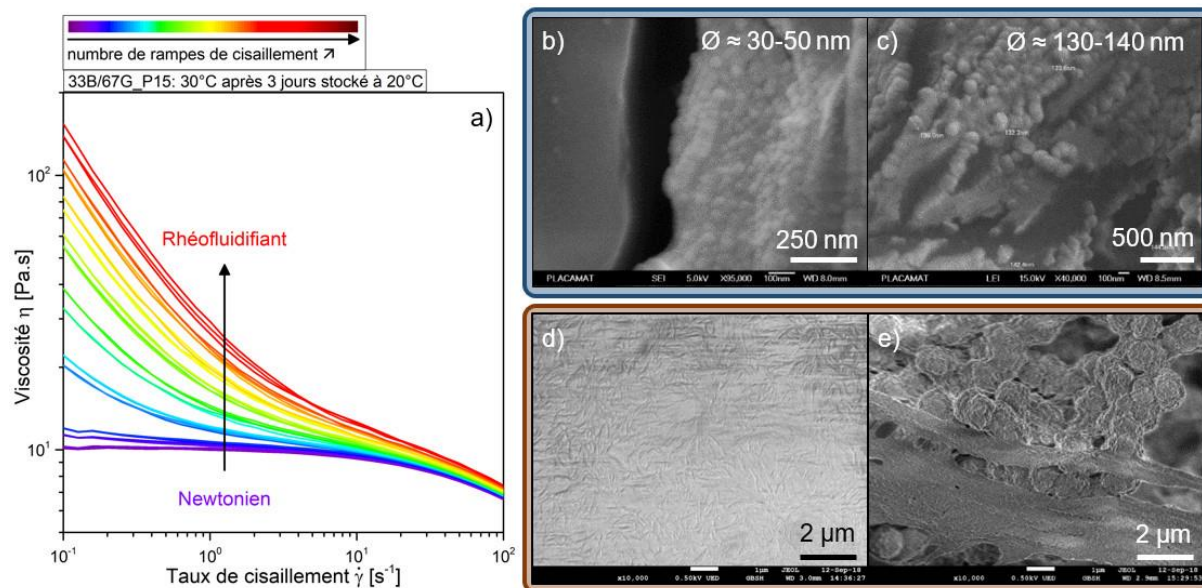


Figure R.4 : a) Propriétés rhéologiques de l'encre composée de 15 %wt P(VDF-TrFE) dans 1/3 alcool benzylique (BzOH) et 2/3  $\gamma$ -butyrolactone (GBL) stockée au préalable 3 jours à 20°C. Mesures réalisées avec un rhéomètre en cisaillement (géométrie cône-plan : diamètre de 50 mm et angle de 1°) : viscosité en fonction du taux de cisaillement obtenu en appliquant de nombreuses rampes croissantes et décroissantes de cisaillement à 30°C ; b) et c) Images cryo-MEB (sans sublimation du solvant) respectivement du mélange de solvants (1/3 BzOH + 2/3 GBL) et de l'encre avec 15 %wt P(VDF-TrFE) dans ce mélange de solvants ; d) et e) Images MEB de films obtenus avec l'encre précédente séchée respectivement à 135°C ou à 23°C.

Les encres Newtoniennes peuvent ainsi devenir rhéofluidifiantes avec de fortes viscosités lorsque de nombreux cycles de cisaillement sont appliqués [Figure R.4-a]. Un protocole précis doit être utilisé pour préparer des encres utilisant des températures appropriées à la sérigraphie. Les films obtenus peuvent être soit poreux, s'ils sont séchés à température ambiante, soit denses et homogènes, s'ils sont séchés à forte température (135°C) [Figure R.4-d-e]. Les films poreux peuvent devenir homogènes s'ils sont recuits à forte température. Les films poreux peuvent être utilisés en tant que membrane de séparation dans les batteries lithium-ion.

## Capteurs de pression

Enfin, des capteurs de pression utilisant les encres précédentes ont été réalisés en encapsulant une couche de P(VDF-TrFE) entre deux électrodes imprimées à partir des encres de PEDOT ou par évaporation de métal. Ils ont été déposés sur un substrat en PDMS ou en utilisant des films de P(VDF-TrFE) sans substrat (pour être intégré dans un cœur imprimé en 3D en vue de la formation d'étudiants en chirurgie cardiaque [Figure R.5-e-f]), et sur des substrats en PET pour comparer les différentes formulations de P(VDF-TrFE).

La Figure R.5-a-b montre une image microscopique d'un dispositif obtenu, ainsi que le schéma d'une matrice de capteurs de pression. Une fois celui-ci polarisé en appliquant successivement des champs électriques sinusoïdaux [Figure R.5-d], une réponse électrique peut être mesurée lorsque le dispositif est déplacé sous l'action d'une pression extérieure [Figure R.5-c].

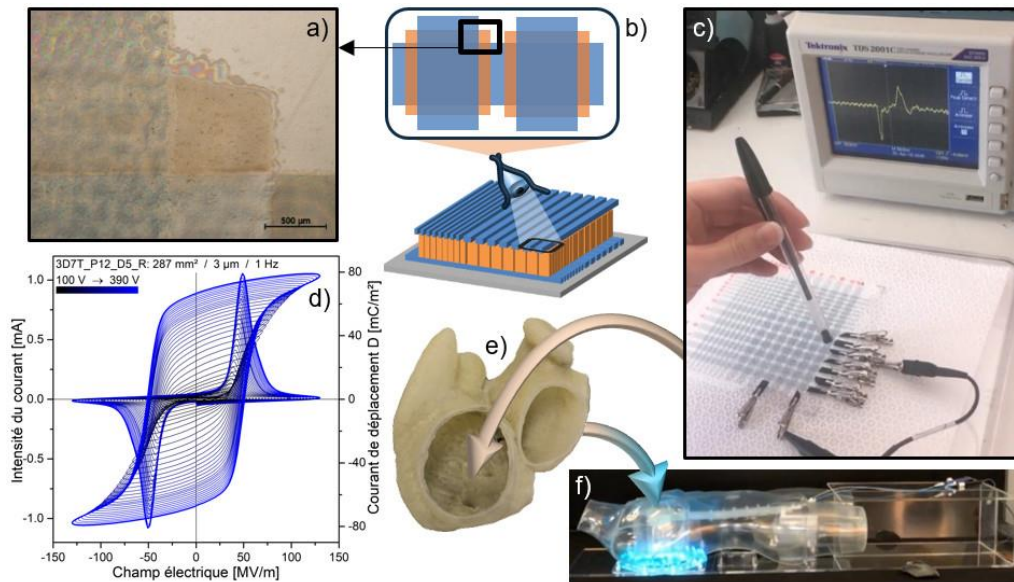


Figure R.5 : a) Image microscopique de l'intersection des différentes couches d'un capteur de pression imprimé en sérigraphie (encre PEDOT:PSS<sub>EL-P5015</sub> pour les électrodes et T\_P10\_D5\_R pour la couche active) ; b) Schéma du dispositif piézoélectrique : en bleu les électrodes et en orange le P(VDF-TrFE) ; c) Photo de la matrice de capteurs de pression et de la mesure de la réponse électrique à une pression après leur polarisation ; d) Polarisation d'un dispositif en appliquant des champs électriques sinusoïdaux avec des amplitudes croissantes : courant de déplacement sous forme de courbe d'hystérésis, et intensité du courant ; e) Cœur imprimé en 3D dans lequel la matrice de dispositifs doit être intégrée ; f) simulateur de corps humain dans lequel le cœur est inséré.

Bien que les substrats en PDMS possèdent une flexibilité adéquate pour incorporer les dispositifs dans le cœur imprimé en 3D, le mouillage et l'adhésion des encres PEDOT sur ces substrats ne sont pas optimaux. Des pré-couches sur les substrats de PDMS peuvent être développées pour augmenter le mouillage et l'adhésion des solutions aqueuses de PEDOT.

Les dispositifs avec des électrodes métalliques ont montré de bonnes propriétés électriques, mais leur manque de flexibilité empêche leur intégration dans le cœur imprimé en 3D. Les encres PEDOT utilisées pour imprimer les électrodes doivent être formulées avec de l'éthylène glycol et non du DMSO. En effet, l'utilisation du DMSO, qui est également un bon solvant du P(VDF-TrFE), a engendré des courts-circuits lorsque les films de P(VDF-TrFE) ont été mis entre deux électrodes de PEDOT.

Les dépôts par spray ou lame rigide en utilisant un masque ont mené respectivement à des fuites entre l'électrode du haut et du bas, à cause de la rugosité, ou entre deux mêmes électrodes de dispositifs voisins, à cause de la mauvaise adhésion entre le masque et le substrat. Cependant, de bonnes propriétés électroniques ont été obtenues en imprimant les encres de PEDOT:PSTFSI

en jet d'encre et les encres de P(VDF-TrFE) en doctor blade, ou en imprimant une encre commerciale de PEDOT:PSS en sérigraphie et les formulations de P(VDF-TrFE) en sérigraphie ou impression pochoir.

D'importantes optimisations des procédés ont été nécessaires pour obtenir des surfaces lisses avec le moins de défauts possibles et ainsi améliorer les propriétés électriques des dispositifs. Les dispositifs imprimés avec les trois encres P(VDF-TrFE) (commerciale et formulations maisons avec agent gélifiant) ont montré des propriétés similaires : hystérésis de polarisation et pics de courant bien définis. Ces dispositifs peuvent être utilisés dans des applications utilisant des capteurs de pression. Des caractérisations supplémentaires en matière de cristallinité devraient être réalisées pour mieux comprendre les différences entre les différents dispositifs.

## Conclusion

Les propriétés des encres PEDOT:PSTFSI et P(VDF-TrFE), deux solutions à base de polymères, ont été explorées dans ce travail. Différentes formulations étaient nécessaires pour optimiser le comportement rhéologique de ces encres, pour permettre leur dépôt en utilisant différents procédés d'impression. Des capteurs de pression ont ensuite été conçus et fabriqués pour démontrer l'applicabilité de ces encres fonctionnelles organiques dans des dispositifs organiques.

Dans le deuxième chapitre, il a été montré que contrairement aux encres PEDOT:PSS, les encres PEDOT:PSTFSI ne nécessitent l'ajout d'aucun additif pour modifier leurs propriétés rhéologiques: un simple ajustement de la concentration en polymère ou de la masse molaire du polyanion leur permet de passer d'un comportement Newtonien à rhéofluidifiant avec des propriétés de gel. En revanche, divers additifs ont été ajoutés pour améliorer les propriétés de mouillage, d'élasticité des encres, et de conductivité des films une fois ceux-ci séchés.

Dans le troisième chapitre, deux formulations d'encres P(VDF-TrFE) pour la sérigraphie ont été réalisées. L'objectif était de rendre la solution de polymère rhéofluidifiante. La première encre utilise un agent gélifiant comme additif, le 1,3:2,4-bis(3,4-diméthylbenzylidène) sorbitol (DMDBS). Lorsque celui-ci est correctement solubilisé dans du triéthylphosphate ou du DMSO, et lorsqu'il est ajouté en bonnes proportions, les encres P(VDF-TrFE) deviennent rhéofluidifiantes. Pour comprendre la modification du comportement rhéologique de l'encre lors de l'ajout de l'agent gélifiant, une étude structurale a été réalisée en cryo-MEB. Des films homogènes ont alors pu être déposés.

Le deuxième type d'encre utilise deux solvants : un bon et un mauvais solvant du polymère. Lorsqu'un protocole précis est suivi, à des températures dépendant de la formulation, l'encre peut se déstabiliser sous l'action d'un cisaillement et d'une diminution de la température. Il a ainsi été possible de formuler des encres P(VDF-TrFE) pour la sérigraphie. Cependant quelques problèmes de compatibilités avec les masques des écrans sont encore présents et restent à étudier.

Le dernier chapitre a permis de combiner les encres précédemment formulées pour créer des dispositifs fonctionnels : les encres PEDOT pour former les électrodes, et les encres P(VDF-TrFE) pour constituer la couche piézoélectrique entre les électrodes. La possibilité d'encapsuler une matrice de dispositifs dans un cœur imprimé en 3D pour former des étudiants en chirurgie cardiaque a été démontrée. La comparaison des formulations de P(VDF-TrFE) a par ailleurs mis en évidence des résultats similaires entre les formulations maison et l'encre commerciale.

Au final, il a été montré que les encres PEDOT:PSTFSI et P(VDF-TrFE) étudiées peuvent être formulées de manière adéquate en vue de dépôts utilisant des procédés d'impression variés dans le but de fabriquer des capteurs de pression fonctionnels. Un travail additionnel est cependant nécessaire pour optimiser de tels dispositifs.

Comme perspectives générales, les encres PEDOT pourraient être modifiées chimiquement pour les rendre sensibles à des molécules biologiques par exemple, en vue d'applications dans des transistors électrochimiques organiques, tout en conservant la facilité de leur dépôt par différents procédés d'impression. Les deux types d'encres, P(VDF-TrFE) et PEDOT, pourraient être développées de manière à devenir réticulables, ce qui devrait réduire les risques de fuite dans les dispositifs. Plus généralement, la démarche originale utilisée, allant de la synthèse à la caractérisation de dispositifs en passant par celle des matériaux et par les dépôts, pourrait être appliquée à d'autres matériaux pour d'autres applications, et cela en vue de contribuer au développement de l'électronique imprimée.

# List of Abbreviations

<b>Acronym</b>	<b>Signification</b>
AFM	Atomic Force Microscopy
AIBN	2,2'-azobis(2-methylpropionitrile)
BTA	tris-tert -butyl-1,3,5-benzenetrisamide
BzOH	Benzyl Alcohol
CTA	Chain Transfer Agent
DBS	1,3:2,4-(dibenzylidene)sorbitol
DLS	Dynamic Light Scattering
DMDBS	1,3:2,4-bis(3,4-dimethylbenzylidene) sorbitol
DMF	N,N-dimethylformamide
DMSO	Dimethyl sulfoxide
DoD	Drops on Demand (Inkjet technique)
DSC	Differential Scanning Calorimetry
EDOT	3,4-ethylene dioxythiophene
EDX	Energy Dispersive X-ray spectrometry
EG	Ethylene Glycol
FoM	Figure of Merit
GBL	$\gamma$ -butyrolactone
GBSH	Super-High resolution Gentle Beam
HB	Herschel-Bulkley
HOMO	Highest Occupied Molecular Orbital
HOPG	Highly Ordered Pyrolytic Graphite
HPF	High Pressure Freezing
ITO	Indium-Tin Oxide
LUMO	Lowest Unoccupied Molecular Orbital
MEK	Methyl Ethyl Ketone (or Butanone)
MFI	Melt flow index
NIR	Near-Infrared
OECT	Organic Electrochemical Transistors
OFET	Organic Field-Effect Transistor
OLED	Organic Light-Emitting Diode

---

<b>Acronym</b>	<b>Signification</b>
OPV	Organic PhotoVoltaic
OTS	Octadecyltrichlorosilane
PDMS	Polydimethylsiloxane
PEDOT	Poly(3,4-ethylene dioxythiophene)
PEO	Polyethylene Oxide
PET	Polyethylene Terephthalate
PL	Power-Law
PMMA	Poly(methyl methacrylate)
PS	Polystyrene
PSS	Poly(4-styrenesulfonate)
PSTFSI	Poly(4-styrene trifluoromethyl (bissulfonylimide))
PTFE	Polytetrafluoroethylene
PVDF	Polyvinylidene fluoride
P(VDF-TrFE)	Poly(vinylidene fluoride- <i>co</i> -trifluoroethylene)
NMR	Nuclear Magnetic Resonance
SEC	Size Exclusion Chromatography
(Cryo-)SEM	(Cryogenic-)Scanning Electron Microscope
STFSIK	Potassium 4-styrene trifluoromethyl (bissulfonylimide)
TEP	Triethylphosphate
THF	Tetrahydrofuran
UV	Ultraviolet

# List of Symbols and Physical Constants

Symbol	Unit	Signification
$Ca$	[-]	Capillary Number
$C^*$	[%wt] or [g·m <sup>-1</sup> ]	Critical Concentration
$D$	[C·m <sup>-2</sup> ]	Displacement
$d_{33}$	[C·N <sup>-1</sup> ]	Transverse Piezoelectric Coefficient
$E$	[V·m <sup>-1</sup> ]	Electric Field
$E_c$	[V·m <sup>-1</sup> ]	Coercive Field
$\epsilon_0$	[F·m <sup>-1</sup> ]	Vacuum Permittivity = $8.854 \times 10^{-12}$ F·m <sup>-1</sup>
$\epsilon_r$	[F·m <sup>-1</sup> ]	Relative Permittivity (or dielectric constant)
$f$	[s <sup>-1</sup> ]	Frequency
$g$	[m·s <sup>-2</sup> ]	Gravitational Force = 9.81 m·s <sup>-2</sup>
$G^*$	[Pa]	Complex Shear Modulus
$G'$	[Pa]	Storage Modulus
$G''$	[Pa]	Loss Modulus
$\gamma$	[%]	Deformation
$\dot{\gamma}$	[s <sup>-1</sup> ]	Shear Rate
$\Gamma$	[mN·m <sup>-1</sup> ]	Surface Tension
$\Delta H$	[cal·mol <sup>-1</sup> ] or [J·g <sup>-1</sup> ]	Enthalpy
$k$	[Pa]	Flow Consistency Index
$m$	[g]	Weight
$M_w$	[Da=g·mol <sup>-1</sup> ]	Molar Mass
$\eta$	[Pa·s]	Viscosity
$n$	[-]	Flow Behavior Index
$\omega$	[rad·s]	Angular Frequency
$P$	[C·m <sup>-2</sup> ]	Polarization
$P_r$	[C·m <sup>-2</sup> ]	Remanent Polarization
$P_s$	[C·m <sup>-2</sup> ]	Saturated Polarization (or Spontaneous Polarization)
$P$	[Pa]	Pressure

---

<b>Symbol</b>	<b>Unit</b>	<b>Signification</b>
$\pi$	[-]	3.14
$R, r$	[m]	Radii
$R_s$	[ $\Omega \cdot \text{sq}^{-1}$ ]	Sheet Resistance
$R_q$	[m]	Roughness
$\sigma$	[ $\text{S} \cdot \text{cm}^{-1}$ ]	Conductivity
$t$	[nm]	Thickness
$T$	[%]	Transmittance
T	[°C]	Temperature
$T_c$	[°C]	Curie Temperature
$T_m$	[°C]	Melting Temperature
$\tau$	[Pa]	Shear Stress
$\tau_0$	[Pa]	Yield Stress
$\mu$	[C·m]	Electric Dipole Moment
$v$	[ $\text{m} \cdot \text{s}^{-1}$ ]	Speed
$\Delta X_c$	[%]	Degree of Crystallinity
$\chi_i$	[-]	Electronegativity of the Atom i

# General Introduction

Polymers are known to be insulators. However, depending on their chemical composition and on their structural conformation, they can possess different electronic properties: from completely insulator, to dielectric, to semi-conductors. Polyacetylene is the first semiconducting polymer discovered in 1977. The conductivity comes from the conjugated backbone and can be increased by improving the packing of the chains and by doping the polymer. Nowadays, poly(3,4-ethylenedioxythiophene) (PEDOT) is the most representative conducting polymer. It is even commercialized in the form of PEDOT:PSS aqueous inks.

Other polymers have dielectric properties and thus can be polarized under an electric field. Among them, polyvinylidene fluoride (PVDF) is well studied. It can crystallize in different phases and become polarized; the polarization can be maintained after removal of the electric field. It is then a piezoelectric material. One of its copolymers, poly(vinylidene fluoride-*co*-trifluoroethylene) (P(VDFTrFE)), crystallizes more easily in an all trans conformation, and gives rise to better polarization. It was discovered in the early 1980s. Both types of polymers are used in printed electronics.

The advantage of polymers compared to other materials with electric properties is that they can be easily processed using solution deposition, well-known in the print media industry. Very high temperatures or pressures are not required, which is the case for ceramic deposition, hence the recent development of organic printed electronics.

A wide variety of applications of polymers in organic printed electronics exist. Among them, Organic Light-Emitting Diodes (OLED), Organic Field-Effect Transistors (OEFT) and Organic Solar Cells (OSC) are well known. Other applications exist such as implantable drug delivery devices, electrochromic displays, thermoelectric devices, actuators, pressure sensors, acoustic devices, etc. Each device is composed of several layers with different properties. Every layer needs a specific thickness, specific patterns, and specific experimental conditions (temperature, inert atmosphere, etc.). Flexible devices can be designed, paving the way to a wide range of mobile applications.

To obtain these devices, the polymeric solutions can be deposited using various deposition techniques. A wide range of printing techniques exist. Principally used in print media, they have been well developed since the first printing presses of the mid-15<sup>th</sup> century. Some of the common printing techniques can be used to deposit functional inks in printed electronics. Each type of deposition has advantages and drawbacks in terms of film thickness, resolution, patterning, homogeneity, etc. Each deposition requires different properties for the inks. Depending on the

process, capillary interactions may occur between the ink and a mesh, a nozzle, blade, etc... It is noteworthy that the wetting properties of the inks on different substrates play a major role. In all these cases, the capillary and the wetting properties of the inks have to be tuned. Indeed, in printed electronics, numerous layers of different functional materials are deposited on top of each other to form devices and the formulations have to be optimized. Besides capillary properties, the rheological behavior of the inks has to be tailored as well: a very fluid ink is needed for depositions using nozzles, while more viscous solutions are required for deposition using a blade. The rheological behavior of polymeric solutions is then essential to enable their deposition using different solution processes.

In this work, two types of organic electronic inks, containing respectively a semi-conducting polymer and a piezoelectric polymer, have been studied.

The first ink is composed of a complex between the semi-conducting polymer, poly(3,4-ethylene dioxythiophene) (PEDOT), and an insulator polyanion, the poly(4-styrene trifluoromethyl (bissulfonylimide)) (PSTFSI) which stabilizes PEDOT in water. The structure of this ink and its rheological behavior as well as the properties of films deposited by inkjet printing, doctor blading, screen-printing and using a soft blade deposition were studied. The effect of the concentration of the PEDOT:PSTFSI complex in water on the rheological properties of the ink was investigated.

The second type of ink is composed of a piezoelectric copolymer, poly(vinylidene fluoride-*co*-trifluoroethylene)(P(VDF-TrFE)), in organic solvents. Due to the structure of the polymer, dipolar moments are induced in the backbone of the polymeric chain and can be oriented through an external electric field. The presence of dipoles in the polymeric material is used in piezoelectric devices to obtain a displacement by applying a voltage or to obtain a voltage by applying a displacement. In this case, the piezoelectric polymer has to be encapsulated between two electrodes. The response of the device is increased when the thickness of the active layer is increased. Among the printing techniques, the thickest patterned layers can be obtained by screen-printing. This technique needs highly viscous but shear-thinning inks. P(VDF-TrFE) inks were formulated to become shear-thinning using a gelifying agent. A more complex pathway using a good and a bad solvent of P(VDF-TrFE) was explored.

Finally, the inks previously formulated were used to create piezoelectric devices. The PEDOT inks become the electrodes, and the P(VDF-TrFE) inks generate the piezoelectric layer. Two goals were targeted. The first one was to develop a matrix of flexible pressure sensors. These sensors should allow the exact localization and the measurement of the applied force on the inside

of a 3D-printed heart. It will be used to train students on cardiovascular diseases surgery. The second aim was to compare the properties of pressure sensors using the various formulations of P(VDF-TrFE) inks.

In this manuscript, the basics of polymers with electronic properties and of printing techniques will first be reviewed. In a second chapter, the properties of PEDOT:PSTFSI inks will be analyzed versus various printing processes. Then, the properties of P(VDF-TrFE) inks formulated for screen-printing will be detailed. In a last chapter, the properties of piezoelectric devices, printed using the inks formulated in the previous chapters, will be examined.



# 1 Organics electronics and printing technologies

1.1 Organic electronics .....	24
1.1.1 Poly(3,4-ethylenedioxythiophene) (PEDOT): a semiconducting polymer .....	24
1.1.1.1 History of semiconducting polymers .....	24
1.1.1.2 Various synthesis pathways of PEDOT:Counterion .....	26
1.1.1.3 Formulation of PEDOT:PSS solutions to increase the conductivity of films .....	29
1.1.1.4 Electronic structure and transport properties of PEDOT:PSS: from single chain to thin film and application in electrochromic devices.....	31
1.1.1.5 Temperature dependence of PEDOT electrical conductivity and application in thermoelectric devices.....	34
1.1.1.6 Applications of the coupling between the ionic and electronic transport in PEDOT films.....	36
1.1.1.7 PEDOT:PSS films as transparent organic electrodes.....	37
1.1.2 Poly(vinylidene fluoride- <i>co</i> -trifluoroethylene) P(VDF-TrFE): a piezoelectric polymers .....	41
1.1.2.1 Dielectric materials.....	41
1.1.2.2 PVDF and PVDF derivatives among the piezoelectric polymers .....	43
1.1.2.3 Synthesis pathways of P(VDF-TrFE).....	45
1.1.2.4 Properties of P(VDF-TrFE).....	45
1.1.2.5 Applications.....	48
1.2 Printing technologies.....	50
1.2.1 Printing processes overview .....	50
1.2.1.1 Small history of printing.....	50
1.2.1.2 Printing processes and properties.....	50
1.2.2 The rheological behavior of inks.....	57
1.3 Conclusion.....	59

## 1.1 Organic electronics

Polymers are generally known to be insulators. However, different types of polymers with electrical properties have been discovered and studied during the last century. This section will explore the properties of semiconducting  $\pi$ -conjugated polymers in a first part, and of piezoelectric polymers in a second part. Both will be compared to traditional conducting and piezoelectric materials in terms of properties and processing.

### 1.1.1 Poly(3,4-ethylenedioxythiophene) (PEDOT):

#### a semiconducting polymer

##### 1.1.1.1 History of semiconducting polymers

$\pi$ -conjugated polymers are polymers with alternated double and single bonds between the carbon atoms. An overlapping between the  $\pi$ -orbitals can create pathways to the electrons. Doping these polymers can decrease the band gap between the  $\pi$ -bonding and  $\pi^*$ -anti-bonding orbitals, increasing the conductivity of the polymer by several orders of magnitude.<sup>1</sup> Various doping strategies exist including electrical doping, which consists of adding a donor or an acceptor of electrons close to the polymer. A charge transfer takes place between the polymer and the dopant, giving rise to a delocalized electron in the polymer, neutralized by a counter ion (derived from the dopant). The polymer is generally oxidized in a cation and the dopant reduced in an anion.<sup>2</sup>

Semiconducting polymers were discovered in 1977 with the study of polyacetylene doped with halogens<sup>3,4</sup>. Later, doped polypyrrole<sup>5</sup> and poly(p-phenylene)<sup>6</sup> were reported in 1979. Figure 1.1 displays the structure of different conjugated polymers studied since.<sup>7,8</sup> All consist of a conjugated backbone. The packing of the chains, the degree of order when dried, the impurity density, and the structural defects influence the charge transport in all these semiconducting polymers.

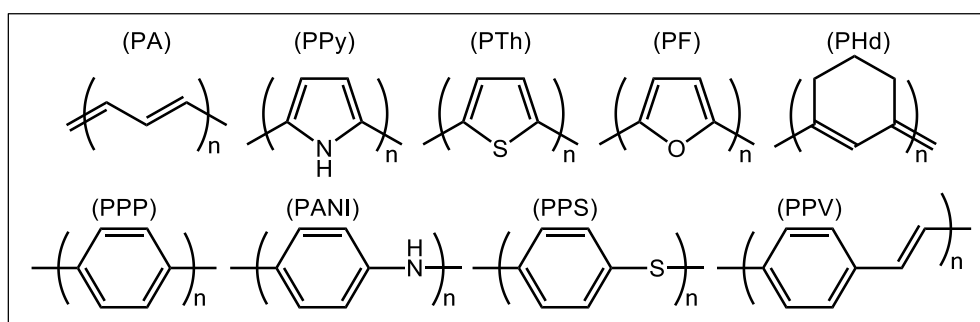


Figure 1.1: Structure of various conducting polymers: Polyacetylene (PA), Polypyrrole (PPy), Polythiophene (PTh), Polyfuran (PF), poly(1,6-heptadiyne) (PHd), Poly(p-phenylene) (PPP), Polyaniline (PANI), Poly(p-phenylene-sulfide) (PPS), Poly(p-phenylene-vinylene) (PPV) (from<sup>7,8</sup>)

The conductivities of these conductive polymers are compared to common materials in Figure 1.2. Without doping, the conductivity of polymers is very low (smaller than  $10^{-5}$  S/cm). However, by doping the structure and allowing better-organisation, the conductivity can increase and can approach that of copper.

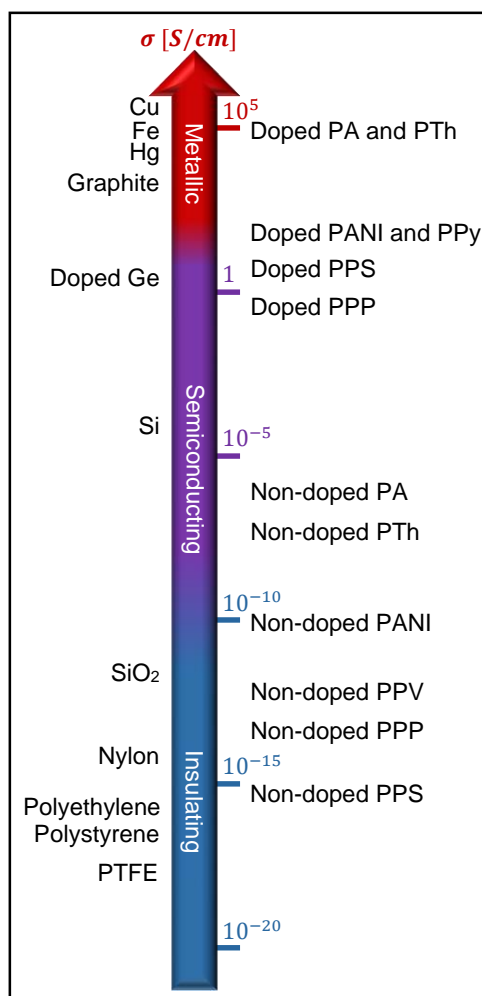


Figure 1.2: Conductivity of conjugated polymers compared to common materials (adapted from<sup>1,9</sup>)

Among the polythiophene derivatives<sup>10,11</sup>, poly(3,4-ethylenedioxythiophene) (PEDOT) is the most representative and studied conducting polymer. Its structure in neutral and oxidized forms is displayed in Figure 1.3.

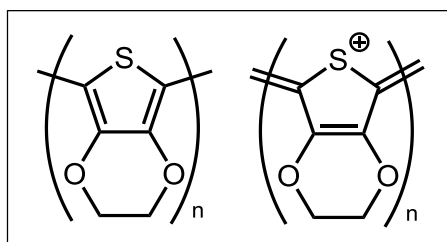


Figure 1.3: Structure of PEDOT: neutral form (left) and oxidized form (right) (from<sup>12</sup>)

To obtain high conductivity, PEDOT polymers have to be doped. An anion can be added to compensate the charge of the oxidized form: the PEDOT is then p-doped, i.e. it is positively

charged. In solid state, very high conductivity can then be reached, up to 8800 S/cm, the highest value recorded for PEDOT single-crystal nanowires.<sup>13</sup>

### 1.1.1.2 Various synthesis pathways of PEDOT:Counterion

PEDOT can be synthesized directly onto a substrate or in solution and then deposited with various solution processes. In this second case, PEDOT have to be stabilized in water with a polyanion as it is insoluble in water. Usually the polyanion poly(styrenesulfonate) (PSS) is used to create the dispersion. The polyanion has then two purposes: to stabilize PEDOT in water as well as to stabilize the charges in the doped units of PEDOT and thus increase its conductivity. PEDOT is more stable than polyacetylene both in air and under heating. This is attributed to the aromatic ring which stabilizes the positive charge, and the dioxy ring which stabilizes free radicals in the conjugated backbone.<sup>11</sup>

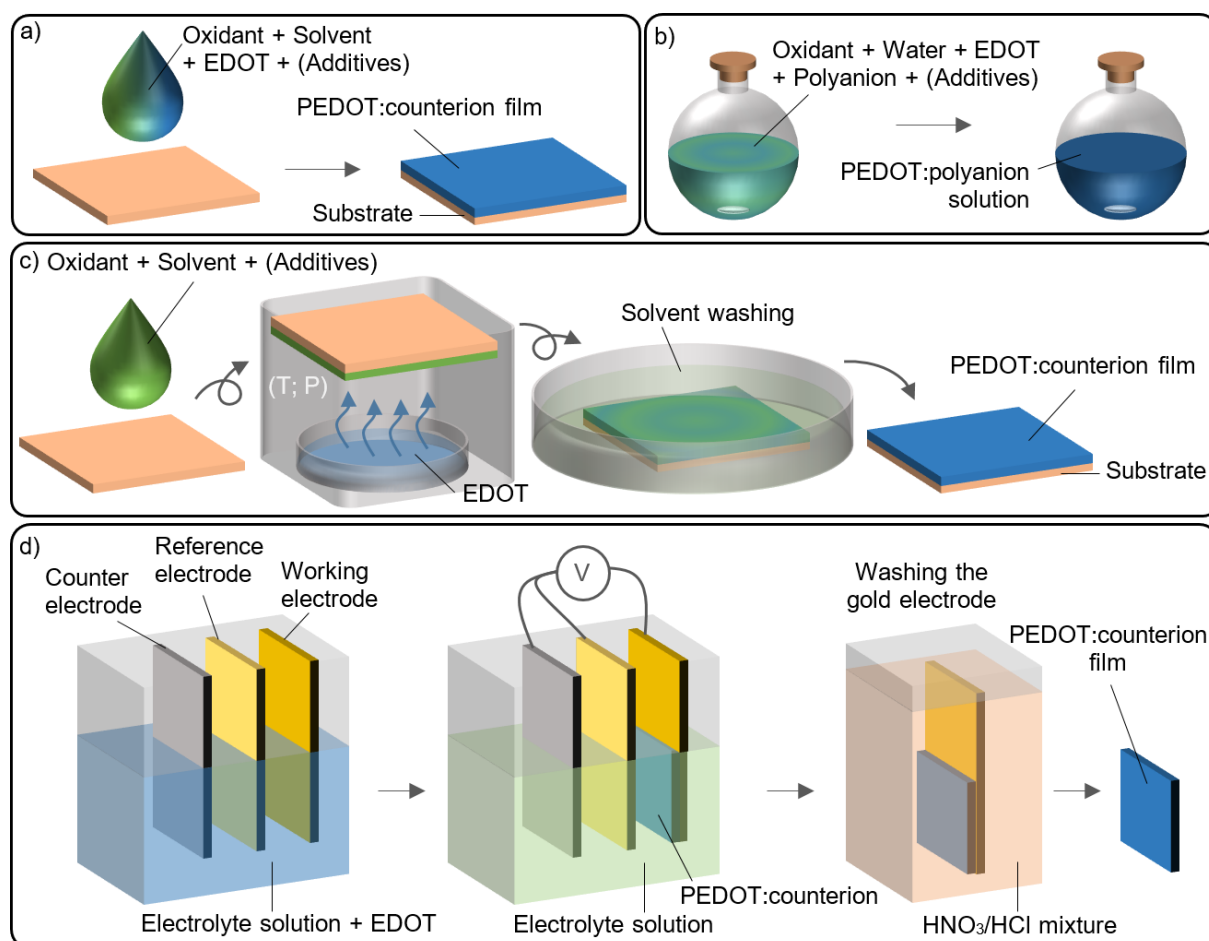


Figure 1.4: Different methods to polymerized EDOT: a) In situ polymerization, b) dispersion polymerization, c) Vapor phase polymerization, d) electro-polymerization (based on<sup>14</sup>)

To synthesize PEDOT, EDOT monomer is oxidized by an oxidant, usually  $\text{Fe}^{3+}$ . The rate of polymerization is reduced by adding a base, which allows the formation of higher molar mass PEDOT, while an anion is added to compensate the charge and stabilize the doped the polymer.<sup>15</sup> Depending of the counterion, the morphology and properties of the complex PEDOT:counterion are different. For example, PEDOT:Cl or PEDOT:Tos are not soluble in water, the counterion being an atom or molecule and not a polymer. The conductivity of PEDOT films with small counterions (obtained by in situ polymerization, chemical vapor polymerization or electro-polymerization) is higher than those obtained by solution processing with a polyanion which is an insulator. The different methods used to polymerize EDOT are schematized in Figure 1.4. For the in situ polymerisation, an oxidant (which can act as counterion), a base and EDOT are mixed together onto the substrate where the polymerization occurs. For vapor phase polymerization, a film of the oxidant is made and then exposed to a vapor of EDOT under vacuum at high temperature. Finally, the excess of EDOT and oxidant is washed out in a bath of good solvents of both constituents (water and ethanol). For electro-polymerization, three electrodes (the working electrode, the reference electrode and the counter electrode) are placed in an electrolyte solution containing the electrolyte (whose anion will become the counterion), a solvent, and EDOT monomers. A voltage is applied to the working electrode where EDOT will be oxidized and polymerized in the form of an insoluble film. The electrode can then be dissolved using an Aqua Regia mixture (composed of nitric acid and hydrochloric acid).<sup>14</sup> The conductivity ( $10^0 - 10^3$  S/cm) then depends on the counterion used. Table 1.1 gives the conductivity, at room temperature, of PEDOT:counterion films obtained by electro-polymerization of EDOT using various counterions and different polymerization methods as detailed in Table 1.2.<sup>16</sup>

Method	A	B	C	D	E	F	G
Counterion	Conductivity [S/cm]						
$\text{ClO}_4^-$			400-650	55	30	780	650
$\text{BF}_4^-$		30	280	24	121		
$\text{PF}_6^-$	105	200	120-150	49			
$\text{NO}_3^-$				79			
$\text{SO}_4^-$				41			
$\text{Tos}^-$				36			125-450
$\text{N}(\text{SO}_2\text{CF}_3)_2^-$	8.5				130		
$\text{N}(\text{SO}_2\text{C}_2\text{F}_5)_2^-$					108		
$\text{N}(\text{SO}_2\text{C}_3\text{F}_7)_2^-$					106		
$\text{N}(\text{SO}_2\text{C}_4\text{F}_9)_2^-$					25		
$\text{CF}_3\text{SO}_3^-$	95	50	200		86		
$\text{C}_4\text{F}_9\text{SO}_3^-$					91		
$\text{C}_8\text{F}_{17}\text{SO}_3^-$					8		
$\text{PSS}^-$			50-80				50-80

Table 1.1: Conductivity at room temperature of PEDOT:counterion films obtained by electro-polymerization of EDOT using various counterion for different polymerization methods detailed in Table 1.2 (from<sup>16</sup>)

Method	Solvent	T [°C]	I [mA/cm <sup>2</sup> ]	E [eV]	U [V]
A	Propylene carbonate	-30°C	0.04		
B	Propylene carbonate	-30°C	0.01 – 0.06mA		
C	Acetonitrile	RT		0.85 – 1.1	
D	Water + surfactant	RT			Sweeps -1/+1
E	Acetonitrile				*
F	Acetonitrile**				1.3
G	Acetonitrile***				0.8

Table 1.2: electro-polymerization methods used in Table 1.1. (\*series of potentials above the half-wave oxidation potential; \*\*on microfiltration membranes; \*\*\*with water for PSS) (adapted from<sup>16</sup>)

Adding copolymers such as poly(ethylene glycol)-poly(propylene glycol) (PEG-PPG) has been shown to increase the crystallinity of resulting PEDOT films in vapor phase polymerisation, by distributing more homogeneously the oxidant and by creating a template where the PEDOT polymerized with a better organisation. An increase in the conductivity is then observed (up to 3400 S/cm).<sup>17</sup>

The three previous methods (in situ polymerisation, vapor phase polymerization, and electro-polymerization) create insoluble PEDOT:counterion films. However, these methods do not allow patterning surfaces PEDOT:counterion films. Dispersion polymerization resolves this problem. This technique uses a polyanion to stabilize PEDOT in water to create a dispersion of nanoparticles of PEDOT. The polyanion poly(4-styrenesulfonate) (PSS) is now widely used and commercialized. The negative charge of PSS compensates the positive charge of doped PEDOT, via electrostatic interactions, and stabilizes the colloidal dispersion.<sup>14</sup> The concentration in polyanion is then very important for those two purposes. It has been shown that after polymerization, PEDOT is doped (oxidized) at 33 %, which means that there is one charge per three monomer units.<sup>18,19</sup> The excess in negative charges of the polyanion is used for stabilisation: it creates an electrostatically stabilizing shell around the discrete soluble gel particles. The size of the colloidal particles is related to the concentration of salt in water: by increasing this concentration, the size first decreases and then increases. Indeed, it has been shown that for polyelectrolytes, the chains of polymer are stiff in the absence of mobile ions due to Coulomb repulsion between the negative charges of the polymer itself. By adding salt, the polyanion becomes more flexible by compensating some of its charges allowing the chain to adapt its conformation and better stabilize the particles. If too much salt is added, electrostatic interactions are screened, leading to aggregation of the microgel particles.<sup>16,20</sup> It has been shown that a minimum molar mass of the polyanion is required to form a stable polyelectrolyte complex in water, and that high molar masses and weak ionic groups result in more stable polyelectrolytes.<sup>16</sup> The structure of PEDOT:PSS is displayed in Figure 1.5.

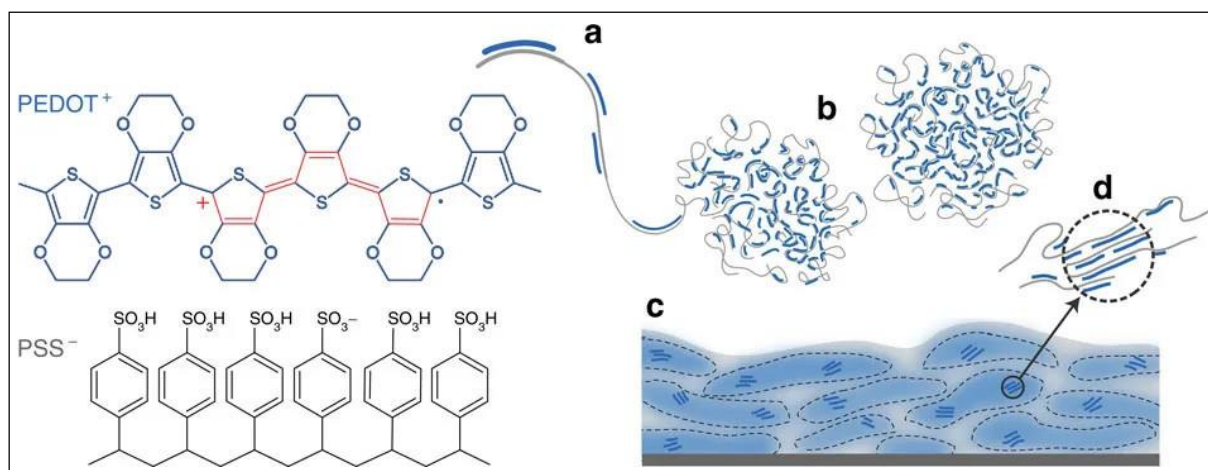


Figure 1.5: The chemical structure of PEDOT:PSS and commonly described microstructure of the conducting polymer system (a) synthesis onto PSS template, (b) formation of colloidal gel particles in dispersion and (c) resulting film with PEDOT:PSS-rich (blue) and PSS-rich (grey) phases. (d) Aggregates/crystallites support enhanced electronic transport. (from<sup>21</sup>)

### 1.1.1.3 Formulation of PEDOT:PSS solutions to increase the conductivity of films

To increase the conductivity of PEDOT:PSS films, a secondary doping effect can be used. It consists of adding a dopant (such as organic solvents, salts and acids). Figure 1.6 shows the progress in terms of conductivity of the films as a function of the nature of the secondary dopant used and for different pre- or post-treatments. Polar organic solvents like DMSO or EG were studied as well as polyols such as sorbitol or glycerol.<sup>22-26</sup> It was found that to act as a secondary dopant, the additive should be highly soluble in water, have a high boiling point and have a high dielectric constant.<sup>27</sup>

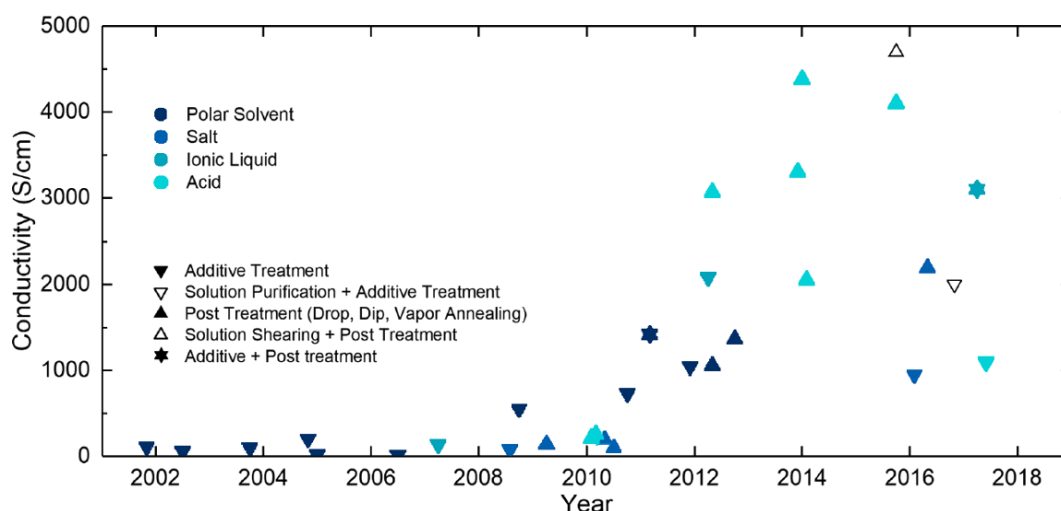


Figure 1.6: Timeline of conductivity enhancement in PEDOT:PSS through secondary doping process (from<sup>14</sup>)

The increase of conductivity was attributed to a phase separation between excess PSS and PEDOT:PSS. It occurs during the drying, when the proportion of water becomes smaller than the concentration of the secondary dopant. This reduces the isolating shell that encapsulates the

conductive particles rich in PEDOT, leading to a better 3D percolation network. It is illustrated in Figure 1.7 which displays the change in electrical conductivity of PEDOT:PSS films formulated with or without EG, as well as schematics of the structural modifications.

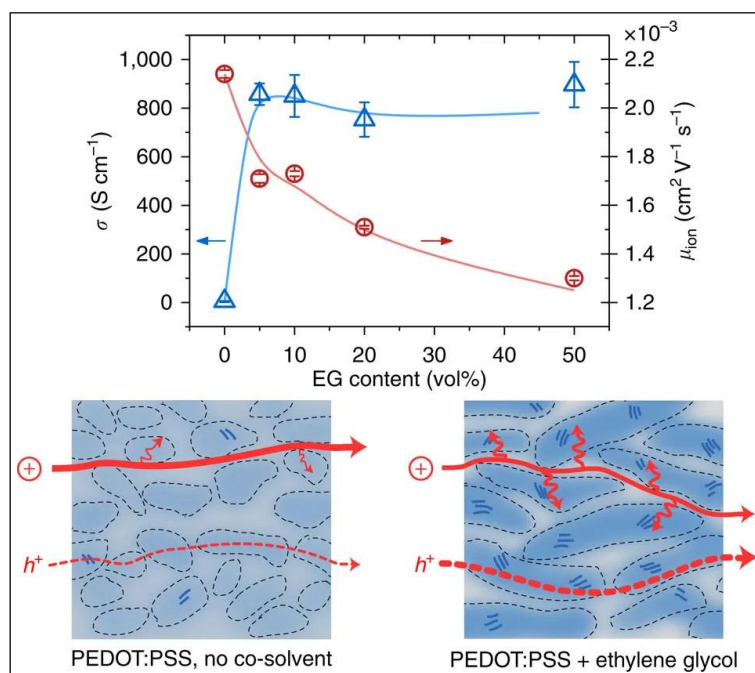


Figure 1.7: Electronic conductivity and ion mobility of PEDOT:PSS films with different contents of EG, and schematic of the morphological changes and associated transport of ions and holes viewed in the cross section of bulk film of PEDOT:PSS with or without EG. Addition of EG varies the PEDOT content, size/purity of PEDOT:PSS rich phases, and amount of PEDOT:PSS aggregates/crystallites. (from<sup>21</sup>)

The secondary dopant can be added in the formulation of the PEDOT ink in small amounts, or can be used during a post-treatment stage. In the second case, dried films of PEDOT:PSS are immersed in the solution of the secondary dopant and then dried again. During this process, excess PSS is removed, which leads to a higher density of PEDOT: reduction of the  $\pi$ - $\pi$  stacking distance in the crystallites, increase of the crystallite size,<sup>28,29</sup> and better orientation of PEDOT crystallites (edge-on for post-treatment with EG, and face on with addition of glycerol).<sup>25</sup>

Ionic compounds (salts,<sup>30</sup> acids,<sup>31</sup> and zwitterions<sup>32</sup> which are molecules possessing both a cation and an anion) are other types of secondary dopant.<sup>29</sup> The increase of conductivity in this case is attributed to charge screening that can lead to some counterion exchange between PEDOT:PSS and the ionic compound. It results in structural modifications from amorphous granular structure to highly ordered nano-fibrils of PEDOT:PSS/ionic liquid composite.

Post-treatment with acid, such as sulfuric acid or nitric acid, is another way to enhance greatly the conductivity of PEDOT films up to 4380 S/cm [Figure 1.8]. It has been explained by a slight increase of the degree of oxidation of PEDOT and a removal of excess of PSS, which provoke structural changes to more linear PEDOT chains and a more crystalline phase.<sup>29,33</sup>

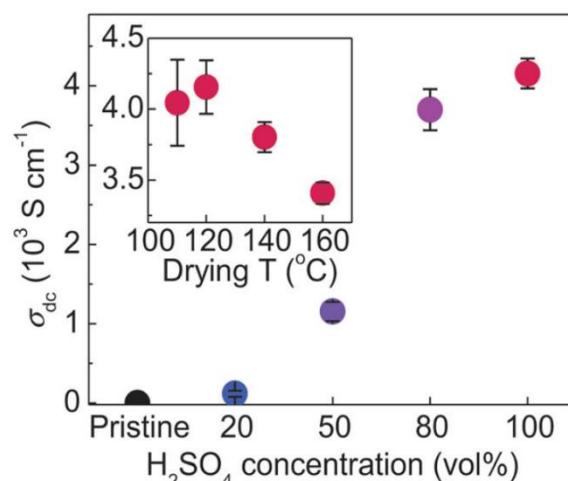


Figure 1.8: Electrical conductivities of PEDOT:PSS films treated with various concentrations of H<sub>2</sub>SO<sub>4</sub>. The inset presents the conductivity of PEDOT:PSS films as a function of the drying T after 100% H<sub>2</sub>SO<sub>4</sub> treatments. (from<sup>33</sup>)

In conclusion, various secondary dopants can be used to increase the conductivity of PEDOT:PSS films. The mechanism of conductivity enhancement has possible explanations: phase separation between excess PSS and PEDOT:PSS seems to be the more recognized one. With charge screening, it can be the cause of an increase in crystallite number, size, density, and organization. A possible increase of the degree of oxidation of PEDOT has also to be taken into account.

#### 1.1.1.4 Electronic structure and transport properties of PEDOT:PSS: from single chain to thin film and application in electrochromic devices

The electronic properties of PEDOT:PSS and the optical properties of PEDOT films and thus PEDOT-based devices are linked. First, the nature of the charge carrier at the scale of a single PEDOT chain will be discussed and then the structure of thin films (with PEDOT crystallites embedded in the amorphous polymer matrix) will be described.

Figure 1.9 shows the evolution of the band structure of PEDOT chain when electrons are removed: positively charged polaron and bipolaron states are reached.<sup>34</sup> The band gap is the gap between the HOMO (highest occupied electronic state) and the LUMO (lowest unoccupied state in the conducting band). By removing electrons, positive charges are formed which modify the band gap and empty polaronic states, corresponding to the missing electrons, appear in the gap. As a result, the bond lengths are modified with formation of quinoid instead of aromatic structure. Polaronic and bipolaronic structures are consecutively formed by removal of odd and even numbers of electrons. The case with the removal of 6 electrons in a chain of 18 units corresponds to a doping level of 33 % (one positive charge every three monomer units) of pristine PEDOT. The band structure, the charge localisation and the wave function of polaron and bipolaron states are similar, which suggest similar electron transport.<sup>34</sup> Furthermore, PEDOT chains are usually short (around 15 monomer units)<sup>16</sup>, which means that intrachain electron hopping rate should be

strongly higher than interchain hopping: the interchain motion being the limiting factor in the electron mobility.

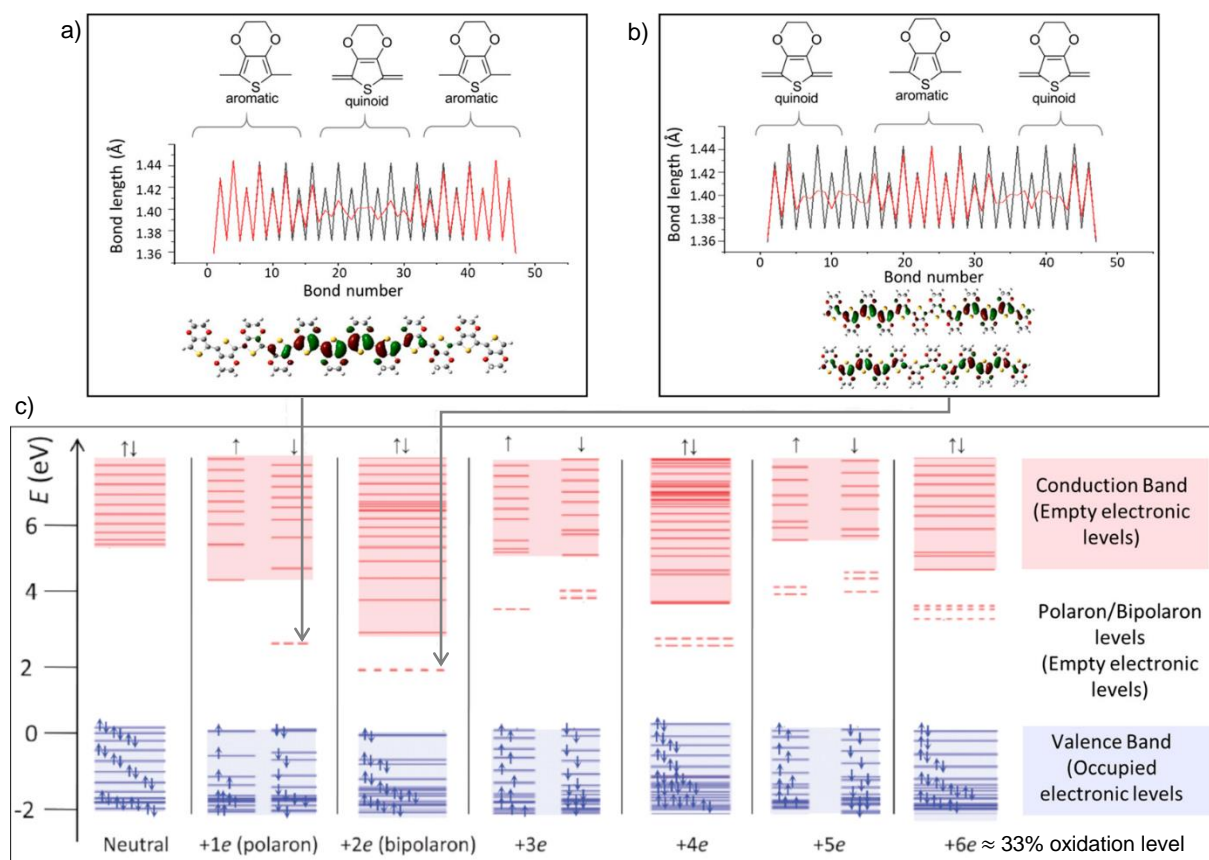


Figure 1.9: Positively charged polaron and bipolaron states in a PEDOT chain (18 units). Bond length alternation and electron density distribution in a PEDOT chain with a) a polaron +1e or b) a bipolaron +2e (the black lines correspond to the bond length alternation for a neutral chain), and band diagram for the polaron and bipolaron states of PEDOT chain when it is successively charged from 0 to +6e. All band diagrams are aligned setting  $E_{LUMO} = 0$ . (from<sup>14,34</sup>)

Not only the oxidation level is important for the properties of PEDOT films, the morphology of the film (crystallites, which are stacking of 3 to 10 PEDOT chains, embedded in amorphous regions) greatly impacts its density of states. Indeed, as shown in Figure 1.10, the energy structure of a crystallite (composed of 5  $\pi$ - $\pi$  stacked chains) comprises a bipolaronic band with a number of states being the number of positive charges of the crystallite. Depending on the position of the counterions, the position of the bipolaronic states are shifted. That is why a density of state (average of the band structures) is more representative for PEDOT films which is composed of numerous crystallites.

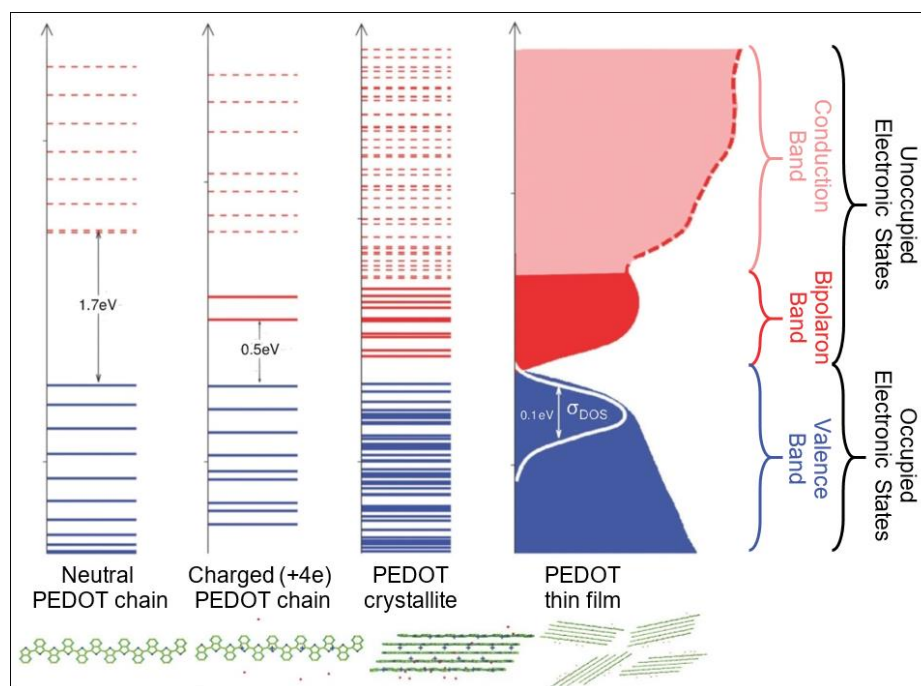


Figure 1.10: Energy structure diagram and the density of states (DOS) of PEDOT: from a single chain (neutral or with two bipolarons) to a thin film (single crystallite to poly-crystallites embedded in amorphous matrix). (adapted from<sup>35</sup>)

For polymeric films with identical crystalline structure, the optical absorption of the films is dependant on its oxidation level (and so of the polaronic or bipolaronic state). To have modifications of the absorbance spectra in the visible range, the conjugated polymer should have an appropriate band gap between 1.0 and 2.5 eV. Indeed, higher band gap results in transitions in the UV region, and lower band gap in the NIR region.<sup>14</sup> Absorbance spectra of PEDOT is modified in a wide wavelength range, including the visible range. By applying a potential to oxidize PEDOT, the film goes from dark blue (fully neutral state at - 0.9 V) to almost transparent sky blue (fully oxidized state at + 1.0 V) passing by at least 20 oxidation and so color steps [Figure 1.11].<sup>36</sup>

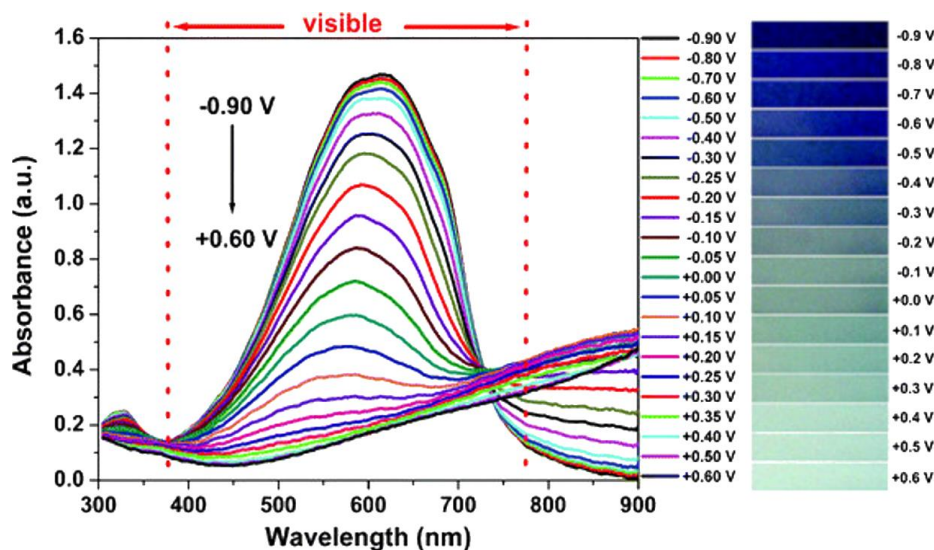


Figure 1.11: Spectroelectrochemistry of PEDOT film: optical variation in the visible region as a function of applied potentials (left), and respective produced colors (right). (from<sup>36</sup>)

One great advantage of conjugated polymers compared to other electrochromic materials is that they have a wide range of oxidation states and can therefore produce color palettes instead of only two colors (corresponding to the neutral and oxidized state of the material). Combining three conjugated polymers (for red, green and blue colors) in an electrochromic device can then give a wide range of colors for display applications. Polymers with red, green and blue emission are shown in Figure 1.12.

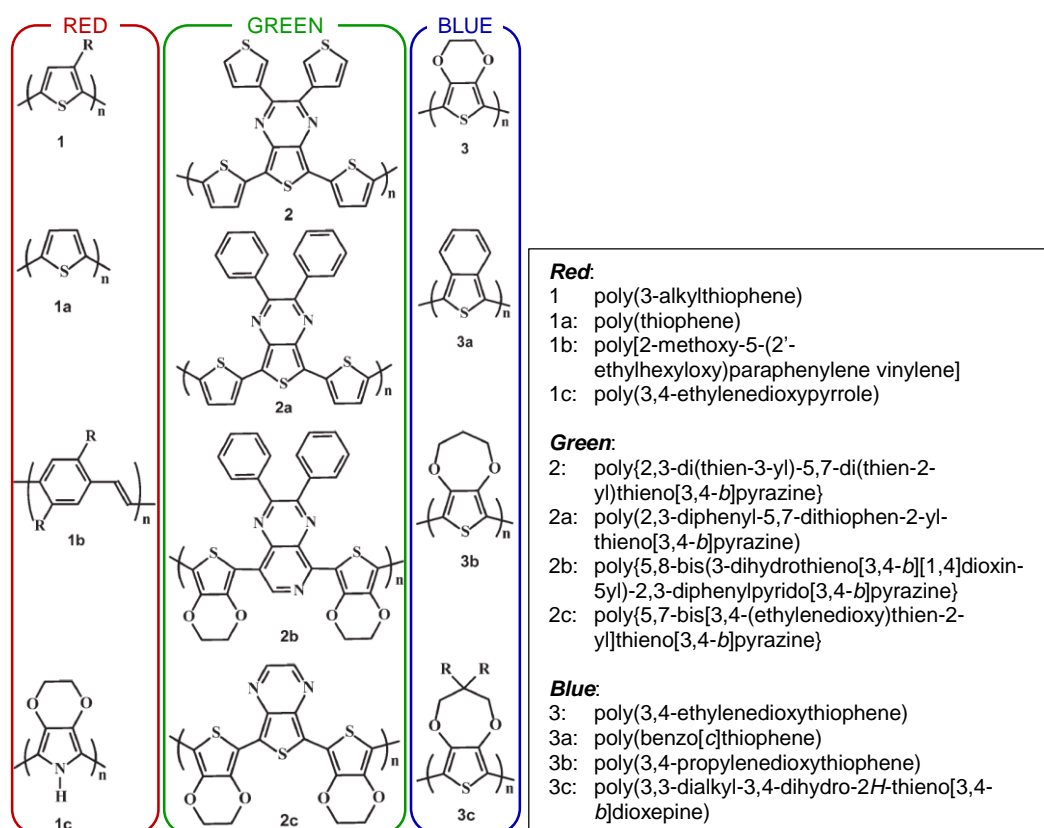


Figure 1.12: Examples of polymers reflecting RGB colours. (from<sup>36</sup>)

### 1.1.1.5 Temperature dependence of PEDOT electrical conductivity and application in thermoelectric devices

The electrical conductivity of PEDOT is also dependent on the temperature and is well described by Mott's variable-range hopping (VRH) model:  $\sigma(T) = \sigma_0 \exp\left(-\left(\frac{T_0}{T}\right)^{\frac{1}{1+D}}\right)$  where  $\sigma_0$  is the conductivity at infinite temperature  $T$ ,  $T_0$  is a characteristic temperature of the polymer related to the localization parameter and the density of states at the Fermi energy, and  $D$  is the dimensionality of the system. For pristine PEDOT films,  $D=1.75$  which indicates a 2D displacement of the electrons. Treatment with secondary dopant induced a transition from an insulating regime to a metallic regime with a weak temperature dependence [Figure 1.13]. In this

case, a fluctuation-induced tunneling (FIT) model is more relevant, due to morphological and structural changes induced by the secondary dopant.<sup>37</sup>

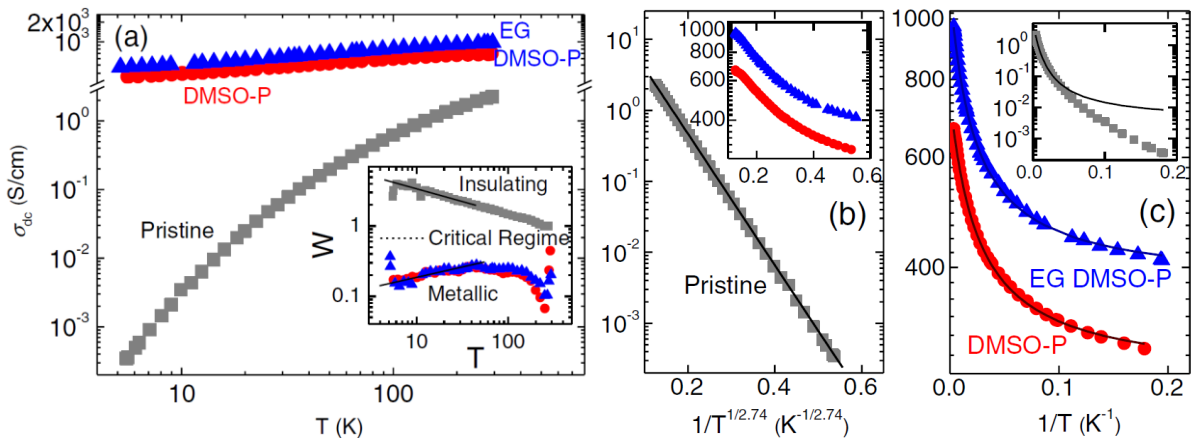


Figure 1.13: a) Temperature dependence of the conductivity of three types of PEDOT:PSS films before (pristine) and after the treatment with secondary dopants. DMSO-P denotes the sample coated from a PEDOT:PSS solution containing 5 %wt DMSO, and EG DMSO-P denotes the sample achieved after immersing the DMSO-P sample into an EG bath. The inset plots the reduced activation energy  $W(T) = \ln(\sigma)/\ln(T)$ . b) VHR model of the pristine sample ( $x=1.74$ ) and c) FIT model for the two treated samples. Solid lines are fits. (from<sup>37</sup>)

PEDOT films correctly treated with secondary dopant can then have a high electrical conductivity but also low thermal conductivity. These are requirements for materials used in thermoelectric generators. Indeed, both electrical and thermal currents are involved. An electrical current is applied to the thermoelectric device [Figure 1.14], and a thermal current (heat flux) is generated [Figure 1.14]. The properties of thermoelectricity are combined in the following figure of merit:  $ZT = \frac{\sigma S^2}{\kappa} T$  where S is the Seebeck coefficient,  $\sigma$  is the electric conductivity, T is the temperature, and  $\kappa$  is the thermal conductivity. PEDOT can be n or p-type doped to form the thermoelectric legs of the device. By increasing the doping level of PEDOT, the electrical conductivity increases while the Seebeck coefficient decreases. A good compromise has to be found, taking into account the thermal conductivity. A ZT of 0.25 was reached using PEDOT:Tos, which nearly fulfills a requirement for efficient energy conversion.<sup>38,39</sup>

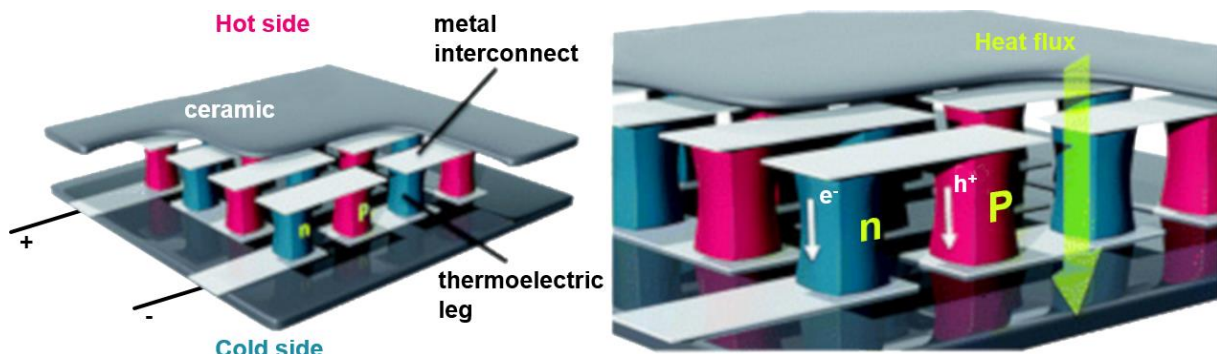


Figure 1.14: Schematic of a thermoelectric module composed of p-type and n-type legs. (adapted from<sup>38</sup>)

### 1.1.1.6 Applications of the coupling between the ionic and electronic transport in PEDOT films

The conductivity of PEDOT is not only related to electron transfer, but also to ion mobility when the films are hydrated. Ionic and electronic charge carriers are strongly coupled in PEDOT. This has applications in electrochemical modulation of color and conductivity used in bioelectronics. The aim is then to measure the presence of a molecule via the output voltage of a bioelectronics sensor, or to regulate physiology processes in cells using bioelectronics actuators. A wide range of devices using both electron and ion transport exists: super-capacitors, organic electrochemical transistors, electrochromic displays, organic electronic ion pumps, implantable drug delivery devices, and neural probes [Figure 1.15].

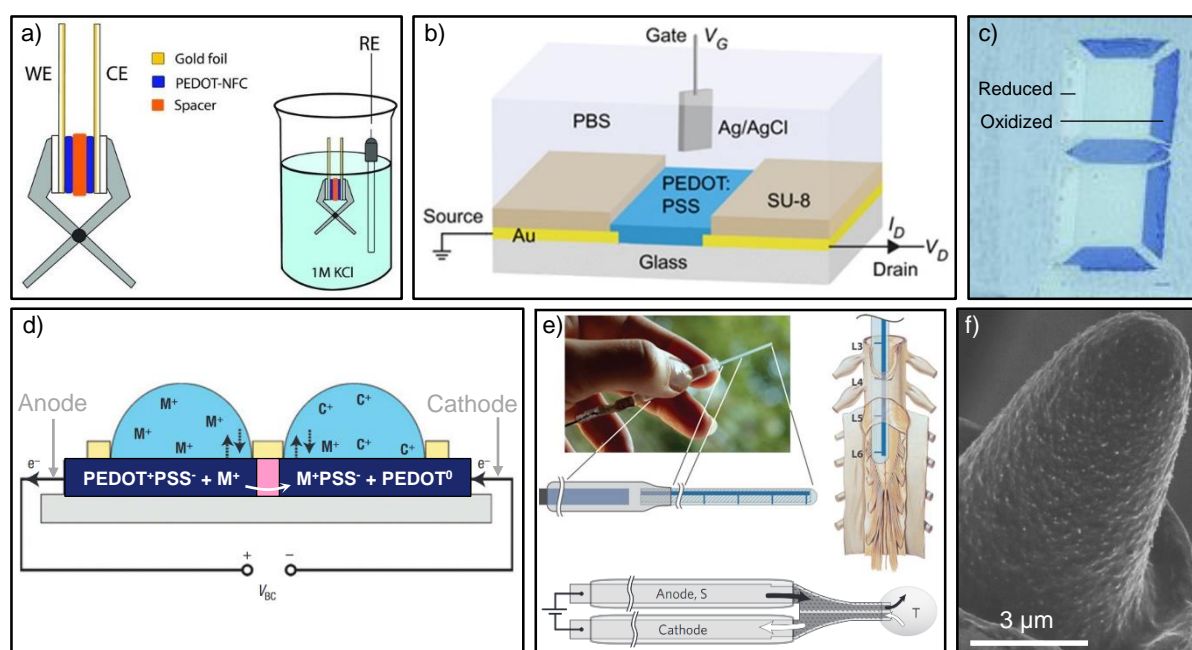


Figure 1.15: a) Super-capacitor cell and three-electrode-electrochemical setup (from<sup>40</sup>), b) Organic electrochemical transistor (adapted from<sup>41</sup>), c) Electrochromic display (adapted from<sup>42</sup>), d) Organic electronic ion pump (from<sup>43</sup>), e) Implanted drug delivery device (adapted from<sup>44,45</sup>), f) Neural probe (from<sup>46</sup>).

In the case of PEDOT super-capacitor cells, two layers of PEDOT are separated with a spacer and linked to two electrodes. The device is immersed in an electrolyte solution. By applying a voltage to the working electrode, ions from the electrolyte migrate into the polymer matrix and dope or de-dope it, which charges or discharges the super-capacitor cell.<sup>40</sup>

Organic electrochemical transistors (OECT) are composed of the active material (PEDOT) deposited between the source and the drain electrodes, and surrounded by an electrolyte in which the gate is submerged. When no voltage is applied to the gate, PEDOT is doped which results in a high source-drain current. When a positive potential is applied to the gate, cations from the electrolyte migrate into the polymeric matrix and de-dope it. This reduces the source-drain current. Contrary to organic field-effect transistor (OFET) [Figure 1.18], the electron transport

takes place in the bulk of the active material and not at its surface.<sup>40,47</sup> EDOT derivatives can be used to synthesize PEDOT derivatives to have both the conductivity of PEDOT and the sensitivity to biological molecules allowing their use as biological sensors.<sup>48,49</sup>

As discussed previously, PEDOT can be used as the active material in electrochromic displays as its absorption wavelength depends on its doping state. The display is encapsulated in an electrolyte and the oxidation of PEDOT occurs when a voltage is applied to the gate, as for OECT, which results in color changes from transparent to blue.<sup>36,42</sup>

Organic electronic ion pumps (OEIP) are devices that translate an electronic signal into a flux of ions. Two PEDOT films are linked respectively to an anode and to a cathode. They are separated by a membrane that is ionically conductive and electronically insulating. The PEDOT film at the anode side is in contact with the source electrolyte tank, containing a high concentration of cations  $M^+$ . When a voltage is applied, PEDOT is oxidized in the anode. To compensate the charge of PEDOT, excess of the polyanion (PSS<sup>-</sup>) interacts with PEDOT and releases the cation  $M^+$  that was linked to it. In the cathode side, PEDOT is reduced, which releases PSS<sup>-</sup> that are neutralized by the cations  $M^+$  coming from the anode side. This generates a flow of cations from the anode to the cathode: the cations are pumped into the targeted electrolyte tank at the cathode side.<sup>14,43</sup> This principle is used for implanted drug delivery devices: the device is implanted in the body at a specific place, and by applying a voltage, biological molecules and neurotransmitters can be delivered at specific times in controlled amounts.<sup>44,45</sup>

Neural probes are metallic probes that record the activity of the brain. They are in direct contact with the neurons. They can be coated with a thin layer of PEDOT. The aim of the coating is to improve the compatibility between the electrode and biological tissues, for in vivo measurements, while keeping the performance of traditional neural probes.<sup>46</sup>

### 1.1.1.7 PEDOT:PSS films as transparent organic electrodes

Various applications can be found for PEDOT:PSS. It can be used as an electrode in various devices such as organic light-emitting diode (OLED), organic photovoltaic (OPV), organic field effect transistor (OFET), capacitors (piezoelectric devices), etc.

PEDOT:PSS is a good candidate to substitute indium-tin oxide (ITO) for transparent electrodes in flexible devices. High transmittance and high conductivity<sup>50</sup> are required for transparent electrodes. Different materials are used to elaborate such transparent electrodes. The most widely used is ITO due to its low sheet resistance ( $10 < R_s < 50 \Omega/\square$ ), high transparency ( $80 < T < 95 \%$ ) and high stability.<sup>51</sup> However, the raw material is expensive and the processing conditions require high temperatures (which is not compatible with top electrodes for organic

devices) and high vacuum. Furthermore, ITO based electrodes are not flexible. Indeed, ITO films crack when bended and their sheet resistance can be increased by several order of magnitude when the curvature radius is under 8 mm. That is not the case for PEDOT:PSS films that have stable sheet resistance at this radius.<sup>52</sup> Moreover, ITO need post treatment to tune its work function (in the range of 4.1-5.53 eV<sup>51,53</sup>) to make it compatible with the organic layers used in OLED and OPV. Various alternatives to ITO have been developed for flexible transparent electrodes: metal layers, nanomaterials and conductive polymers. To increase transparency, metals have to be deposited in ultra-thin layers, which leads to higher sheet resistance ( $1 < R_s < 80 \Omega/\square$ ) without necessarily improving the transmittance ( $40 < T < 60 \%$ ). Metals can also be deposited in grid patterns which improves the resistance ( $6 < R_s < 50 \Omega/\square$ ) and the transmittance ( $T \approx 80 \%$ ). Metal nanowires ( $5 < R_s < 200 \Omega/\square$  and  $70 < T < 90 \%$ ), carbon nanotubes ( $20 < R_s < 1000 \Omega/\square$  and  $50 < T < 95 \%$ ), or graphene ( $100 < R_s < 3000 \Omega/\square$  and  $60 < T < 95 \%$ ) have also been proposed as alternatives.<sup>51</sup> However, in all these cases, the process to deposit the pattern (grids) or synthesize the nanomaterials is complicated and/or energy consuming. Also the patterns may have other defects such as electrical voids.<sup>51,54</sup> The interest of PEDOT:PSS in this case is that it is easily processable and it have interesting sheet resistance ( $50 < R_s < 1000 \Omega/\square$ ) and transmittance ( $75 < T < 90 \%$ ).<sup>51</sup> The relation between the transmittance and the sheet resistance for different materials used for transparent electrodes is shown in Figure 1.16.

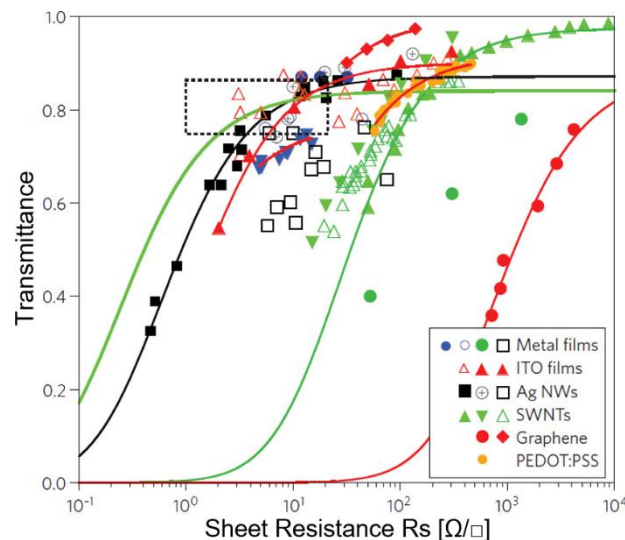


Figure 1.16: Transmittance versus sheet resistance for transparent conductive films made of different materials. (adapted from<sup>114</sup>)

Besides transparent electrodes in OLED and OPV, PEDOT:PSS can be used as hole transport layer or as a buffer layer between ITO and a photoactive layer. Figure 1.17 displays the energy levels of an OLED and the displacement of holes and electrons.

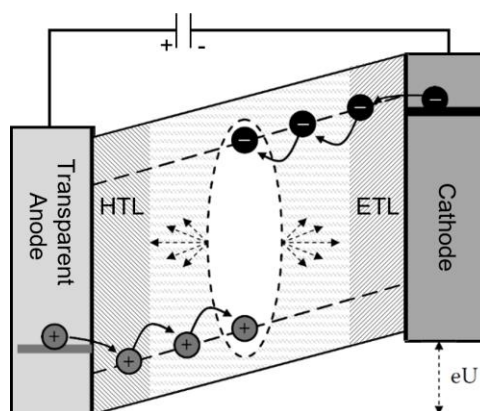


Figure 1.17: Energy levels of an Organic Light Emitting Diodes (OLED) and illustration of the origin of the electroluminescence. Depicted are hole and electron injection from the two electrodes, charge transport and electron-hole pair formation. (HTL = Hole Transport Layer; ETL = Electron Transport Layer) (adapted from<sup>16</sup>)

An OLED is composed of a transparent anode, several organic layers that act as hole and electron transport layers, and a metallic cathode. By applying an external bias, holes are created at the anode, and electrons at the cathode. To allow the displacement of the holes and electrons in the layers under the electric field, the work function of the different layers should be appropriate. The work function of the transparent electrode should be high enough to enable the injection of holes in the HOMO (highest occupied molecular orbital) of the next layer, while the work function of the cathode should be low enough to allow the displacement of the electrons in the LUMO (lowest unoccupied molecular orbital) of the next layer. Each layer should have suitable LUMO and HOMO levels to guide the holes and electrons until they form an electron-hole pair, recombine and create an electroluminescence. PEDOT:PSS can be used as a hole-injection layer. Indeed, a high conductivity is reached and the Fermi level of PEDOT:PSS of 4.5 – 4.9 eV is suitable with the organic compounds used in the OLED. PEDOT:PSS is often added on top of ITO layers to reduce the roughness of the surface (which improves the injection of the holes) and to reduce the HOMO level to get it closer to the one of the electroluminescent material.<sup>16</sup>

Last, PEDOT:PSS can be used for various purposes in organic field-effect transistors (OFET) [Figure 1.18]: as electrode, as interlayer on top of the metallic source and drain, or as the active material (undoped semiconductor that forms a conductive channel at the interface with the dielectric, when a negative bias is applied at the gate).<sup>16</sup>

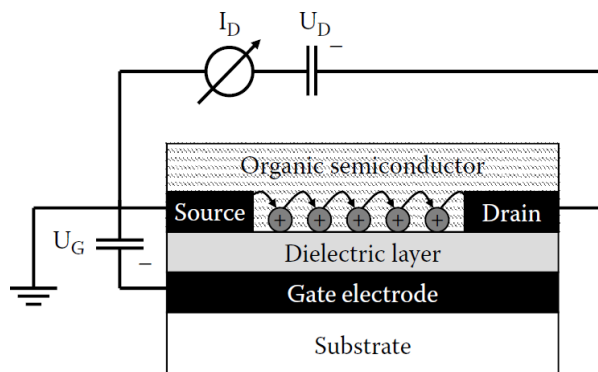


Figure 1.18: Cross-section of an organic field-effect transistors (OFET) with bottom electrode geometry. A conductive channel is created at the interface between the p-type semiconductor and the dielectric layer when a negative bias is applied at the gate electrode. (from<sup>16</sup>)

PEDOT:PSS has thus a large variety of applications. The coupling between the ionic and electronic transport in PEDOT films make it an excellent material for applications in super-capacitors, organic electrochemical transistors, electrochromic displays, organic electronic ion pumps, implantable drug delivery devices, and neural probes. When n- or p-doped, PEDOT films can be used as active materials in thermoelectric devices. The relatively high transparency of PEDOT films can be exploited to create transparent flexible electrodes in optoelectronic devices such as OLED and OPV. Due to their better smoothness than ITO, PEDOT can be used as a buffer layer between ITO and photoactive layers in such devices. PEDOT is also used as a hole transport layer in OLED as well as an undoped semiconductor material in OFET.

To conclude this first part, synthesis pathways of the semi-conducting polymer PEDOT have been explored, as well as formulation with secondary dopant or post-treatments used to increase the conductivity of dried PEDOT films. Insight of probable structural changes has been discussed. The electronic transport alongside the polymeric chain was detailed and consequently the impact of the doping on the conductivity and the color of the polymeric films. The temperature dependence of the conductivity of the PEDOT films and the ionic transport within the film was associated to various applications.

In the next part, another polymer with piezoelectric properties will be discussed: poly(vinylidene fluoride-co-trifluoroethylene) (P(VDF-TrFE)). The interest to study PEDOT along with P(VDF-TrFE) is that they can be used in combination to form piezoelectric devices: PEDOT is used as the electrode layers, and P(VDF-TrFE) as the active piezoelectric material.

## 1.1.2 Poly(vinylidene fluoride-*co*-trifluoroethylene) P(VDF-TrFE): a piezoelectric polymers

### 1.1.2.1 Dielectric materials

Dielectrics are materials that can be polarized under an electric field. Dielectrics have very low conductivity and are used as insulators (they have an energy band gap higher than 3 eV). When the electric field is applied, the positive charges of an elemental volume are forced in the direction of the field, and the negative charges in the opposite direction. The global material remains neutral: no macroscopic charge migration occurs, as it is the case in conductors. The short displacement of the charges creates an electric dipole moment  $\mu = qr$  where  $q$  is the absolute value of the charge, and  $r$  the distance between the two charges. The polarization  $P$  of dielectric materials (in  $C.m^{-2}$ ) is then the ratio between the sum of all the dipole moments in the material and the volume of the material. The electric field  $E$  is defined as  $E = \frac{F}{q}$  where  $F$  is the force exerted on a unit charge when the charge is inside the field. The dielectric displacement  $D$  is then given by  $D = \epsilon_0 E + P$  where  $\epsilon_0 = 8.854 \cdot 10^{-12} F.m^{-1}$  is the vacuum permittivity. The displacement can also be defined as  $D = \epsilon_0 \epsilon_r E$  where  $\epsilon_r$  is the relative permittivity (or dielectric constant).<sup>55</sup>

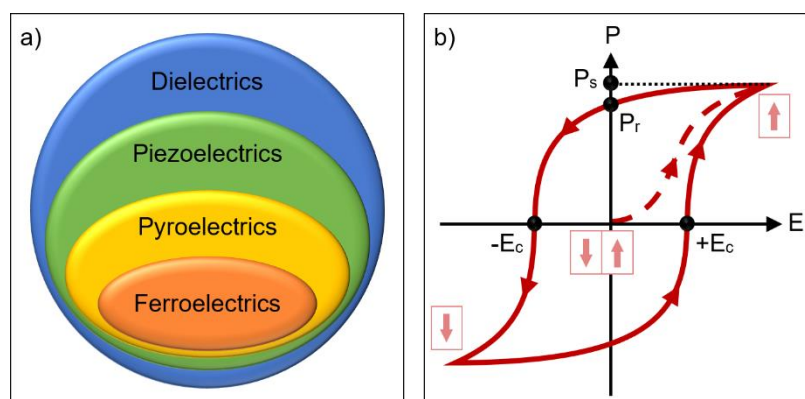


Figure 1.19: a) The schematic relationships among dielectric, piezoelectric, pyroelectric and ferroelectric materials; b) Polarization hysteresis loop of ferroelectrics and schematic of the switching of their bipolar state by an external electric field (adapted from<sup>56</sup>)

Dielectric materials can have different behaviors. The relationship between the different subdivisions of the dielectrics is displayed in Figure 1.19, a). Piezoelectric materials are dielectrics that can be polarized not only in the presence of the electric field, but also when the field is removed. The word piezoelectricity comes from two Greek words meaning that pressure develops electricity. To be piezoelectric, a dielectric should not have rotational symmetry. The properties of piezoelectric materials depend of their crystal structure: if they possess a unique polar axis, the material is also pyroelectric and its spontaneous polarization is temperature dependant. If furthermore this spontaneous polarization can be reversed by an external electric field, the pyroelectric material is also ferroelectric. During the switch of the polarization, a hysteresis loop

of the polarization versus the applied electric field can be observed [Figure 1.19, b)].  $E_c$  is the coercive field defined as the minimum field that has to be applied to go from one polarization to the opposite polarization. The saturated polarization  $P_s$  is the maximum polarization that can be reached when a certain field is applied. It is also called the spontaneous polarization. And  $P_r$  is the remanent polarization that remains after switching down the current.<sup>56</sup>

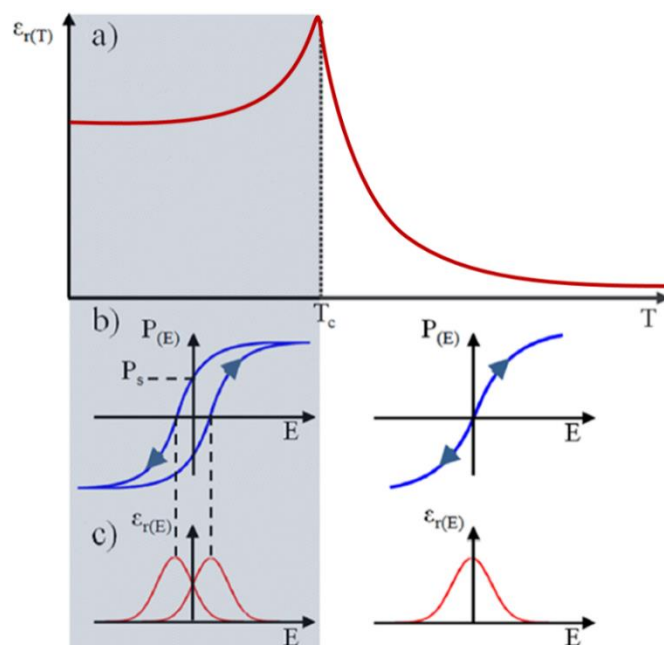


Figure 1.20: a) Temperature dependence of the dielectric constant of a ferroelectric material: a transition from a polar ferroelectric to a nonpolar paraelectric phase occurs at the Curie temperature  $T_c$ . Corresponding b) polarization and c) dielectric constant as a function of applied field below and above  $T_c$ . (adapted from<sup>57</sup>)

The properties of ferroelectric materials depend on the temperature. At the Curie temperature  $T_c$  (under the melting temperature), a structural change occurs from a ferroelectric to a paraelectric phase. In the ferroelectric phase, the crystals have low symmetry and are polar, while in the paraelectric phase, the crystals have more symmetry and are nonpolar. The spontaneous polarisation occurs only in the ferroelectric phase, which means at a temperature under  $T_c$ . The changes in dielectric constant and polarization hysteresis depending on the ferro- or para-electric phase are displayed in Figure 1.20.<sup>56,57</sup> Well known ferroelectric materials are ceramics such as barium titanate.<sup>58</sup> The disadvantage of ceramics is that they are not flexible and need very high pressure and temperature to form dense thin continuous films from synthesized powder.<sup>59</sup> They are therefore not compatible with organic materials.

### 1.1.2.2 PVDF and PVDF derivatives among the piezoelectric polymers

Polymers, usually insulators, can also have dielectric behavior. Indeed, if they are not semi-conductors and have monomer units which are not symmetrical, they can have an internal polarisation along the chain. Electronic, atomic, ionic, orientational and interfacial polarisations can occur in piezoelectric polymers. Depending on the frequency used for the applied external field, different polarisations are involved [Figure 1.21].

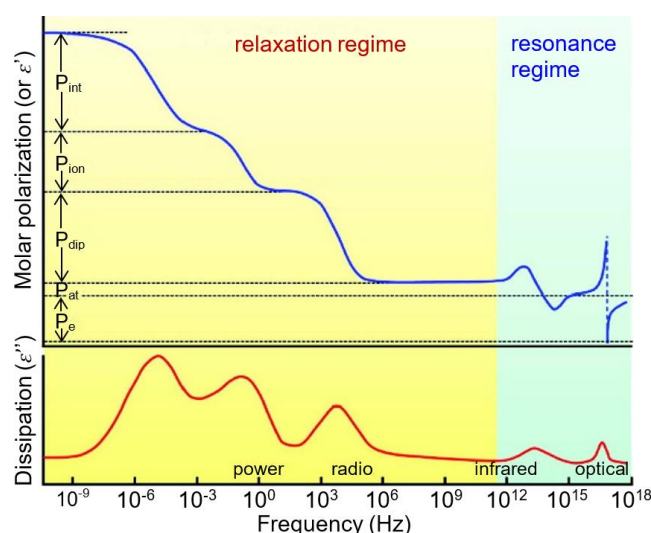


Figure 1.21: Different types of polarization as a function of frequency in polymers.  $P_e$ : electronic polarization,  $P_{at}$ : atomic (or vibrational) polarization,  $P_{dip}$ : dipolar (or orientational) polarization,  $P_{ion}$ : ionic polarization, and  $P_{int}$ : interfacial polarization. The top panel shows the molar polarization (the real part of permittivity), and the bottom panel shows the dissipation factor (the imaginary part of permittivity). (adapted from<sup>60</sup>)

Piezoelectric polymers can be classified in two main classes: ionic electroactive polymers when the polarization is induced by ionic motion in the polymer in response to an external field, or dielectric electroactive polymers when the polarisation is induced by the response of the dipoles inside the polymeric chain to an external field. The second class can be subdivided into dielectric elastomers and ferroelectric polymers.<sup>61</sup> Among the ferroelectric polymers, semi-crystalline fluorinated polymers are of interest. Figure 1.22 displays the structure of polyvinylidene fluoride (PVDF) and of one of its copolymers: poly(vinylidene fluoride-co-trifluoroethylene) (P(VDF-TrFE)).

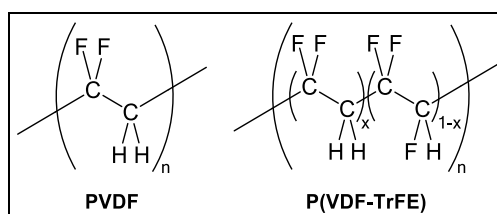


Figure 1.22: Structure of polyvinylidene fluoride (PVDF) and poly(vinylidene fluoride-co-trifluoroethylene) (P(VDF-TrFE)) with monomer units in proportions  $x$  for the VDF unit, and  $1-x$  for the TrFE unit.

The piezoelectricity of PVDF was discovered in 1969 by Kawai,<sup>62</sup> its pyroelectricity two years later by Bergman et al.<sup>63</sup> The ferroelectricity of PVDF was demonstrated in 1974 by Tamura

et al.<sup>64</sup> It was then found by Higashihata et al.<sup>65</sup> and Ohigashi et al.<sup>66</sup> that the copolymer P(VDF-TrFE) can have higher piezoelectric properties than PVDF. Furthermore, It was shown that P(VDF-TrFE) does not need to be oriented to exhibit strong ferroelectric properties.<sup>67</sup> Other derivatives of PVDF, ter- or tetra-polymers with three or four different monomer units, are studied for relaxor purpose.<sup>61</sup>

The crystallinity of PVDF and P(VDF-TrFE) comes from the asymmetrical structure of their polymeric chains, with strong electrical dipole moments ( $3.5 - 7 \cdot 10^{-30}$  C·m)<sup>68</sup> due to the strong electronegativity of the fluorine atom. Different crystalline phases exist. Figure 1.23 schematised the possible crystalline phases in PVDF. The  $\alpha$  phase corresponds to an alternation of trans-gauche conformations, and the different chains in the crystal are in opposite directions. As a result, the crystal unit cell is nonpolar. It is the most stable phase thermodynamically. The  $\beta$  phase corresponds to an all-trans conformation, which is thermodynamically unstable, but has the highest dipole. It is the most interesting phase. This phase is hard to obtain: only using specific polar solvents such as DMF (N,N-dimethylformamide) or by stretching and poling PVDF films from the  $\alpha$  phase. The interest of P(VDF-TrFE) is that by adding some defects (more than 11 %)<sup>69</sup> in the PVDF chain (i.e. adding some TrFE unit with one fluorine substituted by a hydrogen atom), the crystallisation from solvent casting or melt occurs directly in an all-trans conformation similar to the  $\beta$  phase of the PVDF.<sup>61</sup>

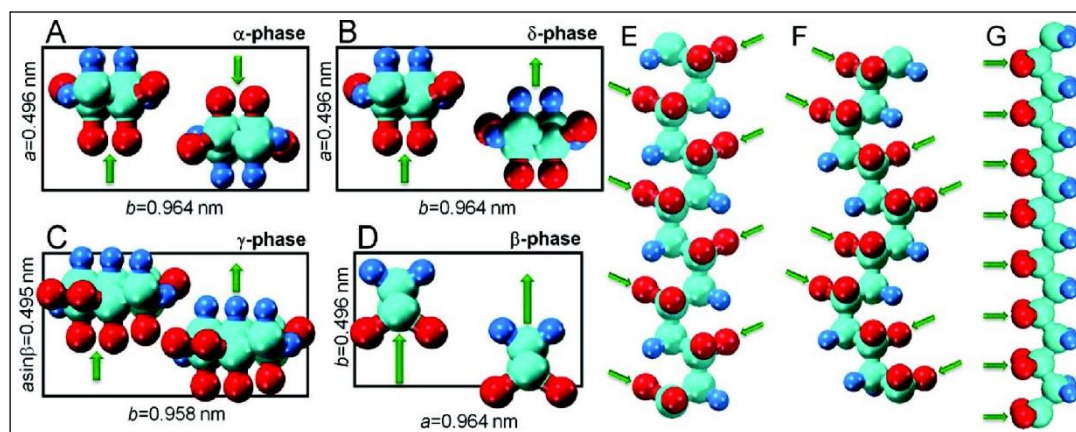


Figure 1.23: Unit cells of (A)  $\alpha$ , (B)  $\delta$ , (C)  $\gamma$ , and (D)  $\beta$  forms of PVDF crystals viewed along the  $c$ -axes and schematic chain conformations for (E)  $TG TG'$  ( $\alpha/\delta$ ), (F)  $TTTG TTTG'$  ( $\gamma$ ), and (G) all-trans ( $\beta$ ) rotational sequences. Red, cyan, and blue spheres represent F, C, and H atoms. The projections of dipole directions are indicated by green arrows. (from<sup>60</sup>)

The properties of the copolymer depend on the ratio between VDF and TrFE units as shown in Figure 1.24: thick ferroelectric lamellar phases are obtained for a concentration of TrFE above 18 %. The ratio 80/20 will be used in chapter 3 and 4.

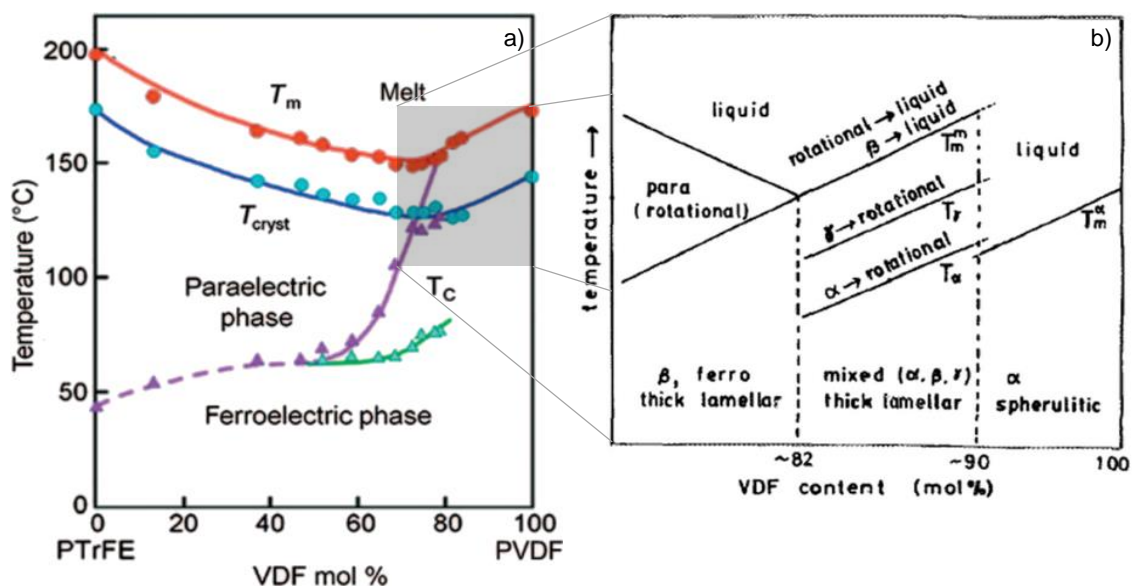


Figure 1.24: a) Phase diagram of P(VDF-TrFE): melting temperature in red, crystallization temperature in blue, curie temperature on heating in purple, and curie temperature on cooling in green. b) Schematic drawing of the phase diagram of unpoled P(VDF-TrFE) crystallized by annealing near the melting point or crystallized slowly from the melts. (adapted from<sup>55,70</sup>)

### 1.1.2.3 Synthesis pathways of P(VDF-TrFE)

P(VDF-TrFE) can be synthesized via conventional radical polymerisation. In this case, various temperatures, initiators, reaction times, and processes (in solution or in dispersed media: suspension, emulsion, or micro-emulsion) can be used.<sup>61</sup> When surfactant or stabilizers are used, their properties are important. Indeed, they can affect the dielectric properties of P(VDF-TrFE) films. The polymer used in the following chapters were synthesized by conventional radical polymerisation using a peroxydicarbonate type initiator.

Other syntheses exist, such as synthesizing other derivatives of PVDF with halogens, and then reducing the halogen to obtain P(VDF-TrFE). In this case, no use of the hazardous TrFE monomer is needed. Reversible deactivation radical polymerizations, such as iodine transfer polymerization, RAFT process (using xanthates as chain transfer agents), can be used but lead to low molar masses.<sup>61</sup>

### 1.1.2.4 Properties of P(VDF-TrFE)

Transitions between different crystalline phases can occur when the polymer is annealed, stretched or poled (i.e. when a high electric field is applied). Furthermore, it has been shown that poling can increase the crystal size and the overall crystallinity, and reduce the packing in the crystallites, for P(VDF-TrFE) films annealed above  $T_c$ .<sup>71</sup> By poling using increasing electric fields, more and more dipoles align with the field, which increases the remanent polarization. Bargain et al.<sup>72</sup> have shown that annealing and poling P(VDF-TrFE) films can increase the size of the crystals in the ferroelectric phase [Figure 1.25]. During the evaporation of the solvent, P(VDF-TrFE)

crystallizes into a ferroelectric phase. The conformational defects become the amorphous phase. During annealing at a temperature above  $T_c$ , the ferroelectric phase becomes a paraelectric phase. The conformational defects can be included in this phase. During the cooling, the defects convert partially into ferroelectric crystals, and in so called defect ferroelectric crystals at the edge of the ferroelectric lamellar crystals. If poled at room temperature, the dipoles of the defect ferroelectric phase align with the field, which removes the conformational defects and converts them into ferroelectric crystals.

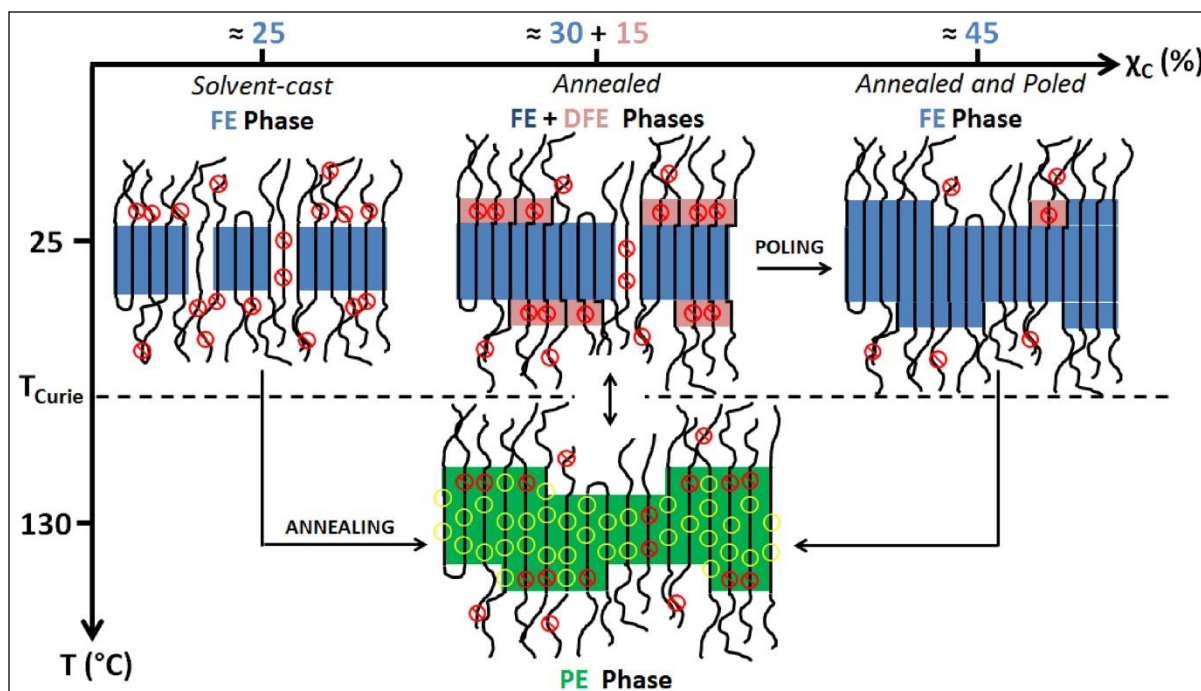


Figure 1.25: Schematic representation (not to scale) of crystal phase evolution in a crystalline lamella of P(VDF-TrFE) 72/28 %<sub>mol</sub> film from as-cast to annealed and poled. As-cast film at 25°C, with all-trans ferroelectric (FE) phase (blue). At 130°C, paraelectric (PE) phase (green) with trans and gauche conformations. At 25°C after annealing, defect ferroelectric (DFE) phase (pink) and FE phase. After poling, only FE phase is present.  $\ominus$  represents irreversible gauche conformations (chemical defects) while  $\circ$  represents reversible gauche conformations appearing at temperature higher than  $T_c$ . (from<sup>72</sup>)

P(VDF-TrFE) was characterized in terms of polarization versus field. The coercive field  $E_c$  is of circa 50 MV/m, and the remanent polarization can reach 110 mC/m<sup>2</sup>. The theoretical maximum polarization was calculated to be 130 mC/m<sup>2</sup> for PVDF, and 65 mC/m<sup>2</sup> for PTrFE. For the copolymer P(VDF-TrFE), the theoretical maximum polarization can be calculated by weight averaging of these two values in the absence of mutual interactions.<sup>73,74</sup> However, the crystals lattices differ from PVDF to PTrFE and this has to be taken into account in the calculation of the total polarization of the compound.

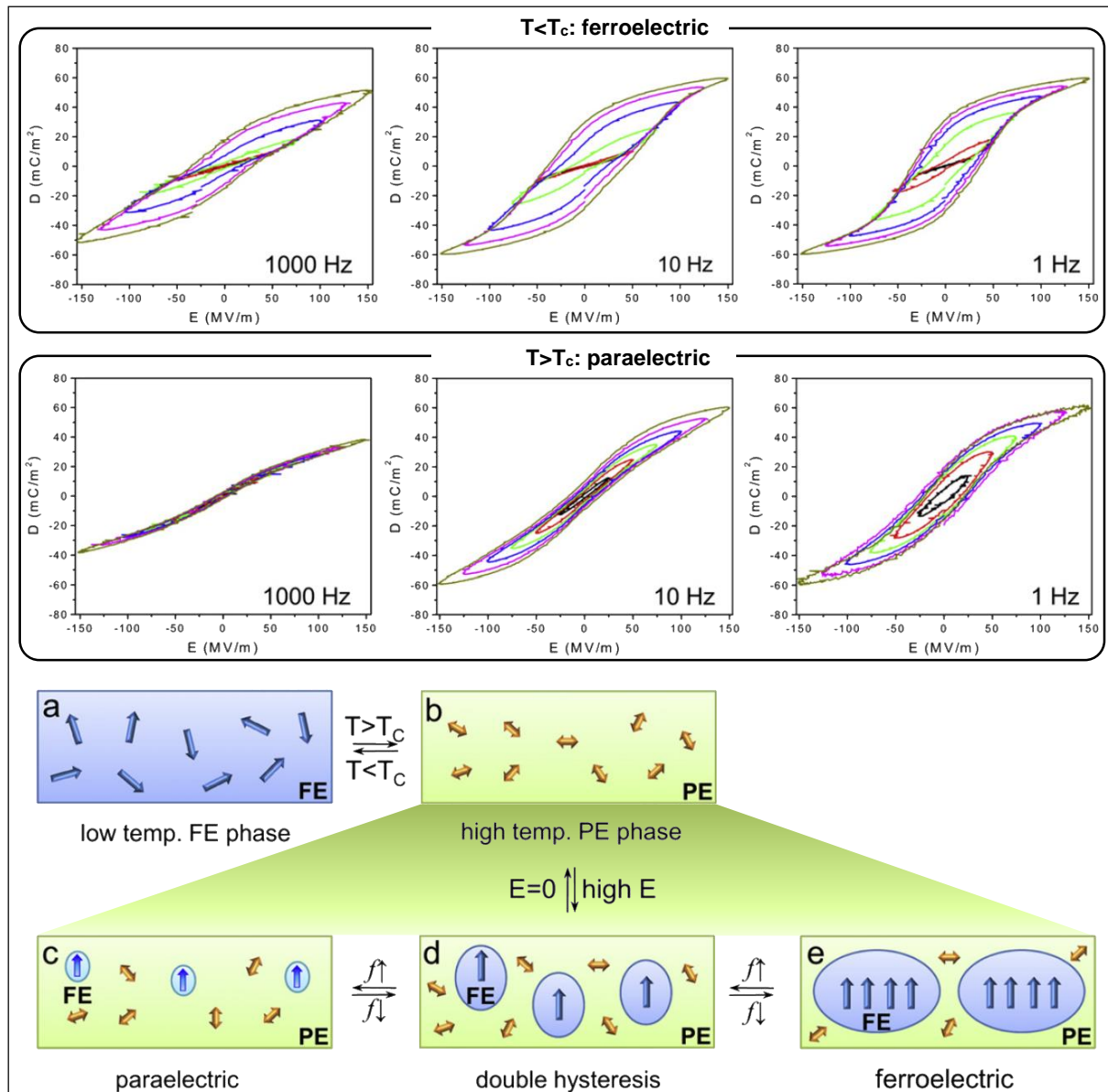


Figure 1.26: Bipolar hysteresis D-E loops for a uniaxially stretched 50/50 mol% P(VDF-TrFE) film in the ferroelectric (FE) and paraelectric (PE) phases at low ( $25^\circ\text{C}$ ) and high ( $100^\circ\text{C}$ ) temperatures and at three different frequency (1000 Hz, 10 Hz and 1 Hz). The poling field (a sinusoidal waveform) starts at 25 MV/m and increases with 25 MV/m increments. a-e: Schematic illustration of the ferroelectric-to-paraelectric Curie phase transition and electric field-induced ferroelectric domain nucleation/growth and corresponding ferroelectric behaviors in the paraelectric phase. Dark blue arrows represent large dipoles in the ferroelectric crystal (light blue rectangle) or domains (light blue ovals). Orange double arrows represent weak dipoles in the paraelectric crystal (light green rectangles). (adapted from<sup>74,75</sup>)

Depending on the temperature, the polarization curves differ in shape. Figure 1.26 displays the displacement versus field of a P(VDF-TrFE) film in the ferroelectric phase (at a temperature below  $T_c$ ) and in the paraelectric phase (at a temperature above  $T_c$ ) for three different frequencies. For the measurements at low temperature, a hysteresis loop is recorded and the phase is only ferroelectric for each frequency. The remanent polarisation decreases at high frequency: the bigger ferroelectric domains cannot follow rapid changes of polarization. For the high temperatures, at high frequency (1000 Hz), there is no remanent polarization: the phase is only paraelectric. By decreasing the frequency, a double hysteresis appears: ferroelectric domains

start to grow. At even lower frequency, the hysteresis loop continues to open: the ferroelectric domains become bigger. The temperature and frequency of poling is then important. At room temperature, all P(VDF-TrFE) with ratio higher than 55 % of VDF have a  $T_C$  higher than 60°C, and thus the measurements at room temperature are done in the ferroelectric phase.

Material	$d_{33}$ [pC/N]
Quartz	2 ( $d_{11}$ )
BaTiO <sub>3</sub> crystal	85.6
BaTiO <sub>3</sub> ceramic	191
PZT (PbZr <sub>1-x</sub> Ti <sub>x</sub> O <sub>3</sub> )	171 – 300
PVDF	-33
75/25 % <sub>mol</sub> P(VDF-TrFE)	-38
Cellular polypropylene	200

Table 1.3: Comparison of some remarkable transverse piezoelectric coefficients of polymeric materials and ceramics. PZT stands for Lead-Zirconate-Titanate, and BaTiO<sub>3</sub> stands for barium titanate. (from<sup>61,76</sup>)

The piezoelectric properties of materials are characterized by the piezoelectric coefficient  $d_{ij}$  where  $d_{31}$  and  $d_{32}$  are the longitudinal piezoelectric coefficients and  $d_{33}$  is the transverse piezoelectric coefficient.  $d_{33}$  of P(VDF-TrFE) has a value from -40 to -20 pC/N: the polymeric film contracts in the polarization direction in response to an external electric field.<sup>61</sup> The values for ceramics are much higher [Table 1.3], but P(VDF-TrFE) has other advantages: it is solution processable, light-weight, flexible, and has lower permittivity.

### 1.1.2.5 Applications

P(VDF-TrFE) can be used in many devices such as actuators, pressure sensors, acoustic devices, etc. Figure 1.27 displays the possible applications recorded for piezoelectric polymers.

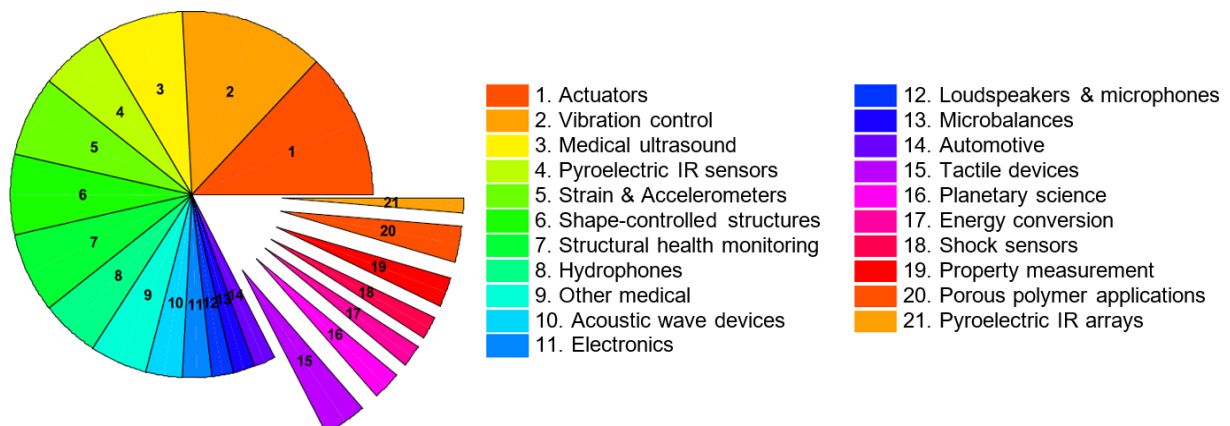


Figure 1.27: Piezoelectric and pyroelectric applications of electroactive polymers during the years from 1999 to 2004 (adapted from<sup>77</sup>)

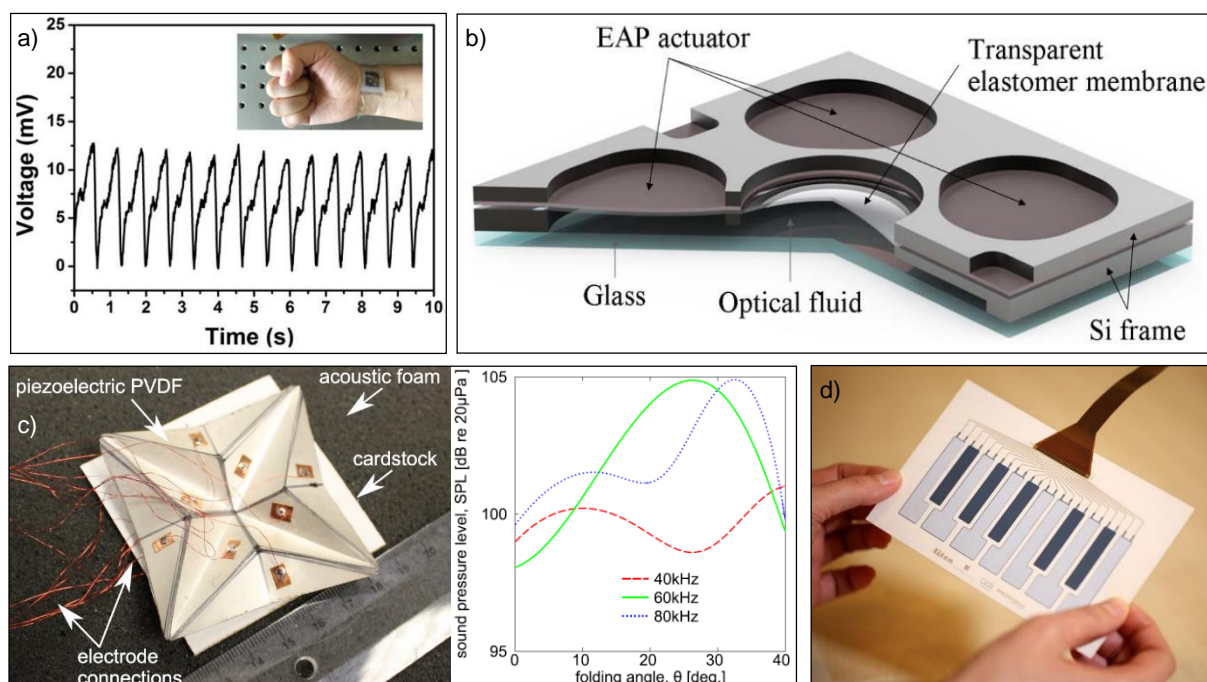


Figure 1.28: Example of applications using P(VDF-TrFE): a) health monitoring pressure sensor (from<sup>78</sup>), b) micro-lens with variable focal (from<sup>79</sup>), c) adaptive acoustic transducer (from<sup>80</sup>), d) flexible keyboard (from<sup>61</sup>).

Four examples are displayed in Figure 1.28. First a pressure sensor where P(VDF-TrFE) is sandwiched between two PEDOT electrodes and encapsulated in silicone rubber. This pressure sensor is used to monitor health and measure heart beat. The second device is a micro-lens with variable focal. The variation of the focal length is induced by the modification of the shape of a transparent elastomer membrane filled with optical liquid. The deformation of the membrane is caused by the displacement of actuators (using a fluorinated polymer as active layer). The third device is an adaptive acoustic transducer. In this case, P(VDF-TrFE) is used as actuator to tune the folding angle of an acoustic foam. Depending on this angle, the response to each frequency varies. And last, pressure sensors can also be used as human-machine interface such as a flexible keyboard. In this case, the information measured has to be translated into a specific sound.

In this part, dielectric materials were described. This category of materials can be subdivided in piezoelectric, pyroelectric and ferroelectric materials. The corresponding properties have been detailed. Not just ceramics possess piezoelectric properties; polymers such as PVDF and P(VDF-TrFE) also display interesting properties and have the advantages with respect to ceramics to be easily processable and flexible. The possible synthesis pathways of P(VDF-TrFE) were given. The variation of the crystallinity of these polymers was correlated to the temperature and to the ratio between the VDF and the TrFE unit. The most interesting phase, the  $\beta$  phase, is obtained directly from solvent casting for P(VDF-TrFE) with more than 11 % TrFE at

room temperature. The influence of annealing and poling onto the ferro-, defect ferro- and para-electric phases were described.

The two types of polymers previously studied are used in printed electronics. They can be deposited using solution processes. The next session describes the possible printing processes for functional inks such as PEDOT:PSS or P(VDF-TrFE).

## 1.2 Printing technologies

### 1.2.1 Printing processes overview

#### 1.2.1.1 Small history of printing

The objective of printing techniques is to reproduce an image or a text without having to draw it manually. Numerous printing techniques exist. Since ancient times, woodcut technique was used to transfer a design carved on wood onto a paper or a textile. First used in Asia in the 7<sup>th</sup> century, it appears in Europe in the 15<sup>th</sup> century. Movable types were first created in China in the early 11<sup>th</sup> century using porcelain, clay, wood, and then copper. Bronze types were created in Korea in the early 13<sup>th</sup> century. Gutenberg introduced the first press with movable types (in an alloy of lead, tin, antimony, copper and bismuth) in Europe in mid-15<sup>th</sup> century. That is the starting point of printing presses. The presses were first flat, printing one sheet at a time. The first roll-to-roll press appears in mid-19<sup>th</sup> century. Non-contact printing was developed later in the 20<sup>th</sup> century.<sup>81</sup>

#### 1.2.1.2 Printing processes and properties

Various printing technologies exist. They are principally used in print media but some of them can be used to deposit functional inks in printed electronics. The other are not suitable due to their way of working. For example, the processes using toner need charged or magnetic particles with relatively low melting temperature to be melt onto the substrate. That is not the case for polymers used in printed electronics. Figure 1.29 depicts all the printing processes and highlights those that are appropriate for printed electronics. Two main types of depositions exist: with or without contact. In the first case, the ink is deposited on a substrate using a master, which is the image carrier (it stores a static design like a stamp). In the second case, the ink is directly deposited to the substrate, and the printed design can be different from one substrate to the other.

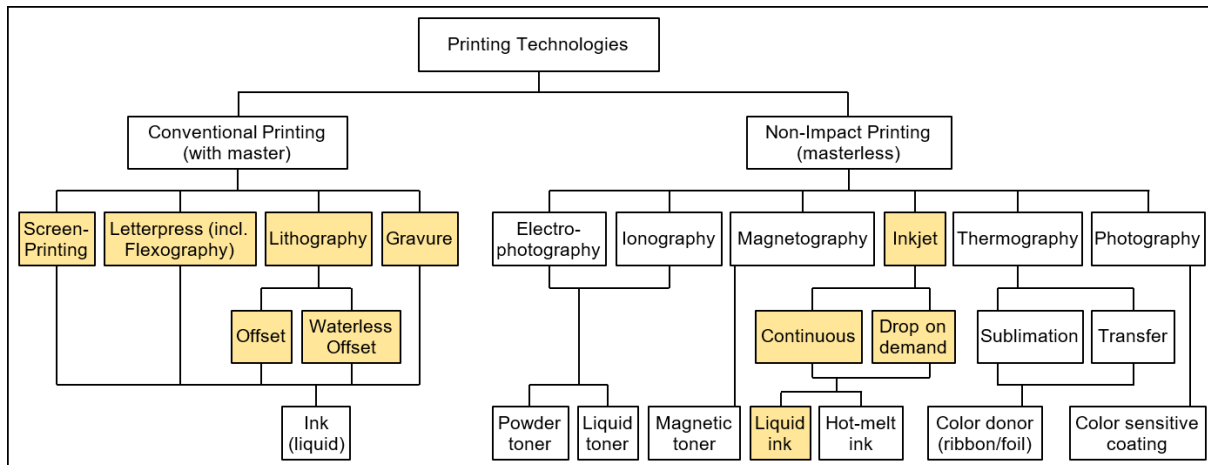


Figure 1.29: Printing technologies (adapted from<sup>81</sup>). In yellow processes used in printed electronics.

Figure 1.30 displays a schematic of screen-printing: the master is then a screen covered with a mask. The ink is pushed through the holes with a squeegee at a certain speed and pressure, and with a certain air gap between the substrate and the mask. During the deposition, the mask is slightly distorted and comes into contact with the substrate at the position of the squeegee. The ink has to be shear thinning: viscous at low shear to stay on the screen, and very fluid at high shear to pass through the meshes. Then the ink has to become viscous again so as not to spread out before drying. This technique allows the deposition of thick layers. It is more and more used in printed electronics.<sup>82-84</sup>

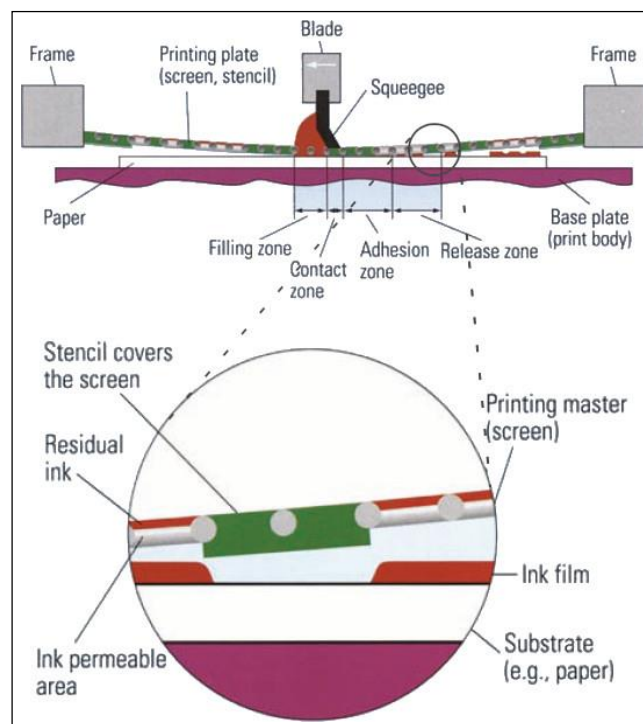


Figure 1.30: Schematic of screen-printing. (adapted from<sup>81</sup>)

Figure 1.31 displays a schematic of flexography printing. The principle is the same as stamps: a thick and soft printing plate, which has in relief the design to be deposited, is inked and pressed onto the substrate. The inking is done by an anilox roller, which is a metallic roll with numerous small holes filed in an ink chamber. The disadvantage of this process is the poor resolution caused by the pressing of the soft printing plate onto the substrate. However, this technology evolved and the resolution is more and more increased, which explains its use in printed electronics.<sup>85,86</sup>

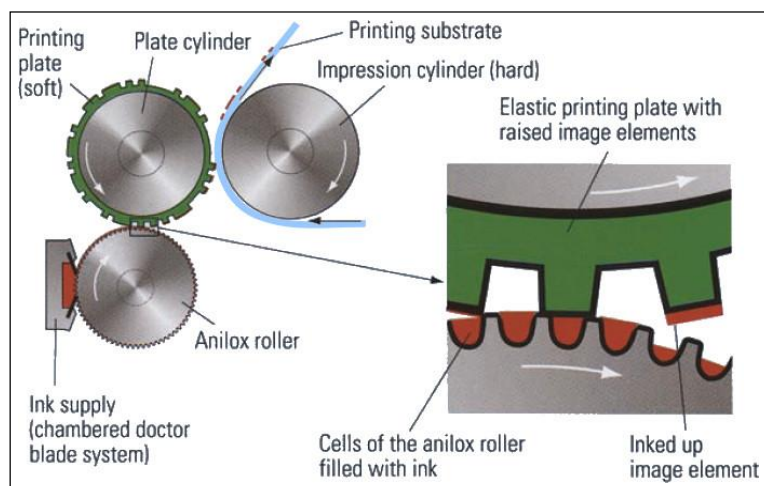


Figure 1.31: Schematic of flexography printing. (adapted from<sup>81</sup>)

Figure 1.32 displays a schematic of offset printing. The printing plate is very thin and hard contrary to flexography printing. The differentiation between the hydrophobic printing areas and the hydrophilic non-printing areas is done by physical means: the plate is first dampened, the water covers the non-printing area, and then the oil-based ink is added and covers only the area without water. Everything is transferred to a soft polymeric blanket that conveys the ink to the substrate. The ink has to be viscous so as not to spread onto the blanket before being transferred to the substrate. Another offset technique can be used without water with a plate that is covered with a 2  $\mu\text{m}$  silicone layer that repels the ink at the non-printing area, and silicone oil is added to the ink. Very high resolution can be obtained. The high resolution is interesting and can be used to miniaturize devices.<sup>87,88</sup> Offset can also be combined with other printing processes, for example with screen-printing: the ink is screen-printed on a blanket that absorbs organic solvent, for better resolution, and then the ink is transferred to the substrate.<sup>89,90</sup>

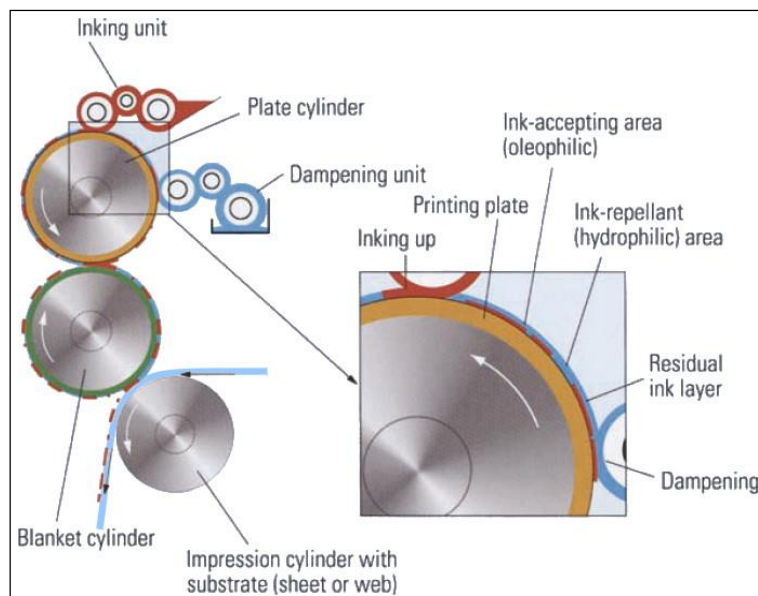


Figure 1.32: Schematic of offset printing. (adapted from<sup>81</sup>)

Figure 1.33 displays a schematic of gravure printing. The master is a steel cylinder covered by a copper layer that is engraved with very tiny holes. The holes are equally spaced with variable depth or variable area or both. The holes are filled with the very fluid ink via an ink fountain and a doctor blade. The ink is transferred to an absorbent substrate, when it is pressed to the gravure cylinder, by capillary mechanisms. It can be used to deposit very thin patterns of functional ink.<sup>91-93</sup>

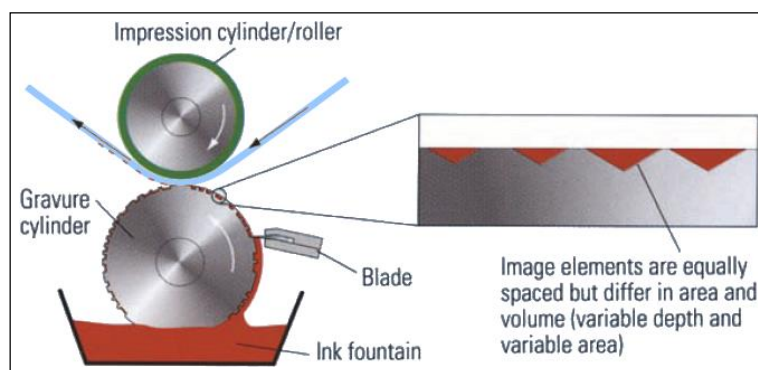


Figure 1.33: Schematic of gravure printing. (adapted from<sup>81</sup>)

Contrary to the previous printing techniques, inkjet printing is a non-contact deposition. Figure 1.34 displays schematics of the different inkjet printing techniques. For continuous inkjet, drops are ejected via a pump at a fixed interval, and the drop that should not be printed are deflected using a high voltage field. For drops on demand (DoD) inkjet, only the drops that have to be printed are ejected. Two mechanisms exist. Thermal inkjet uses the evaporation of a part of the solvent in the jet chamber when a heat is applied to create a gas bubble that ejects the corresponding ink volume. Piezo inkjet uses a piezoelectric material, that is deformed when a voltage is applied, to change the volume of the jet chamber and then to eject an ink drop. The advantage of this technique is that printing can be carried out on complex surfaces not only flat substrates and the design can be modified from one printing task to the other. It is widely used in device fabrication.<sup>91,94,95</sup>

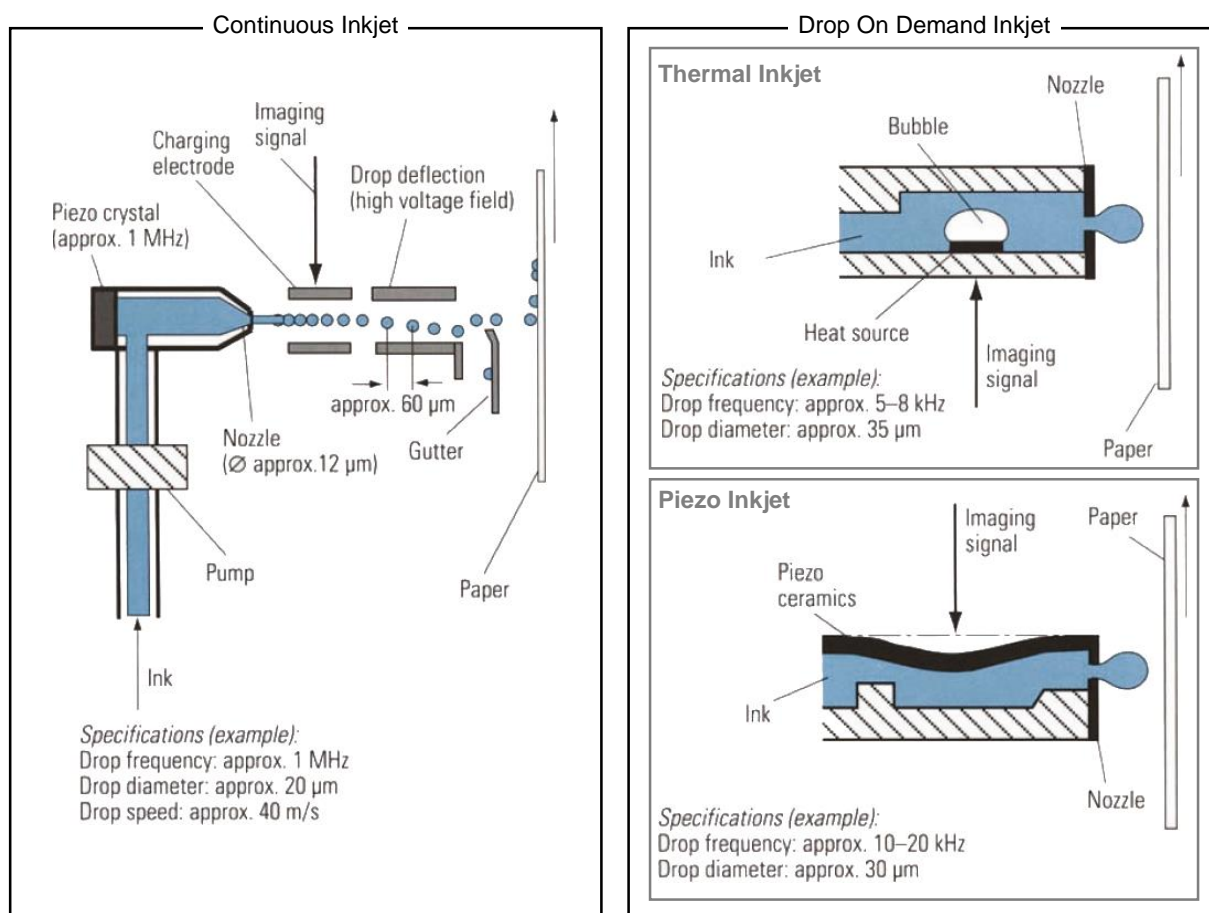


Figure 1.34: Schematic of inkjet technologies. (adapted from<sup>91</sup>)

Table 1.4 summarize the mechanisms, drying process and inks properties of the printing processes that can be used in printed electronics.

Printing	Ink type	Transfer mechanism	Drying	Ink properties: Viscosity [mPa.s] (Layer thickness [ $\mu\text{m}$ ])	Proportion of ink to be cured on the substrate [%]	Comments
Offset	Oil-based	Ink splitting, Pressure about 1 MPa in contact zone	Physically: Absorption Chemically: cross-linking / oxidation	40.10 <sup>3</sup> -100.10 <sup>3</sup> (0.5-1.5)	90-100	Slow drying, high print quality
	UV/EB curing		Radiation cross-linking			
Gravure	Solvent	Ink splitting, emptying of cells, Pressure approx. 3 MPa in the contact zone	Evaporation of solvents (H <sub>2</sub> O/Toluene)	50-200 (0.8-1)	25	Absorbent substrate, Solvent recycling
	UV curing		Radiation cross-linking	50-200 (5-8)	100	Thick ink layers possible
Flexography	Solvent	Ink splitting Pressure about 0.3 MPa in contact zone	Evaporation of solvents (H <sub>2</sub> O, alcohol, etc.)	50-500 (0.8-1)	20-30	Medium quality, Solvent recycling
	UV curing		Radiation cross-linking	50-500 (Up to 2.5)	100	High ink layer, Thickness possible, Better quality
Screen	Solvent	Pressing ink through holes in the screen	Evaporation of solvents or radiation cross-linking	Shear-thinning (Dependent on the mesh width up to ~12 $\mu\text{m}$ )	Dependent on ink type	Versatile application, Low quality
	UV curing					
Inkjet	Thermal technology (DoD)	Pressure impulse, Drop volume: 6-30 pL	Evaporation / absorption	1-5 (<0.5)	3-5	Avoiding bleeding in the substrate by means of special coating
	Conventional ink	Pressure impulse, Drop volume: 4-30 pL	Evaporation / absorption	5-20 (<0.5)	5	
	Hot-melt (Pigments in melted polymers/wax, 80-100°C)	Pressure impulse, Drop volume: 20-30 pL	Hardening through cooling	10-30 (12-18)	100	Thick ink layer, sensitive to scratching
	UV (Pigments in liquid monomers, etc.)	Pressure impulse, Drop volume: 10-30 pL	Radiation cross-linking	15-30 (10-20)	100	Thick ink layer on non-absorbent substrates
	Continuous technology (dyes in solvent. water, MEK, etc.)	Ink drop jet, splitting up into drops of 5-100 pL	Evaporation / absorption	1-5 (<0.5)	<5	Avoiding bleeding in the substrate by means of special coating

Table 1.4: Properties of different types of ink in printing process. (adapted from<sup>81</sup>)

In fact, other solution processes, not used in traditional printing because they allow the deposition of only complete films or of patterns in one direction, can be used in printed electronics. Figure 1.35 schematize most of them. Dip coating consists of dipping a substrate in a solution and removing the substrate at a constant speed. Depending on the speed and interactions between the solution and the substrate, a film can be deposited with a certain thickness. For doctor blade, the thickness of the film depends on the speed of the blade, of the air gap between the blade and the substrate, and of the viscosity of the solution. In metering rod technique, the ink goes through a spiral hole in the rod. The thickness of the deposited film depends on the depth and the wavelength of the spiral hole. In spray coating, very thin droplets of the solution are ejected using gas pressure and a nozzle. The thickness of the deposited film depends then on the time of deposition. The films are not very homogeneous due to the fact that the quantity of droplets is lower at the border than at the center.

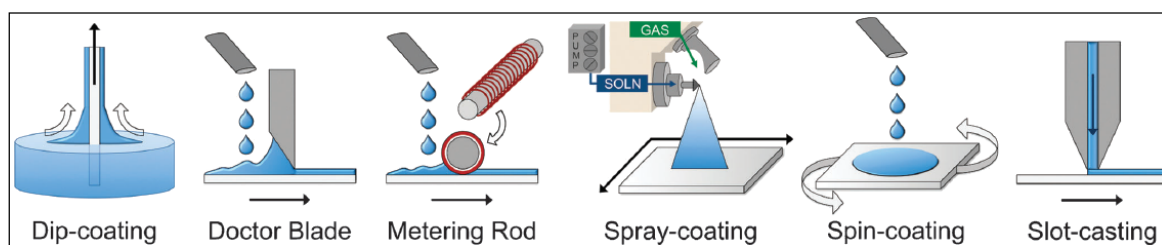


Figure 1.35: Schematic of various solution deposition methods used in functional printing. (adapted from<sup>96</sup>)

Spin coating technique is more detailed in Figure 1.36. It consists of the deposition of a drop of the solution onto the substrate. The ink flows outwards during the rotation of the substrate at high speed due to centrifugal force. Finally, excess solution is ejected from the substrate and very thin films are obtained. The solvent is either evaporated during the process, if they are very volatile, or afterward by heating the substrate. Spin coating is widely used at the laboratory scale to study materials for device applications.<sup>97-99</sup>

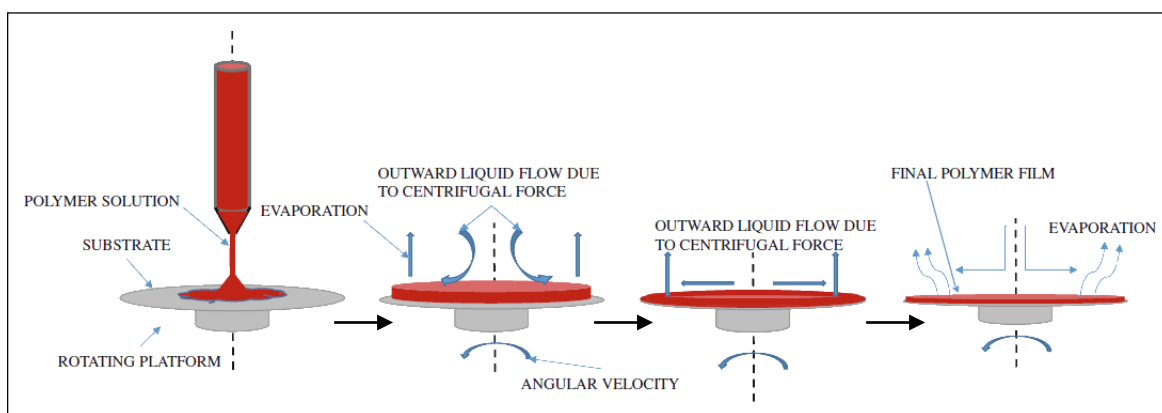


Figure 1.36: Schematic of spin coating. (adapted from<sup>100</sup>)

The slot die coating is detailed in Figure 1.37. The ink is pushed through the slot of a head using a certain pressure and the substrate is moved at a constant speed. A shim can be added in the slot to block some space and enable the deposition of lines. This technique is used to deposit very thin and homogeneous films. It is used to create layers of devices.<sup>91,101,102</sup>

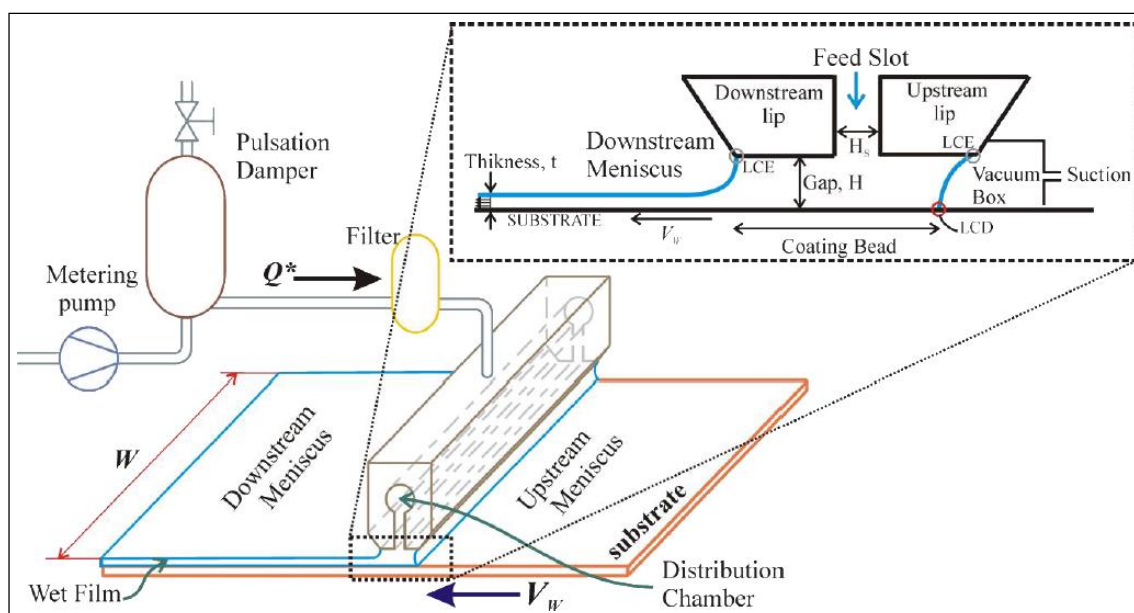


Figure 1.37: Schematic of slot die coating. (from<sup>103</sup>)

Numerous deposition processes can then be used to deposit patterns or homogeneous films of functional inks to create flexible devices using low temperature and low pressure. For each process, the ink needs specific properties.<sup>104,105</sup> Indeed, capillary interactions between ink and mesh, nozzle, slot and holes are important. Depending on the substrate, wettability problems can occur and specific formulation can improve the wetting properties. Furthermore, rheological behavior has to be considered: for some deposition processes a very fluid ink is needed, as for inkjet (5 – 40 mPa.s)<sup>106,107</sup>, and for others a very high viscosity with shear thinning and elastic behavior is required, as for doctor blade or screen-printing.<sup>108</sup> In the next part, a brief view of rheological behaviors will be exposed.

## 1.2.2 The rheological behavior of inks

The rheological properties of an ink may depend on different parameters such as the deformation  $\gamma$ , the processing time  $t$  (thixotropic behavior), the processing shear rate  $\dot{\gamma} = \frac{d\gamma}{dt}$ , the temperature  $T$ , etc. Inks may also have a yield stress  $\tau_0$ , that is the minimum shear stress  $\tau$  above which the ink can flow.

To obtain the rheological properties of a solution, rheometers are usually used. To measure the solution viscosity, a shear rate  $\dot{\gamma}$  is applied to the ink contained in different geometry cells and

the corresponding shear stress  $\tau$  is measured. The viscosity is calculated with the relation  $\eta = \frac{\tau}{\dot{\gamma}}$ . Newtonian fluids, for example, follow the relation  $\tau = \eta\dot{\gamma}$  where the viscosity  $\eta$  is constant. For so called Bingham fluids<sup>109</sup>, a yield stress  $\tau_0$  is present and the stress is written as  $\tau = \tau_0 + k\dot{\gamma}$ . Power-law fluids follow the Ostwald - de Waele relationship<sup>110</sup>  $\tau = k\dot{\gamma}^n = \eta(\dot{\gamma})\dot{\gamma}$  which leads to  $\eta(\dot{\gamma}) = k\dot{\gamma}^{n-1}$ . For  $n < 1$  the solution is shear thinning. For  $n > 1$ , on the other hand, the fluid is shear thickening which is a behavior to avoid for printing processes. The Herschel-Bulkley model<sup>111</sup> covers a large spectrum of behaviors using the yield stress  $\tau_0$ , the flow consistency index  $k$ , and the flow behavior index  $n$ : the stress is given by  $\tau = \tau_0 + k\dot{\gamma}^n$ . Figure 1.38 depicts the six main classes of rheological behavior: Newtonian, Bingham plastic, shear thinning with and without a yield stress, and shear thickening with or without a yield stress.

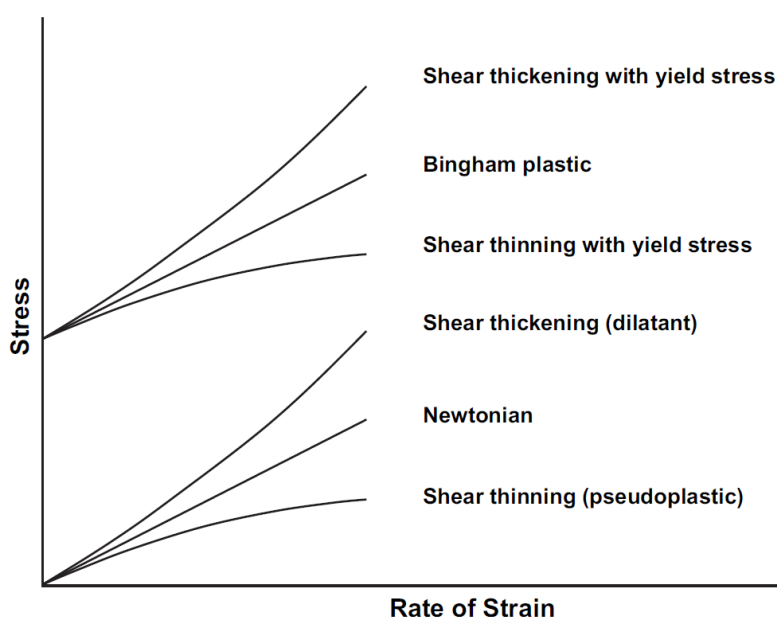


Figure 1.38: The six main classes of the time-independent fluids presented in a generic graph of stress against strain rate in shear flow. (from<sup>112</sup>)

Inks may also show elastic behavior. The elasticity of the ink is an important property to take into account. It can be determined using dynamic oscillation stress sweep. The complex shear modulus  $G^* = G' + iG''$  is measured and can be decomposed into two parts: the storage modulus  $G'$  represents the elastic behavior of the ink, and the loss modulus  $G''$  gives the viscous contribution. Both are constant in the linear viscoelastic range. Hook's law models ideal elastic fluids:  $G^* = \frac{\tau(t)}{\gamma(t)} = cst$ . In the case of ideal elastic fluid,  $G'' = 0$ ; for an ideal viscous fluid,  $G' = 0$ . In the general case of a so called viscoelastic fluid: if  $G'' > G'$  the fluid is a viscoelastic liquid, and if  $G' > G''$  the fluid is a viscoelastic gel (or soft solid).<sup>113</sup>

These methods to measure rheological behavior will be used in the next chapters to characterize organic inks for different processing purpose.

## 1.3 Conclusion

In this chapter, the properties of two different types of polymer used in printing electronic devices were described. First PEDOT semi-conducting polymers were discussed in terms of syntheses and formulations or post-treatments to modify the doping level and to increase the conductivity of PEDOT films. Probable structural modifications and mechanisms of the electronic transport with the impact on the doping level and the color of the polymer were explored.

Then the properties of a dielectric polymer, PVDF, and its copolymer P(VDF-TrFE) were described. The relation between the ratio VDF/TrFE on the crystallinity, as well as the influence of annealing and poling onto the different electric phases (ferro-, defect ferro- and para-electric phases) was discussed.

These two polymers can be deposited with solution processes. The different printing methods used in printed electronics were described. For each process, the inks need specific properties, taking into account the capillary interactions during the deposition, the rheological behavior needed for the process, and the wettability of the substrate. The variety of rheological behaviors were also discussed.

In the following chapters, two functional inks for printed electronics, PEDOT based inks and P(VDF-TrFE) inks, will be formulated for various deposition processes. Additives will enable the modification of the wettability properties of the inks and rheological behaviors. Films will be deposited and characterized. Finally, pressure sensors using these formulations will be created and characterized.

## Bibliography

- (1) Moliton, A.; Hiorns, R. C. Review of Electronic and Optical Properties of Semiconducting  $\pi$ -Conjugated Polymers: Applications in Optoelectronics. *Polym. Int.* **2004**, *53* (10), 1397–1412. <https://doi.org/10.1002/pi.1587>.
- (2) Street, G. B.; Clarke, T. C. Conducting Polymers: A Review of Recent Work. *IBM J. Res. Dev.* **1981**, *25* (1), 51–57. <https://doi.org/10.1147/rd.251.0051>.
- (3) Shirakawa, H.; Louis, E. J.; MacDiarmid, A. G.; Chiang, C. K.; Heeger, A. J. Synthesis of Electrically Conducting Organic Polymers: Halogen Derivatives of Polyacetylene, (CH)<sub>x</sub>. *J. Chem. Soc. Chem. Commun.* **1977**, No. 16, 578–580. <https://doi.org/10.1039/C39770000578>.
- (4) Skotheim, T. A.; Reynolds, J. *Conjugated Polymers: Processing and Applications*; CRC Press, 2006.
- (5) Kanazawa, K. K.; Diaz, A. F.; Geiss, R. H.; Gill, W. D.; Kwak, J. F.; Logan, J. A.; Rabolt, J. F.; Street, G. B. 'Organic Metals': Polypyrrole, a Stable Synthetic 'Metallic' Polymer. *J. Chem. Soc. Chem. Commun.* **1979**, No. 19, 854–855. <https://doi.org/10.1039/C39790000854>.
- (6) Ivory, D. M.; Miller, G. G.; Sowa, J. M.; Shacklette, L. W.; Chance, R. R.; Baughman, R. H. Highly Conducting Charge-transfer Complexes of Poly(P-phenylene). *J. Chem. Phys.* **1979**, *71* (3), 1506–1507. <https://doi.org/10.1063/1.438420>.
- (7) Das, T. K.; Prusty, S. Review on Conducting Polymers and Their Applications. *Polym.-Plast. Technol. Eng.* **2012**, *51* (14), 1487–1500. <https://doi.org/10.1080/03602559.2012.710697>.
- (8) Wynne, K. J.; Street, G. B. Conducting Polymers. A Short Review. *Ind. Eng. Chem. Prod. Res. Dev.* **1982**, *21* (1), 23–28. <https://doi.org/10.1021/i300005a005>.
- (9) Bidan, G. Electroconducting Conjugated Polymers: New Sensitive Matrices to Build up Chemical or Electrochemical Sensors. A Review. *Sens. Actuators B Chem.* **1992**, *6* (1), 45–56. [https://doi.org/10.1016/0925-4005\(92\)80029-W](https://doi.org/10.1016/0925-4005(92)80029-W).
- (10) Groenendaal, L.; Jonas, F.; Freitag, D.; Pielartzik, H.; Reynolds, J. R. Poly(3,4-Ethylenedioxythiophene) and Its Derivatives: Past, Present, and Future. *Adv. Mater.* **2000**, *12* (7), 481–494. [https://doi.org/10.1002/\(SICI\)1521-4095\(200004\)12:7<481::AID-ADMA481>3.0.CO;2-C](https://doi.org/10.1002/(SICI)1521-4095(200004)12:7<481::AID-ADMA481>3.0.CO;2-C).
- (11) Heywang, G.; Jonas, F. Poly(Alkylenedioxythiophene)S—new, Very Stable Conducting Polymers. *Adv. Mater.* **1992**, *4* (2), 116–118. <https://doi.org/10.1002/adma.19920040213>.
- (12) Mitraka, E.; Jafari, M. J.; Vagin, M.; Liu, X.; Fahlman, M.; Ederth, T.; Berggren, M.; Jonsson, M. P.; Crispin, X. Oxygen-Induced Doping on Reduced PEDOT. *J. Mater. Chem. A* **2017**, *5* (9), 4404–4412. <https://doi.org/10.1039/C6TA10521A>.
- (13) Cho, B.; Park, K. S.; Baek, J.; Oh, H. S.; Koo Lee, Y.-E.; Sung, M. M. Single-Crystal Poly(3,4-Ethylenedioxythiophene) Nanowires with Ultrahigh Conductivity. *Nano Lett.* **2014**, *14* (6), 3321–3327. <https://doi.org/10.1021/nl500748y>.
- (14) Reynolds, J. R.; Thompson, B. C.; Skotheim, T. A. *Conjugated Polymers: Properties, Processing, and Applications*; CRC Press, 2019.
- (15) Ha, Y.-H.; Nikolov, N.; Pollack, S. K.; Mastrangelo, J.; Martin, B. D.; Shashidhar, R. Towards a Transparent, Highly Conductive Poly(3,4-Ethylenedioxythiophene). *Adv. Funct. Mater.* **2004**, *14* (6), 615–622. <https://doi.org/10.1002/adfm.200305059>.
- (16) Elschner, A.; Kirchmeyer, S.; Lovenich, W.; Merker, U.; Reuter, K.; Kirchmeyer, S.; Lovenich, W.; Merker, U.; Reuter, K. *PEDOT: Principles and Applications of an Intrinsically Conductive Polymer*; CRC Press, 2010. <https://doi.org/10.1201/b10318>.
- (17) Fabretto, M. V.; Evans, D. R.; Mueller, M.; Zuber, K.; Hojati-Talemi, P.; Short, R. D.; Wallace, G. G.; Murphy, P. J. Polymeric Material with Metal-Like Conductivity for Next Generation Organic Electronic Devices. *Chem. Mater.* **2012**, *24* (20), 3998–4003. <https://doi.org/10.1021/cm302899v>.

- (18) Zotti, G.; Zecchin, S.; Schiavon, G.; Louwet, F.; Groenendaal, L.; Crispin, X.; Osikowicz, W.; Salaneck, W.; Fahlman, M. Electrochemical and XPS Studies toward the Role of Monomeric and Polymeric Sulfonate Counterions in the Synthesis, Composition, and Properties of Poly(3,4-Ethylenedioxythiophene). *Macromolecules* **2003**, *36* (9), 3337–3344. <https://doi.org/10.1021/ma021715k>.
- (19) Kim, D.; Zozoulenko, I. Why Is Pristine PEDOT Oxidized to 33%? A Density Functional Theory Study of Oxidative Polymerization Mechanism. *J. Phys. Chem. B* **2019**, *123* (24), 5160–5167. <https://doi.org/10.1021/acs.jpcc.9b01745>.
- (20) Dautzenberg, H. Polyelectrolyte Complex Formation in Highly Aggregating Systems. 1. Effect of Salt: Polyelectrolyte Complex Formation in the Presence of NaCl. *Macromolecules* **1997**, *30* (25), 7810–7815. <https://doi.org/10.1021/ma970803f>.
- (21) Rivnay, J.; Inal, S.; Collins, B. A.; Sessolo, M.; Stavrinidou, E.; Strakosas, X.; Tassone, C.; Delongchamp, D. M.; Malliaras, G. G. Structural Control of Mixed Ionic and Electronic Transport in Conducting Polymers. *Nat. Commun.* **2016**, *7* (1), 1–9. <https://doi.org/10.1038/ncomms11287>.
- (22) Zhang, S.; Kumar, P.; Nouas, A. S.; Fontaine, L.; Tang, H.; Cicoira, F. Solvent-Induced Changes in PEDOT:PSS Films for Organic Electrochemical Transistors. *APL Mater.* **2015**, *3* (1), 014911–014911.7. <https://doi.org/10.1063/1.4905154>.
- (23) He, H.; Zhang, L.; Guan, X.; Cheng, H.; Liu, X.; Yu, S.; Wei, J.; Ouyang, J. Biocompatible Conductive Polymers with High Conductivity and High Stretchability. *ACS Appl. Mater. Interfaces* **2019**. <https://doi.org/10.1021/acsami.9b07325>.
- (24) Wang, G.-F.; Tao, X.-M.; Xin, J. H.; Fei, B. Modification of Conductive Polymer for Polymeric Anodes of Flexible Organic Light-Emitting Diodes. *Nanoscale Res. Lett.* **2009**, *4* (7), 613–617. <https://doi.org/10.1007/s11671-009-9288-8>.
- (25) Palumbiny, C. M.; Heller, C.; Schaffer, C. J.; Körstgens, V.; Santoro, G.; Roth, S. V.; Müller-Buschbaum, P. Molecular Reorientation and Structural Changes in Cosolvent-Treated Highly Conductive PEDOT:PSS Electrodes for Flexible Indium Tin Oxide-Free Organic Electronics. *J. Phys. Chem. C* **2014**, *118* (25), 13598–13606. <https://doi.org/10.1021/jp501540y>.
- (26) Mengistie, D. A.; Wang, P.-C.; Chu, C.-W. Effect of Molecular Weight of Additives on the Conductivity of PEDOT:PSS and Efficiency for ITO-Free Organic Solar Cells. *J. Mater. Chem. A* **2013**, *1* (34), 9907–9915. <https://doi.org/10.1039/C3TA11726J>.
- (27) Crispin, X.; Jakobsson, F. L. E.; Crispin, A.; Grim, P. C. M.; Andersson, P.; Volodin, A.; van Haesendonck, C.; der Auweraer, M. V.; Salaneck, W. R.; Berggren, M. The Origin of the High Conductivity of Poly(3,4-Ethylenedioxythiophene)–Poly(Styrenesulfonate) (PEDOT–PSS) Plastic Electrodes. *Chem. Mater.* **18** (18), 4354–4360.
- (28) Ouyang, J.; Xu, Q.; Chu, C.-W.; Yang, Y.; Li, G.; Shinar, J. On the Mechanism of Conductivity Enhancement in Poly(3,4-Ethylenedioxythiophene):Poly(Styrene Sulfonate) Film through Solvent Treatment. *Polymer* **2004**, *45* (25), 8443–8450. <https://doi.org/10.1016/j.polymer.2004.10.001>.
- (29) Shi, H.; Liu, C.; Jiang, Q.; Xu, J. Effective Approaches to Improve the Electrical Conductivity of PEDOT:PSS: A Review. *Adv. Electron. Mater.* **2015**, *1* (4), n/a-n/a. <https://doi.org/10.1002/aelm.201500017>.
- (30) Xia, Y.; Ouyang, J. Salt-Induced Charge Screening and Significant Conductivity Enhancement of Conducting Poly(3,4-Ethylenedioxythiophene):Poly(Styrenesulfonate). *Macromolecules* **2009**, *42* (12), 4141–4147. <https://doi.org/10.1021/ma900327d>.
- (31) Xia, Y.; Ouyang, J. Significant Conductivity Enhancement of Conductive Poly(3,4-Ethylenedioxythiophene): Poly(Styrenesulfonate) Films through a Treatment with Organic Carboxylic Acids and Inorganic Acids. *ACS Appl. Mater. Interfaces* **2010**, *2* (2), 474–483. <https://doi.org/10.1021/am900708x>.
- (32) Xia, Y.; Zhang, H.; Ouyang, J. Highly Conductive PEDOT:PSS Films Prepared through a Treatment with Zwitterions and Their Application in Polymer Photovoltaic Cells. *J. Mater. Chem.* **2010**, *20* (43), 9740–9747. <https://doi.org/10.1039/C0JM01593H>.

- (33) Kim, N.; Kee, S.; Lee, S. H.; Lee, B. H.; Kahng, Y. H.; Jo, Y.-R.; Kim, B.-J.; Lee, K. Highly Conductive PEDOT:PSS Nanofibrils Induced by Solution-Processed Crystallization. *Adv. Mater. Deerfield Beach Fla* **2014**, *26* (14), 2268–2272, 2109. <https://doi.org/10.1002/adma.201304611>.
- (34) Zozoulenko, I.; Singh, A.; Singh, S. K.; Gueskine, V.; Crispin, X.; Berggren, M. Polarons, Bipolarons, And Absorption Spectroscopy of PEDOT. *ACS Appl. Polym. Mater.* **2019**, *1* (1), 83–94. <https://doi.org/10.1021/acsapm.8b00061>.
- (35) Muñoz, W. A.; Crispin, X.; Fahlman, M.; Zozoulenko, I. V. Understanding the Impact of Film Disorder and Local Surface Potential in Ultraviolet Photoelectron Spectroscopy of PEDOT. *Macromol. Rapid Commun.* **2018**, *39* (4), 1700533. <https://doi.org/10.1002/marc.201700533>.
- (36) Sonmez, G. Polymeric Electrochromics. *Chem. Commun.* **2005**, No. 42, 5251–5259. <https://doi.org/10.1039/B510230H>.
- (37) Kim, N.; Lee, B. H.; Choi, D.; Kim, G.; Kim, H.; Kim, J.-R.; Lee, J.; Kahng, Y. H.; Lee, K. Role of Interchain Coupling in the Metallic State of Conducting Polymers. *Phys. Rev. Lett.* **2012**, *109* (10), 106405. <https://doi.org/10.1103/PhysRevLett.109.106405>.
- (38) Bubnova, O.; Crispin, X. Towards Polymer-Based Organic Thermoelectric Generators. *Energy Environ. Sci.* **2012**, *5* (11), 9345–9362. <https://doi.org/10.1039/C2EE22777K>.
- (39) Bubnova, O.; Khan, Z. U.; Malti, A.; Braun, S.; Fahlman, M.; Berggren, M.; Crispin, X. Optimization of the Thermoelectric Figure of Merit in the Conducting Polymer Poly(3,4-Ethylenedioxythiophene). *Nat. Mater.* **2011**, *10* (6), 429–433. <https://doi.org/10.1038/nmat3012>.
- (40) Malti, A.; Edberg, J.; Granberg, H.; Khan, Z. U.; Andreasen, J. W.; Liu, X.; Zhao, D.; Zhang, H.; Yao, Y.; Brill, J. W.; et al. An Organic Mixed Ion–Electron Conductor for Power Electronics. *Adv. Sci.* **2016**, *3* (2), 1500305. <https://doi.org/10.1002/advs.201500305>.
- (41) Tybrandt, K.; Zozoulenko, I. V.; Berggren, M. Chemical Potential–electric Double Layer Coupling in Conjugated Polymer–polyelectrolyte Blends. *Sci. Adv.* **2017**, *3* (12), ea03659. <https://doi.org/10.1126/sciadv.aao3659>.
- (42) Tehrani, P.; Hennerdal, L.-O.; Dyer, A. L.; Reynolds, J. R.; Berggren, M. Improving the Contrast of All-Printed Electrochromic Polymer on Paper Displays. *J. Mater. Chem.* **2009**, *19* (13), 1799–1802. <https://doi.org/10.1039/B820677E>.
- (43) Isaksson, J.; Kjäll, P.; Nilsson, D.; Robinson, N.; Berggren, M.; Richter-Dahlfors, A. Electronic Control of Ca<sup>2+</sup> Signalling in Neuronal Cells Using an Organic Electronic Ion Pump. *Nat. Mater.* **2007**, *6* (9), 673–679. <https://doi.org/10.1038/nmat1963>.
- (44) Jonsson, A.; Song, Z.; Nilsson, D.; Meyerson, B. A.; Simon, D. T.; Linderöth, B.; Berggren, M. Therapy Using Implanted Organic Bioelectronics. *Sci. Adv.* **2015**, *1* (4), e1500039. <https://doi.org/10.1126/sciadv.1500039>.
- (45) Simon, D. T.; Kurup, S.; Larsson, K. C.; Hori, R.; Tybrandt, K.; Gojny, M.; Jäger, E. W. H.; Berggren, M.; Canlon, B.; Richter-Dahlfors, A. Organic Electronics for Precise Delivery of Neurotransmitters to Modulate Mammalian Sensory Function. *Nat. Mater.* **2009**, *8* (9), 742–746. <https://doi.org/10.1038/nmat2494>.
- (46) Alba, N. A.; Du, Z. J.; Catt, K. A.; Kozai, T. D. Y.; Cui, X. T. In Vivo Electrochemical Analysis of a PEDOT/MWCNT Neural Electrode Coating. *Biosensors* **2015**, *5* (4), 618–646. <https://doi.org/10.3390/bios5040618>.
- (47) Rivnay, J.; Inal, S.; Salleo, A.; Owens, R. M.; Berggren, M.; Malliaras, G. G. Organic Electrochemical Transistors. *Nat. Rev. Mater.* **2018**, *3* (2), 1–14. <https://doi.org/10.1038/natrevmats.2017.86>.
- (48) Kros, A.; Nolte, R. J. M.; Sommerdijk, N. A. J. M. Poly(3,4-Ethylenedioxythiophene)-Based Copolymers for Biosensor Applications. *J. Polym. Sci. Part Polym. Chem.* **2002**, *40* (6), 738–747. <https://doi.org/10.1002/pola.10159>.
- (49) Tekbaşoğlu, T. Y.; Soganci, T.; Ak, M.; Koca, A.; Şener, M. K. Enhancing Biosensor Properties of Conducting Polymers via Copolymerization: Synthesis of EDOT-Substituted Bis(2-Pyridylimino)Isoindolato-Palladium Complex and Electrochemical Sensing of Glucose by

- Its Copolymerized Film. *Biosens. Bioelectron.* **2017**, *87*, 81–88. <https://doi.org/10.1016/j.bios.2016.08.020>.
- (50) De, S.; Lyons, P. E.; Sorel, S.; Doherty, E. M.; King, P. J.; Blau, W. J.; Nirmalraj, P. N.; Boland, J. J.; Scardaci, V.; Joimel, J.; et al. Transparent, Flexible, and Highly Conductive Thin Films Based on Polymer–Nanotube Composites. *ACS Nano* **2009**, *3* (3), 714–720. <https://doi.org/10.1021/nn800858w>.
- (51) Cao, W.; Li, J.; Chen, H.; Xue, J. Transparent Electrodes for Organic Optoelectronic Devices: A Review. *J. Photonics Energy* **2014**, *4* (1), 040990. <https://doi.org/10.1117/1.JPE.4.040990>.
- (52) Paetzold, R.; Heuser, K.; Henseler, D.; Roeger, S.; Wittmann, G.; Winnacker, A. Performance of Flexible Polymeric Light-Emitting Diodes under Bending Conditions. *Appl. Phys. Lett.* **2003**, *82* (19), 3342–3344. <https://doi.org/10.1063/1.1574400>.
- (53) Park, Y.; Choong, V.; Gao, Y.; Hsieh, B. R.; Tang, C. W. Work Function of Indium Tin Oxide Transparent Conductor Measured by Photoelectron Spectroscopy. *Appl. Phys. Lett.* **1996**, *68* (19), 2699–2701. <https://doi.org/10.1063/1.116313>.
- (54) A Review of Flexible OLEDs Toward Highly Durable Unusual Displays - IEEE Journals & Magazine <https://ieeexplore.ieee.org/abstract/document/7827119> (accessed Feb 28, 2019).
- (55) Dang, Z.-M. *Dielectric Polymer Materials for High-Density Energy Storage*; William Andrew, 2018.
- (56) Li, J.; Liu, Y.; Zhang, Y.; Cai, H.-L.; Xiong, R.-G. Molecular Ferroelectrics: Where Electronics Meet Biology. *Phys. Chem. Chem. Phys.* **2013**, *15* (48), 20786–20796. <https://doi.org/10.1039/C3CP52501E>.
- (57) Dragoman, M. MoS<sub>2</sub> Thin Films as Electrically Tunable Materials for Microwave Applications. *Appl. Phys. Lett.* **2015**, *Applied Physics Letters*, 243109. <https://doi.org/10.1063/1.4938145>.
- (58) Jaffe, B. *Piezoelectric Ceramics*; Elsevier, 2012.
- (59) Zhu, X. Piezoelectric Ceramic Materials: Processing, Properties, Characterization, and Applications. *Piezoelectric Mater. Struct. Prop. Appl.* **2010**, 1–36.
- (60) Zhu, L.; Wang, Q. Novel Ferroelectric Polymers for High Energy Density and Low Loss Dielectrics. *Macromolecules* **2012**, *45* (7), 2937–2954. <https://doi.org/10.1021/ma2024057>.
- (61) Soulestin, T.; Ladmiral, V.; Dos Santos, F. D.; Améduri, B. Vinylidene Fluoride- and Trifluoroethylene-Containing Fluorinated Electroactive Copolymers. How Does Chemistry Impact Properties? *Prog. Polym. Sci.* **2017**, *72*, 16–60. <https://doi.org/10.1016/j.progpolymsci.2017.04.004>.
- (62) Kawai, H. The Piezoelectricity of Poly (Vinylidene Fluoride). *Jpn. J. Appl. Phys.* **1969**, *8* (7), 975. <https://doi.org/10.1143/JJAP.8.975>.
- (63) Bergman, J. G.; McFee, J. H.; Crane, G. R. Pyroelectricity and Optical Second Harmonic Generation in Polyvinylidene Fluoride Films. *Appl. Phys. Lett.* **1971**, *18* (5), 203–205. <https://doi.org/10.1063/1.1653624>.
- (64) Tamura, M.; Ogasawara, K.; Ono, N.; Hagiwara, S. Piezoelectricity in Uniaxially Stretched Poly(Vinylidene Fluoride). *J. Appl. Phys.* **1974**, *45* (9), 3768–3771. <https://doi.org/10.1063/1.1663857>.
- (65) Higashihata, Y.; Sako, J.; Yagi, T. Piezoelectricity of Vinylidene Fluoride-Trifluoroethylene Copolymers. *Ferroelectrics* **1981**, *32* (1), 85–92. <https://doi.org/10.1080/00150198108238678>.
- (66) Ohigashi, H.; Koga, K. Ferroelectric Copolymers of Vinylidene fluoride and Trifluoroethylene with a Large Electromechanical Coupling Factor. *Jpn. J. Appl. Phys.* **1982**, *21* (8A), L455. <https://doi.org/10.1143/JJAP.21.L455>.
- (67) Defebvin, J.; Barrau, S.; Stoclet, G.; Rochas, C.; Lefebvre, J.-M. In Situ SAXS/WAXS Investigation of the Structural Evolution of Poly(Vinylidene Fluoride) upon Uniaxial Stretching. *Polymer* **2016**, *84*, 148–157. <https://doi.org/10.1016/j.polymer.2015.12.041>.

- (68) Heremans, P.; Gelinck, G. H.; Müller, R.; Baeg, K.-J.; Kim, D.-Y.; Noh, Y.-Y. Polymer and Organic Nonvolatile Memory Devices. *Chem. Mater.* **2011**, *23* (3), 341–358. <https://doi.org/10.1021/cm102006v>.
- (69) Farmer, B. L.; Hopfinger, A. J.; Lando, J. B. Polymorphism of Poly(Vinylidene Fluoride): Potential Energy Calculations of the Effects of Head-to-head Units on the Chain Conformation and Packing of Poly(Vinylidene Fluoride). *J. Appl. Phys.* **1972**, *43* (11), 4293–4303. <https://doi.org/10.1063/1.1660919>.
- (70) Furukawa, T. Structure and Functional Properties of Ferroelectric Polymers. *Adv. Colloid Interface Sci.* **1997**, *71–72*, 183–208. [https://doi.org/10.1016/S0001-8686\(97\)90017-8](https://doi.org/10.1016/S0001-8686(97)90017-8).
- (71) Koga, K.; Ohigashi, H. Piezoelectricity and Related Properties of Vinylidene Fluoride and Trifluoroethylene Copolymers. *J. Appl. Phys.* **1986**, *59* (6), 2142–2150. <https://doi.org/10.1063/1.336351>.
- (72) Bargain, F.; Panine, P.; Domingues Dos Santos, F.; Tencé-Girault, S. From Solvent-Cast to Annealed and Poled Poly(VDF-Co-TrFE) Films: New Insights on the Defective Ferroelectric Phase. *Polymer* **2016**, *105*, 144–156. <https://doi.org/10.1016/j.polymer.2016.10.010>.
- (73) Al-Jishi, R.; Taylor, P. L. Equilibrium Polarization and Piezoelectric and Pyroelectric Coefficients in Poly(Vinylidene Fluoride). *J. Appl. Phys.* **1985**, *57* (3), 902–905. <https://doi.org/10.1063/1.334690>.
- (74) Su, R.; Tseng, J.-K.; Lu, M.-S.; Lin, M.; Fu, Q.; Zhu, L. Ferroelectric Behavior in the High Temperature Paraelectric Phase in a Poly(Vinylidene Fluoride-Co-Trifluoroethylene) Random Copolymer. *Polymer* **2012**, *53* (3), 728–739. <https://doi.org/10.1016/j.polymer.2012.01.001>.
- (75) Yang, L.; Li, X.; Allahyarov, E.; Taylor, P. L.; Zhang, Q. M.; Zhu, L. Novel Polymer Ferroelectric Behavior via Crystal Isomorphism and the Nanoconfinement Effect. *Polymer* **2013**, *54* (7), 1709–1728. <https://doi.org/10.1016/j.polymer.2013.01.035>.
- (76) Gao, J.; Xue, D.; Liu, W.; Zhou, C.; Ren, X. Recent Progress on BaTiO<sub>3</sub>-Based Piezoelectric Ceramics for Actuator Applications. *Actuators* **2017**, *6* (3), 24. <https://doi.org/10.3390/act6030024>.
- (77) Lang, S. B.; Muensit, S. Review of Some Lesser-Known Applications of Piezoelectric and Pyroelectric Polymers. *Appl. Phys. A* **2006**, *85* (2), 125–134. <https://doi.org/10.1007/s00339-006-3688-8>.
- (78) Wang, A.; Hu, M.; Zhou, L.; Qiang, X. Self-Powered Wearable Pressure Sensors with Enhanced Piezoelectric Properties of Aligned P(VDF-TrFE)/MWCNT Composites for Monitoring Human Physiological and Muscle Motion Signs. *Nanomaterials* **2018**, *8* (12). <https://doi.org/10.3390/nano8121021>.
- (79) Choi, S. T.; Lee, J. Y.; Kwon, J. O.; Lee, S.; Kim, W. Varifocal Liquid-Filled Microlens Operated by an Electroactive Polymer Actuator. *Opt. Lett.* **2011**, *36* (10), 1920–1922. <https://doi.org/10.1364/OL.36.001920>.
- (80) Zou, C.; Harne, R. L. Adaptive Acoustic Energy Delivery to near and Far Fields Using Foldable, Tessellated Star Transducers. *Smart Mater. Struct.* **2017**, *26* (5), 055021. <https://doi.org/10.1088/1361-665X/aa6a93>.
- (81) *Handbook of Print Media: Technologies and Production Methods*; Kipphan, H., Ed.; Springer-Verlag: Berlin Heidelberg, 2001. <https://doi.org/10.1007/978-3-540-29900-4>.
- (82) Ng, L. W. T.; Zhu, X.; Hu, G.; Macadam, N.; Um, D.; Wu, T.-C.; Moal, F. L.; Jones, C.; Hasan, T. Conformal Printing of Graphene for Single- and Multilayered Devices onto Arbitrarily Shaped 3D Surfaces. *Adv. Funct. Mater.* **2019**, *29* (36), 1807933. <https://doi.org/10.1002/adfm.201807933>.
- (83) He, P.; Cao, J.; Ding, H.; Liu, C.; Neilson, J.; Li, Z.; Kinloch, I. A.; Derby, B. Screen-Printing of a Highly Conductive Graphene Ink for Flexible Printed Electronics. *ACS Appl. Mater. Interfaces* **2019**, *11* (35), 32225–32234. <https://doi.org/10.1021/acsami.9b04589>.
- (84) Saleh, M.; Abbass, Y.; Ibrahim, A.; Valle, M. Experimental Assessment of the Interface Electronic System for PVDF-Based Piezoelectric Tactile Sensors. *Sensors* **2019**, *19* (20), 4437. <https://doi.org/10.3390/s19204437>.

- (85) Krebs, F. C.; Fyenbo, J.; Jørgensen, M. Product Integration of Compact Roll-to-Roll Processed Polymer Solar Cell Modules: Methods and Manufacture Using Flexographic Printing, Slot-Die Coating and Rotary Screen Printing. *J. Mater. Chem.* **2010**, *20* (41), 8994–9001. <https://doi.org/10.1039/C0JM01178A>.
- (86) F. Huebner, C.; B. Carroll, J.; D. Evanoff, D.; Ying, Y.; J. Stevenson, B.; R. Lawrence, J.; Michael Houchins, J.; L. Foguth, A.; Sperry, J.; H. Foulger, S. Electroluminescent Colloidal Inks for Flexographic Roll-to-Roll Printing. *J. Mater. Chem.* **2008**, *18* (41), 4942–4948. <https://doi.org/10.1039/B809450K>.
- (87) Rehman, M. M.; Siddiqui, G. U.; Gul, J. Z.; Kim, S.-W.; Lim, J. H.; Choi, K. H. Resistive Switching in All-Printed, Flexible and Hybrid MoS<sub>2</sub>-PVA Nanocomposite Based Memristive Device Fabricated by Reverse Offset. *Sci. Rep.* **2016**, *6*, 36195. <https://doi.org/10.1038/srep36195>.
- (88) Pudas, M.; Hagberg, J.; Leppävuori, S. Printing Parameters and Ink Components Affecting Ultra-Fine-Line Gravure-Offset Printing for Electronics Applications. *J. Eur. Ceram. Soc.* **2004**, *24* (10), 2943–2950. <https://doi.org/10.1016/j.jeurceramsoc.2003.11.011>.
- (89) Nomura, K.; Kusaka, Y.; Ushijima, H.; Nagase, K.; Ikedo, H.; Mitsui, R.; Takahashi, S.; Nakajima, S.; Iwata, S. Continuous Fine Pattern Formation by Screen-Offset Printing Using a Silicone Blanket. *J. Micromechanics Microengineering* **2014**, *24* (9), 095021. <https://doi.org/10.1088/0960-1317/24/9/095021>.
- (90) Takei, Y.; Nomura, K.; Horii, Y.; Zymelka, D.; Ushijima, H.; Kobayashi, T. Fabrication of Simultaneously Implementing “Wired Face-Up and Face-Down Ultrathin Piezoresistive Si Chips” on a Film Substrate by Screen-Offset Printing. *Micromachines* **2019**, *10* (9), 563. <https://doi.org/10.3390/mi10090563>.
- (91) Merklein, L.; Daume, D.; Braig, F.; Schlisske, S.; Rödlmeier, T.; Mink, M.; Kourkoulos, D.; Ulber, B.; Di Biase, M.; Meerholz, K.; et al. Comparative Study of Printed Multilayer OLED Fabrication through Slot Die Coating, Gravure and Inkjet Printing, and Their Combination. *Colloids Interfaces* **2019**, *3* (1), 32. <https://doi.org/10.3390/colloids3010032>.
- (92) Vaklev, N. L.; Steinke, J. H. G.; Campbell, A. J. Gravure Printed Ultrathin Dielectric for Low Voltage Flexible Organic Field-Effect Transistors. *Adv. Mater. Interfaces* **2019**, *6* (11), 1900173. <https://doi.org/10.1002/admi.201900173>.
- (93) Hamsch, M.; Reuter, K.; Stanel, M.; Schmidt, G.; Kempa, H.; Fügmann, U.; Hahn, U.; Hübner, A. C. Uniformity of Fully Gravure Printed Organic Field-Effect Transistors. *Mater. Sci. Eng. B* **2010**, *170* (1), 93–98. <https://doi.org/10.1016/j.mseb.2010.02.035>.
- (94) Lim, D. U.; Choi, S.; Kim, S.; Choi, Y. J.; Lee, S.; Kang, M. S.; Kim, Y.-H.; Cho, J. H. All-Inkjet-Printed Vertical Heterostructure for Wafer-Scale Electronics. *ACS Nano* **2019**, *13* (7), 8213–8221. <https://doi.org/10.1021/acsnano.9b03428>.
- (95) D. Garma, L.; M. Ferrari, L.; Scognamiglio, P.; Greco, F.; Santoro, F. Inkjet-Printed PEDOT:PSS Multi-Electrode Arrays for Low-Cost in Vitro Electrophysiology. *Lab. Chip* **2019**. <https://doi.org/10.1039/C9LC00636B>.
- (96) Pasquarelli, R. M.; Ginley, D. S.; O’Hayre, R. Solution Processing of Transparent Conductors: From Flask to Film. *Chem. Soc. Rev.* **2011**, *40* (11), 5406–5441. <https://doi.org/10.1039/C1CS15065K>.
- (97) Chen, W.-H.; Qiu, L.; Zhang, P.; Jiang, P.-C.; Du, P.; Song, L.; Xiong, J.; Ko, F. Simple Fabrication of a Highly Conductive and Passivated PEDOT:PSS Film via Cryo-Controlled Quasi-Congeeing Spin-Coating for Flexible Perovskite Solar Cells. *J. Mater. Chem. C* **2019**, *7* (33), 10247–10256. <https://doi.org/10.1039/C9TC02744K>.
- (98) Roopa, T. S.; Murthy, H. N. N.; Swathi, H. S.; Angadi, G.; Harish, D. V. N. Synthesis and Characterization of Spin-Coated Clay/PVDF Thin Films. *Bull. Mater. Sci.* **2019**, *42* (1), 15. <https://doi.org/10.1007/s12034-018-1683-2>.
- (99) Mitzi, D. B.; Kosbar, L. L.; Murray, C. E.; Copel, M.; Afzali, A. High-Mobility Ultrathin Semiconducting Films Prepared by Spin Coating. *Nature* **2004**, *428* (6980), 299–303. <https://doi.org/10.1038/nature02389>.

- (100) Das, R.; Chanda, A. Fabrication and Properties of Spin-Coated Polymer Films; 2016; pp 283–306. [https://doi.org/10.1007/978-3-319-39715-3\\_10](https://doi.org/10.1007/978-3-319-39715-3_10).
- (101) Bodner, M.; García, H. R.; Steenberg, T.; Terkelsen, C.; Alfaro, S. M.; Avcioglu, G. S.; Vassiliev, A.; Primdahl, S.; Hjuler, H. A. Enabling Industrial Production of Electrodes by Use of Slot-Die Coating for HT-PEM Fuel Cells. *Int. J. Hydrog. Energy* **2019**, *44* (25), 12793–12801. <https://doi.org/10.1016/j.ijhydene.2018.11.091>.
- (102) Merklein, L.; Mink, M.; Kourkoulos, D.; Ulber, B.; Raupp, S. M.; Meerholz, K.; Scharfer, P.; Schabel, W. Multilayer OLEDs with Four Slot Die-Coated Layers. *J. Coat. Technol. Res.* **2019**. <https://doi.org/10.1007/s11998-019-00225-2>.
- (103) Maza Quinones, D.; Carvalho, M. EFFECT OF DIE LIP CONFIGURATION ON THE OPERATING WINDOW OF SLOT COATING PROCESS. **2006**.
- (104) Izdebska, J.; Thomas, S. *Printing on Polymers: Fundamentals and Applications*; William Andrew, 2015.
- (105) Cui, Z. *Printed Electronics: Materials, Technologies and Applications*; John Wiley & Sons, 2016.
- (106) Hoath, S. D. *Fundamentals of Inkjet Printing: The Science of Inkjet and Droplets*; John Wiley & Sons / Wiley-VCH Verlag GmbH & CoKGaA: Weinheim, Germany, 2016.
- (107) Zapka, W. *Handbook of Industrial Inkjet Printing: A Full System Approach*; John Wiley & Sons, 2018.
- (108) Abbott, S. *How to Be a Great Screen Printer*, Macdermid Autotype Limited.; HowTo eBook; 2008.
- (109) Bingham, E. C. An Investigation of the Laws of Plastic Flow. *Bull. Bur. Stand.* **1916**, *13* (2), 309. <https://doi.org/10.6028/bulletin.304>.
- (110) Ostwald, W. Ueber die Geschwindigkeitsfunktion der Viskosität disperser Systeme. I. *Kolloid-Z.* **1925**, *36* (2), 99–117. <https://doi.org/10.1007/BF01431449>.
- (111) Herschel, W. H.; Bulkley, R. Konsistenzmessungen von Gummi-Benzollösungen. *Kolloid-Z.* **1926**, *39* (4), 291–300. <https://doi.org/10.1007/BF01432034>.
- (112) Sochi, T. Non-Newtonian Flow in Porous Media. *Polymer* **2010**, *51* (22), 5007–5023. <https://doi.org/10.1016/j.polymer.2010.07.047>.
- (113) Mezger, T. G. *The Rheology Handbook: For Users of Rotational and Oscillatory Rheometers*; Vincentz Network GmbH & Co KG, 2006.
- (114) Ellmer, K. Past Achievements and Future Challenges in the Development of Optically Transparent Electrodes. *Nat. Photonics* **2012**, *6* (12), 809–817. <https://doi.org/10.1038/nphoton.2012.282>.

# 2 PEDOT:PSTFSI inks for various deposition processes

2.1 Introduction.....	68
2.2 Materials & Methods .....	70
2.2.1 Materials .....	70
2.2.2 Synthesis: from monomer to polyanion to complex PEDOT:PSTFSI .....	70
2.2.3 Formulations of PEDOT:PSTFSI solutions .....	73
2.2.4 Characterization of PEDOT:PSTFSI solutions.....	75
2.2.5 Substrate preparation .....	76
2.2.6 Deposition and drying of PEDOT:PSTFSI solutions .....	77
2.2.7 Characterization of the depositions.....	78
2.3 PEDOT:PSTFSI inks characterization.....	79
2.3.1 Polymer structure and conformation in solution .....	79
2.3.2 Shear rheology: from Newtonian to shear thinning behavior .....	84
2.3.3 From liquid to gel like solutions.....	87
2.3.4 Wettability: inks' surface tension versus substrate's surface energy .....	89
2.4 PEDOT:PSTFSI inks processing: inkjet printing, doctor blading, screen-printing, and soft-blading.....	91
2.5 Film characterization.....	95
2.5.1 Film topology .....	95
2.5.2 Films conductivity at the surface.....	97
2.5.3 Optoelectronic properties for transparent electrodes .....	102
2.6 Conclusion .....	104

## 2.1 Introduction

Organic semi-conducting polymers are attractive for their competitive price and low processability requirements. Aqueous solutions of these polymers can be deposited with a variety of processes to make thin, flexible and transparent conductive films. Such films can be used as transparent electrodes in organic light emitting diodes or organic photovoltaic cells. Poly(3,4-ethylene dioxythiophene):poly(styrenesulfonate) (PEDOT:PSS) [Figure 2.1] is the only PEDOT:polyanion system which is commercially available. It has interesting properties: sheet resistance  $R_s$  in the range  $50 < R_s < 1000 \Omega/\square$  and transmittance  $T$  in the range  $75 < T < 90 \%$ .<sup>1</sup> To produce thin films using this ink, different deposition processes are used: flexography,<sup>2</sup> screen-printing,<sup>3</sup> rotogravure,<sup>4,5</sup> inkjet,<sup>6,7</sup> offset, slot-dye,<sup>8</sup> doctor blade,<sup>9</sup> 3D printing<sup>10</sup> etc. Each process has its benefits and drawbacks and needs an ink with specific rheological properties.<sup>11</sup> For example, a fluid ink with low viscosity (5-40 mPa.s) is needed for inkjet printing,<sup>12,13</sup> while a viscous shear thinning ink with elastic behavior or possessing a yield stress is required for doctor-blading and screen-printing.<sup>14</sup> A key property to allow a good processability of the ink is therefore its viscosity and its rheological behavior.

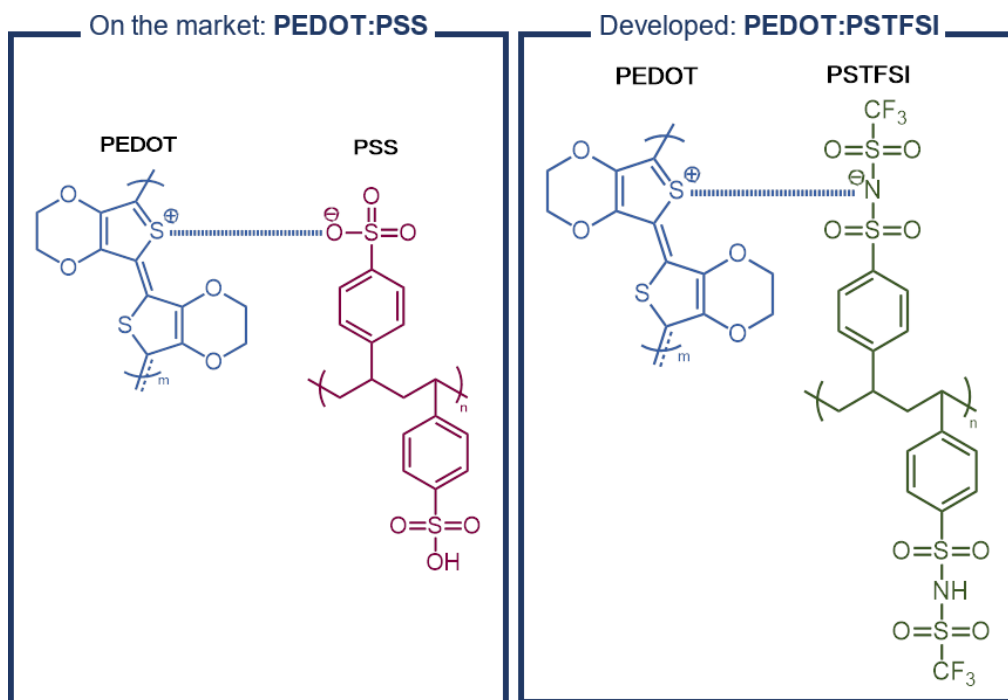


Figure 2.1: Structure of the commercial complex PEDOT:PSS (poly(3,4-ethylene dioxythiophene):poly(styrenesulfonate)) and the home made complex PEDOT:PSTFSI (poly(3,4-ethylenedioxythiophene):poly(4-styrene trifluoromethyl (bissulfonamide)))

Other counterions than PSS exist to stabilize PEDOT via ionic bounds in aqueous solvents such as poly(4-styrene trifluoromethyl(bissulfonylimide)) (PSTFSI)<sup>15</sup> [Figure 2.1]. It will be shown that PSTFSI give comparable conductivity and transparency properties to the films. However, the rheological properties of PEDOT:PSS and PEDOT:PSTFSI inks are especially different. For example PEDOT:PSTFSI inks can form a physical gel even at low concentrations, making it attractive for processing purposes while PEDOT:PSS shows only minor shear thinning behavior for concentrations as high as 1 %<sub>wt</sub>. This difference in behavior is in part due to structural differences between the polyanions: PSTFSI favors hydrogen bonds while PSS does not.

In this chapter, the structure of the home-made PEDOT:PSTFSI inks will be explored as well as their rheological properties and wettability. Then the films properties will be studied in function of the deposition process: doctor blade, screen-printing, inkjet, and soft blade deposition. It will be shown that PEDOT:PSTFSI inks can be adapted to each of these processes by simply tuning the concentration, making their formulation simple while keeping comparable optoelectronic properties as commercial inks.

## 2.2 Materials & Methods

### 2.2.1 Materials

To synthesize the anion STFSIK, the polyanion PSTFSIK and then the complex PEDOT:PSTFSIK, numerous chemicals were used: N,N-dimethylformamide (DMF) and dry-acetonitrile (from Acros Organics); ethanol, acetone, isopropanol, hydrochloric acid, oxalyl chloride, dichloromethane, sodium 4-vinylbenzenesulfonate, 2,2'-azobis(2-methylpropionitrile) (AIBN), potassium carbonate, iron III chloride and ammonium persulfate (from Sigma Aldrich); sodium bicarbonate and triethylamine (from Fisher); S-dodecyl-S'-( $\alpha,\alpha'$ -dimethyl- $\alpha''$ -acetic acid) trithiocarbonate (Chain Transfer Agent: CTA) and trifluoromethanesulfonamide (from ABCR); Lewatit MP 62 WS and S100 KR (from Lanxess). All products were used without further purification.

To formulate the different inks, Zonyl FS-300 fluorosurfactant, dimethyl sulfoxide (DMSO), polyethylene oxide (PEO) ( $M_w$ : 8000kDa) (from Sigma Aldrich) and ethylene glycol (EG) (from Fisher) were used.

To render glass or gold substrate more hydrophobic, toluene, chloroform, octadecyltrichlorosilane (OTS), and octane-thiol (from Sigma Aldrich) were used.

### 2.2.2 Synthesis: from monomer to polyanion to complex PEDOT:PSTFSI

To stabilize PEDOT in water, ionic interactions with potassium salt of poly(4-styrene trifluoromethyl (bissulfonylimide)) (PSTFSIK) were used. PSTFSIK is however not commercially available, as its monomer. For this reason, we have synthesized the potassium 4-styrene trifluoromethyl (bissulfonylimide) (STFSIK) monomer, the PSTFSIK polyanion, and then the complex PEDOT:PSTFSI.

The synthesis of the STFSIK monomer was inspired from the literature<sup>16</sup> [Figure 2.2]. Oxalyl chloride and N,N-dimethylformamide (DMF) were mixed in dry-acetonitrile in presence of 4-vinylbenzenesulfonate of sodium to form a Vilsmeier reagent. The trifluoromethanesulfonamide nucleophile was added with triethylamine base. The salts were eliminated using potassium carbonate and hydrochloride acid. The counterion was replaced by potassium ion using potassium carbonate solution. The monomer precipitated and was then dried at 50°C under vacuum with a yield around 40 %.

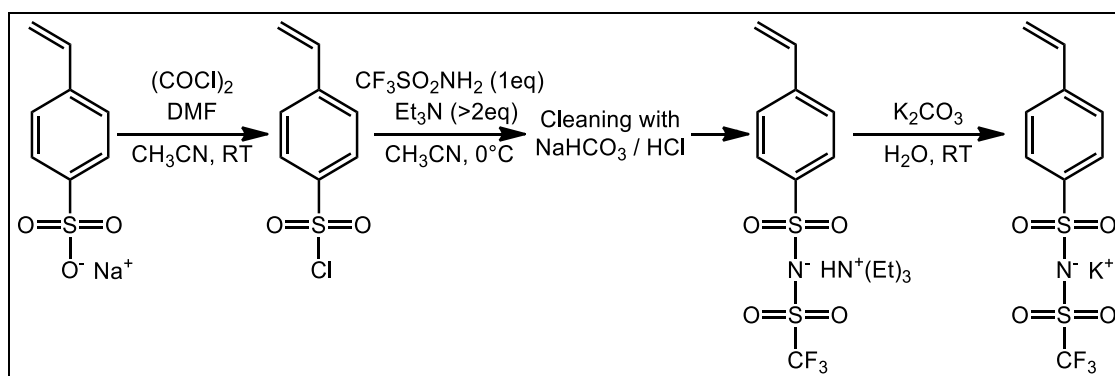


Figure 2.2: Synthesis of potassium 4-styrene trifluoromethyl (bissulfonylimide) (STFSIK)

The synthesis of the PSTFSIK polyanion followed previous studies<sup>17</sup> [Figure 2.3]: the monomer STFSIK was mixed with 2,2'-azobis(2-methylpropionitrile) (AIBN) and the RAFT chain transfer agent S-dodecyl-S'-( $\alpha,\alpha'$ -dimethyl- $\alpha''$ -acetic acid) trithiocarbonate (CTA) in DMF at 68°C during some days. Then more monomer was added. At the end of the reaction, the polymer PSTFSIK was precipitated in THF, diethyl ether and some methanol two times (after redissolving in DMSO). The polymer was then dried at 60°C under vacuum (yield  $\approx$  50 %).

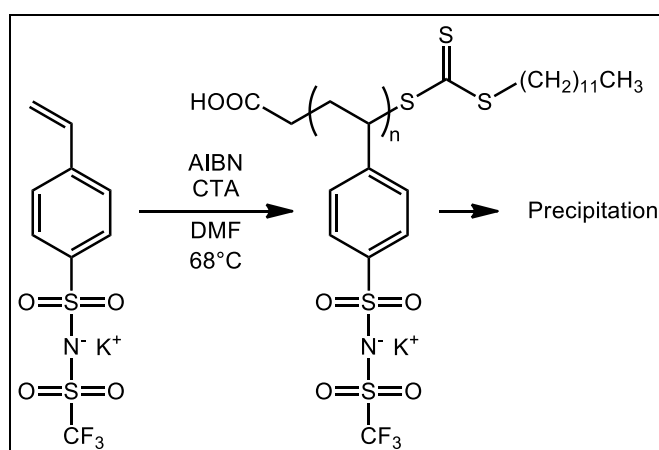


Figure 2.3: Synthesis of potassium poly(4-styrene trifluoromethyl (bissulfonylimide)) (PSTFSIK)

The chemical structures of the monomer STFSIK and polyanion PSTFSIK were checked using  $^1\text{H-NMR}$  spectroscopy (recorded on a Bruker Avance III HD 400 equipped with a 5 mm Bruker multinuclear direct probe) in deuterated DMSO at 298 K and 100.7 MHz [Figure 2.4 and Figure 2.5].

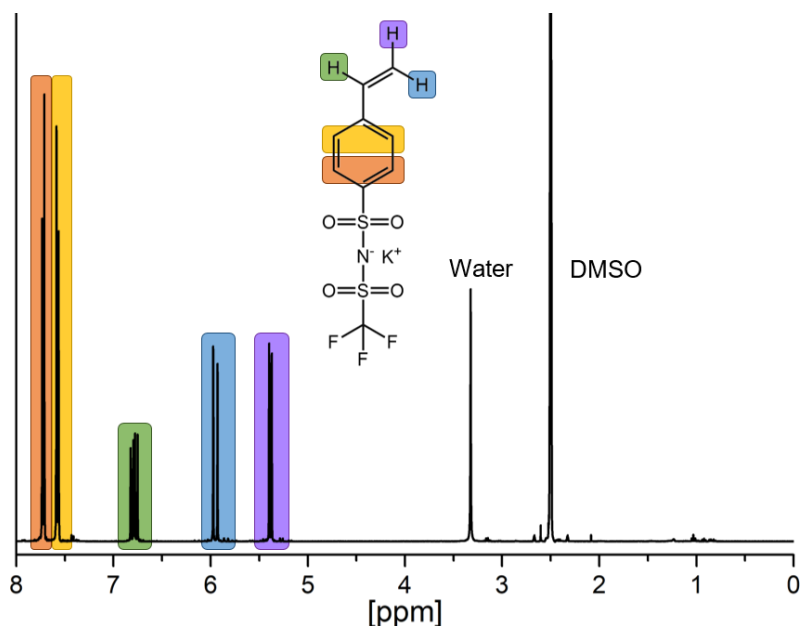


Figure 2.4:  $^1\text{H-NMR}$  spectroscopy of STFSIK in dimethylsulfoxide- $D_6$ .

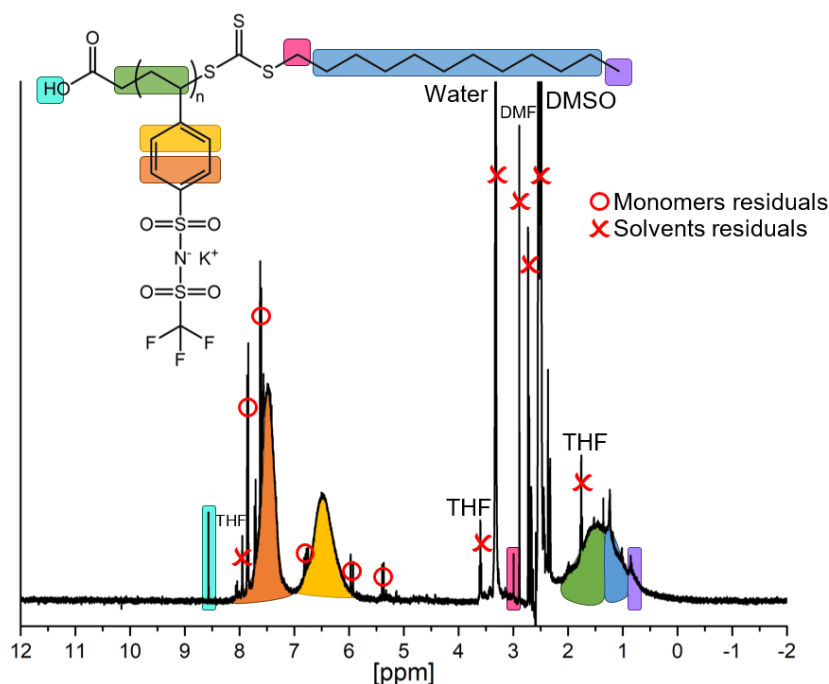


Figure 2.5:  $^1\text{H-NMR}$  spectroscopy of PSTFSIK in dimethylsulfoxide- $D_6$ .

The molar mass of the polyanion was tracked by size-exclusion chromatography (SEC) [See Appendix 2: Figure A.2-1] recorded on an Agilent PL-GPC 220 High Temperature Chromatograph calibrated with polystyrene standards using three-columns sets: Shodex GF-1G 7B column and two-times Shodex Asahipak GF-7M-HQ columns with a 0.6 mL/min flow at 75°C in DMF with 0.1 mol/L LiBr using 0.15 % toluene as flow marker. Polymers with different molar masses were obtained: i.e. 80, 90 and 250 kDa [See Appendix 2: Table A.2-1].

The complex poly(3,4-ethylenedioxythiophene):poly(4-styrene trifluoromethyl (bissulfonyl-imide)) (PEDOT:PSTFSI) was then synthesized using an oxidative polymerization of

EDOT in presence of ammonium persulfate, iron III chloride and PSTFSI in water [Figure 2.6].<sup>18</sup> Purification of the complexions was done by using a cationic and an anionic ion-exchange resins (Lewatit S100 KR and MP 62 WS). The solution was then concentrated using an ultrafiltration cell. The concentration was determined by measuring the absorbance of the solution in a 1 mm optical glass cell with a UV-360 Shimadzu UV-Vis-NIR-Spectrophotometer. The relation between the absorbance and the concentration was determined previously using the Beer-Lambert law:  $C = 0.565 \times \text{Abs}$ .

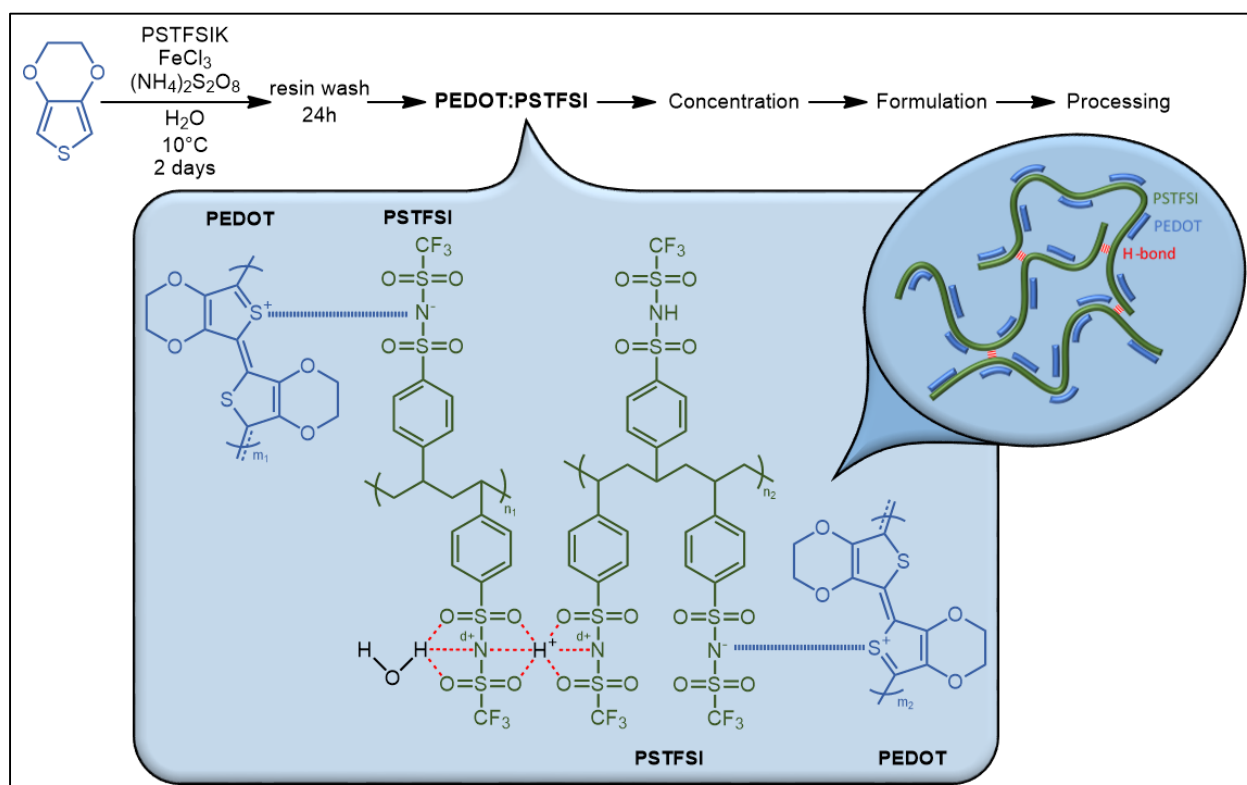


Figure 2.6: Synthesis and structure of the complex poly(3,4-ethylenedioxythiophene):poly(4-styrene trifluoromethyl (bissulfonylimide)) (PEDOT:PSTFSI)

### 2.2.3 Formulations of PEDOT:PSTFSI solutions

The obtained solutions of PEDOT:PSTFSI were then formulated by changing the concentration of the complex in water and adding additives: 5 %<sub>vol</sub> of a high boiling point solvent (DMSO or EG) was used to enhance the conductivity of the films after drying as explained in the literature<sup>19,20</sup>, and 0.04 % of an anionic fluorosurfactant surfactant (Zonyl FS-300) was added to improve the wettability of the ink. Indeed, the addition of surfactant decreases the surface tension of the ink (from close to the one of water, 72 mN/m, to 24 mN/m). This allows deposition onto plastic substrates by doctor blading or inkjet printing, or could allow the ink to flow through the mesh of the screen in screen-printing. The concentration 0.04 %<sub>w</sub> of surfactant was chosen as it is just above the critical micelle concentration of the surfactant in water [Figure 2.7].

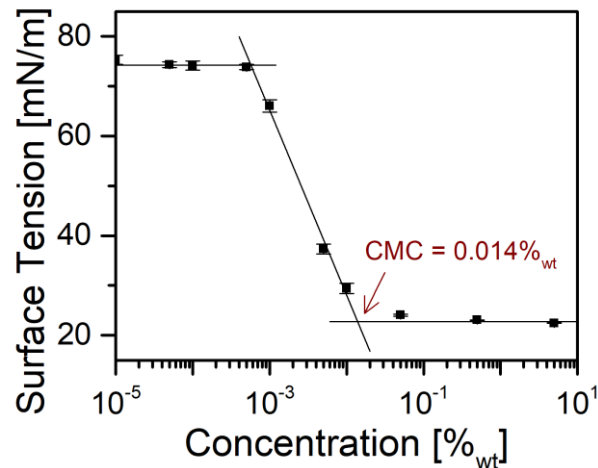


Figure 2.7: Surface tension of solutions of Zonyl FS-300 fluorosurfactant in water for different concentrations: determination of the CMC = 0.01 %wt.

The rheological properties [Figure 2.8] and surface tension [Table 2.1] of PEDOT:PSTFSI inks formulated with and without surfactant and/or high boiling point solvent were measured. It is found that the low concentration of additives (DMSO or EG) have no significant influences on the viscosity and surface tension.

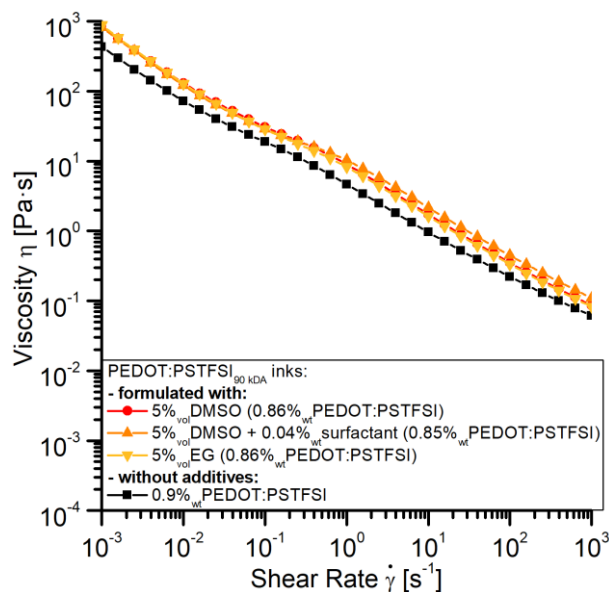


Figure 2.8: Rheological behavior of PEDOT:PSTFSI inks formulated with a high boiling point solvent (DMSO or EG) and/or with a surfactant (Zonyl FS-300 fluorosurfactant). Measures were done with a shear rheometer (cone plate geometry: 50 mm diameter and 1° angle): viscosity versus shear rate obtained by applying shear rate ramps at 18°C.

Solution	Surface tension (mN/m)
Water	72.2±0.8
Water + 5 % <sub>vol</sub> DMSO	66.7±0.3
Water + 5 % <sub>vol</sub> EG	68.3±0.5
Water + 0.04 % <sub>wt</sub> surfactant	24.1±0.2
Water + 5 % <sub>vol</sub> DMSO + 0.04 % <sub>wt</sub> surfactant	23.1±0.3
Water + 5 % <sub>vol</sub> EG + 0.04 % <sub>wt</sub> surfactant	23.7±0.1

Table 2.1: Surface tensions of water with DMSO or EG (5%<sub>vol</sub>) and/or Zonyl (0.04%<sub>mass</sub>) as additives.

For the soft blade deposition, a high molar mass neutral polymer (PEO<sub>8000</sub> kDa) was used to increase the elasticity of the ink.

## 2.2.4 Characterization of PEDOT:PSTFSI solutions

The solutions were then characterized in terms of rheological behaviors.

An Anton Paar MCR302 rheometer was used with a CP50-1° geometry (cone 50 mm – 1° / plate) [Figure 2.9]. Different temperatures, shear rates and shear stresses were applied to measure the shear viscosity and viscoelastic behavior of the solutions.

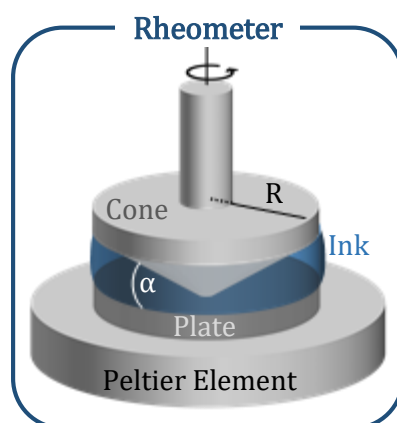


Figure 2.9: Rheometers schematic with a cone / plate geometry

A Krüss Drop Shape Analyzer DSA100 was used with a pendant drop method and a Young-Laplace model<sup>21,22</sup>:  $\Delta P = (P_{int} - P_{ext}) = \Gamma \left( \frac{1}{R_1} + \frac{1}{R_2} \right)$  where  $\Gamma$  is the surface tension of the fluid,  $\Delta P$  is the pressure difference at the interface between the drop and the surrounding air,  $R_1$  and  $R_2$  are the principal radii of the drop. For concentrated solutions with gel behaviors, it was not possible to use this technique. In that case, the surface tension was measured using Tate's law<sup>23,24</sup>:  $m_{drop} \times g = 2\pi \times r_{capillary} \times \Gamma$  where  $\Gamma$  is the surface tension of the fluid,  $m_{drop}$  is the weight of one drop,  $r_{capillary}$  is the internal radius of the needle, and  $g$  is the gravitational force.

The structure of the complex PEDOT:PSTFSI in solution was determined by liquid Atomic Force Microscopy (AFM), Dynamic Light Scattering (DLS) and cryo-Scanning Electron Microscopy (cryo-SEM). Liquid AFM was performed on a Bruker Dimension FastScan AFM, with very diluted solutions of polymers deposited on HOPG (Highly Ordered Pyrolytic Graphite) using a tapping mode. Hydrodynamic radius was extracted from DLS measurement of diluted solutions of PEDOT:PSTFSI done on a ALV / CGS-3 Compact Goniometer System equipped with a helium-neon laser ( $\lambda=632.8$  nm).

Cryo-Scanning Electron Microscopy (cryo-SEM) was performed at BIC (Bordeaux Imaging Center) (Zeiss Gemini 300) platform. The solutions were frozen with high pressure freezing (HPF) to obtain amorphous water ice not to damage the polymer during the freezing with ice crystals

(250 bars / liquid nitrogen / 6 s). The frozen solutions were then sublimated (10 – 20 min at 95°C) and observed at 3 kV.

After characterizing the solutions, and before depositing the solutions, substrates need to be prepared.

## 2.2.5 Substrate preparation

Generally, microscope slides were used as substrates. Before printing, they were cleaned by sonication for 15 minutes in ethanol, acetone and isopropanol, respectively. Some depositions were done on poly(ethylene terephthalate) (PET). In this case, the PET was rinsed with acetone and dried with compressed air.

To change the wetting properties of the glass substrates, glass slides were silanized [Figure 2.10]. The purpose of this reaction is to functionalize a hydrophilic surface containing hydroxyl groups (like glass) and render it hydrophobic. The slides were cleaned as before, dried over night in an oven at 100°C, treated 15 min by UV-ozone, placed 20 min in a glass container filled with a solution of 0.5 %<sub>vol</sub> Octadecyltrichlorosilane (OTS)<sup>25</sup> in toluene,<sup>26</sup> then placed in chloroform bath for a few hours before being rinsed with toluene. A Krüss Drop Shape Analyzer DSA100 was used with a contact angle method to check the surface free energy of the silanized glasses:  $20 \pm 3$  mN/m were found with almost only a dispersive contribution. In contrast, the surface free energy of untreated glass was measured at  $60 \pm 39$  mN/m and of PET at  $40 \pm 18$  mN/m. The contact angle of water drops on the silanized glass obtained is  $105 \pm 1^\circ$ , while the contact angle of water on untreated glass is  $15 \pm 3^\circ$ , and  $66 \pm 2^\circ$  on PET.

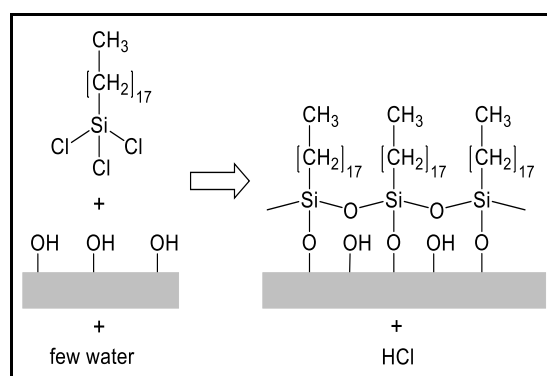


Figure 2.10: Silanization reaction on hydrophilic substrate. (adapted from<sup>27</sup>)

For conductive AFM, ITO substrates were used, as well as glass substrate on which 10 nm of chrome and 100 nm of gold were thermally evaporated. Some of these gold substrates were then rendered more hydrophobic using one hour bath of octane-thiol concentrated at 0.01 mol/L in ethanol.<sup>28</sup> For small substrates, the contact angle increases from  $91 \pm 3^\circ$  to  $103 \pm 1^\circ$ . For large

substrates, used for the soft blade deposition, the contact angle only increases from  $81 \pm 6^\circ$  to  $97 \pm 1^\circ$  for a three days bath.

## 2.2.6 Deposition and drying of PEDOT:PSTFSI solutions

Four depositions processes were used: doctor blade to deposit flat tint, screen-printing, inkjet printing and soft blading to print patterns (with and without contact) [Figure 2.11].

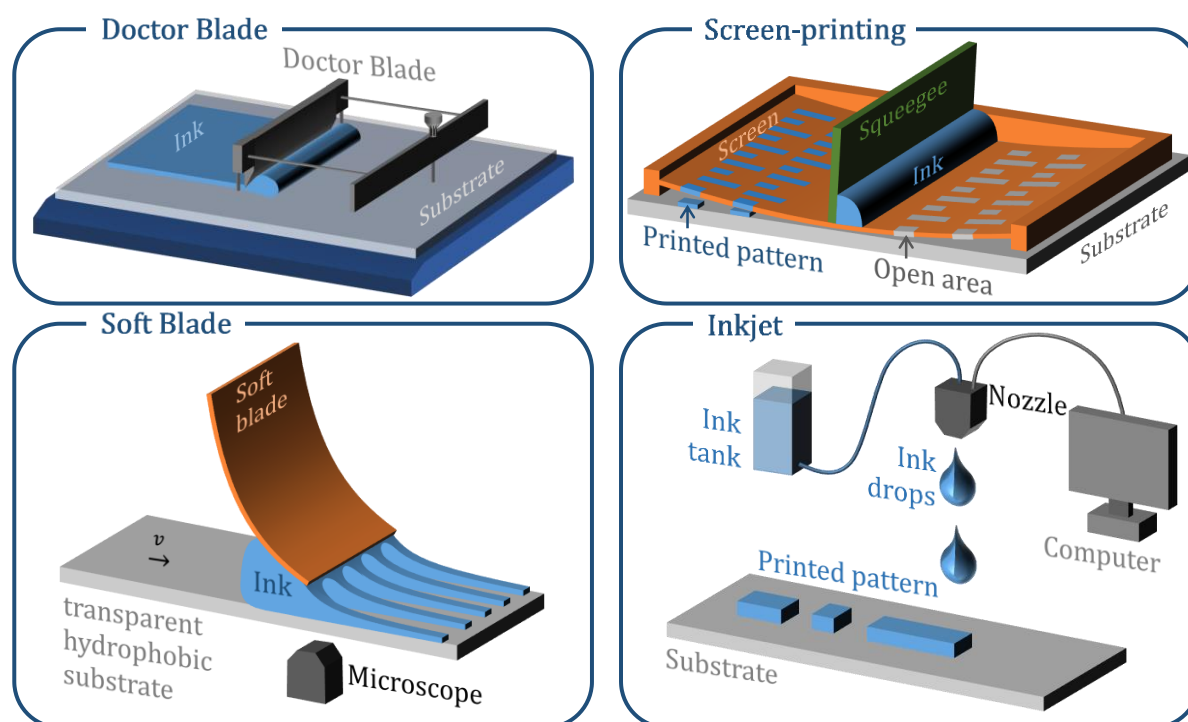


Figure 2.11: Schematics of the deposition processes: doctor blade, screen-printing, soft blade and inkjet

An Erichsen Doctor Blade was used to deposit inks on microscope slides with different air gaps (between 50 and 150  $\mu\text{m}$ ) and speeds (5 or 10 mm/s).

A single nozzle Microfab Jetlab4 inkjet printer was used with a MJ-ATP-01-050 nozzle. Different parameters were adjusted to stabilize drops. Printing was done on glass.

For screen-printing, a mask was first created on a screen (mesh size of 150 wires/cm with a diameter of the wires of 30  $\mu\text{m}$ ) [Figure 2.12]: the designed pattern was printed firstly with a Studio 3005AC Toshiba copier two times on PET to create a mask. Then a CDF Vision 15  $\mu\text{m}$  emulsion (a diazo dual-cure capillary film) was placed on the screen with deionized-water. After drying, the mask was exposed 7 minutes to UV-light and then revealed using a Kärcher pressure washing. An EKRA X5 screen-printer was then used with squeegee in modified polyurethane and the dried screen. The ink was deposited with a pressure of 120 N, an air gap between the screen and the substrate of 1 mm, and a squeegee speed of 180 mm/s.

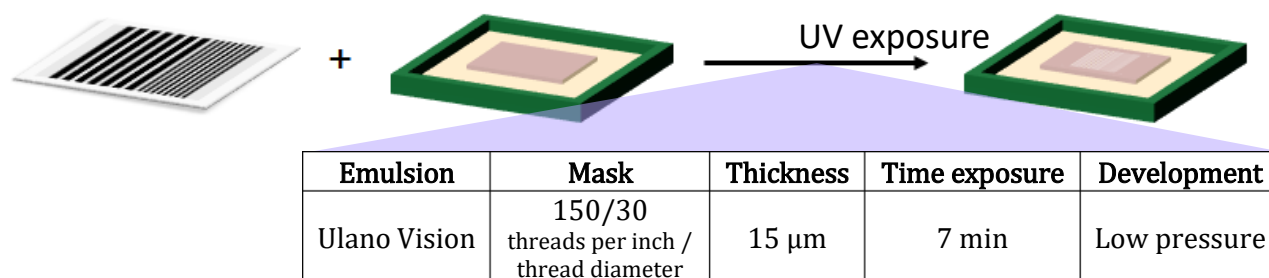


Figure 2.12: Creating a screen with mask for screen-printing

For the last process, a soft blade was used. The purpose of this deposition is to create lines of a water-based polymeric ink on a hydrophobic substrate by using the instability of the contact line near the soft blade. It has been shown that lines should be obtained for highly shear-thinning polymer solution.<sup>25</sup> A soft blade (a sheet of Mylar 1.5 x 4 cm<sup>2</sup> with a thickness of 200  $\mu\text{m}$ ) was fixed to a Marzhauser Wetzlar (SCAN IM 130 x 100) translation stage on a Zeiss Axio observer A1 inverted microscope. Depositions were done at speed from 0.02 mm/s to 20 mm/s on silanized glass or gold treated with octane-thiol and recorded with a Hamamatsu Orca flash 2.8 fast camera.

After deposition, PEDOT:PSTFSI films were dried 5 minutes at 120°C. For the last deposition, the lines dried before the end of the deposition at ambient temperature.

After deposition of the solutions and drying of the films, they were characterized using different techniques.

## 2.2.7 Characterization of the depositions

To characterize the topology of the films, two techniques were used. A Bruker Dimension FastScan AFM (in solid state and tapping mode) allows the determination of the topology of surfaces from 30 by 30 to 1 by 1  $\mu\text{m}^2$ . A conductive mode was also employed to measure the surface conductivity of the films. While a Jeol 7800-E Prime Scanning Electron Microscope (SEM) enables the observation from very large scale of the film (700  $\mu\text{m}$ ) to very low scale (up to 0.5  $\mu\text{m}$ ). It was used with a GBSH (Super-High resolution Gentle Beam) mode to see the PEDOT films without having to metalize it, and so it was possible to see the polymer itself and not the cracks of the platinum.

To obtain the conductivity  $\sigma$  of the films, the thickness  $t$  was firstly measured with a Bruker Dektak XT-A profilometer, and the sheet resistance  $R_s$  with a Jandel RM3-AR four point probes. The conductivity was then calculate using the relation:  $\sigma = \frac{1}{t \times R_s}$ .

## 2.3 PEDOT:PSTFSI inks characterization

In the following part, the properties of PEDOT:PSTFSI inks will be discussed, starting with the structure of the inks, then their rheological properties in shear and extension, and finally their wettability behavior. The aim is to formulate the PEDOT:PSTFSI inks for different deposition processes. Two important properties control the processability of the inks: the rheological properties controlled by the concentration as well as the structure of the polymers, and the wetting properties, partially controlled by the surface tension of the inks (which has to be compared with the free surface energy of the substrate).

### 2.3.1 Polymer structure and conformation in solution

The structure of commercial PEDOT:PSS solutions and of home-made PEDOT:PSTFSI solutions was determined by three different methods: Dynamic Light Scattering (DLS), liquid Atomic Force Microscopy (AFM), and cryo-Scanning Electron Microscopy.

The hydrodynamic radii of the complex PEDOT:PSTFSI<sub>80 kDa</sub>, and of the commercial PEDOT:PSS<sub>PH 1000</sub> were extracted from DLS measurements on very diluted solutions. Figure 2.13 displays the normalized correlation function  $g$  measured for a very diluted PEDOT:PSTFSI<sub>80 kDa</sub> solution at five different angles, and the corresponding fit function:  $g(t) = e^{-t/T}$  where  $T$  is the relaxation time following the relation  $\frac{1}{T} = 2Dq^2$  with  $q = \frac{4\pi n \sin(\theta/2)}{\lambda}$  the wave vector,  $D$  the diffusion coefficient,  $n$  the refractive index of the solvent (1.33 for water), and  $\lambda$  the wavelength of the laser. The hydrodynamic radius  $R_h$  can then be extracted from the Stokes-Einstein law:  $D = \frac{kT}{6\pi R_h \eta}$ , where  $k = 1.380649 \cdot 10^{-23}$  J/K is the Boltzmann constant,  $T$  the temperature in kelvin degree,  $\eta$  the solvent viscosity, and  $D$  the diffusion coefficient.<sup>29,30</sup>

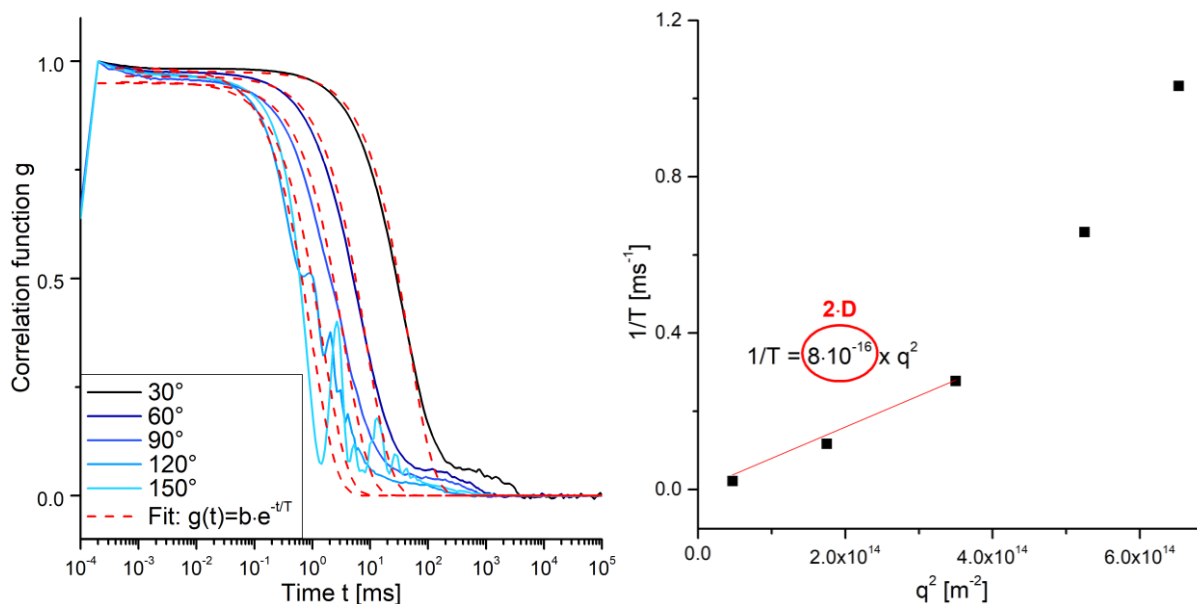


Figure 2.13: a) Correlation function  $g$  recorded during 15 min of a diluted solution of PEDOT:PSTFSI<sub>80 kDa</sub> at five different angles (30°, 60°, 90°, 120° and 150°) with corresponding exponential fit, and b) the inverse of the relaxation time versus the wave vector.

Ink	$R_h$ [nm]
PEDOT:PSS <sub>PH 1000</sub>	425-480
PEDOT:PSTFSI <sub>80 kDa</sub>	510-570

Table 2.2: Hydrodynamic radius of two PEDOT:polyanion inks

Hydrodynamic radius around 510 – 570 nm was obtained for PEDOT:PSTFSI<sub>80 kDa</sub> solution, and around 425 – 480 nm for commercial PEDOT:PSS<sub>PH 1000</sub>. Solutions [Table 2.2].

Further characterization of the complex was performed using liquid AFM and cryo-SEM. Liquid AFM allows the visualisation of the topology of polymers in very diluted solutions deposited on HOPG (Highly Ordered Pyrolytic Graphite) [Figure 2.14]: the complex PEDOT:PSTFSI<sub>80 kDa</sub> forms aggregates while PEDOT:PSS (PH 1000 or IJ 000) chains stay far one from each other. In any cases, the polymers sink to the substrate. The measured thickness of one polymeric chain is in the range of a few nanometers (1.5 – 4 nm), and a width in the range of 10 – 30 nm. The difference of one order of magnitude between the thickness and the width can be explained by the fact that the polymer lies flat on the substrate during the measurement.

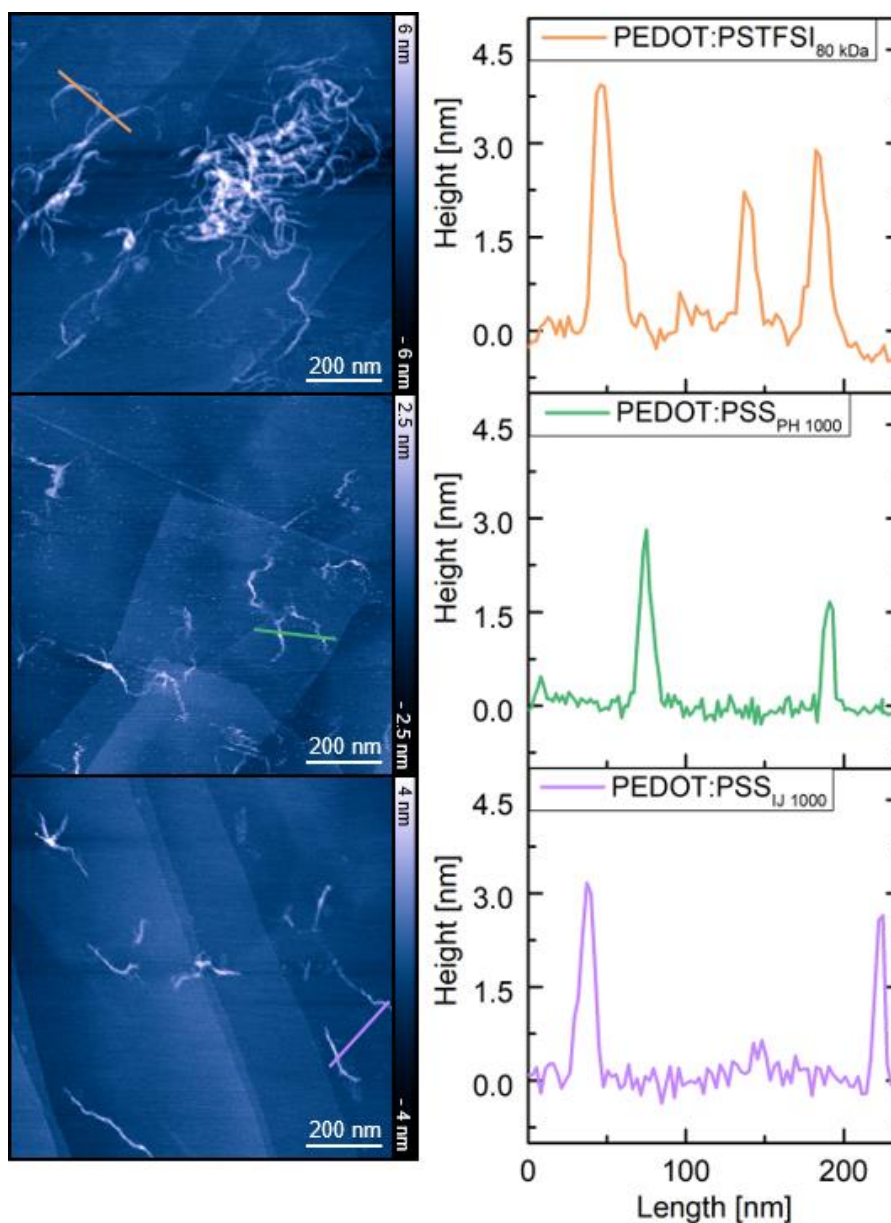


Figure 2.14: liquid AFM images (tapping mode) of very diluted PEDOT:PSTFSI<sub>80 kDa</sub>, commercial PEDOT:PSS<sub>PH 1000</sub> and PEDOT:PSS<sub>IJ 1000</sub> in water on HOPG (Highly Ordered Pyrolytic Graphite) and respective profiles.

Cryo-SEM measurements were done on solutions of PEDOT:PSTFSI<sub>80 kDa</sub> concentrated at 1 %<sub>wt</sub> [Figure 2.15] and 0.5 %<sub>wt</sub> [Figure 2.16], and on one solution of PEDOT:PSS commercial (PH 1000) [Figure 2.17]. For both inks with PSTFSI as polyanion [Figure 2.15 and Figure 2.16], a random network was found, and the thickness of one PSTFSI chain was estimated in the order of 4 – 10 nm, which is in accordance with the values found in AFM. Small particles are also visible beside the long polyanionic chains and should be PEDOT chains: their dimensions are in the order of 5 – 15 nm. For the lower concentration, the structure started to collapse because of the high sublimation needed (with lower sublimation, nothing was visible).

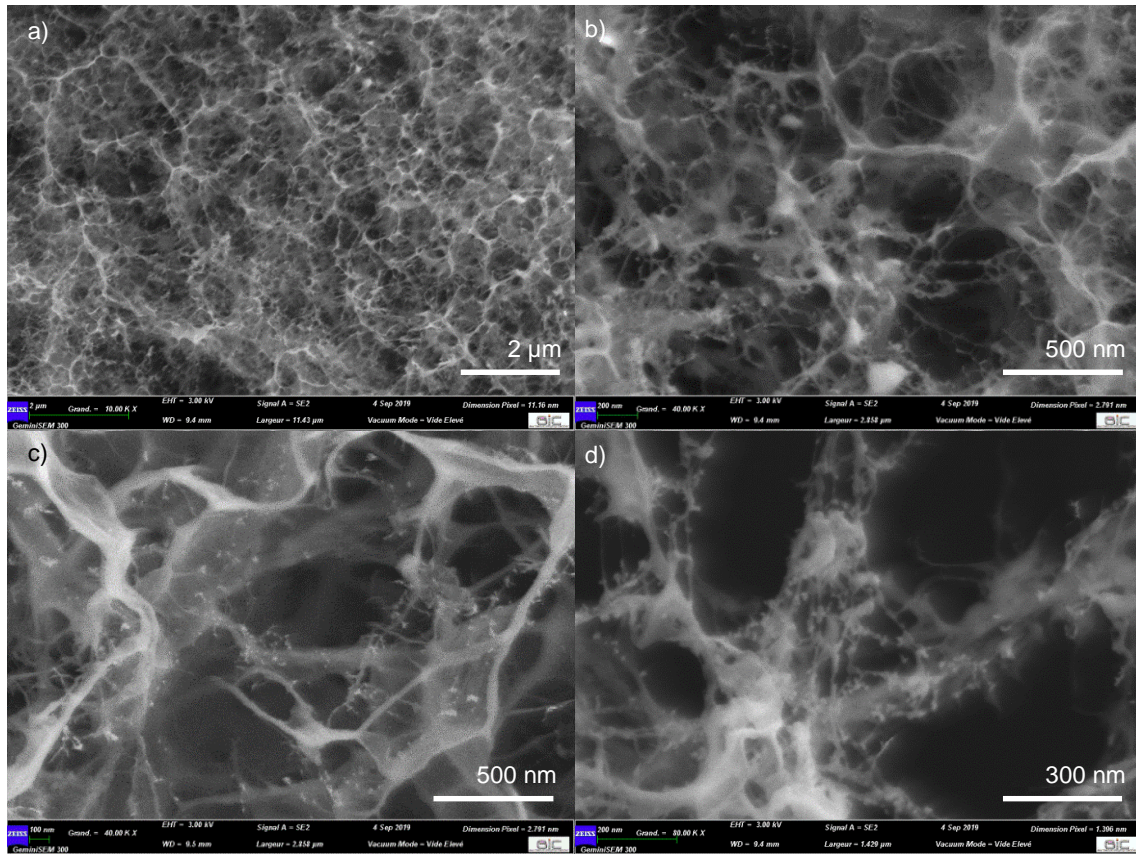


Figure 2.15: Scanning Electron Microscopy (SEM) pictures of a solution of PEDOT:PSTFSI  $_{80}$  kDa concentrated at 1 %wt sublimated 10 min at  $-95^{\circ}\text{C}$  (x10K, x40K, x40K, x80K respectively)

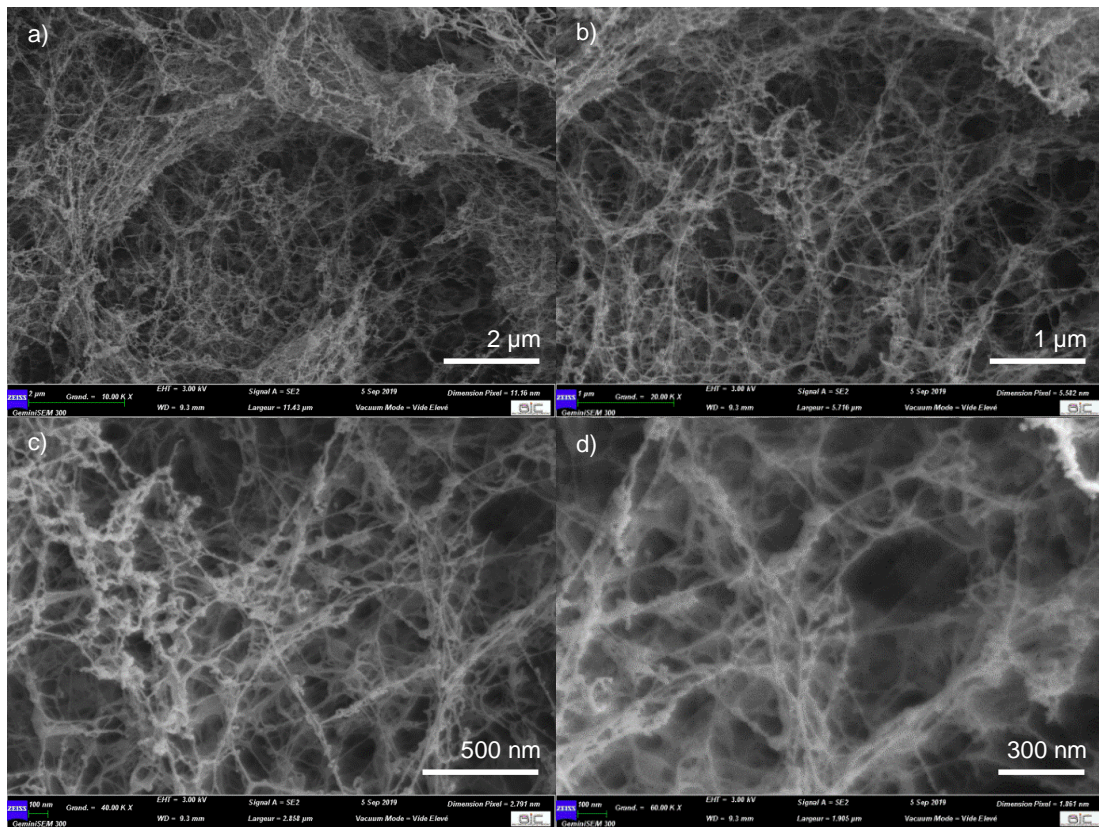


Figure 2.16: Scanning Electron Microscopy (SEM) pictures of a solution of PEDOT:PSTFSI  $_{80}$  kDa concentrated at 0.5 %wt sublimated 20 min at  $-95^{\circ}\text{C}$  (x10K, x20K, x40K, x60K respectively)

For the PEDOT:PSS<sub>PH 1000</sub> ink, a well organised matrix structure in the shape of honeycomb was found [Figure 2.17]. This structure could perhaps be explained by the utilisation of monodisperse molar mass polyanion, or by the addition of unknown additives in this commercial ink. The sublimation was not complete to keep the spatial structure. Figure 2.17.c shows one block turned over after the sublimation: all the filled walls are amorphous glass of water. The structure started to collapse in Figure 2.17.d. The thickness of one PSS polymeric chain was found in the order of 7 – 13 nm, and the small PEDOT chains in the order of 14 – 18 nm.

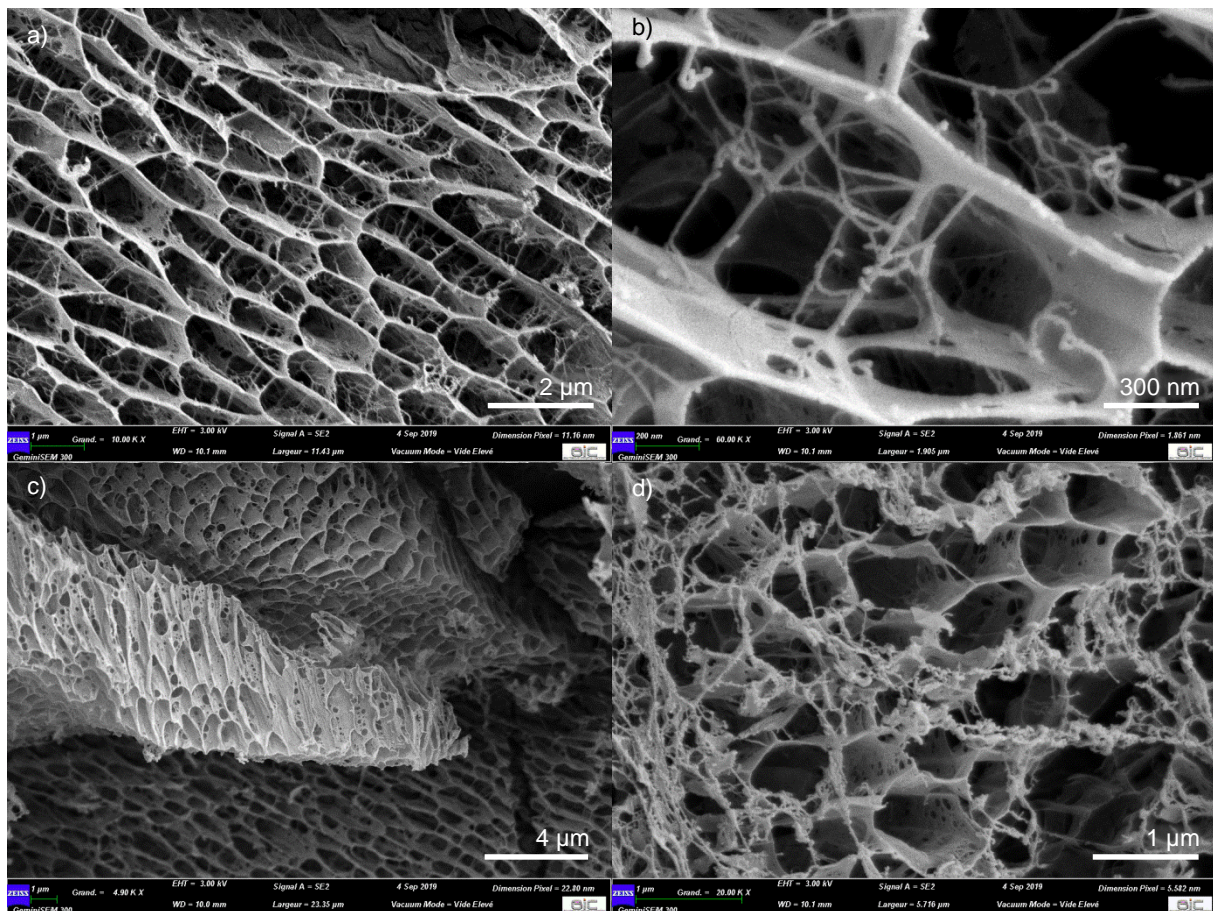


Figure 2.17: Scanning Electron Microscopy (SEM) pictures of a solution of PEDOT:PSS<sub>PH 1000</sub> sublimated 20 min at -95°C (x10K, x60K, x5K, x20K respectively)

In the case of the three inks, the polymers are then homogeneously distributed and form a network.

The rheological measurement resulting from those structural properties will be explored in the next part.

### 2.3.2 Shear rheology: from Newtonian to shear thinning behavior

Rheological measurements of PEDOT:PSTFSI solutions at different concentrations are displayed in Figure 2.18. Shear rate  $\dot{\gamma}$  ramp were applied and corresponding shear stress  $\tau$  were recorded. The viscosity was then obtained with the relation  $\eta = \frac{\tau}{\dot{\gamma}}$ .

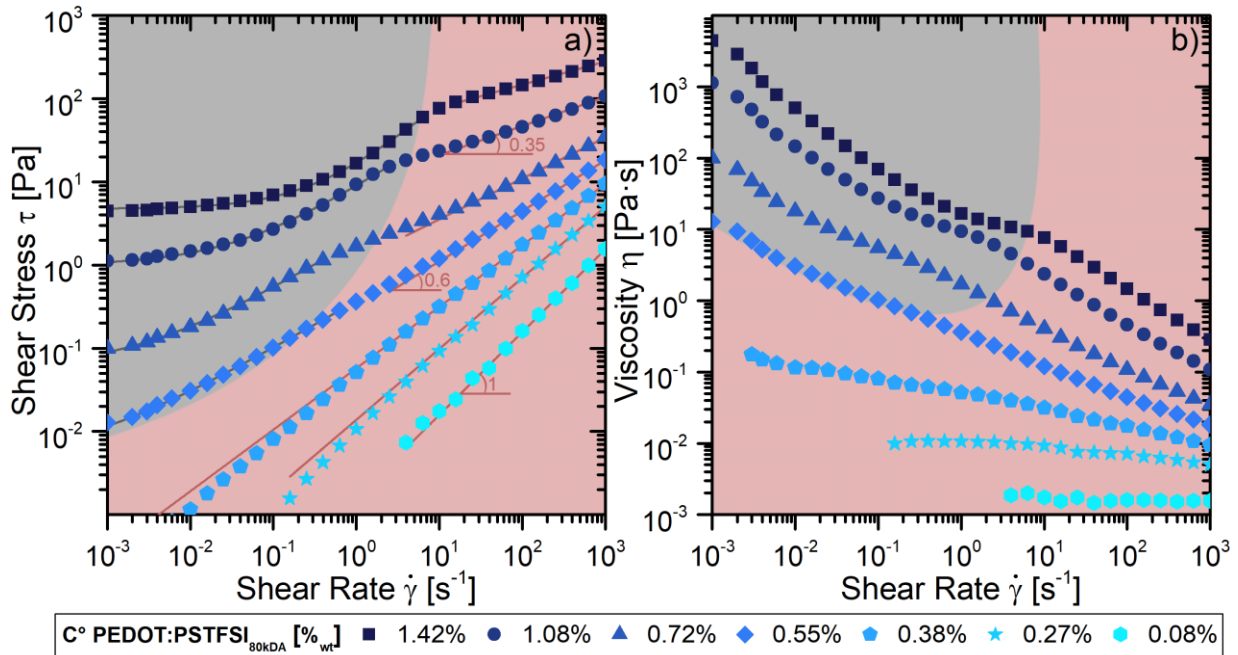


Figure 2.18: Rheological behavior of PEDOT:PSTFSI inks measured with a shear rheometer (cone plate geometry: 50 mm diameter and  $1^\circ$  angle): a) shear stress versus shear rate and b) viscosity versus shear rate obtained by applying shear rate ramps at  $18^\circ\text{C}$ . The lines are fits to the data using the power model (red) or the HB model (grey). The numbers are the values of the parameter  $n$ .

For low concentrations, the stress varies linearly with the shear rate. In consequence, the viscosity is almost constant: the solutions behave as Newtonian fluids. By increasing the concentration, the viscosity becomes shear dependant. This can be modeled using the power-law (PL) model<sup>31</sup>  $\tau = k\dot{\gamma}^n$ . For higher concentrations, two regimes appear. The fluid continues to behave as a PL fluid for high shear rates. However, for lower shears the rheological behavior changes and the Herschel-Bulkley (HB) model<sup>32</sup> becomes more relevant:  $\tau = \tau_0 + k\dot{\gamma}^n$ .

Two regimes are therefore observed (grey and red regions in Figure 2.18). In the grey region, for low shear rate and high concentrations, the solutions behave according to the HB model. In the red region on the other hand, the yield stress is either too low to be measured or completely absent and the solutions behave as PL fluids. Figure 2.19 shows the yield stress  $\tau_0$  [Figure 2.19.a] and the flow behavior index  $n$  [Figure 2.19.b]. The yield stress becomes measurable after a threshold near 0.5 %<sub>wt</sub> and increases with the concentration. The flow behavior index  $n$  starts near 1 for low concentrations, which behave as Newtonian fluids, and decreases with the increase of the concentration, indicating that the ink becomes more and more

shear thinning. The value of  $n$  extracted in the HB regime depends mildly on concentration and has a value near 0.6. For the high concentrations, the increase in shear rate at which the change in regime for a HB to a PL fluid occurs is not constant and increases with the concentration. We believe that this change in behavior comes from the fact that the PSTFSI polyanion creates hydrogen bonds near the nitrogen atom<sup>33</sup> [Figure 2.20] and that the yield stress is the result of these hydrogen bonds. This is consistent with the increase in the yield stress with concentration. The increase in shear must break such bonds and therefore drastically reduce the yield stress and induce a change in the rheological behavior from an HB fluid to a PL fluid.

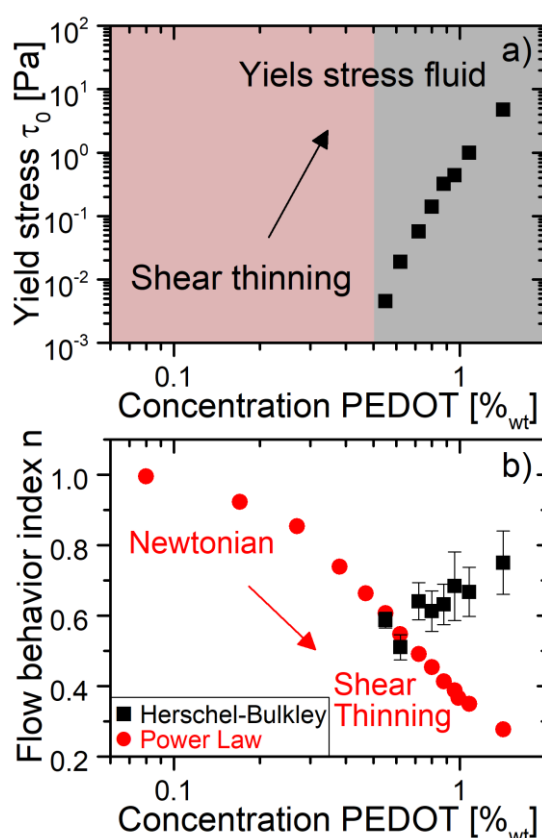


Figure 2.19. Herschel-Bulkley regime (grey region) and power-law regime (red region) parameters obtained from the shear stress curves of PEDOT:PSTFSI<sub>80kDa</sub> inks [Figure 2.18]: a) yield stress  $\tau_0$  and b) flow behavior index  $n$ .

Besides concentration effects, both the viscosity and the yield stress can be varied by changing the molar mass of the polyanion. Experiments using different molar masses of the polyanion have shown that higher molar masses lead to higher viscosities as expected. Further, increasing the molar mass also increases the yield stress: for a polyanion of 250 kDa molar mass instead of 80 kDa as for the above results, the yield stress increases by almost an order of magnitude for identical concentrations [Figure 2.21].

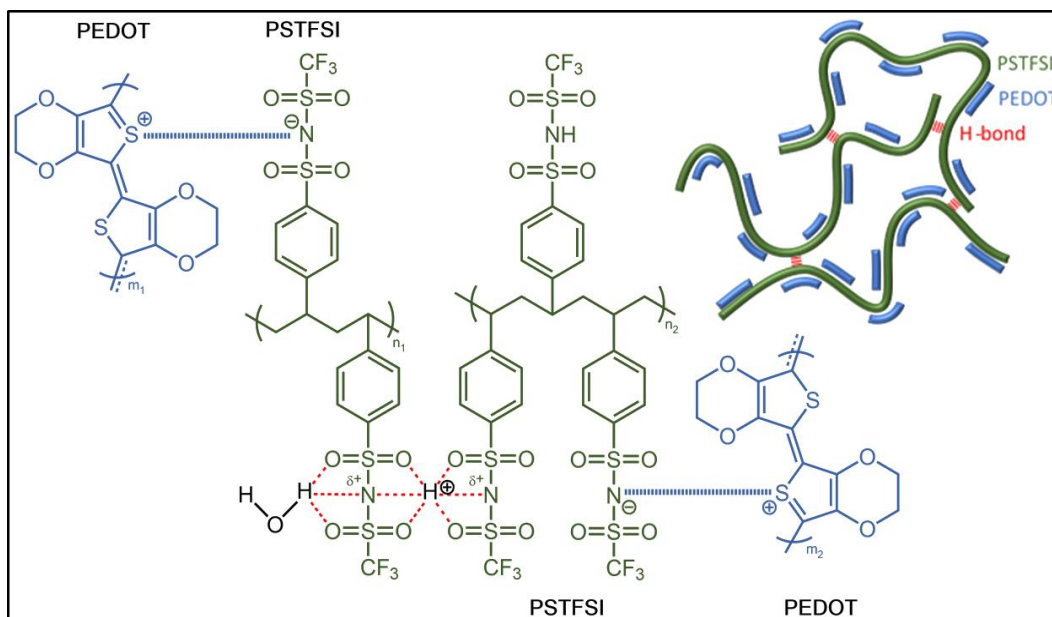


Figure 2.20: Structure and schematic representation of the complex PEDOT:PSTFSI (poly(3,4-ethylene dioxythiophene):poly(4-styrene trifluoromethyl (bissulfonylimide))) showing probable hydrogen bonds<sup>33</sup> between polyanions.

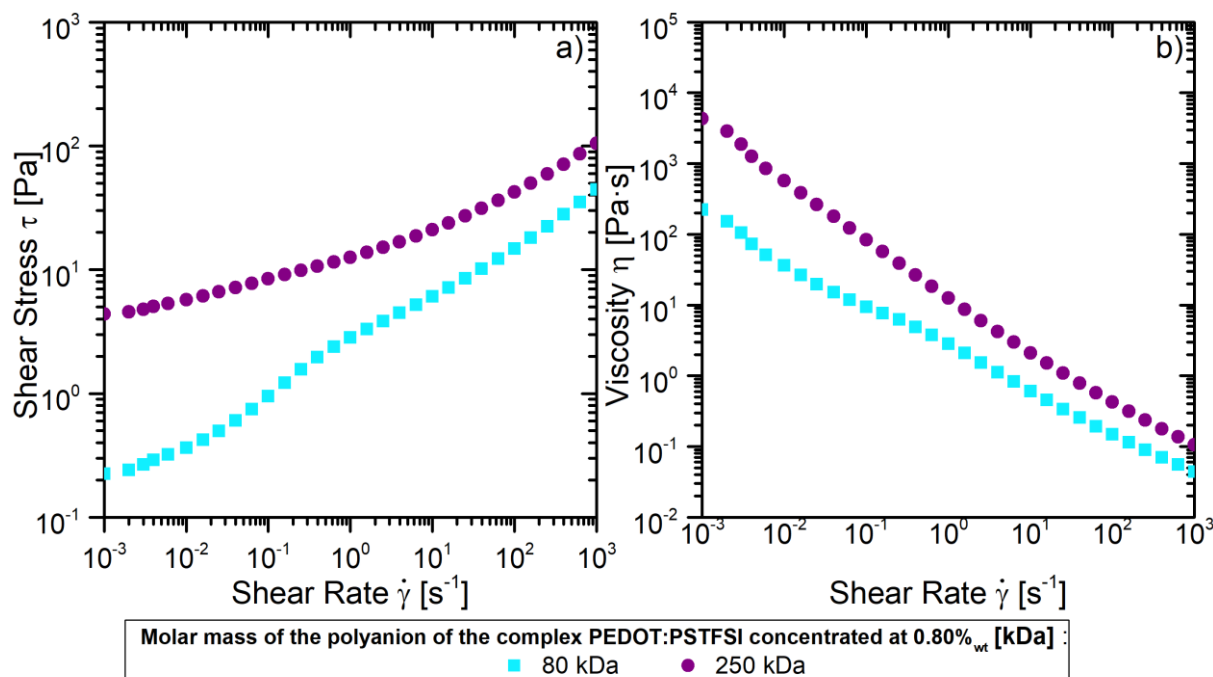


Figure 2.21: Rheological behavior of PEDOT: PSTFSI inks of two different molar masses (80 and 250 kDa) measured with a shear rheometer (cone plate geometry: 50 mm diameter and 1° angle): a) shear stress versus shear rate and b) viscosity versus shear rate obtained by applying shear rate ramps at 18°C.

Similar behavior was found in extensional rheology [See Appendix A.2].

### 2.3.3 From liquid to gel like solutions

To complete the above rheology measurements, dynamic oscillatory stress sweep measurements were performed: a sinusoidal shear stress  $\tau(t) = \tau_A \cdot \sin(\omega t)$  is imposed to the fluid and the corresponding deformation  $\gamma(t) = \gamma_A \cdot \sin(\omega t + \varphi)$  is measured (where  $\gamma_A$  and  $\tau_A$  are amplitudes,  $\omega = 2\pi \cdot f$  is the imposed angular frequency which was fixed at  $2\pi$ , and  $\varphi$  is the phase shift between the deformation and the shear stress). The complex dynamic modulus  $G^*$  is then expressed as:  $G^* = \frac{\tau(t)}{\gamma(t)} = G' + iG''$  where the storage modulus  $G'$  and loss modulus  $G''$  represent the elastic and viscous parts of the viscoelastic behavior. When  $G'$  is higher than  $G''$ , the ink has a gel-like behavior.<sup>34</sup> The higher  $G'$  and  $G''$  are, the more elastic the gel is. The gel behaviors of PEDOT:PSTFSI<sub>80kDa</sub> inks are displayed in Figure 2.22. For concentrations under 0.55 %, i.e. in the red region where we have previously shown that the ink has no yield stress, the ink is more viscous than elastic. By increasing the concentration,  $G'$  and  $G''$  increase and  $G''$  becomes smaller than  $G'$ : the ink becomes more elastic. The limit between the two regimes appears when  $G' = G'' \approx 50$  mPa and corresponds to a concentration of about 0.6 %. This is precisely where the H.B. behavior sets in and the solution becomes a yield-stress fluid.

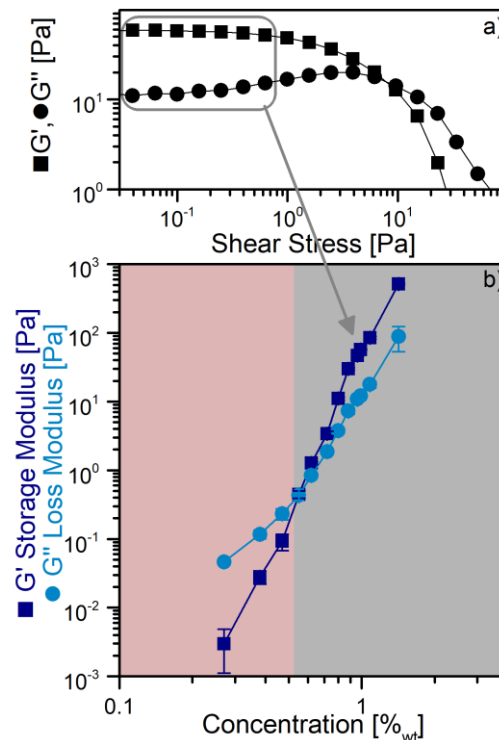


Figure 2.22. Rheological behavior of PEDOT:PSTFSI inks measured with a shear rheometer (cone plate geometry 50 mm /  $1^\circ$ ): a) storage  $G'$  and loss  $G''$  modulus obtained at a frequency of 1 Hz at  $18^\circ$  C for PEDOT:PSTFSI<sub>80 kDa</sub> at 0.99 %wt in water versus stress. b) average value of  $G'$  and  $G''$  in the linear viscoelastic range (i.e. in the plateau region of Figure 2.22.a) versus concentration.

For a polyanion with higher molar mass, both storage and loss moduli increase at identical concentrations, as if the curves of  $G'$  and  $G''$  were shifted to higher concentration for the higher

molar mass although the weight concentration and the number of atoms are the same. That could be explained by the fact the higher molar mass means a larger number of nitrogen sites on one polyanion chain, which can result in hydrogen bounds with more polymers and so increases both the viscosity and the storage and loss moduli.

M <sub>w</sub> of the polyanion	Moduli of PEDOT:PSTFSI 0.8 %wt	
	G'	G''
80 kDa	11.0±0.6	3.8±0.3
250 kDa	53.1±12.0	17.4±3.8

*Table 2.3: Rheological behavior of PEDOT:PSTFSI inks of two different molecular weight (80 and 250 kDa) concentrated at 0.8 %wt and measured with a shear rheometer (cone plate geometry 50 mm/1°): storage G' and loss G'' modulus obtained at a frequency of 1 Hz at 18°C. The average of G' and G'' in the linear viscoelastic range are displayed.*

To summarize these rheology measurements, we have shown that the viscosity and elasticity of PEDOT:PSTFSI inks can be tuned by simply varying the concentration. This renders the formulation of such inks simple for different deposition processes going from inkjet printing which requires low viscosity Newtonian solutions to screen printing which requires elastic fluids. Changing the molar mass of the polyanion is also another means to tune the rheological behavior as it changes the viscosity, the yield stress, as well as the elasticity of the solutions.

PEDOT:PSTFSI solutions compare favorably with commercial PEDOT:PSS inks. For example, the properties of two commercial inks, Orgacon IJ 1000 (from Sigma Aldrich) and Clevios PH 1000 (from Heraeus), which can be used in inkjet printing, were measured. A slightly shear thinning behavior for the two inks was found with values of the viscosities in the range 0.3 – 1.4 Pa.s for 10<sup>-3</sup> s<sup>-1</sup> and 0.01 – 0.02 Pa.s for 10<sup>3</sup> s<sup>-1</sup>. The storage and loss moduli for the two solutions were, respectively,  $G' = 0.44 \pm 0.01 \text{ Pa} < G'' = 0.71 \pm 0.01 \text{ Pa}$  and  $G' = 0.11 \pm 0.01 \text{ Pa} < G'' = 0.50 \pm 0.01 \text{ Pa}$ . Another commercial ink used in screen-printing, Orgacon EL-P 5015 (from Sigma Aldrich) was characterized: a high shear thinning behavior was found with viscosities in the range 1.2 · 10<sup>5</sup> Pa.s for 10<sup>-3</sup> s<sup>-1</sup> and 1.7 Pa.s for 10<sup>3</sup> s<sup>-1</sup>, and a storage modulus  $G' = 237 \pm 6 \text{ Pa}$  higher than the loss modulus  $G'' = 99 \pm 2 \text{ Pa}$ . To obtain this behavior for the commercial inks, PEDOT:PSS inks have to be concentrated to more than 5 %wt, which is energy and time consuming. It must be emphasized that commercial PEDOT inks are already formulated complex fluids with a variety of different additives to tune their rheological properties. For the PEDOT:PSTFSI solutions studied here, only the concentration was changed to go from fluid like solutions to gel like ones.

### 2.3.4 Wettability: inks' surface tension versus substrate's surface energy

While rheology controls a number of properties relevant to the processing of inks, another important feature is the wettability of the substrate. The wettability is in part controlled by the surface tension of the solution: adapting surface tensions allows good wetting and a good adhesion of the ink onto the substrate. The inks used here have therefore been characterized by measuring their static surface tensions  $\Gamma$  [Table 2.4]. For dilute solutions of PEDOT:PSTFSI (0.5 %<sub>wt</sub>) we obtain the same surface tension as water ( $\approx 72$  mN/m). By adding 0.04 %<sub>wt</sub> surfactant (Zonyl FS-300 fluorosurfactant) or more to PEDOT:PSTFSI, the surface tension of the inks decreases drastically to almost 24 mN/m. The concentration 0.04 %<sub>wt</sub> of surfactant was chosen as it is above and near the critical micelle concentration of the surfactant in pure water [Figure 2.7].

For higher concentrations of PEDOT:PSTFSI (near 1 %<sub>wt</sub>) without surfactant, we obtain a surface tension of roughly 55 mN/m. For these high concentrations, the PSTFSI itself is surface active as solutions of this polyanion at a concentration of 1 % have surface tensions near 60 mN/m [Figure 2.23]. The addition of surfactant (0.04 %<sub>wt</sub> of Zonyl FS-300) to these high concentration solutions reduces the surface tension further to values near 24 mN/m. The addition of surfactant may change the rheology of the solutions, however, measurements with and without surfactant show similar viscosities [Figure 2.8 and Table 2.1].

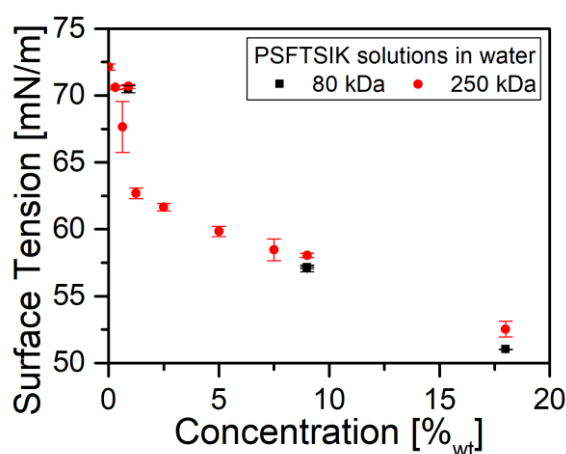


Figure 2.23: Surface tension of solutions of PSTFSIK in water for different concentrations.

More stable drops after ejection were obtained when surfactant was added in the solution, most likely because of a worse wettability with the nozzle.

Solution	Surface tension $\Gamma$ [mN/m]	
	Pendant drop	Tate's Law
Water (formulated with DMSO, or EG, or pure water) without surfactant	69±2	70
Water (formulated with DMSO, or EG, or pure water) with surfactant (Zonyl)	24±1	20
PEDOT:PSS <sub>PH 1000</sub>	69±1	-
PEDOT:PSS <sub>IJ 1000</sub>	26±1	-
PEDOT:PSTFSI <sub>90 kDa</sub> < 0,5 % <sub>wt</sub>	72±1	70
PEDOT:PSTFSI <sub>90 kDa</sub> < 0,5 % <sub>wt</sub> + surfactant	24±2	-
PEDOT:PSTFSI <sub>90 kDa</sub> 0.96 % <sub>wt</sub>	-	55

Table 2.4: Surface tension of water (formulated with DMSO or EG or pure water) with or without surfactant, PEDOT:PSS solutions (PH 1000 and IJ 000), PEDOT:PSTFSI<sub>90 kDa</sub> at different concentrations.

For inkjet printing, surfactant must be added not only to have stable drops, but also for better wettability of the substrate. Indeed, in the absence of surfactant, dewetting of drops on a glass substrate is observed leading to non-homogeneous films. Addition of surfactant in this case, improves the homogeneity of the films.

For doctor blade processing, the 1 %<sub>wt</sub> PEDOT:PSTFSI allowed a good deposition on glass surfaces without need of surfactant. However, surfactant must be added for plastics substrate like PET: the surface tension of the liquid needs to be lower than the surface energy of the substrate to have a complete wettability. The surface energy of glass was measured at  $60 \pm 39$  mJ/m<sup>2</sup> with an equal polar and dispersive part compared to the one of PET which was measured at  $40 \pm 18$  mJ/m<sup>2</sup> with a polar part ten times lower than the dispersive part. For the 1 %<sub>wt</sub> PEDOT:PSTFSI, good wettability is obtained on glass (contact angle of 15°) while on PET the contact angle is four times higher and surfactant has to be added for good wettability.

For screen-printing, the screen has, with its roughness, a surface free energy of  $20 \pm 1$  mN/m almost completely dispersive ( $18.5 \pm 1$  mN). As we will see below, this partially explains the difficulty of the ink to flow through the mesh of the screen and the consequent inhomogeneity of the films obtained. The addition of surfactant in this case does not change the outcome considerably.

## 2.4 PEDOT:PSTFSI inks processing: inkjet printing, doctor blading, screen-printing, and soft-blading

In general and in order to process inks using different techniques, different formulations have to be used. These formulations based on the use of different additives, adapt the rheological properties of the inks to the requirements of the printing technique. For example, inks for inkjet printing need to be of low viscosity and possess little elasticity. On the other hand, inks adapted for doctor blading need to be shear thinning and, ideally, possess a yield stress. For screen-printing applications, gel like shear thinning solutions are preferred. In all these cases, the wetting properties of the inks on the substrates used have to be controlled as well.

The interest of the present system (PEDOT:PSTFSI), as it was shown in part 2.3, is that one can go from a very fluid system to a gel like solution by simply changing its concentration. A change of the polyanion molar mass is also another means to modify the solution behavior. Thus, as far as the rheology is concerned, the formulation is simple.

These solutions can also be formulated to tune the wettability of the substrates through the addition of surfactant. For PEDOT based systems, it has also been shown that the addition of a high boiling point solvent (dimethyl sulfoxide (DMSO) or ethylene glycol (EG)) can enhance the conductivity of the films several fold.<sup>19</sup> For this purpose, we have used 0.04 %<sub>wt</sub> surfactant (Zonyl FS-300 fluorosurfactant) to enhance the wettability of the glass substrates used and 5 %<sub>vol</sub> of a high boiling point solvent (DMSO, but test using EG have also been carried out with similar results) to enhance their conductivity. We have checked that the rheological and wettability properties are reasonably the same with and without 5 %<sub>vol</sub> of DMSO or EG [Figure 2.8 and Table 2.1].

This section focuses on processing the PEDOT:PSTFSI inks using different techniques: inkjet printing, doctor blading, screen printing, and soft blading.

For inkjet processing, Newtonian low viscosity solutions are recommended. In our case, a PEDOT:PSTFSI<sub>80 kDA</sub> ink at concentrations under 0.55 %<sub>wt</sub> has no yield stress and may even be Newtonian at lower concentrations. The viscosity of our inks at 0.5 %<sub>wt</sub> is similar to that of the commercial PEDOT:PSS inks (Clevios PH 1000 and Orgacon IJ 1000).

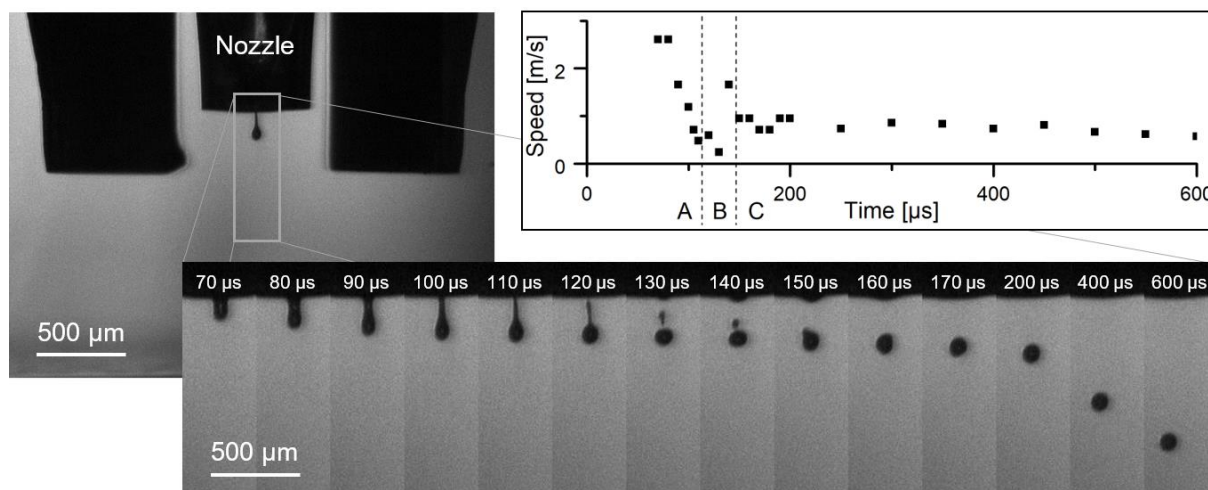


Figure 2.24. Photos of a drop (illuminated with a stroboscopic light at different frequency) of 0.5 %<sub>wt</sub> PEDOT:PSTFSI<sub>80 kDa</sub> ink ejected during inkjet printing from a 50 μm nozzle and schematic of the speed of the drop divided in three zone : A) drop attached to the capillary, B) detachment of the drops (one principal and one satellite) and then merging of the satellite drop with the principal drop, C) free falling of the drop at a speed near 1 m/s.

The 0.5 %<sub>wt.</sub> solution was used to print films using an inkjet printer. Before use, the solution was sonicated for a few seconds and filtered with a 0.45 μm PTFE filter. Very stable drops can be obtained from the printer nozzle. For higher concentrations however, 0.7 %<sub>wt.</sub> for example, printing becomes very difficult, and the drops are highly unstable and create several satellite drops. Clearly, low concentrations and absence of yield stress play an important role. Considering that the drop ejection speed is of the order of 1 – 10 m/s (<sup>13</sup> and [Figure 2.24]) and that the inkjet nozzle diameter is 50 μm, the shear rate at the nozzle can be very high and roughly  $\dot{\gamma} \approx \frac{v}{d} = 2 \cdot 10^4 - 2 \cdot 10^5 \text{ s}^{-1}$ . The viscosity of the solution at 0.5 %<sub>wt</sub> can be extrapolated to this shear rate by using the power law parameters, as  $\eta = k\dot{\gamma}^{n-1} = 2 - 7 \text{ mPa} \cdot \text{s}$  which is close to the viscosity recommended for inkjet printers (5 – 40 mPa.s).<sup>12,13</sup>

For doctor blading, a viscous ink is recommended to reduce retraction or spreading effects near the contact line. The presence of a yield stress and an elastic modulus are beneficial since spreading or retraction can also be reduced or inhibited. We have used a concentration of 1 %<sub>wt</sub> of PEDOT:PSTFSI<sub>80 kDa</sub> which has a yield stress  $\tau_0$  of about 1 Pa and an elastic modulus  $G'$  of about 100 Pa.

The films obtained using the inkjet printer as well as the doctor blade are shown in Figure 2.25. The schematics give a brief overview of the techniques and the photographs show the obtained films. For both techniques, the films are relatively homogeneous.

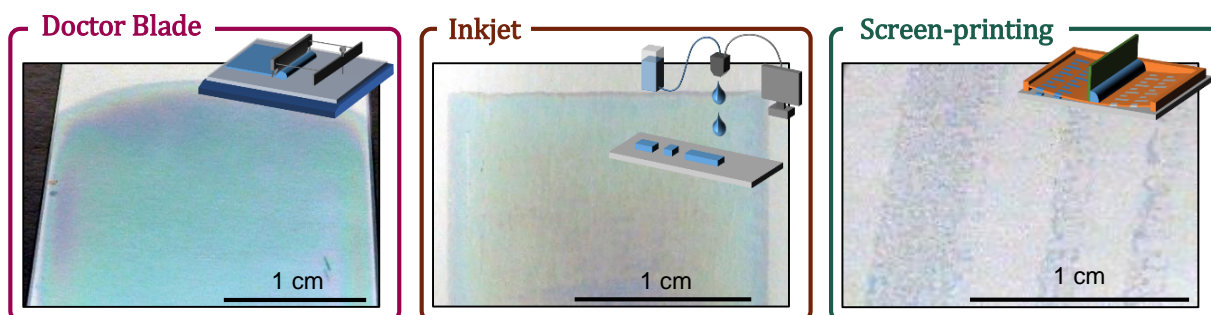


Figure 2.25: Photos of films deposited by doctor blade, inkjet and screen-printing.

For screen-printing, the inks need to be highly shear thinning and to have sufficient elastic moduli. The ink should be able to flow through the mesh when the squeegee applies a high shear, but the ink layer should gel on the substrate to hold in place. For this last deposition process, we have used different solution concentrations between 0.9 and 1.4 %<sub>wt</sub>. All these solutions have the right viscoelastic properties. However, and despite the fact that the rheology of the fluid is in the desired range, heterogeneous films were obtained [Figure 2.25]. We believe that the heterogeneity is due to wettability problems of the solutions with respect to the screens used as alluded to in part 2.3.4.

Last, an attempt at printing heterogeneous patterns in the form of parallel lines has been carried out. It has been shown that for aqueous shear thinning solutions, with a high extensional viscosity and capillary number  $Ca = \frac{\eta(\dot{\gamma}) \times v}{r}$  in the range of  $10^{-3} - 10^{-1}$ , thin lines can be deposited by using a soft blade deposition technique on hydrophobic substrates.<sup>25</sup> The extensional properties of 1 %<sub>wt</sub> PEDOT:PSTFSI<sub>80 kDa</sub> inks, which have a  $Ca$  in the desired range [Figure 2.26], are not sufficient and the deposition gives rise to aligned drops as can be seen in Figure 2.27.a. In order to increase the extensional properties of the solution, a high molar mass neutral polymer, PEO<sub>8 000 kDa</sub>, was added. High molar mass polymers such as PEO are known to increase the extensional properties of aqueous solutions.<sup>35</sup> The rheology of the solution, and therefore the value of the capillary number, was tuned by varying both the concentration of PEO and PEDOT:PSTFSI. The optimized formulation of 0.3 %<sub>wt</sub> PEDOT:PSTFSI<sub>80 kDa</sub> and 5 000 ppm PEO<sub>8 000 kDa</sub> allows to form lines using deposition speeds between 0.1 and 2 mm/s. Figure 2.27.b shows both the formation of lines and drops connected by lines during the deposition process and Figure 2.27.c shows more developed lines observed after the drying of the ink. No surfactant was added for these experiments. Indeed, in this technique the dewetting of the ink onto the hydrophobic substrate is essential.

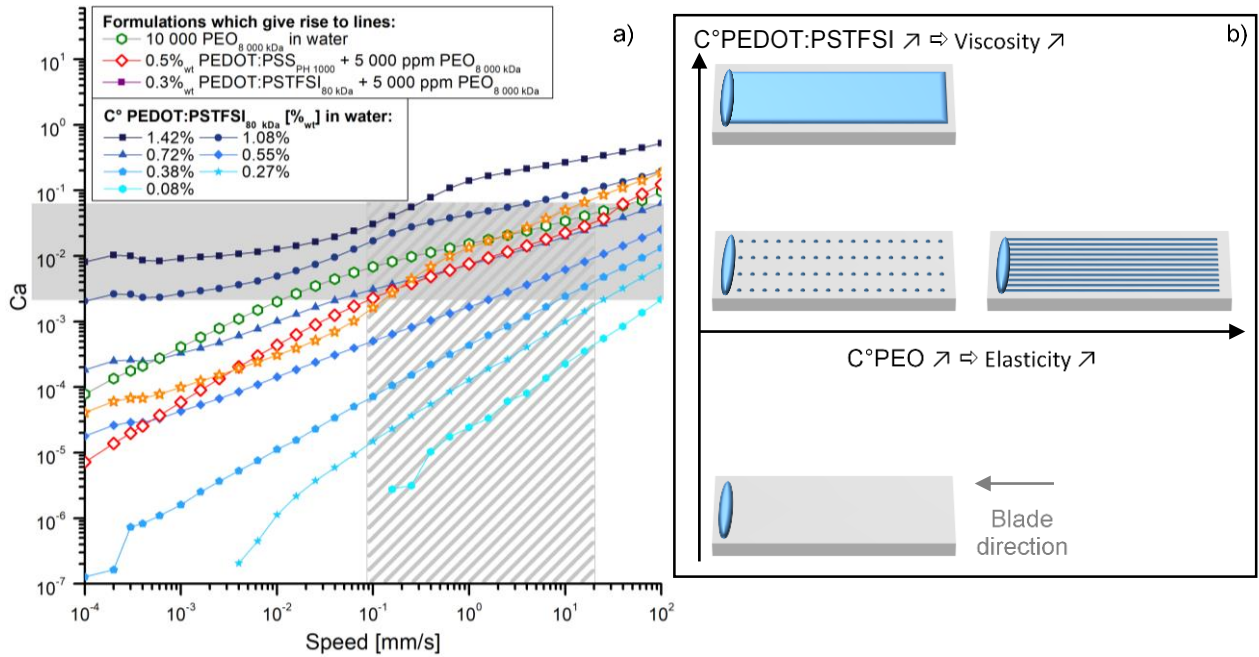


Figure 2.26: a) Capillary number of different aqueous inks calculated from their shear viscosity: PEDOT:PSTFAI<sub>80 kDa</sub> at different concentrations, 10 000 ppm (=0.01 %<sub>wt</sub>) PEO, and 0.5 %<sub>wt</sub> PEDOT:PSS<sub>PH 1000</sub> or 0.3 %<sub>wt</sub> PEDOT:PSTFSI<sub>80 kDa</sub> with 5 000 ppm (=0.005 %<sub>wt</sub>) PEO. The grey area is the region reported in the literature where lines should be deposited. The hatched area is the speed used to obtain lines with the PEDOT formulations with PEO. b) Schematic of the deposition of the formulated PEDOT:polyanion inks in function of the concentration of PEDOT and PEO: from no deposition at all, to aligned dots or lines, to complete film deposition.

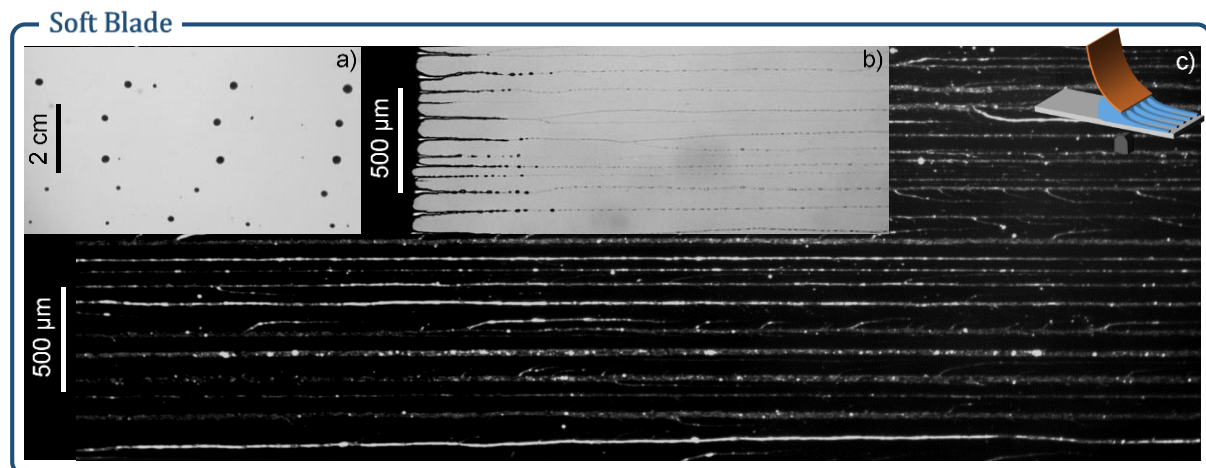


Figure 2.27: Schematic of the soft blade depositions process (the ink was deposited under the blade and the substrate, a silanized glass, was then moved at different speeds) and photo of the depositions: a) aligned dots (1 %<sub>wt</sub> PEDOT:PSTFSI<sub>80 kDa</sub>); b) lines of 0.3 %<sub>wt</sub> PEDOT:PSTFSI<sub>80 kDa</sub> + 5 000 ppm PEO<sub>8 000 kDa</sub> during the deposition, and c) after drying (phase contrast image).

## 2.5 Film characterization

The obtained films were then characterized in terms of topology, conductivity at the surface and optoelectronic properties.

### 2.5.1 Film topology

The topology was determined by AFM and SEM measurements on PEDOT:PSTFSI<sub>80 kDa</sub> films deposited by doctor blade or inkjet printing [Figure 2.28 and Figure 2.29]. Two scales of roughness are visible and summarized in Table 2.5: in a 30  $\mu\text{m}$  x 30  $\mu\text{m}$  observation window, the roughness is two times lower ( $14 \pm 5$  nm instead of  $32 \pm 6$  nm) for the films deposited by inkjet in comparison to the one deposited by doctor blade. That could come from the fact that inkjet inks were sonicated for a few seconds and filtered with a 0.45  $\mu\text{m}$  PTFE filter, while doctor blade inks were too viscous and didn't received any treatment. The 1  $\mu\text{m}$  square observations give a roughness in the range of the polymer thickness (Figure 2.14: 1.5 – 4 nm):  $2.5 \pm 0.3$  nm for inkjet and  $2.9 \pm 1.4$  nm for doctor blade. The structure of the polymer is better defined for the film deposited by inkjet than by doctor blade: one possible explanation could be that the ink is highly sheared (See 0:  $2 \cdot 10^4 - 2 \cdot 10^5 \text{ s}^{-1}$ ) during the ejection of the drop, which could help to remove the interactions between the polyanion and separate better the chains.

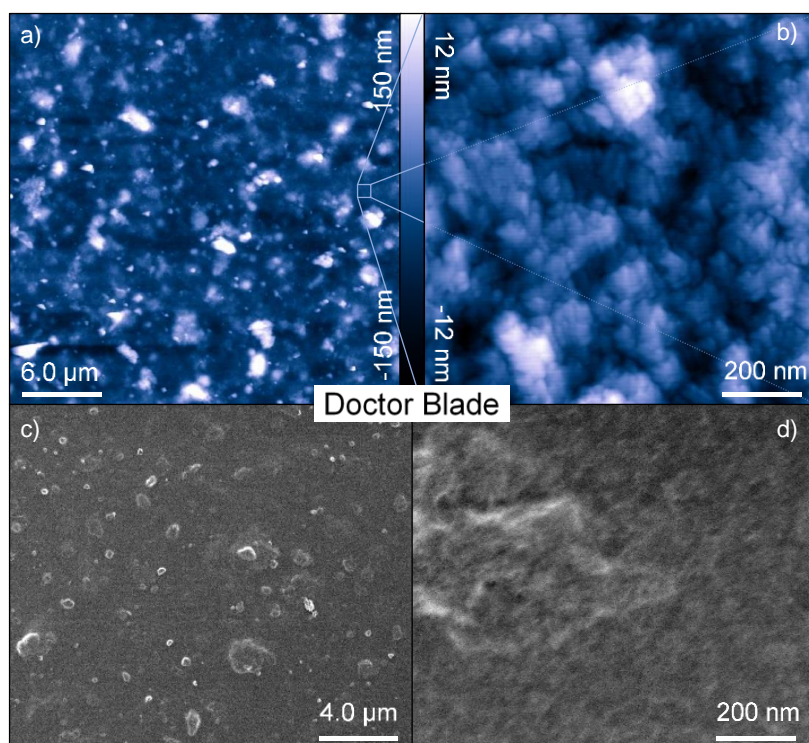


Figure 2.28: Microscopy of PEDOT:PSTFSI<sub>80 kDa</sub> films deposited by doctor blade on glass substrate : solid AFM image (in blue: a) 30x30  $\mu\text{m}^2$  and b) 1x1  $\mu\text{m}^2$ ) and SEM (0.5 kV - UED - GBSH - WD 3 mm - c) x 5 000 and d) x 100 000).

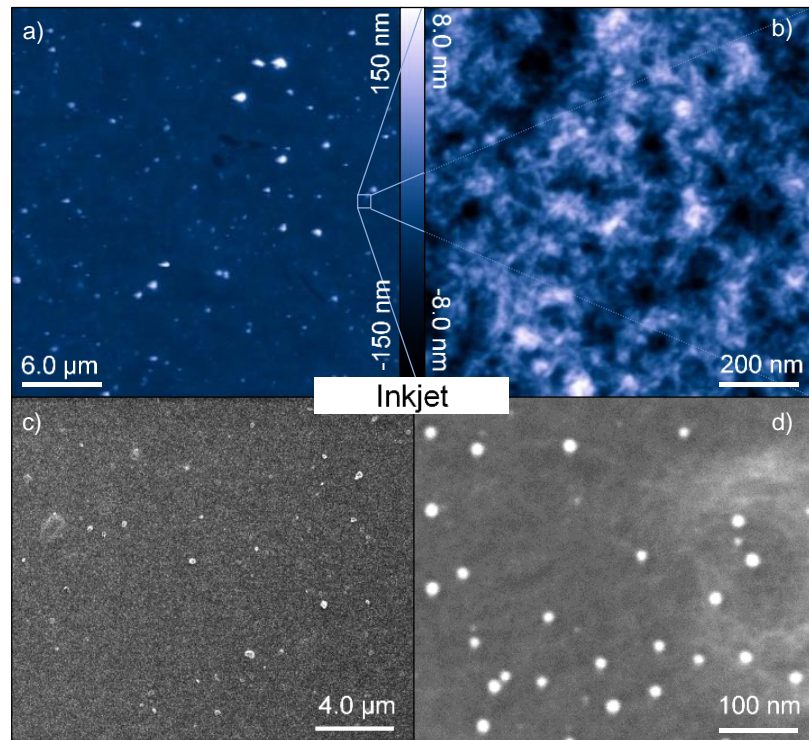


Figure 2.29: Microscopy of PEDOT:PSTFSI  $_{80 \text{ kDa}}$  films deposited by inkjet printing on glass substrate : solid AFM image (in blue: a)  $30 \times 30 \mu\text{m}^2$  and b)  $1 \times 1 \mu\text{m}^2$ ) and SEM ( $0.5 \text{ kV} - \text{UED} - \text{GBSH} - \text{WD } 3 \text{ mm} - \text{c} \times 5 \text{ 000}$  and d)  $\times 150 \text{ 000}$ ).

Process	Roughness [nm]	
	$1 \times 1 \mu\text{m}^2$	$30 \times 30 \mu\text{m}^2$
Inkjet	$2.5 \pm 0.3$	$14 \pm 5$
Doctor Blade	$2.9 \pm 1.4$	$32 \pm 6$

Table 2.5: Roughness of PEDOT:PSTFSI  $_{80 \text{ kDa}}$  films deposited by doctor blade or inkjet measured by AFM.

The SEM image of films deposited by inkjet printing shows shiny points [Figure 2.29.d]. These dots most probably come from the glass substrate itself [See Appendix A.3].

Figure 2.30 displays microscopy pictures of lines of  $0.3 \text{ \%}_{\text{wt}}$  PEDOT:PSTFSI  $_{80 \text{ kDa}}$  with  $5 \text{ 000 ppm}$  PEO  $_{8 \text{ 000 kDa}}$  deposited with a soft blade on PET substrate. Because the PET is not as hydrophobic as the silanized glass (the contact angle of water is  $105 \pm 1^\circ$  on silanized glass, and  $66 \pm 2^\circ$  on PET), two different types of lines are obtained: thin and wide lines were the dewetting was not high enough ( $60 - 130 \text{ nm}$  thickness and  $50 - 60 \text{ nm}$  width), and thick with thin width were the dewetting performed well as on silanized glass ( $690 - 730 \text{ nm}$  thickness and  $20 - 25 \text{ nm}$  width). In both cases, the surface seems smoother than the deposition in doctor blade or inkjet because the polymers are less well defined, but the general roughness for a  $30 \mu\text{m}$  square is in the same range  $26 \pm 6 \text{ nm}$  for a substrate roughness in the range  $5 - 8 \text{ nm}$ . In the SEM images, some PEDOT:PSTFSI aggregates are visible outside the lines, which means that during the dewetting some aggregates are left on site.

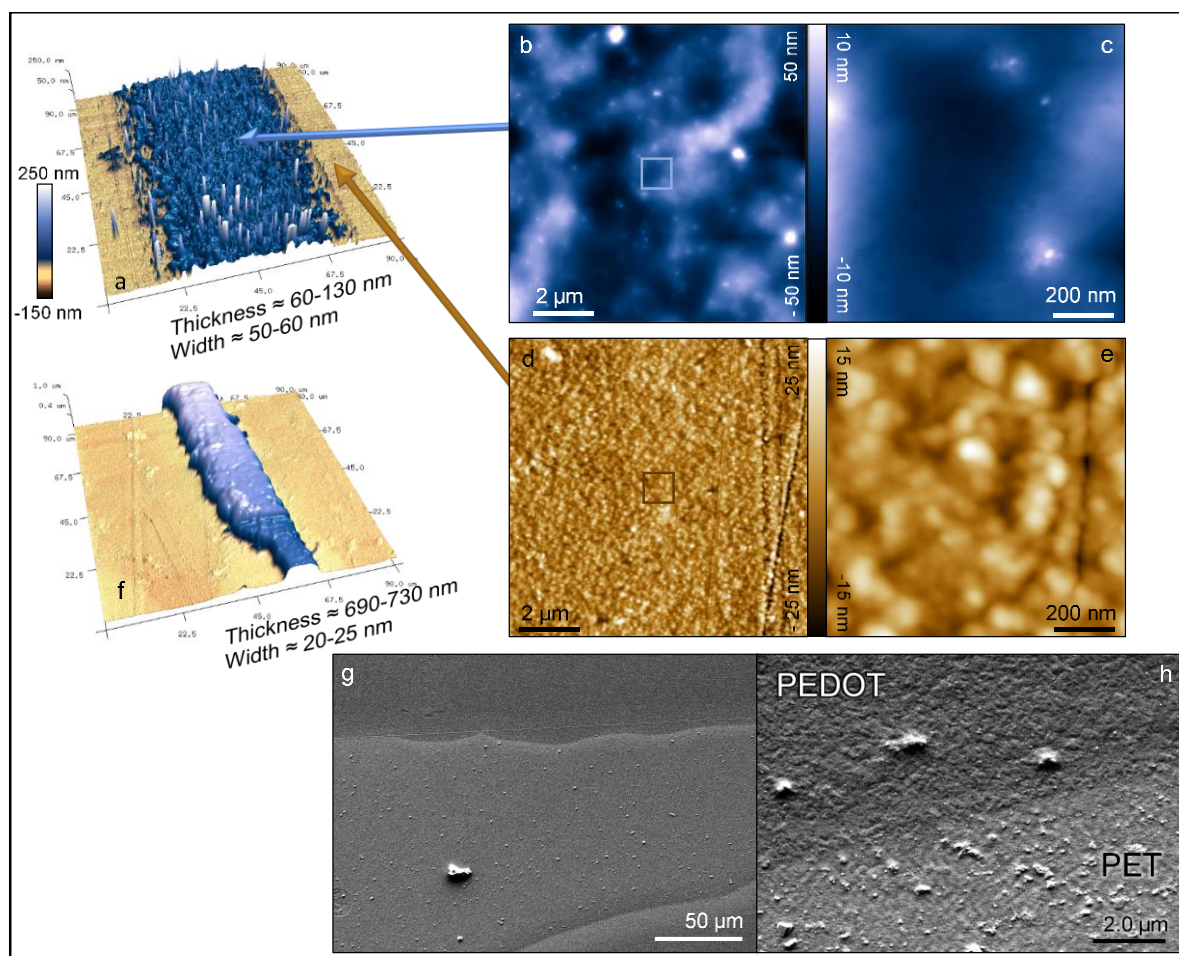


Figure 2.30: Microscopy of lines obtained by deposition of a solution of 0.3 %wt PEDOT:PSTFSI 80 kDa and 5 000 ppm PEO 8 000 kDa with a soft blade on an hydrophobic surface: solid AFM image of two lines on PET (a-f: scale: 90  $\mu\text{m}$ , 10  $\mu\text{m}$  or 1  $\mu\text{m}$ ) and SEM of metallised lines on PET (g-h: 1kV – LED – WD 10 mm – x 500 and x 10 000).

The wettability of dried PEDOT films is detailed in Appendix A.4.

## 2.5.2 Films conductivity at the surface

Conductive AFM was performed to visualise the area where the electrons can pass at the surface of films. Thus, PEDOT films were deposited by doctor blade or inkjet on a conductive substrate: ITO or gold. 1V was applied through the substrate, and a tip was measuring the output current at the surface. This method is qualitative and not quantitative. Figure 2.31 and Figure 2.32 display the resulting images respectively for deposition on ITO and gold: the height sensor signals (so the topology) are shown in the 1<sup>st</sup> column, the contact current in 3<sup>rd</sup> column, and in the 2<sup>nd</sup> column the outline between conductive and non conductive parts overlay the topology image. The ink used are PEDOT:PSTFSI (with molar masses of 80 kDa or 250 kDa) and PEDOT:PSS PH 1000 formulated with surfactant and with or without DMSO.

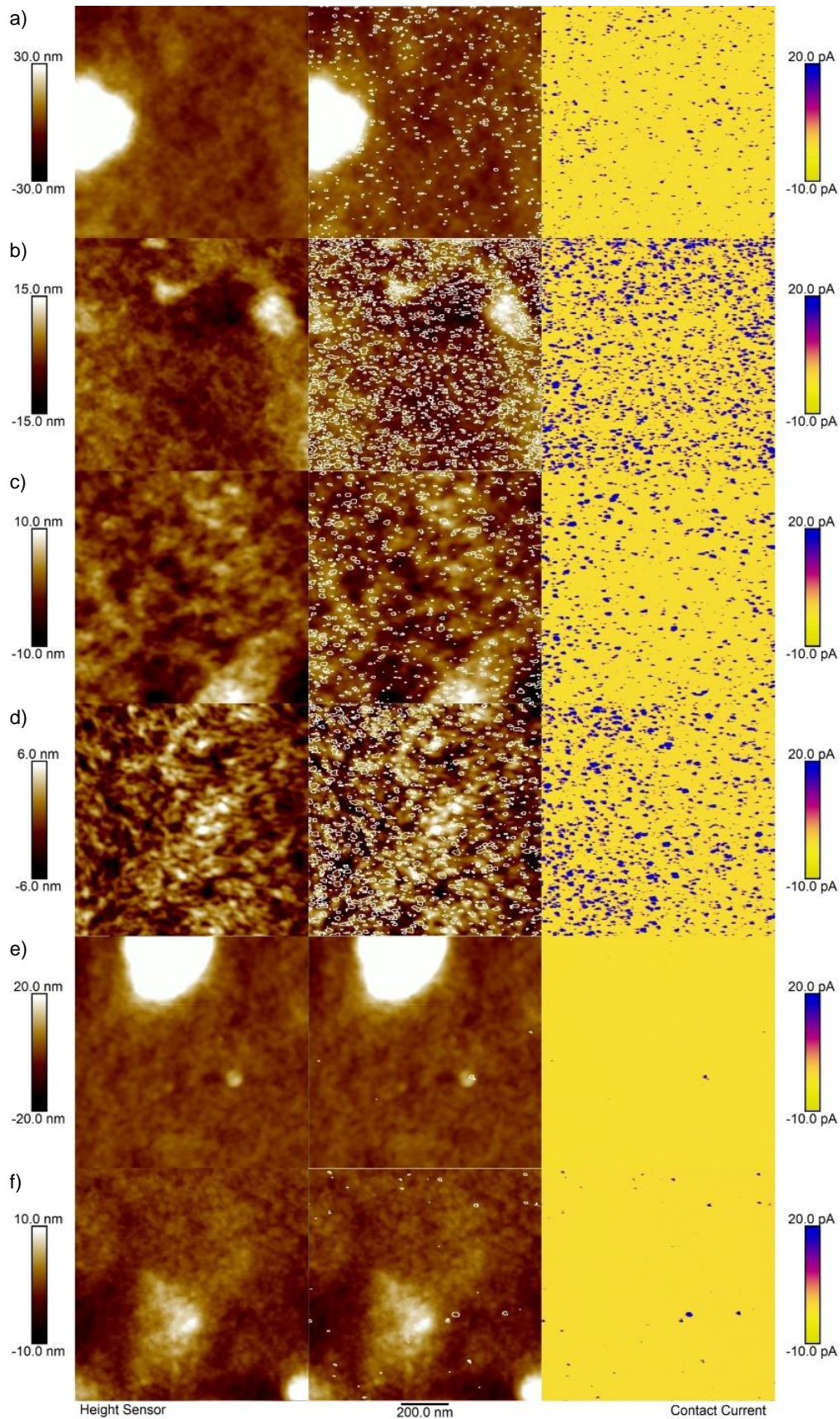


Figure 2.31: Conductive AFM of PEDOT:polyanion deposited on ITO. 1V was applied, Height Sensor (1<sup>st</sup> column) and Contact Current (3<sup>rd</sup> column) were recorded. The blue area are conductive while yellow are less conductive. In the 2<sup>nd</sup> column, the outline between conductive and non conductive parts overlay the topology image. a) PEDOT:PSTFSI<sub>80 kDa</sub> + D + Z (Inkjet), b) PEDOT:PSTFSI<sub>80 kDa</sub> + D + Z (DB), c) PEDOT:PSTFSI<sub>250 kDa</sub> + D + Z (DB), d) PEDOT:PSS<sub>PH1000</sub> + D + Z (DB), e) PEDOT:PSS<sub>PH1000</sub> + Z (DB), f) PEDOT:PSTFSI<sub>80 kDa</sub> + Z (DB). (D=DMSO, Z=Zonyl, DB=Doctor Blade).

Table 2.6 and Table 2.7 sum up the percentage of conductive area at the surface of the films depending of the PEDOT ink and the process used.

Deposition	Ink	Conductive Area [%]
-	ITO Substrate	15
Inkjet	PEDOT:PSTFSI <sub>80 kDa</sub> +D+Z	4
Doctor Blade	PEDOT:PSTFSI <sub>80 kDa</sub> +D+Z	16
	PEDOT:PSTFSI <sub>250 kDa</sub> +D+Z	7
	PEDOT:PSS <sub>PH 1000</sub> +D+Z	13
	PEDOT:PSS <sub>PH 1000</sub> +Z	0.13
	PEDOT:PSTFSI <sub>80 kDa</sub> +Z	0.46

Table 2.6: Percentage of conductive area at the surface of PEDOT:polyanion films on ITO (D=DMSO, Z=Zonyl).

For deposition by doctor blade on ITO [Figure 2.31 and Table 2.6], ink formulated with DMSO shows that for a three-time higher molar mass of the polyanion PSTFSI, the percentage of conductive area at the surface is lower (divided by 2.5). The commercial PEDOT:PSS ink has a comparable percentage to the one of PEDOT:PSTFSI<sub>80 kDa</sub> (13 – 16 %). This last ink was also deposited by inkjet, the low percentage found in this case can come from the fact that the thickness of the film was lower. For the two inks formulated without DMSO, which is used to increase the conductivity of the film, the percentage of conductive area at the surface is very low: less than 0.5 %. Adding a high boiling point solvent is then very important to have a better pathway to the electrons and so better conductivity. Lower molar mass of the polyanion seems to give better conductivity: the polyanion can more easily move during the drying and so a better segregation with the PEDOT occurs.

For films deposited on gold [Figure 2.32 and Table 2.7], the percentage of conductive area is very low (3 – 4 %). But in this case, even the grains of the evaporated gold were not measured very conductive: it should come from a deterioration of the fragile conductive tip in contact with the gold.

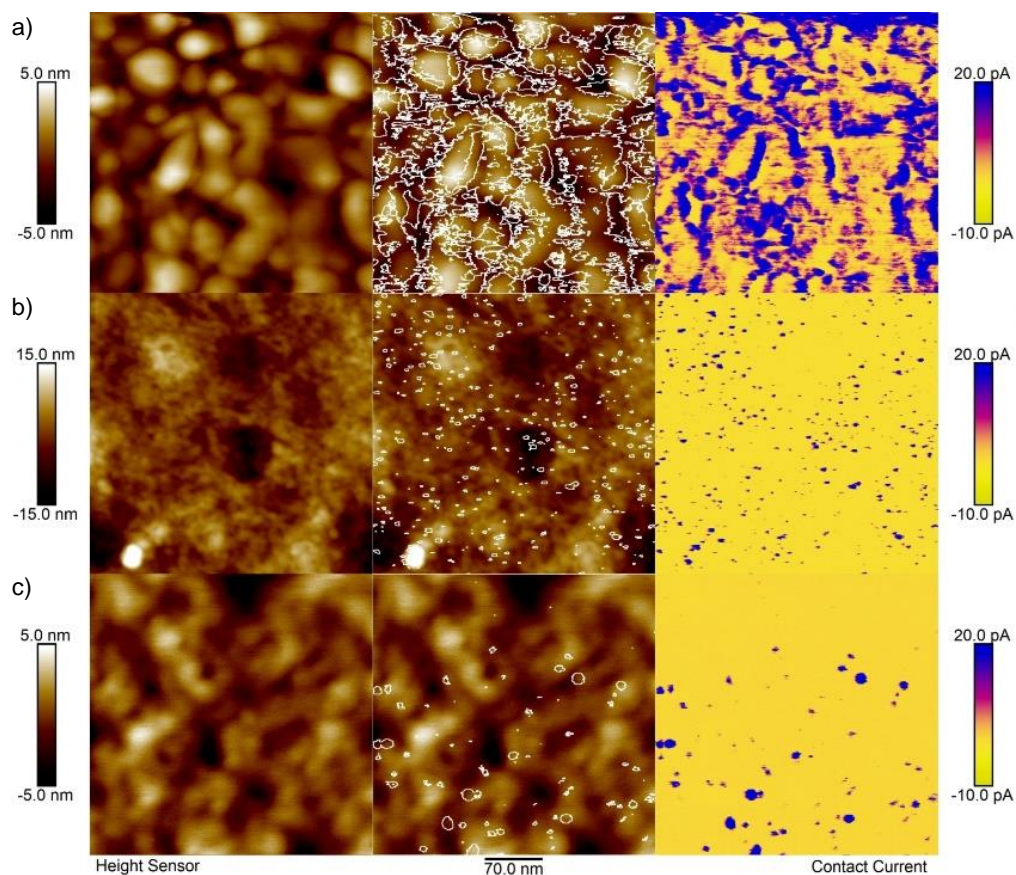


Figure 2.32: Conductive AFM of PEDOT:PSTFSI deposited on gold substrate treated with octane-thiol (for hydrophobicity). 1V was applied, Height Sensor (1<sup>st</sup> column) and Contact Current (3<sup>rd</sup> column) were recorded. In the 2<sup>nd</sup> column, the outline between conductive and non conductive parts overlay the topology image. a) Gold substrate treated with octane-thiol, b) PEDOT:PSTFSI<sub>80 kDa</sub> + D + Z (DB), c) PEDOT:PSTFSI<sub>250 kDa</sub> + D + Z (DB). (D=DMSO, Z=Zonyl, DB=Doctor Blade).

Deposition	Ink	Conductive Area [%]
-	Gold substrate treated with octane-thiol	42
Doctor Blade	PEDOT:PSTFSI <sub>80 kDa</sub> +D+Z	4
	PEDOT:PSTFSI <sub>250 kDa</sub> +D+Z	3

Table 2.7: Percentage of conductive area at the surface of PEDOT:PSTFSI films on gold treated with octane-thiol (D=DMSO, Z=Zonyl).

Figure 2.33 shows conductive AFM images of a conductive line of 0.5 %<sub>w</sub> PEDOT:PSS<sub>PH 1000</sub> + 5000 ppm PEO<sub>8 000 kDa</sub> deposited with a soft blade on gold substrate treated with octane-thiol (for hydrophobicity). The polymers align in the direction of the deposition.

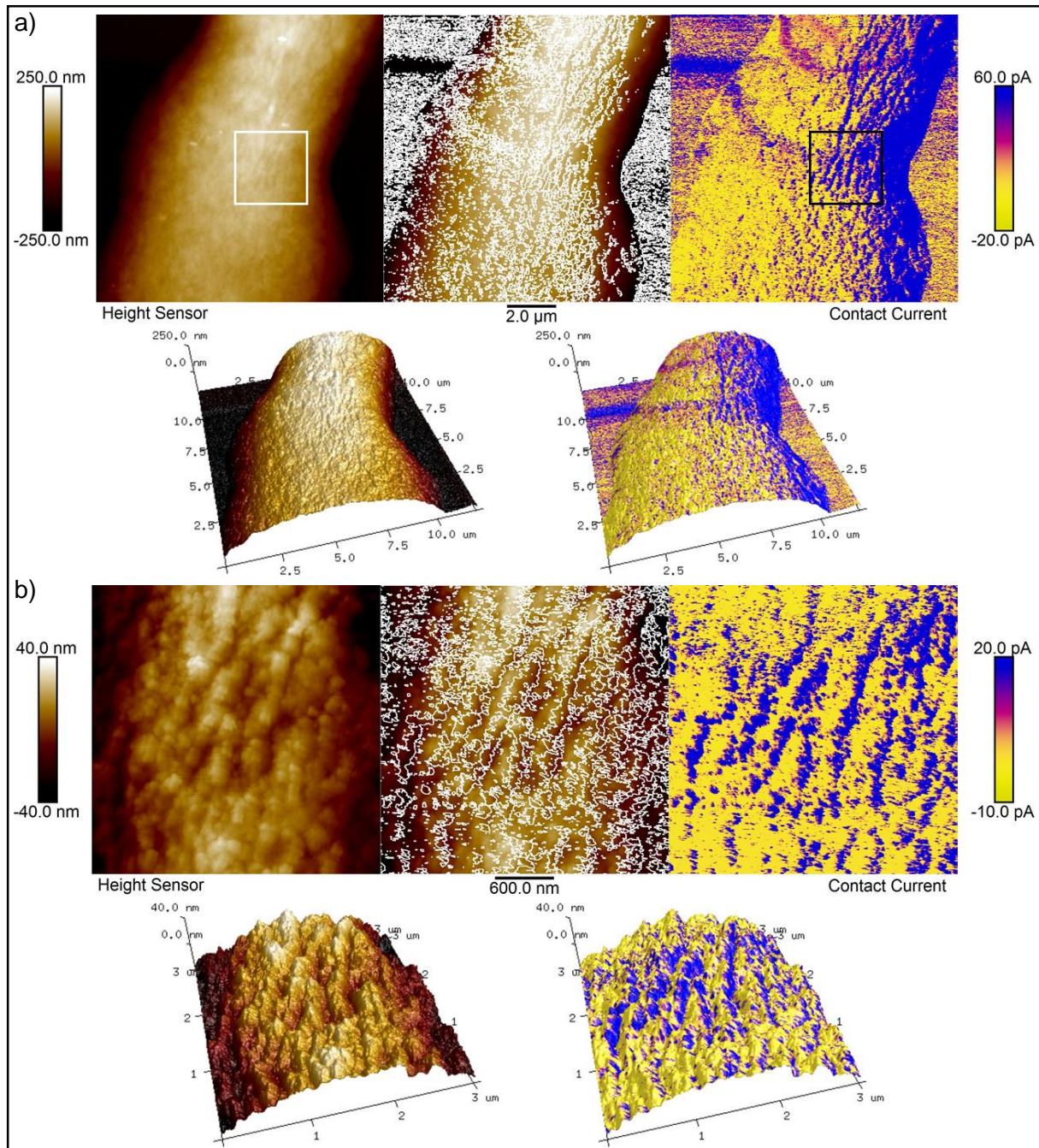


Figure 2.33: Conductive AFM of 0.5 %wt PEDOT:PSS<sub>PH 1000</sub> + 5000 ppm PEO<sub>8 000 kDa</sub>: line obtained by dewetting on a gold substrate treated with octane-thiol (for hydrophobicity). 1V was applied, Height Sensor (left and 3D left) and Contact Current (right and 3D right) were recorded. In the center, the outline between conductive and non conductive parts overlay the topology image. b) is a zoom of a).

### 2.5.3 Optoelectronic properties for transparent electrodes

The optoelectronic properties of the films obtained by doctor blade, inkjet and screen-printing of PEDOT:PSTFSI inks were measured: the conductivity of the films and their transparency.

The electrical conductivity  $\sigma$  of the films, which is the intrinsic property related to the mobility of the material electrical charges, was calculated using the thickness  $t$  (obtained with a profilometer), and the sheet resistance  $R_s$  (measured with a four-point probe) with the relation:  $\sigma = \frac{1}{t \times R_s}$ . The conductivity of lines deposited with a soft blade on silanized glass was measured with a two probe setup under a microscope [Figure 2.34], but only the very large lines at the border of the blade (and so not the real lines) were visible and measurable. That is why this part doesn't go further in the optoelectronic properties of the lines, even if we know from the conductive AFM that they are conductive.

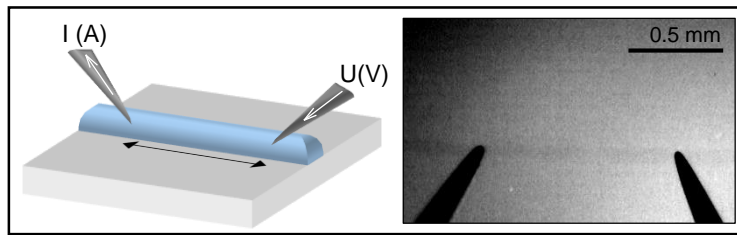


Figure 2.34: Schematic and microscopy image of the two probes measurement of one line.

The transmittance  $T$  of the films was measured with a UV-spectrometer at 550 nm:  $T = \frac{I}{I_0}$  where  $I$  is the transmitted intensity and  $I_0$  is the intensity of the incident light.

To compare transparent electrodes, the most commonly used feature is the so called Figure of Merit ( $FoM$ ).<sup>36,37</sup> This  $FoM$  is the ratio of the electrical conductance  $\sigma_{dc}$  on the optical

conductance  $\sigma_{opt}$  defined as follows:  $FoM = \frac{\sigma_{dc}}{\sigma_{opt}} = \frac{188,5}{\left(\frac{1}{\sqrt{T_{550\text{ nm}}} - 1}\right) R_s}$  where  $R_s$  is the sheet resistance,

and  $T_{550\text{ nm}}$  is the transmittance at 550 nm of the printed films.

The results are summarised in Table 2.8 which shows the rheological properties needed for each process, inkjet, doctor blade, screen-printing, the concentration ranges relevant for these processes, as well as the optoelectronic properties of the films obtained.

Note that sheet resistances in the range 55 – 128  $\Omega/\square$  (doctor blade) and 100 – 180  $\Omega/\square$  (inkjet) were measured for films of thicknesses comprised between 190 nm and 580 nm. The measured conductivities (230 – 320 S/cm) for films obtained with doctor blade coating and

(240 – 380 S/cm) for films obtained using inkjet printing are roughly the same. Such values are comparable, albeit smaller, to the conductivity of ITO (in the range of  $10^3$  S/cm).<sup>1</sup>

Depending on the thickness, different transmittances between 72 and 93 % (72 – 86 % for doctor blade and 85 – 93 % for inkjet printing) were measured, which is in the range of the transmittance of ITO films (80 – 95 %<sup>1</sup>).

Process	Viscosity	Shear thinning	Elasticity & Viscosity	[PEDOT:PSTFSI <sub>80kDa</sub> ] (%wt)	t (nm)	$\sigma$ (S/cm)	T (%)	FoM
Inkjet	Weak 5 – 40 mPa.s	Not necessary	$G' < G''$	$\approx 0.5$	268±102	297±76	90±4	27±4
Doctor Blade	Intermediate (0.1 – 10 Pa.s for 1 – $10^3$ s <sup>-1</sup> )	Not necessary	$G' > G''$	$\approx 0.9 - 1$	458±224	276±33	80±9	19±2
Screen-printing	High (1 – 100 Pa.s for 1 – $10^3$ s <sup>-1</sup> )	Yes	$G' > G''$	$0.9 < C < 1.4$	Inhomogeneous layer [Figure 2.25]			

Table 2.8: Formulation and rheology needed for three depositions processes and corresponding optoelectronic properties

Table 2.8 show that a FoM between 16 and 23 is obtained for films deposited by using doctor blade processing while for films obtained using inkjet printing, which are more transparent but have similar conductivities, a FoM between 23 and 31 is obtained. These results are near the minimum FoM needed for transparent electrodes in industry, evaluated at 35 ( $R_s < 100 \Omega/\square$ , and  $T > 90\%$ ).<sup>38</sup> Clearly, PEDOT:PSTFSI is a good candidate for making transparent and flexible electrodes.

## 2.6 Conclusion

In this chapter, PEDOT:PSTFSI inks have been studied. First STFSIK anion were synthesized as well as PSTFSIK polyanion, to obtained PEDOT:PSTFSI complex. The structural study was done using DLS, liquid AFM and cryo-SEM. It has shown that PEDOT:PSTFSI polymers form a network in water: the network being the polyanion with dimensions in the range of 2 – 10 nm width (AFM and cryo-SEM) and 510 – 570 nm long (DLS), and small PEDOT polymers (5 – 15 nm) are visible alongside. The rheological behaviors of those inks were then systematically studied in function of the concentration in polymer: it has been shown that for low concentration, the ink can have a Newtonian behavior, while for concentrated one, the ink can become shear thinning with gel properties. The extensional rheology has shown the same behavior than in shear, with a slightly lower viscosity. The inks were then formulated with surfactant to give them a better wettability onto hydrophobic substrates: the surface tension goes from near 70 mN/m to near 24 mN/m. A high boiling point solvent (DMSO or EG) was also used to increase the conductivity of the dried films, and to have a better water resistance. Indeed, it has been shown that water drop on PEDOT:polyanion films can break easily the film when no high boiling point solvent was used in the formulation, and it was explained by the fact that a better segregation between PEDOT and the polyanion render the PEDOT less soluble in water.

Four different deposition processes were then used: doctor blade, inkjet, screen-printing, and a soft blade deposition process. On one hand, inhomogeneous films were obtained by screen-printing deposition. It has been explained by capillary problems of the ink into the screen. A systematic study using different screens, and adding for example few high molar mass neutral polymer should be performed to obtain a better formulation of PEDOT:PSTFSI for screen-printing. On the other hand, homogeneous films were obtained by doctor blade and inkjet with PEDOT:PSTFSI solutions concentrated respectively at 1 %<sub>wt</sub> and 0.5 %<sub>wt</sub>: the measured roughness was in the range of 15 – 30 nm for a 30 μm side square, the conductivity in the range 230 – 380 S/cm and the transmittance in the range 72 – 93 %. That has resulted in promising FoM for further industrial and academic developments as transparent electrodes, reaching FoM up to 31. The conductivity at the surface was found to be not homogeneous: only the end of conducting PEDOT pathway was imaged by conducting AFM method, and the use of high boiling point solvent to have better conducting pathway was confirmed.

For the soft blade deposition, lines of PEDOT were obtained only by adding a high neutral polymer (PEO) to increase the extensional properties of the ink. The deposition was done on silanized glass for the better defined lines, on PET to allow SEM measurements, and on evaporated gold treated with octane-thiol for conductive AFM measurements. In the two last cases, the

contact angle of water onto the substrate was lower (respectively  $66^\circ$  and  $90^\circ$  compared to the  $105^\circ$  on silanized glass), and so the lines less well defined. It was shown that it is possible to deposit very thin lines of PEDOT on hydrophobic substrate using only a soft blade: with thickness near 700 nm and width close to 20 – 25 nm in the case of well defined lines. It was not possible to measure the conductivity of those lines with a traditional four probe measurement, even a two probe apparatus under a microscope didn't permit to measure it. However, conductive AFM has shown that the lines are conductive, and that the polymer is aligned in the direction of the deposition thanks to the high molar mass neutral polymer.

To conclude, this study has shown that PEDOT:PSTFSI inks can be easily formulated to be used in various deposition processes. No viscosity enhancers or other additives are needed to obtain viscous or gel like water-based inks. The processability of these inks is controlled by their viscosity and rheological properties, which can be tuned by simply varying the concentration of the solution or the molar mass of the polyanion. Formulation with neutral high molar mass polymers allows increasing the extensional properties of the inks and enables deposition through a soft blade technique for the formation of linear patterns. Finally, formulation with surfactant further improves the wettability of the ink, while the use of high boiling point solvents as conductivity enhancing agents allows increasing the conductivity of the dried ink layers without modifying the rheological properties of the ink. Interestingly, the optoelectronic features of PEDOT transparent conductive films were maintained whatever the deposition technique used. Both doctor blading and inkjet printing showed good promise, for further industrial and academic developments, reaching figures of merit up to 31.

## Bibliography

- (1) Cao, W.; Li, J.; Chen, H.; Xue, J. Transparent Electrodes for Organic Optoelectronic Devices: A Review. *J. Photonics Energy* **2014**, *4* (1), 040990. <https://doi.org/10.1117/1.JPE.4.040990>.
- (2) Raupp, S.; Daume, D.; Tekoglu, S.; Merklein, L.; Lemmer, U.; Hernandez-Sosa, G.; Sauer, H. M.; Dörsam, E.; Scharfer, P.; Schabel, W. Slot Die Coated and Flexo Printed Highly Efficient SMOLEDs. *Adv. Mater. Technol.* **2017**, *2* (2), 1600230. <https://doi.org/10.1002/admt.201600230>.
- (3) Pali, L. S.; Jindal, R.; Garg, A. Screen Printed PEDOT:PSS Films as Transparent Electrode and Its Application in Organic Solar Cells on Opaque Substrates. *J. Mater. Sci. Mater. Electron.* **2018**, *29* (13), 11030–11038. <https://doi.org/10.1007/s10854-018-9185-y>.
- (4) Sico, G.; Montanino, M.; De Girolamo Del Mauro, A.; Imparato, A.; Nobile, G.; Minarini, C. Effects of the Ink Concentration on Multi-Layer Gravure-Printed PEDOT:PSS. *Org. Electron.* **2016**, *28*, 257–262. <https://doi.org/10.1016/j.orgel.2015.10.031>.
- (5) Hrehorova, E. Materials and Processes for Printed Electronics: Evaluation of Gravure Printing in Electronics Manufacture, 2007.
- (6) Kommeren, S.; Coenen, M. J. J.; Eggenhuisen, T. M.; Slaats, T. W. L.; Gorter, H.; Groen, P. Combining Solvents and Surfactants for Inkjet Printing PEDOT:PSS on P3HT/PCBM in Organic Solar Cells. *Org. Electron.* **2018**, *61*, 282–288. <https://doi.org/10.1016/j.orgel.2018.06.004>.
- (7) Hoath, S. D.; Hsiao, W.-K.; Martin, G. D.; Jung, S.; Butler, S. A.; Morrison, N. F.; Harlen, O. G.; Yang, L. S.; Bain, C. D.; Hutchings, I. M. Oscillations of Aqueous PEDOT:PSS Fluid Droplets and the Properties of Complex Fluids in Drop-on-Demand Inkjet Printing. *J. Non-Newton. Fluid Mech.* **2015**, *223*, 28–36. <https://doi.org/10.1016/j.jnnfm.2015.05.006>.
- (8) Yang, J.; Lin, Y.; Zheng, W.; Liu, A.; Cai, W.; Yu, X.; Zhang, F.; Liang, Q.; Wu, H.; Qin, D.; et al. Roll-to-Roll Slot-Die-Printed Polymer Solar Cells by Self-Assembly. *ACS Appl. Mater. Interfaces* **2018**, *10* (26), 22485–22494. <https://doi.org/10.1021/acsami.8b05673>.
- (9) Ji, G.; Wang, Y.; Luo, Q.; Han, K.; Xie, M.; Zhang, L.; Wu, N.; Lin, J.; Xiao, S.; Li, Y.-Q.; et al. Fully Coated Semitransparent Organic Solar Cells with a Doctor-Blade-Coated Composite Anode Buffer Layer of Phosphomolybdic Acid and PEDOT:PSS and a Spray-Coated Silver Nanowire Top Electrode. *ACS Appl. Mater. Interfaces* **2018**, *10* (1), 943–954. <https://doi.org/10.1021/acsami.7b13346>.
- (10) Nadgorny, M.; Ameli, A. Functional Polymers and Nanocomposites for 3D Printing of Smart Structures and Devices. *ACS Appl. Mater. Interfaces* **2018**, *10* (21), 17489–17507. <https://doi.org/10.1021/acsami.8b01786>.
- (11) Izdebska, J.; Thomas, S. *Printing on Polymers: Fundamentals and Applications*; William Andrew, 2015.
- (12) Hoath, S. D. *Fundamentals of Inkjet Printing: The Science of Inkjet and Droplets*; John Wiley & Sons / Wiley-VCH Verlag GmbH & CoKGaA: Weinheim, Germany, 2016.
- (13) Zapka, W. *Handbook of Industrial Inkjet Printing: A Full System Approach*; John Wiley & Sons, 2018.
- (14) Abbott, S. *How to Be a Great Screen Printer*, Macdermid Autotype Limited.; HowTo eBook; 2008.
- (15) Hofmann, A. I.; Smaal, W. T. T.; Mumtaz, M.; Katsigiannopoulos, D.; Brochon, C.; Schütze, F.; Hild, O. R.; Cloutet, E.; Hadziioannou, G. An Alternative Anionic Polyelectrolyte for Aqueous PEDOT Dispersions: Toward Printable Transparent Electrodes. *Angew. Chem. Int. Ed.* **2015**, *54* (29), 8506–8510. <https://doi.org/10.1002/anie.201503024>.
- (16) Meziane, R.; Bonnet, J.-P.; Courty, M.; Djellab, K.; Armand, M. Single-Ion Polymer Electrolytes Based on a Delocalized Polyanion for Lithium Batteries. *Electrochimica Acta* **2011**, *57*, 14–19. <https://doi.org/10.1016/j.electacta.2011.03.074>.
- (17) Mumtaz, M.; Aissou, K.; Katsigiannopoulos, D.; Brochon, C.; Cloutet, E.; Hadziioannou, G. A Well-Defined Polyelectrolyte and Its Copolymers by Reversible Addition Fragmentation

- Chain Transfer (RAFT) Polymerization: Synthesis and Applications. *RSC Adv.* **2015**, *5*(119), 98559–98565. <https://doi.org/10.1039/C5RA19730A>.
- (18) Hofmann, A. I.; Katsigiannopoulos, D.; Mumtaz, M.; Petsagkourakis, I.; Pecastaings, G.; Fleury, G.; Schatz, C.; Pavlopoulou, E.; Brochon, C.; Hadziioannou, G.; et al. How To Choose Polyelectrolytes for Aqueous Dispersions of Conducting PEDOT Complexes. *Macromolecules* **2017**, *50* (5), 1959–1969. <https://doi.org/10.1021/acs.macromol.6b02504>.
- (19) Shi, H.; Liu, C.; Jiang, Q.; Xu, J. Effective Approaches to Improve the Electrical Conductivity of PEDOT:PSS: A Review. *Adv. Electron. Mater.* **2015**, *1* (4), n/a-n/a. <https://doi.org/10.1002/aelm.201500017>.
- (20) Palumbiny, C. M.; Heller, C.; Schaffer, C. J.; Körstgens, V.; Santoro, G.; Roth, S. V.; Müller-Buschbaum, P. Molecular Reorientation and Structural Changes in Cosolvent-Treated Highly Conductive PEDOT:PSS Electrodes for Flexible Indium Tin Oxide-Free Organic Electronics. *J. Phys. Chem. C* **2014**, *118* (25), 13598–13606. <https://doi.org/10.1021/jp501540y>.
- (21) Worthington, A. M. II. On Pendent Drops. *Proc. R. Soc. Lond.* **1881**, *32* (212–215), 362–377. <https://doi.org/10.1098/rspl.1881.0032>.
- (22) Berry, J. D.; Neeson, M. J.; Dagastine, R. R.; Chan, D. Y. C.; Tabor, R. F. Measurement of Surface and Interfacial Tension Using Pendant Drop Tensiometry. *J. Colloid Interface Sci.* **2015**, *454*, 226–237. <https://doi.org/10.1016/j.jcis.2015.05.012>.
- (23) Tate, T. XXX. On the Magnitude of a Drop of Liquid Formed under Different Circumstances. *Lond. Edinb. Dublin Philos. Mag. J. Sci.* **1864**, *27* (181), 176–180. <https://doi.org/10.1080/14786446408643645>.
- (24) Garandet, J. P.; Vinet, B.; Gros, P. Considerations on the Pendant Drop Method: A New Look at Tate's Law and Harkins' Correction Factor. *J. Colloid Interface Sci.* **1994**, *165* (2), 351–354. <https://doi.org/10.1006/jcis.1994.1240>.
- (25) Deblais, A.; Harich, R.; Colin, A.; Kellay, H. Taming Contact Line Instability for Pattern Formation. *Nat. Commun.* **2016**, *7*, 12458. <https://doi.org/10.1038/ncomms12458>.
- (26) McGovern, M. E.; Kallury, K. M. R.; Thompson, M. Role of Solvent on the Silanization of Glass with Octadecyltrichlorosilane. *Langmuir* **1994**, *10* (10), 3607–3614. <https://doi.org/10.1021/la00022a038>.
- (27) Glass, N. R.; Tjeung, R.; Chan, P.; Yeo, L. Y.; Friend, J. R. Organosilane Deposition for Microfluidic Applications. *Biomicrofluidics* **2011**, *5* (3), 036501-036501-7. <https://doi.org/10.1063/1.3625605>.
- (28) Notsu, H.; Kubo, W.; Shitanda, I.; Tatsuma, T. Super-Hydrophobic/Super-Hydrophilic Patterning of Gold Surfaces by Photocatalytic Lithography. *J. Mater. Chem.* **2005**, *15* (15), 1523–1527. <https://doi.org/10.1039/B418884E>.
- (29) Stetefeld, J.; McKenna, S. A.; Patel, T. R. Dynamic Light Scattering: A Practical Guide and Applications in Biomedical Sciences. *Biophys. Rev.* **2016**, *8* (4), 409–427. <https://doi.org/10.1007/s12551-016-0218-6>.
- (30) Mccoy, J. L.; Muthukumar, M. Dynamic Light Scattering Studies of Ionic and Nonionic Polymer Gels with Continuous and Discontinuous Volume Transitions. *J. Polym. Sci. Part B Polym. Phys.* **2010**, *48* (21), 2193–2206. <https://doi.org/10.1002/polb.22101>.
- (31) Ostwald, W. Ueber die Geschwindigkeitsfunktion der Viskosität disperser Systeme. I. *Kolloid-Z.* **1925**, *36* (2), 99–117. <https://doi.org/10.1007/BF01431449>.
- (32) Herschel, W. H.; Bulkley, R. Konsistenzmessungen von Gummi-Benzollösungen. *Kolloid-Z.* **1926**, *39* (4), 291–300. <https://doi.org/10.1007/BF01432034>.
- (33) Hofmann, A. Aqueous Dispersions of Conducting Polymers for Opto-Electronic Applications. Thèse de doctorat, Université de Bordeaux, Bordeaux, 2016.
- (34) Mezger, T. G. *The Rheology Handbook: For Users of Rotational and Oscillatory Rheometers*; Vincentz Network GmbH & Co KG, 2006.
- (35) Ingremau, F.; Kellay, H. Stretching Polymers in Droplet-Pinch-Off Experiments. *Phys. Rev. X* **2013**, *3* (4), 041002. <https://doi.org/10.1103/PhysRevX.3.041002>.

- 
- (36) Li, D.; Han, T.; Ruan, H. Solution-Assembled Ordered Grids Constructed with Silver Nanowires as Transparent Conductive Electrodes. *ACS Omega* **2018**, *3* (7), 7191–7195. <https://doi.org/10.1021/acsomega.8b01320>.
- (37) van de Groep, J.; Spinelli, P.; Polman, A. Transparent Conducting Silver Nanowire Networks. *Nano Lett.* **2012**, *12* (6), 3138–3144. <https://doi.org/10.1021/nl301045a>.
- (38) De, S.; Lyons, P. E.; Sorel, S.; Doherty, E. M.; King, P. J.; Blau, W. J.; Nirmalraj, P. N.; Boland, J. J.; Scardaci, V.; Joimel, J.; et al. Transparent, Flexible, and Highly Conductive Thin Films Based on Polymer–Nanotube Composites. *ACS Nano* **2009**, *3* (3), 714–720. <https://doi.org/10.1021/nn800858w>.

# 3 P(VDF-TrFE) inks for screen-printing

3.1 Introduction.....	110
3.2 Materials & Methods .....	113
3.2.1 Materials .....	113
3.2.2 Characterization methods of the polymer .....	113
3.2.3 Formulation and nomenclature of P(VDF-TrFE) solutions .....	114
3.2.4 Characterization methods of the formulated inks.....	114
3.2.5 Substrate preparation and inks deposition.....	115
3.2.6 Characterization methods of the depositions.....	115
3.3 Characterization of the neat polymer .....	115
3.4 P(VDF-TrFE) solutions with a gelifying agent.....	119
3.4.1 Additives and formulations of T <sub>Px<sub>p</sub></sub> A <sub>x<sub>A</sub></sub> inks .....	119
3.4.2 Rheological behaviors of T <sub>P<sub>0.1-15</sub></sub> D <sub>0.1-10</sub> inks .....	122
3.4.3 Structure of T <sub>P10</sub> , T <sub>D<sub>0.03</sub> g/mL</sub> , and T <sub>P10_D5</sub> inks.....	126
3.4.4 Gelifying agent in a mixture of a good and a bad solvent of DMDBS.....	129
3.4.4.1 Solubility of DMDBS in different solvents.....	129
3.4.4.2 Rheological behavior of 3D7T <sub>P12_D5</sub> and D <sub>P12_D5</sub> inks .....	130
3.4.5 Properties of films.....	131
3.4.5.1 Structure of films obtained using T <sub>P10_D5_R</sub> .....	131
3.4.5.2 Wettability of films .....	132
3.4.5.3 Crystallinity of films .....	133
3.5 P(VDF-TrFE) solutions in a mixture of a good and a bad solvent.....	134
3.5.1 Formulations of x <sub>B</sub> B/x <sub>G</sub> G <sub>Px<sub>p</sub></sub> inks.....	134
3.5.2 Rheological behavior .....	135
3.5.3 Structural study of 33B/67G <sub>P15</sub> ink and 33B/67G solution .....	138
3.6 Conclusion .....	140

### 3.1 Introduction

P(VDF-TrFE) is a piezoelectric polymer. It is widely used in organic electronics as an active layer in pressure sensors, actuators, speakers, etc. For such piezoelectric devices, P(VDF-TrFE) is sandwiched between two electrodes, usually PEDOT:PSS in organic devices, or metals like aluminium, silver or gold in hybrid organic/inorganic devices.

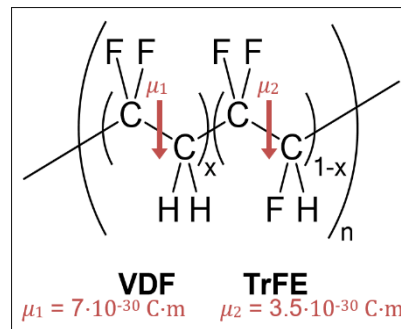


Figure 3.1: Structure of poly(vinylidene fluoride-co-trifluoroethylene) (P(VDF-TrFE)), and dipole moments  $\mu_1$  and  $\mu_2$  of the two monomer units in proportions  $x$  for the VDF unit, and  $1-x$  for the TrFE unit.

Figure 3.1 displays the structure of P(VDF-TrFE). It is a copolymer made of two types of monomers, vinylidene fluoride (VDF) in proportion  $x$  and trifluoroethylene (TrFE) in proportion  $1-x$ . The monomer units contain respectively two and three fluorine atoms. Due to the difference in electronegativity between the fluorine ( $\chi_F = 3.98$ ), carbon ( $\chi_C = 2.2$ ) and hydrogen ( $\chi_H = 2.55$ ) atoms, dipolar moments are created in the polymeric chain. The dipolar moment of the VDF unit,  $\mu_1 = 7 \cdot 10^{-30} \text{ C} \cdot \text{m}$ , is oriented in the same direction as the one of the TrFE unit,  $\mu_2 = 3.5 \cdot 10^{-30} \text{ C} \cdot \text{m}$ .<sup>1</sup> When an electric field is applied to the polymer, the dipoles moments align with the field through a rotation of the chain. The new direction of the atoms remains after removing the electric field. This is called the remanant polarization of the polymeric film and can be used to increase the response of piezoelectric devices. The device can be used either by applying a voltage, which results in a displacement of the P(VDF-TrFE) layer (for actuators or speakers), or by applying a pressure and so a displacement of the layer, which results in the creation of a voltage signal (for pressure sensors). Figure 3.2 displays a schematic of the preparation and use of a piezoelectric device.

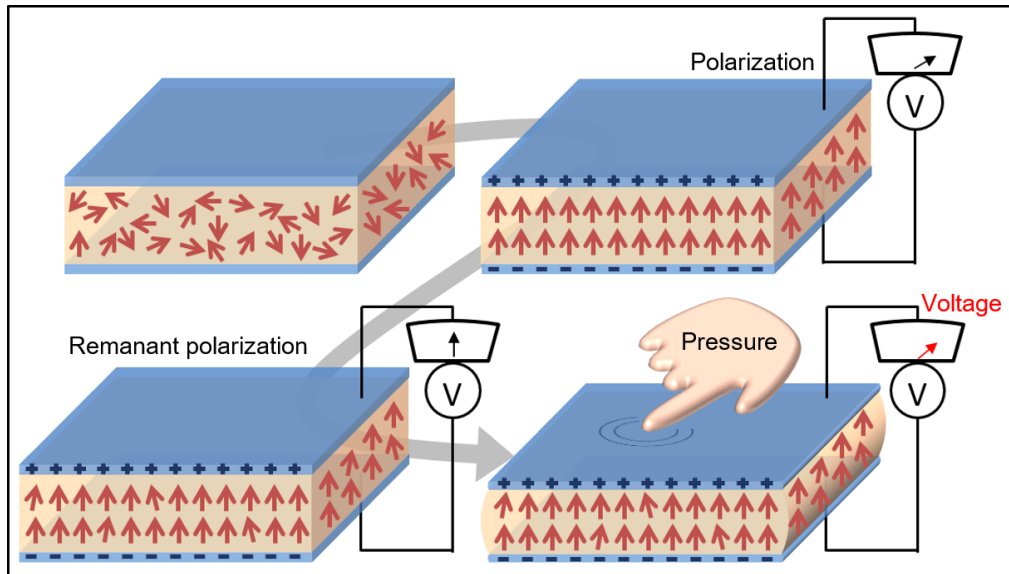


Figure 3.2: Schematic of the preparation and utilisation of a piezoelectric device (e.g. P(VDF-TrFE) layer between to electrodes): polarization of the dipoles of P(VDF-TrFE) by applying a voltage; removal of the voltage results in a remanant polarization; utilisation by applying a pressure and obtaining a voltage as output signal.

To make P(VDF-TrFE) films, different deposition processes can be used. One of the printing processes used is screen-printing [Figure 3.3] which allows to pattern surfaces in a simple way. As explained in chapter 1, specific rheological properties are needed for specific printing processes. In the case of screen-printing, a shear-thinning behavior is desirable<sup>2</sup>. However, commercially available P(VDF-TrFE) inks for screen-printing, such as FC25 Ink P (Arkema), shows a Newtonian behavior as the viscosity is constant versus shear rate, Figure 3.4, except for very high shear where very little shear-thinning is observed. The viscosity of the commercial PEDOT:PSS ink EL-P 5015 (Orgacon), used in screen-printing, is displayed as a reference.

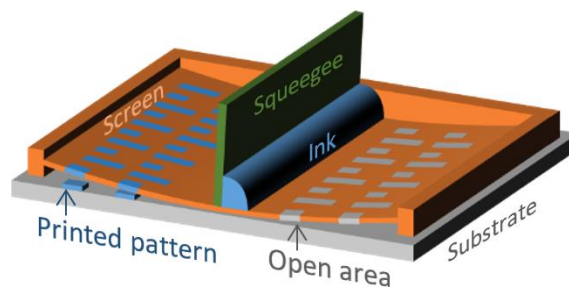


Figure 3.3: Schematics of screen-printing

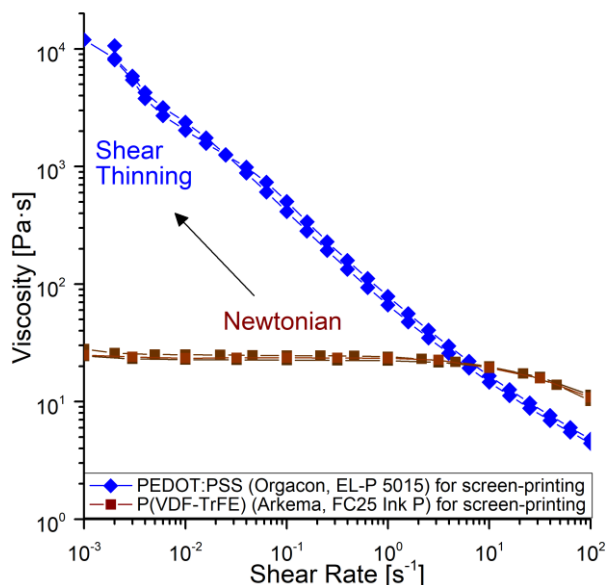


Figure 3.4: Rheological behavior of commercial PEDOT:PSS ink used for screen-printing (Orgacon, EL-P 5015) and commercial P(VDF-TrFE) for screen-printing (Arkema, FC25 Ink P), measured with a shear rheometer (cone plate geometry: 50 mm diameter and 1° angle): viscosity versus shear rate obtained by applying shear rate ramps at 20°C.

The aim of the following study is to modify the behavior of P(VDF-TrFE) inks to render them shear-thinning. Different approaches were examined. The simplest and straightforward method uses a gelifying agent in a good solvent of P(VDF-TrFE). The solvent used is triethylphosphate. High temperatures (130 – 140°C) are needed to dissolve the gelifying agent in the solvent. In order to avoid high temperatures, the gelifying agent can first be dissolved in DMSO before being blended with the P(VDF-TrFE) solution. In this case, the temperature used during the preparation of the ink can be lowered to 60°C: that is the second method. Finally, a more complex pathway will be explored using phase separation by mixing a good and a bad solvent of P(VDF-TrFE). This procedure leads to inks that are less resistant to shear, but can have an interest in the formation of porous films for application in lithium-ion battery.

## 3.2 Materials & Methods

### 3.2.1 Materials

The composition of poly(vinylidene fluoride-*co*-trifluoroethylene) (P(VDF-TrFE)) used in this study is 79.4 %<sub>wt</sub> of VDF unit and 20.6 %<sub>wt</sub> of TrFE unit. Two batches were investigated: FC20 62-053 and FC20 62-054 (from Arkema). To formulate them in solutions, different solvents and additives were used:  $\gamma$ -butyrolactone (GBL) (from Acros Organics), Benzyl Alcohol (BzOH) (from Sigma Aldrich) and Triethylphosphate (TEP) (from Acros Organics) as solvent, 1,3:2,4-bis(3,4-dimethylbenzylidene)sorbitol (DMDBS) (from TCI) and tris-tert-butyl-1,3,5-benzenetrisamide (BTA) (from Irgaclear, XT 386) as additives. To compare the home made formulations, a commercial ink of P(VDF-TrFE) in triethylphosphate was used: FC25 InkP (from Arkema).

### 3.2.2 Characterization methods of the polymer

The molar mass of the two batches of polymer was determined by size-exclusion chromatography (SEC) using three-columns sets: Shodex GF-1G 7B column and two-times Shodex Asahipak GF-7M-HQ columns with a 0.6 mL/min flow at 75°C in DMF with 0.1 mol/L LiBr using 0.15 % toluene as flow marker; or Agilent PL1113-1300 column and two times Agilent PL1113-6300 columns with a 0.8 mL/min flow at 30°C in THF using 0.15 % trichlorobenzene as flow marker. Calibration was done with polystyrene or poly(methyl methacrylate) standards.

Differential Scanning Calorimetry (DSC) of P(VDF-TrFE) films were performed on a TA instrument DSC Q100 RCS. The films were obtained by drop casting solutions of 10 %<sub>wt</sub> P(VDF-TrFE) in TEP on glass. Different temperatures were used to dry them, and an annealing was sometimes pursued (135°C or 130°C / 30 min). The hotplate was left to cool down at room temperature before removing the sample. The films were then detached from the substrate and left overnight under vacuum at room temperature to remove all remaining solvent. The sample was measured in aluminium caps using the following recipe: equilibration at -70°C, 1<sup>st</sup> heating to 200°C, 1<sup>st</sup> cooling to -70°C, 2<sup>nd</sup> heating to 200°C, 2<sup>nd</sup> cooling to 20°C, using a ramp rate of 20°C/min and a 5 min stabilisation period between each ramp [Figure 3.5].

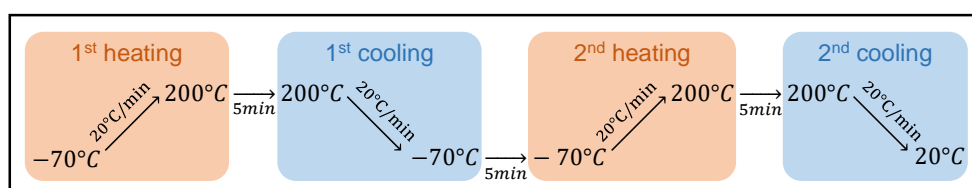


Figure 3.5: DSC method

### 3.2.3 Formulation and nomenclature of P(VDF-TrFE) solutions

Different formulations of P(VDF-TrFE) were done. A certain amount of the polymer was dissolved in a solvent S or in two solvents  $S_1 + S_2$  in volume proportions  $x_{S_1}$  and  $x_{S_2}$ . The dissolution was speed up by heating the solution at 50 – 60°C. The weight proportion of the polymer with respect to the total weight is  $x_p$ . For some formulations, an additive A was added in weight proportion with respect to the weight of the polymer. The nomenclature of the inks is the following:  $x_{S_1}S_1/x_{S_2}S_2 - Px_p - Ax_A$  using the abbreviations detailed in Table 3.1.

	Name	Abbreviation in text	Abbreviation in nomenclature
Polymer	poly(vinylidene fluoride- <i>co</i> -trifluoroethylene)	P(VDF-TrFE)	P
Solvents	$\gamma$ -butyrolactone	GBL	G
	Benzyl alcohol	BzOH	B
	Triethylphosphate	TEP	T
Additives	1,3:2,4-Bis(3,4-dimethylbenzylidene)sorbitol)	DMDBS	D
	tris-tert-butyl-1,3,5-benzenetrisamide)	BTA	B

Table 3.1: Abbreviations in text and in the nomenclature of P(VDF-TrFE) inks of the components.

For example, 33B/67G\_P15 means that 15 %<sub>wt</sub> of P(VDF-TrFE) was mixed in 67 %<sub>vol</sub>  $\gamma$ -butyrolactone and 33 %<sub>vol</sub> benzyl alcohol, while 3D/7T\_P12\_B5 means that 30 %<sub>vol</sub> of DMSO and 70 %<sub>vol</sub> of triethylphosphate were used with 12 %<sub>wt/total</sub> of P(VDF-TrFE) and 5 %<sub>wt/polymer</sub> of BTA.

Magnetic stirrer was firstly used, helped with manual stirring at the spatula for viscous inks. Then, in a second time, a reactor with a four glass blade stirrer was used to have a better stirring. P(VDF-TrFE) was dissolved for two hours (or more for high concentrations) at 60°C in the different solvents, while the additives were dissolved at higher temperature (130 – 140°C in TEP).

### 3.2.4 Characterization methods of the formulated inks

The solutions were then characterized with different methods. The rheological behaviors were determined as in previous chapter by using an Anton Paar MCR302 rheometer with a CP50-1° geometry (cone 50 mm – 1° / plate). Various temperatures, shear rates and shear stresses were applied to measure the shear viscosity and viscoelastic behavior of the solutions.

The structure in solution was determined by cryo-Scanning Electron Microscopy (cryo-SEM) at PLACAMAT (PLateforme Aquitaine de CARactérisation des MATériaux) (Jeol 6700F) and BIC (Bordeaux Imaging Center) (Zeiss Gemini 300) platforms. In each cases, the solution was frozen in liquid nitrogen and then in nitrogen paste, or directly in nitrogen paste. At PLACAMAT, the frozen solution was then metalized with a mixture of gold/palladium (240 s / 10 mA) without sublimation of the solvent. At BIC, the frozen solution was sublimated using different times

(10, 15, and 20 min at  $-95^{\circ}\text{C}$ ,  $-85^{\circ}\text{C}$  or  $-70^{\circ}\text{C}$ ) and then metallized (gold/palladium, 40 s / 10 mA). The observation was done between 5 and 15 kV at PLACAMAT, and at 3 kV at BIC.

Some liquid DSC was performed in high pressure caps from  $-70$  to  $150^{\circ}\text{C}$  ( $2^{\circ}\text{C}/\text{min}$ ), but no other peak than the ones of the solvent(s) were found. Solid DSC was also carried out using the same protocol as for the neat polymer [see 3.2.2].

### 3.2.5 Substrate preparation and inks deposition

The inks were then deposited by doctor blade (5 mm/min with air gaps between 50 – 150  $\mu\text{m}$ ) or screen-printing (mesh of the screen: 39 – 55 or 90 – 48; speed of the squeegee: 100 mm/s; air gap: 1 mm; pressure: 100 N) on cleaned glass (ultrasound 15 min in ethanol, acetone and then isopropanol) or cleaned PET (washed with acetone). Multilayers were performed, and different drying protocols between each layer were done ( $100^{\circ}\text{C}$  / 5min;  $40^{\circ}\text{C}$  / 3h;  $20^{\circ}\text{C}$  / multiple days).

### 3.2.6 Characterization methods of the depositions

The structure of the film was then checked by microscopy using an optical microscope (Nikon LV100ND) and a scanning electron microscope (Jeol 7800-E Prime). In the last case, no metallisation was performed to image the structure of the polymer. That for the GBSH (Super-High resolution Gentle Beam) mode was necessary with 0.5 kV. A Bruker Dektak XT-A profilometer was used too.

Devices with P(VDF-TrFE) layers between a top and a bottom electrode of PEDOT or metal were characterized in Chapter 4.

## 3.3 Characterization of the neat polymer

The neat polymer (P(VDF-TrFE)) used here, was obtained from Piezotech (Arkema). Two different batches were used. Each characterized by its molar mass. The molar masses given by Piezotech are 512 and 640 kDa for the batch 62-053, and for the batch 62-054 respectively using MFI (Melt flow index). Our own measurements using SEC in THF with PMMA calibration give values of  $M_w$  1.6-1.7 times lower than the ones estimated by the MFI. However, the batch FC20 60-053 has a lower molecular mass in weight than the batch FC20 62-054, which is consistent with the MFI estimate. Additional details on molar mass measurements are given in Appendix A.5.

In order to characterize the different phase transitions in the material, DSC measurements on dried films of P(VDF-TrFE) were carried out for different drying temperatures as the drying temperature is known to influence the quality of the films.<sup>3</sup> On some occasions, annealing at  $135^{\circ}\text{C}$

during 30 min was also performed (temperature and time chosen from the literature<sup>3</sup>). The results for the first and second heating cycles are shown in Figure 3.6: the peak at lower temperature indicates the Curie temperature  $T_C$ . The second peak indicates the melting temperature  $T_m$ . Since the second heating occurs after melting the sample following the first heating cycle, the values of  $T_C$  and  $T_m$  are the same for the different preparations.

For the first heating cycle, when films are dried at 20°C, the Curie peak is broad and at low temperature, which means that the crystalline phase of the polymer is more disorganised and amorphous<sup>4</sup>. For the films dried at 90°C, below  $T_C$ , the Curie peak shifts to a higher temperature indicating a more organized phase.<sup>5</sup> For films dried at 135°C, the Curie peak is at an intermediate temperature, so the ordering is intermediate, most probably because the crystallisation was done at  $T > T_C$  and so in the paraelectric phase.<sup>5</sup> The melting temperature also shifts to a higher temperature. According to reference,<sup>5</sup> this is indicative of an increase in the size of the crystals in the thickness of the film. For films dried at room temperature and then annealed 30 min at 135°C, the Curie peak is at a higher temperature similar to that of films directly dried at 135°C.

Drying the films at high temperature below the Curie temperature and further annealing favors better order and will be used in the following to enhance the properties of the films for device applications.

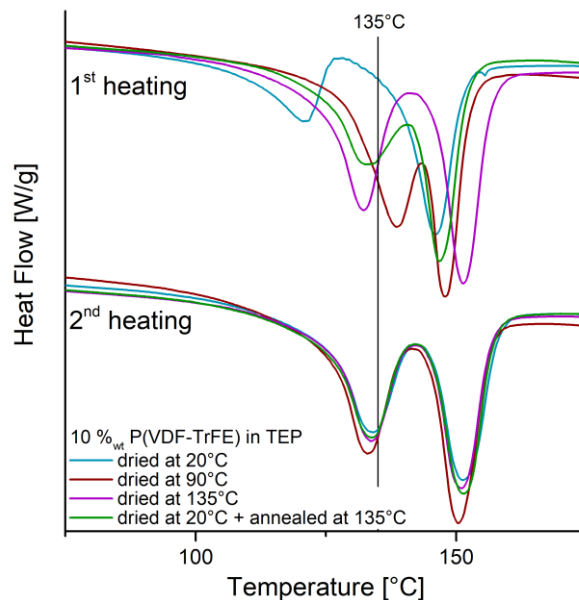


Figure 3.6: Differential Scanning Calorimetry of films of P(VDF-TrFE) obtained by drop casting a solution of 10%wt P(VDF-TrFE) in TEP and dried at 20°C, 90°C 135°C or dried at 20°C and annealed at 135°C.

To complete the study of the neat polymer, rheological measurements of P(VDF-TrFE) solutions at different concentrations (batch FC20-054) in GBL were done at 20°C. Figure 3.7 shows that for low concentrations, only the Newtonian plateau in viscosity is visible. For high concentrations above 20 %wt, shear thinning behavior appears for high shear rates only. At higher

concentrations (30 %<sub>wt</sub>) the solution become shear thinning. Similar measurements were carried out for the batch FC20 62-053 [see Appendix A.6].

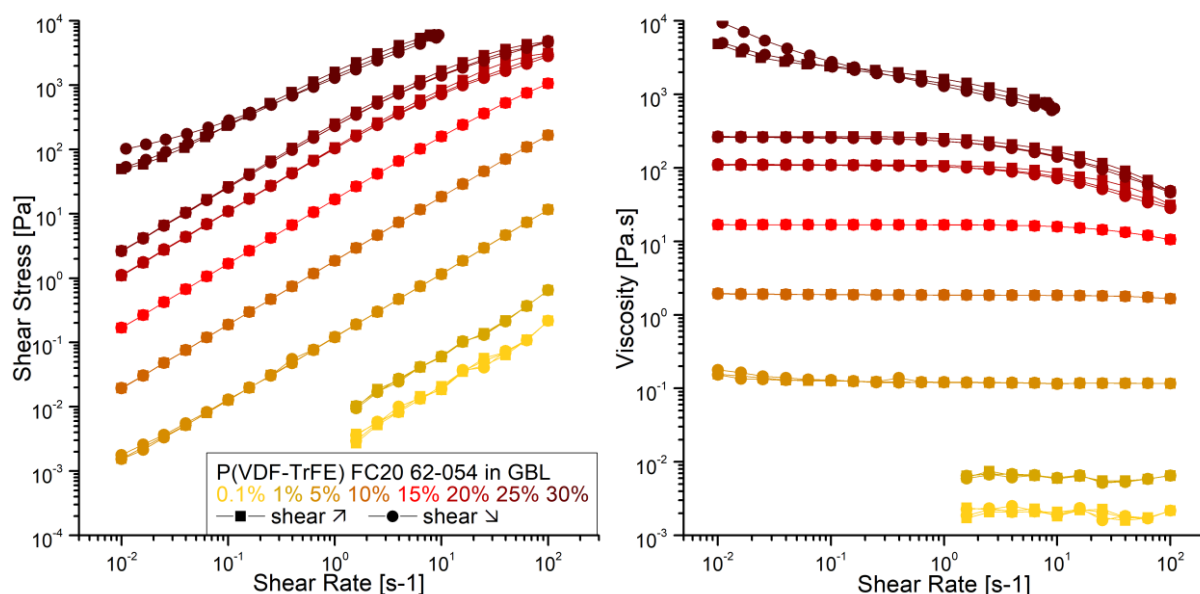


Figure 3.7: Rheological behavior of P(VDF-TrFE) (batch FC20 62-054) in GBL at different concentration measured with a shear rheometer (cone plate geometry: 50 mm diameter and 1° angle): viscosity versus shear rate and shear stress versus shear rate, obtained by applying shear rate ramps at 20°C.

Using the viscosity on the Newtonian plateau, a reduced viscosity was calculated to determine a critical concentration  $C^*$  separating the dilute from the semi-dilute regime. The following relation was used:  $Reduced\ viscosity = \frac{\eta_i}{C_{polymer}}$  where

$$\eta_i = \frac{\eta - \eta_{solvent}}{\eta_{solvent}} = Relative\ viscosity\ increment.^6$$

Figure 3.8 displays the results for the two batches of P(VDF-TrFE):  $C^*$  was found lower for the batch FC20 62-054 than for the batch FC20 62-053: 0.19 g/mL compared to 0.26 g/mL, (which correspond to 14.1 %<sub>wt</sub> compared to 18.7 %<sub>wt</sub> with respect to the total weight). That is consistent with the SEC measurements: the polymers of the FC20 62-054 batch have a higher molar mass.

The current commercial ink used for screen-printing (FC25 InkP, from Arkema) has a concentration close to the  $C^*$  found (15 – 18 %<sub>wt</sub>).

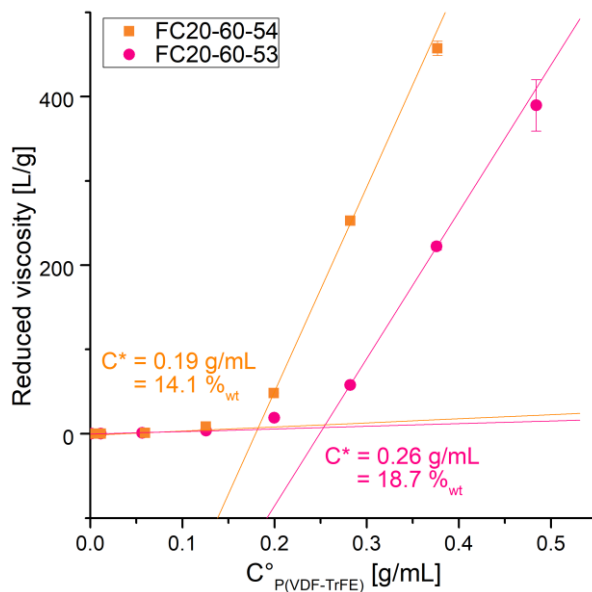


Figure 3.8: Reduced viscosity of two batches of P(VDF-TrFE) in GBL versus Concentration: two characteristic concentrations can be extracted ( $C^*$ )

Further rheological characterization has been carried out to determine whether solutions of P(VDF-TrFE) inks can be gel like. In fact, it has been shown that PVDF alone forms a gel at low temperatures in solvents such as GBL [Figure 3.9].<sup>7</sup>

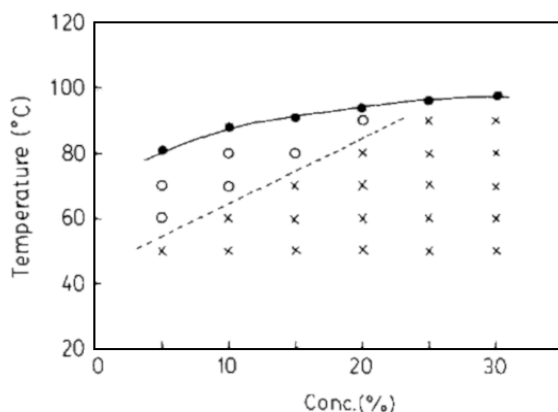


Figure 3.9: Phase diagram of PVDF/ $\gamma$ -butyrolactone solution:  $\bullet$ , gel melting temperatures; ---, sol-gel transition temperatures ( $\circ$ , sol;  $\times$ , gel states) [from <sup>7</sup>]

It is thus important to verify if the copolymer P(VDF-TrFE) presents similar behavior as PVDF. Dynamic oscillatory stress sweep measurements at 20°C [Figure 3.10] show that for all the concentrations, the storage modulus  $G'$  is always smaller than the loss modulus  $G''$ : the viscous contribution is higher than the elastic one even though the ratio of elastic to viscous moduli increases with concentration. The solutions are therefore not in a gel state at 20°C. Furthermore, the viscosity of P(VDF-TrFE) solutions evolves almost linearly with the temperature [See Appendix A.7].

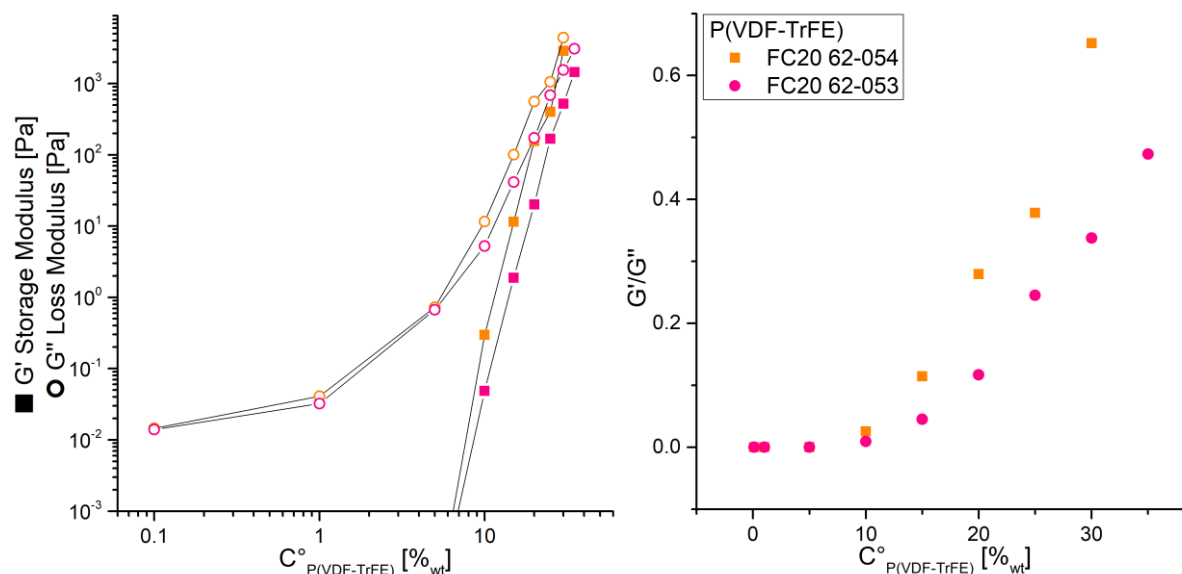


Figure 3.10: (left) Rheological behavior of two batches of P(VDF-TrFE) inks in GBL measured with a shear rheometer (cone plate geometry 50 mm / 1°): average value of storage  $G'$  and loss  $G''$  modulus (obtained at a frequency of 1 Hz at 20°C) in the linear viscoelastic range (i.e. in the plateau region) versus concentration. (right) Ratio between the storage modulus  $G'$  and the loss modulus  $G''$  of two batches of P(VDF-TrFE) inks.

As mentioned above, to process P(VDF-TrFE) inks using screen printing, the solutions need to be formulated properly. Different ways to change the rheological behavior of the ink from Newtonian to shear thinning behavior will be explored. All the following studies were done with the batch FC20 62-054. First, a gelifying agent was added to a solution of P(VDF-TrFE) in good solvents of the polymer.

## 3.4 P(VDF-TrFE) solutions with a gelifying agent

### 3.4.1 Additives and formulations of T<sub>PXP</sub>A<sub>XA</sub> inks

A gelifying agent is a molecule or a polymer that forms a percolated network structure in a solvent. If weak bonds are used to form the three-dimensional network, such as hydrogen bonds, a physical gel can be obtained.<sup>8</sup> On the other hand, a nucleating agent is a molecule that can initialize the crystallisation in materials. It can tune the degree of crystallinity as well as the shape and size of the crystals of crystalline polymers.<sup>9</sup>

Two different gelifying agents were chosen: 1,3:2,4-Bis(3,4-dimethylbenzylidene)sorbitol (DMDBS) [Figure 3.11] and tris-tert-butyl-1,3,5-benzenetrisamide (BTA) [Figure 3.12]. It has been demonstrated that these additives can be used as nucleating agents<sup>10</sup> and as organic gelators in the case of DMDBS.<sup>11</sup> Here we will focus first on the rheological modification and later on the crystalline properties of the films.

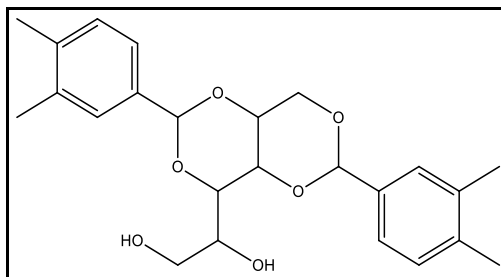


Figure 3.11: Structure of DMDBS (1,3:2,4-Bis(3,4-dimethylbenzylidene)sorbitol).

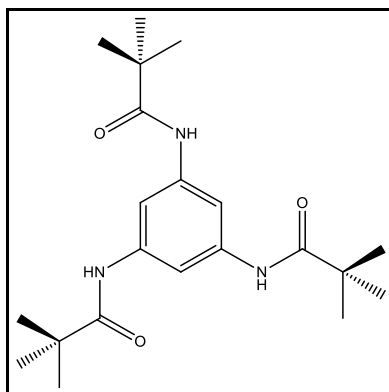


Figure 3.12: Structure of BTA (tris-tert-butyl-1,3,5-benzenetrisamide).

BTA and DMDBS were solubilised in triethylphosphate (TEP), which is the solvent used for the commercial ink, in GBL and in methyl ethyl ketone (MEK), which are two other good solvents of P(VDF-TrFE), at different concentrations. Both gelifying agents are insoluble in the three solvents at room temperature. To solubilize these agents a high temperature is needed.

BTA was soluble only at low concentrations (below 0.5 %<sub>w</sub>) and forms filament like crystals at higher concentrations in TEP or GBL (solubilized at 130°C for 10 – 15 min). In MEK, 0.3 %<sub>w</sub> BTA can be solubilized at 70°C in 10 min, and forms filament like crystals after 10 min at room temperature. Because of the difficulty to solubilize BTA at high concentrations without obtaining crystals, the study focused mainly on DMDBS.

In the case of 0.3 and 3 %<sub>w</sub> DMDBS in TEP or GBL, good dissolution was obtained at 130°C during 10 – 15 min. For the second concentration, a gel started to form after 10 – 30 min at room temperature (white appearance) while the low concentration stayed fluid and transparent. DMDBS was not soluble in MEK even after 2h at 110°C. Other tests of solubility in other solvents of P(VDF-TrFE) were carried out to determine the solubilization temperature of DMDBS [Table 3.2]. The solvent DMSO gives the lowest solubilization temperature.

Solvent	T <sub>solubilization</sub>
TEP	130°C
GBL	130°C
MEK	-
DMSO	60°C
Cyclopentanone	90°C
Cyclohexanone	95°C

Table 3.2: Temperature at which 0.01%<sub>wt</sub> DMDBS start to solubilise in solvents of P(VDF-TrFE): TEP, GBL, MEK, dimethyl sulfoxide (DMSO), Cyclopentanone and cyclohexanone.

Different amounts of DMDBS were added in P(VDF-TrFE) solutions at different concentrations: 0.1 %<sub>wt</sub>, 1 %<sub>wt</sub>, 10 %<sub>wt</sub> and 15 %<sub>wt</sub> of polymer in GBL or TEP. The concentration of DMDBS is given with respect to the polymer weight. Each time, DMDBS was first solubilized in the solvent at 130°C, P(VDF-TrFE) was solubilized in the solvent at 60°C, and then the two solutions were mixed together at 60°C with a magnetic stirrer or a spatula (the DMDBS solution was added while at 130°C in the case of high concentrations to remain fluid and soluble). The solutions at 0.1 %<sub>wt</sub> and 1 %<sub>wt</sub> of P(VDF-TrFE) and concentrations of DMDBS from 0.1 to 10 %<sub>wt</sub> were transparent and very fluid at room temperature. The solutions at 10 %<sub>wt</sub> and 15 %<sub>wt</sub> of P(VDF-TrFE) were more viscous. While the 15 %<sub>wt</sub> solution remained transparent, the 10%<sub>wt</sub> P(VDF-TrFE) displayed some turbidity for the TEP solvent and for concentrations of DMDBS around 5 %<sub>wt</sub> and higher. While the solution at 8 %<sub>wt</sub> and 10 %<sub>wt</sub> DMDBS in TEP started have white domains from the beginning, the 5 %<sub>wt</sub> solution becomes turbid only if sheared [Figure 3.13].

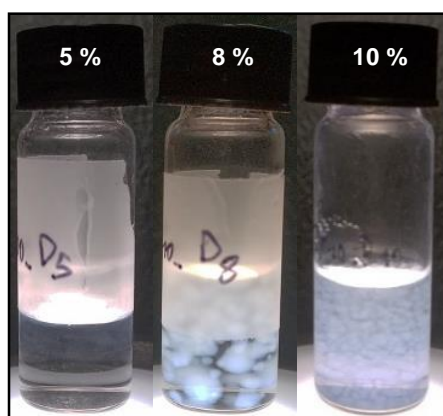


Figure 3.13: three solutions of DMDBS in triethylphosphate with 10%<sub>wt</sub> P(VDF-TrFE) at different concentrations: 5, 8 and 10 %<sub>wt</sub> of DMDBS with respect to the polymer

Rheological measurements were then performed. The solutions of 5 to 10 %<sub>wt</sub> DMDBS in 10 %<sub>wt</sub> P(VDF-TrFE) in GBL or TEP became completely white after the rheological measurements while the rest stayed completely transparent [Table 3.3].

Solvent	TEP	GBL	TEP	GBL	TEP	GBL	TEP	GBL
P(VDF-TrFE) [%wt/total]	0.1		1		10		15	
DMDBS [%wt/polymer]	0.1	T/-	T/-	T/-	T/-	T/-	T/-	(0.07%) T/T
	1	T/-	T/-	T/-	T/-	T/T	T/T	(0.7%) T/T
	5	-	-	-	-	T/W	T/-	(6%) T/T
	8	-	-	-	-	WT/W	T/-	-
	10	T/-	T/-	T/-	T/-	WT/W	T/-	-

Table 3.3: visual aspect of the solutions with different amount of P(VDF-TrFE) and DMDBS in TEP or GBL: before/after rheology (T = transparent; W = completely white; WT = white domains in transparent solution; - = not measured).

### 3.4.2 Rheological behaviors of T\_P0.1-15\_D0.1-10 inks

The first solutions studied were the 15 %wt P(VDF-TrFE) solutions in TEP and GBL. This concentration is close to  $C^*$  measured in part 3.3. Figure 3.14 displays the rheological measurements of this solution at 0 %wt, 0.07 %wt, 0.7 %wt, and 6 %wt of DMDBS or BTA in TEP or GBL. Multiple shear rates were applied at 20°C. The results for commercial PEDOT:PSS (Orgacon EL-P 5015) is displayed as a reference. The results at concentrations between 0 %wt and 0.7 %wt of gelifying agent are very similar and the small differences in viscosity are not significant. All solutions have a Newtonian plateau in the studied shear rate range (0.01 – 100s<sup>-1</sup>). The addition of 6 %wt of DMDBS increases the viscosity by a factor of 3, but the behavior stays the same with a Newtonian plateau.

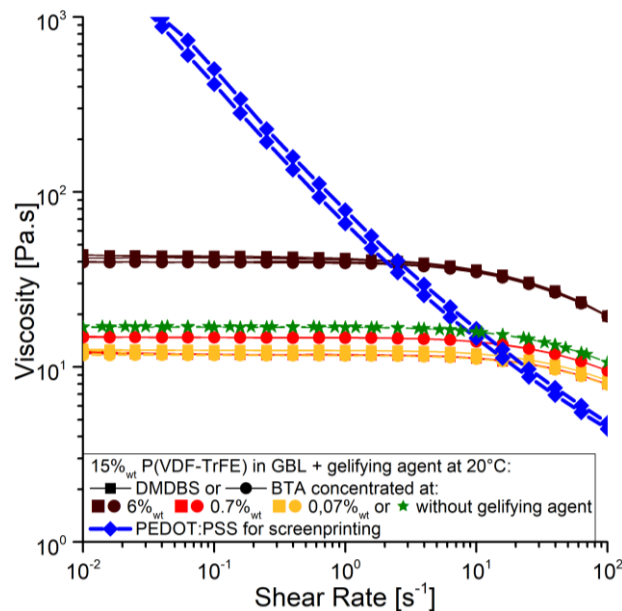


Figure 3.14: Rheological behavior of solution of 15%wt P(VDF-TrFE) in GBL or TEP with 0 %wt, 0.07 %wt, 0.7 %wt, and 6 %wt of DMDBS or BTA, measured with a shear rheometer (cone plate geometry: 50 mm diameter and 1° angle): viscosity versus shear rate obtained by applying multiple shear rate ramps (increasing and decreasing) at 20°C. The curve of commercial PEDOT:PSS (Orgacon EL-P 5015) was added as reference.

All the solutions at 0.1 and 1 %<sub>wt</sub> P(VDF-TrFE) were too fluid and therefore not considered. The rheological measurements of solutions at 10 %<sub>wt</sub> P(VDF-TrFE) and various concentrations of DMDBS are shown in Figure 3.15 and Figure 3.17. For low concentrations of gelifying agent (0 %<sub>wt</sub> or 1 %<sub>wt</sub>), the inks stayed Newtonian even after four shear sweep cycles. For 8 %<sub>wt</sub> or 10 %<sub>wt</sub> DMDBS, the ink is ejected from the rheometer and the measurements are difficult to carry out. For 5 %<sub>wt</sub> DMDBS, the properties of the ink evolve during the measurement: it starts with a Newtonian plateau for the first shear sweep cycle and becomes shear-thinning and more viscous for the following cycles. The ink is anti-thixotropic: the viscosity increases with time and number of shear sweep cycles. After a certain number of such cycles, the viscosity reaches a steady state as the flow curve (stress versus shear) becomes stable and does not change with further cycles. Only a small hysteresis between the increasing and decreasing shear rate ramps is maintained contrary to the initial stages where the hysteresis was large. No ejection from the Rheometer occurs, and the ink after being subjected to several shear cycles, becomes turbid and presents a white appearance.

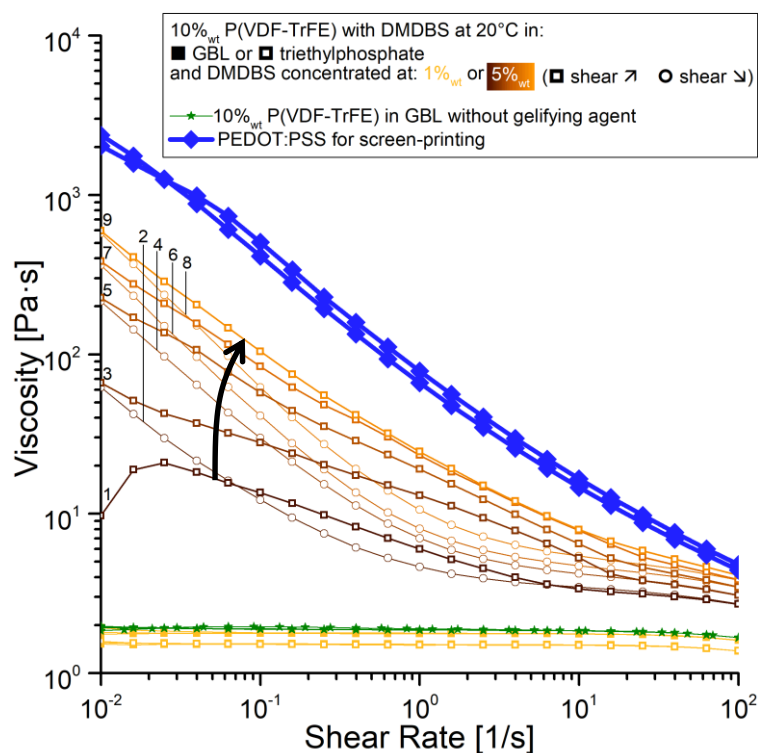


Figure 3.15: Rheological behavior of a solution of 10 %<sub>wt</sub> P(VDF-TrFE) in GBL or TEP with 0 %<sub>wt</sub>, 1 %<sub>wt</sub> or 5 %<sub>wt</sub> of DMDBS or BTA. Measurements were done with a shear rheometer (cone plate geometry: 50 mm diameter and 1° angle): viscosity versus shear rate obtained by applying multiple shear rate ramps (increasing and decreasing) at 20°C. The curve of commercial PEDOT:PSS (Orgacon EL-P 5015) was added as reference. The numbers represent the number of shear rate ramps applied to the sample.

Considering the non-stationary behavior observed for these inks, a new process of formulation was then carried out for the same ink (T\_P10\_D5) in a reactor with a four blade stirrer [Figure 3.16]. The strategy is to obtain an ink with stationary properties by subjecting it to shear in this reactor to produce the stationary shear thinning ink directly.

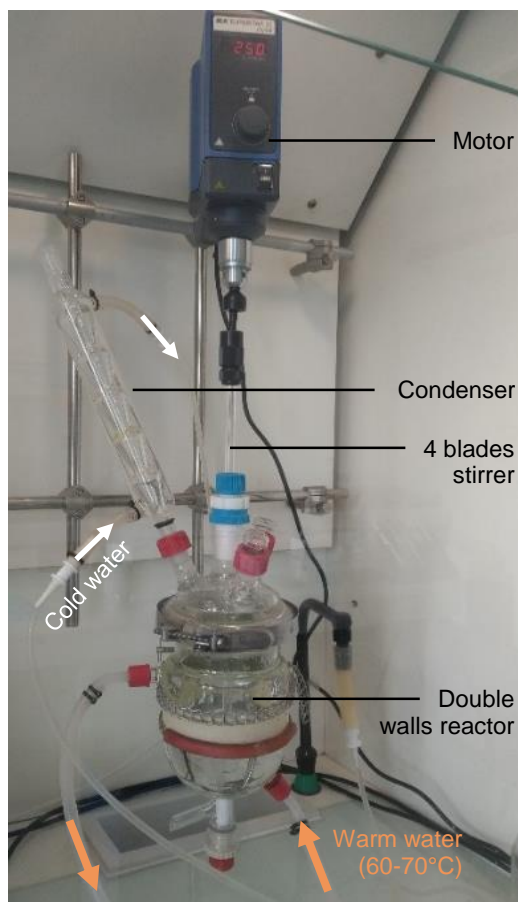


Figure 3.16: Double walls reactor with a four blade glass stirrer used to formulate 200mL of P(VDF-TrFE) inks.

The inks produced using the reactor, will carry the mention “R” at the end of their name: T\_P10\_D5\_R. The properties of this ink are shown as the red curves in Figure 3.17: the behavior is now shear thinning and very stable with 32 shear ramps. The oscillatory measurements, however, show an elastic modulus which is lower than the viscous modulus. Both moduli are however greater than those measured for the ink T\_P10 without gelifying agent (in dark green). A trial of the same kind of ink with the second gelifying agent, BTA, was carried (T\_P12\_B5), but little shear-thinning is observed. If the DMDBS is added directly to the solution of P(VDF-TrFE) in TEP heated at 60°C, the solubilization of the DMDBS is incomplete and most probably remains in powder form, and only Newtonian behavior is obtained. It is thus important to heat and dissolve DMBS correctly before adding it to the solution of polymer.

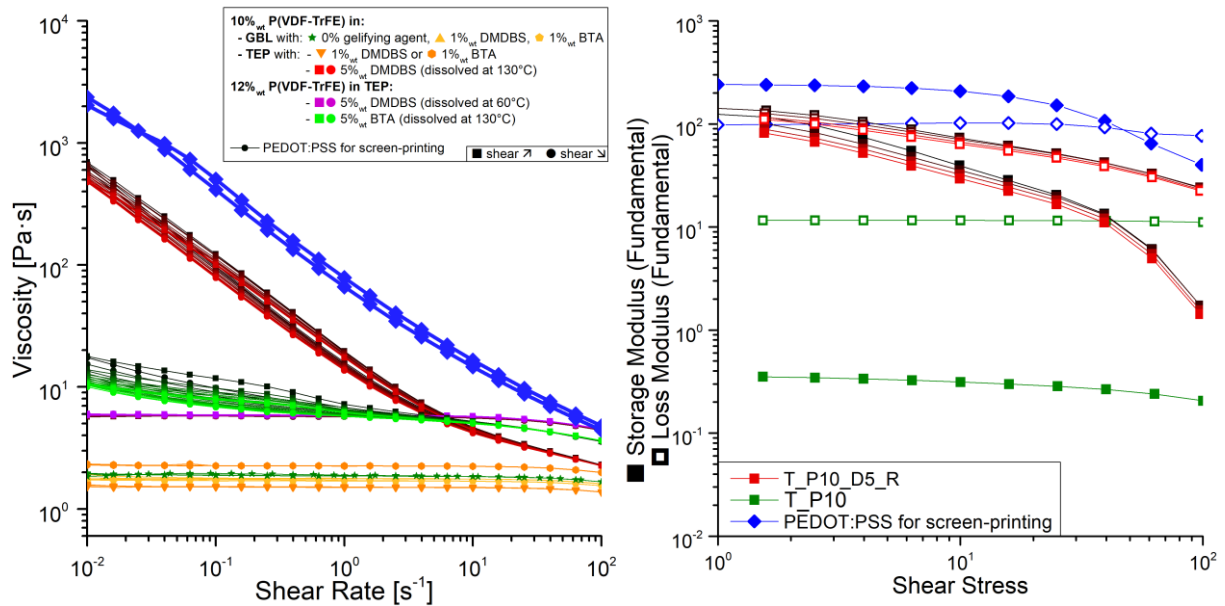


Figure 3.17: Rheological behavior of solutions of 10 or 12 %wt P(VDF-TrFE) in GBL or TEP with 0, 1 or 5 %wt of DMDBS or BTA; the gelifying agents were dissolved at 130°C (or one time at 60°C) and the polymer was dissolved at 60°C. Measurements were done with a shear rheometer (cone plate geometry: 50 mm diameter and 1° angle): viscosity versus shear rate obtained by applying multiple shear rate ramps (increasing and decreasing) at 20°C. The curve of commercial PEDOT:PSS (Orgacon EL-P 5015) was added as reference.

Rheological behavior of solutions of 10 or 12 %wt P(VDF-TrFE) in GBL or TEP with 0 %wt, 1 %wt or 5 %wt of DMDBS or BTA; the gelifying agents were dissolved at 130°C (or one time at 60°C) and the polymer was dissolved at 60°C. Measurements were done with a shear rheometer (cone plate geometry: 50 mm diameter and 1° angle): viscosity versus shear rate obtained by applying multiple shear rate ramps (increasing and decreasing) at 20°C. The curve of commercial PEDOT:PSS (Orgacon EL-P 5015) was added as reference.

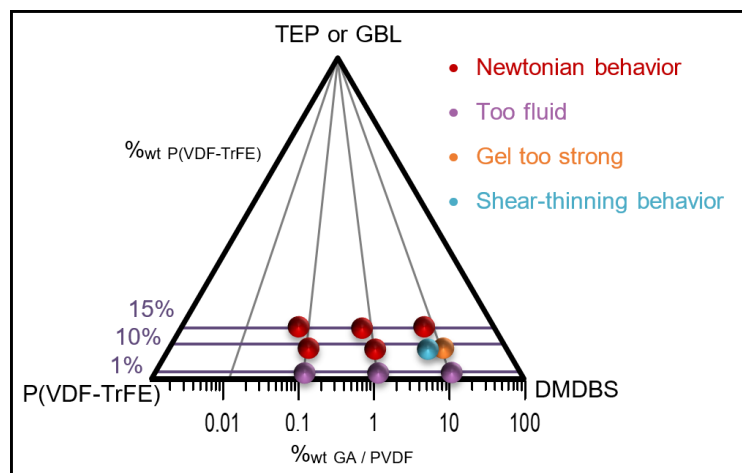


Figure 3.18: Phase diagram of P(VDF-TrFE) and DMDBS in TEP or GBL and corresponding rheological behaviors

Figure 3.18 summarizes the studied inks and their rheological behaviors in a phase diagram. Low concentrations of P(VDF-TrFE) (1 %wt) result in inks of low viscosity unsuitable for screen-printing applications, while high concentrations of polymer (15 %wt) with concentrations of gelifying agent comprised between 0.07 and 6 %wt have a Newtonian behavior. For intermediate

concentrations (10 %<sub>wt</sub>) of P(VDF-TrFE), different regimes are observed: for low concentration in gelifying agent (0.1 – 1 %<sub>wt</sub>), the inks are Newtonian, while for high concentrations (8 – 10 %<sub>wt</sub>), the inks become very strong gels. Finally for an intermediate concentration of 5 %<sub>wt</sub> DMDBS, the ink becomes shear-thinning, acquires high viscosities and elastic moduli in the range of 100 Pa. These properties make this ink the most suitable for screen-printing or doctor blading applications. The last ink, called T\_P10\_D5\_R, was then adopted for further characterization as well as to form films and characterize them after drying.

### 3.4.3 Structure of T\_P10, T\_D0.03 g/mL, and T\_P10\_D5 inks

To try to understand the mechanism that renders the ink shear-thinning, liquid DSC and cryo-SEM were performed. The purpose of liquid DSC was to see if there is any crystallisation in solution. Indeed, DMDBS is not only a gelifying agent,<sup>11</sup> but also a nucleating agent.<sup>10</sup> However, no crystallisation peak was found from -70°C to 150°C except the ones of the solvent. No crystallisation seems to occur in solution. Additional characterizations using cryo-SEM were also performed.

For these characterizations, the samples are first frozen using liquid Nitrogen and then held at a low temperature, which is sample dependent, for a certain period of time to sublimate the solvent. For the ink T\_P10, a temperature of -70°C was used during 10 min [Figure 3.19]. This ink is composed of small polymer spheres in the range of 40 – 50 nm. A solution of 0.03 g/mL DMDBS dissolved in TEP was also observed after becoming a gel at room temperature. The sublimation was carried at -85°C for 20 min. The results are shown in Figure 3.20 where a structure characteristic of the fracturing of spherulitic structures appears with lines diverging from a common point. At higher resolution, small aligned spheres (50 – 70 nm) start to appear; the spacing between the lines is in the range 160 – 520 nm ( $365 \pm 135$  nm).

A mechanism of aggregation has been proposed for DBS (1,3:2,4-(dibenzylidene)sorbitol) another derivative of sorbitol very similar to DMDBS without methyl groups at the ends of the benzyl groups. This molecule is known to have a “butterfly” shape with polar “body” due to the hydroxyl groups, and apolar aromatic “wings”. DBS forms twisted fibers of 10nm in diameter in organic solvents and forms a physical thermo-reversible gel through hydrogen bonds. A similar mechanism may operate for DMDBS.<sup>9,12</sup>

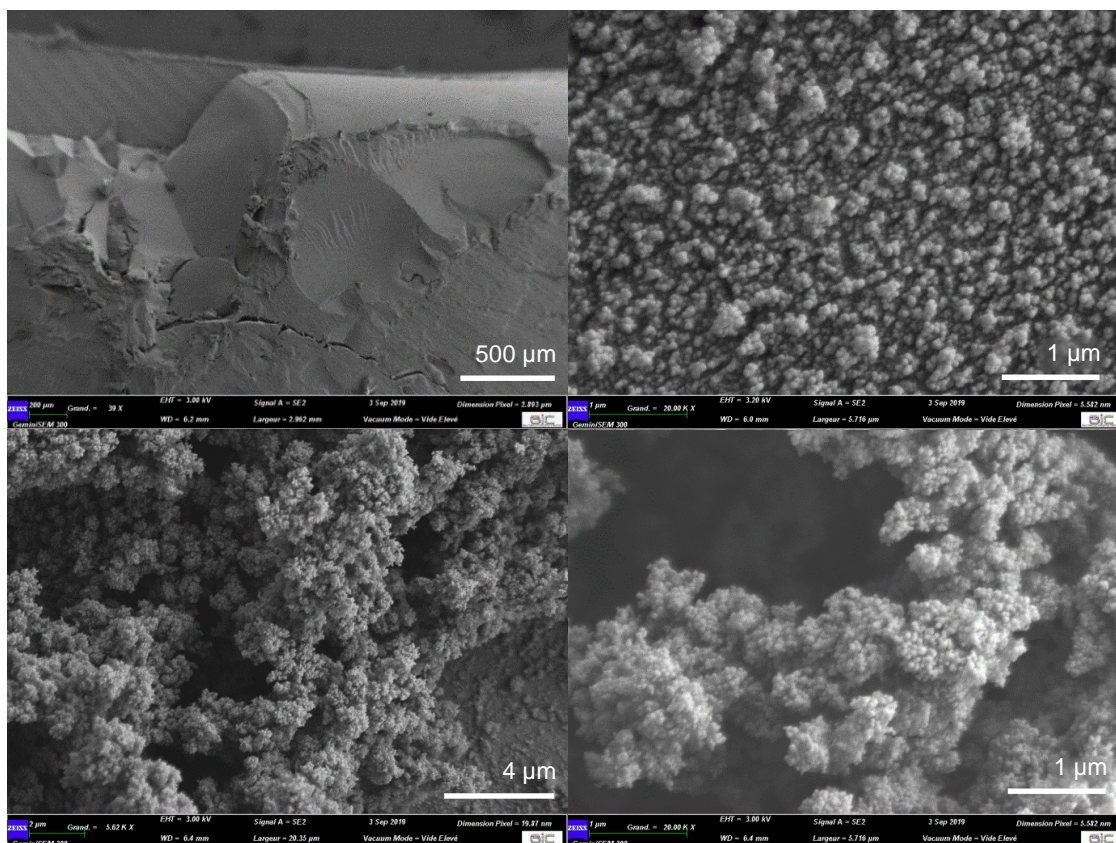


Figure 3.19: cryo-Scanning Electron Microscopy (cryo-SEM) pictures of the ink T<sub>P10</sub> sublimated at -70°C during 10 min and metallised with 10 mA during 40 s (x39, x20K, x5.6K and x20K respectively).

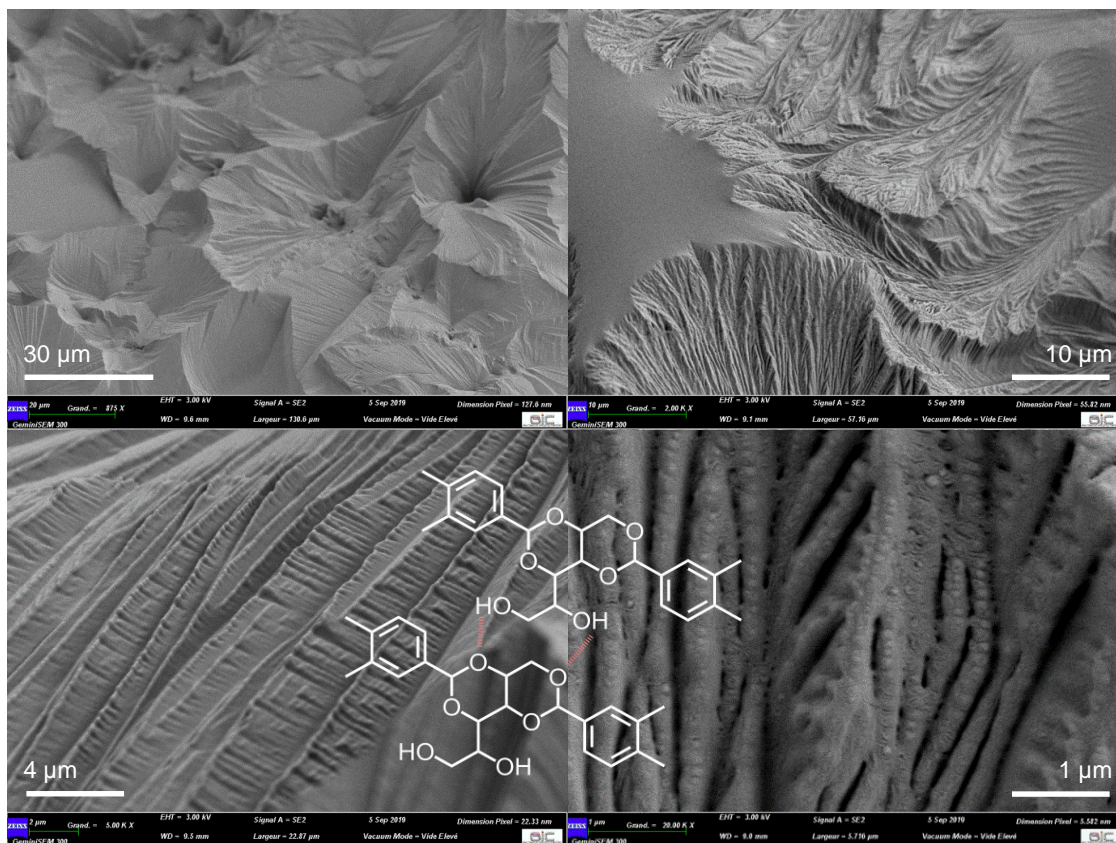


Figure 3.20: cryo-Scanning Electron Microscopy (cryo-SEM) pictures of a solution of DMDBS at 0.03 g/mL in TEP sublimated at -85°C during 20 min and metallised with 10 mA during 40 s (x875, x2K, x5K and x20K respectively), and possible hydrogen bonds between two DMDBS molecules.

For the ink T\_P10\_D5 [Figure 3.21], sublimation was carried out at  $-95^{\circ}\text{C}$  during 15 min or at  $-85^{\circ}\text{C}$  during 10 min.

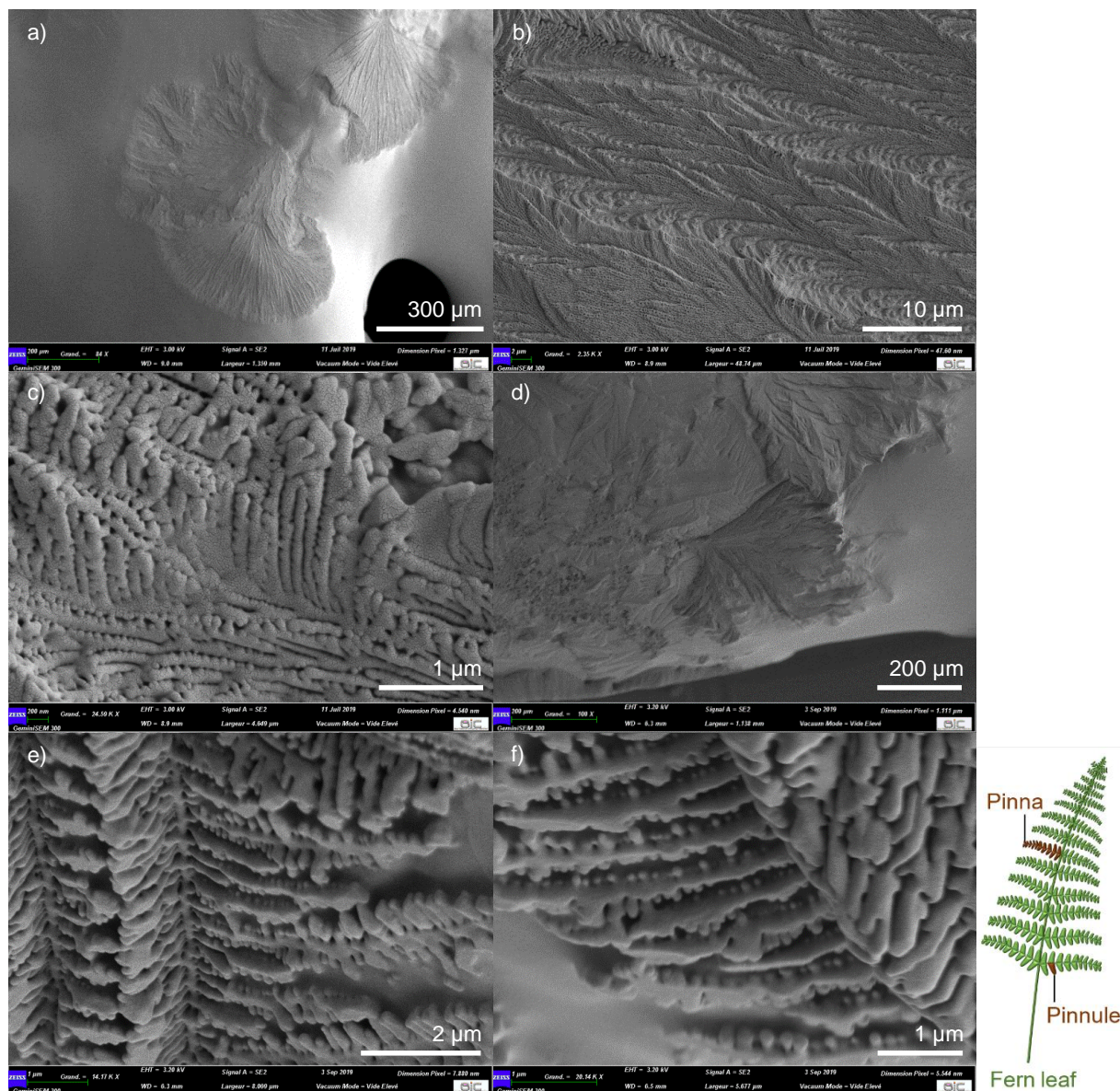


Figure 3.21: cryo-Scanning Electron Microscopy (cryo-SEM) pictures of the ink T\_P10\_D5\_R sublimated at  $-95^{\circ}\text{C}$  during 15 min (a-c) or at  $-85^{\circ}\text{C}$  during 10 min (d-f) and metallised with 10 mA during 40 s (x34, x2.4K, x25K, 100, x14K, x20K respectively).

In Figure 3.21, spherulitic structures appear similarly to the solution of DMDBS in TEP [Figure 3.20]. A closer look revealed that the ordered lines have ramifications with primary and secondary divisions, as the leaves of a fern. Small spheres appear at certain places alongside each line as the pinnules of a fern. The smaller and best defined spheres have a diameter in the range of 50 – 60 nm. The spacing between the lines is in the range 150 – 480 nm ( $350 \pm 100$  nm), which is close to the one found for DMDBS in TEP. It is possible that the small spheres are not observed over the whole sample because sublimation is not efficient and complete over the whole observed area.

In conclusion, the gelifying agent allows the structuring of the ink. In the absence of gelifying agent, the polymers adopt the shape of small spheres without any organisation and which results in a Newtonian behavior for the rheology. For the ink with gelifying agent, the polymers are small spheres organized along lines, a structure which may give rise to a shear thinning behavior: by increasing the shear, the lines may orient and align in the flow direction.

To summarize, the ink T\_P10\_D5\_R can be easily processed as its rheological properties are suitable for screen-printing and doctor blading. Furthermore, this ink allows for the formation of homogeneous P(VDF-TrFE) films as we will see below. The only disadvantage is related to the high temperature (130°C) needed to dissolve the gelifying agent (DMDBS) in the TEP solvent. In the next section, we propose a strategy to decrease this temperature by first dissolving DMDBS in DMSO, which is a good solvent for DMDBS and allows solubilization at 60° C, before blending with the solution of P(VDF-TrFE) in TEP.

### 3.4.4 Gelifying agent in a mixture of a good and a bad solvent of DMDBS

#### 3.4.4.1 Solubility of DMDBS in different solvents

The gelifying agent DMDBS is soluble in DMSO and the solution is liquid like. In order to obtain gels, DMDBS has to be dissolved in a mixture of DMSO and a bad solvent of DMDBS. Since we do not know the proportion of TEP and DMSO necessary to obtain gels with DMDBS, we have examined the solubility properties of DMDBS in the literature.

The solubility of DMDBS in different solvents has been studied previously. Shen et al have shown that DMDBS forms gels in mixtures of DMSO and a variety of bad solvents [see Table 3.4].<sup>13</sup> Gels were obtained in a range of concentrations of the bad solvent comprised between 60 and 80 %<sub>vol</sub> as summarized in Table 3.4. We have therefore tested a mixture of 30% DMSO and 70% TEP which indeed allows the formation of a gel in the presence of DMDBS.

Systems	System 1					System 2				Extreme values
	carbon tetrachloride	mesitylene	toluene	o-xylene	ethylbenzene	methanol	ethanol	propanol	butanol	
Minimum concentration of bad solvent in DMSO to have a gel [%]	50	50	60	60	60	40	50	50	60	60
Maximum concentration of bad solvent in DMSO to have a gel [%]	80	90	90	90	90	60	80	80	90	80

Table 3.4: Summary of the concentration of the solvents (in DMSO) in which DMDBS forms a gel after dissolution

### 3.4.4.2 Rheological behavior of 3D7T\_P12\_D5 and D\_P12\_D5 inks

In fact, TEP acts as a good solvent of DMDBS at high temperatures, but as a bad solvent at room temperature. Different inks were then formulated: 10 or 12 %<sub>wt</sub> P(VDF-TrFE) + 5 %<sub>wt</sub> DMDBS in 30 %<sub>vol</sub> DMSO and 70 %<sub>vol</sub> TEP, which will be compared with inks formulated using DMSO only. The ratio used for TEP in DMSO is in the range where gels are obtained. The results for the viscosity versus shear rate are displayed in Figure 3.22: in 100 % DMSO (D\_P12\_D5), only Newtonian behavior is obtained, while in 70 %<sub>vol</sub> TEP and 30 %<sub>vol</sub> DMSO (3D/7T\_P12\_D5\_R), a shear thinning behavior is obtained. The interest of this ink from the previous working inks (T\_P10\_D5\_R) is that no high temperature is needed (60°C instead of 130°C), which is more comfortable for large scale formulations.

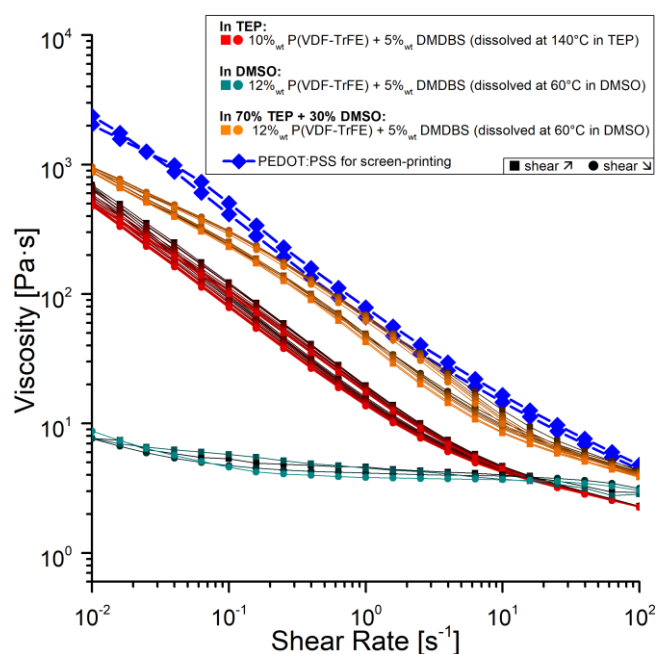


Figure 3.22: Rheological behavior of solution of 5 %<sub>wt</sub> of DMDBS dissolved in TEP at 140°C added at a 10 %<sub>wt</sub> P(VDF-TrFE) solution in TEP at 60°C, 5 %<sub>wt</sub> of DMDBS dissolved in DMSO at 60°C and 12 %<sub>wt</sub> P(VDF-TrFE) added at 60°C, 5 %<sub>wt</sub> of DMDBS dissolved in DMSO at 60°C and added to a solution of P(VDF-TrFE) dissolved in TEP at 60°C (result: 70 % TEP + 30 % DMSO, 5 %<sub>wt/polymer</sub> DMDBS + 12 %<sub>wt/total</sub> P(VDF-TrFE)). Measurements were done with a shear rheometer (cone plate geometry: 50 mm diameter and 1° angle): viscosity versus shear rate obtained by applying multiple shear rate ramps (increasing and decreasing) at 20°C. The curve of commercial PEDOT:PSS (Orgacon EL-P 5015) was added as reference.

To summarize, the use of a gelifying agent in the P(VDF-TrFE) solutions allows to obtain shear thinning solutions with stationary properties (independent of time and history) once prepared using the home made reactor. Further, and to work at lower temperatures, the gelifying agent can be dissolved in small amounts of DMSO, a good solvent, before being blended with the polymer solution.

In the next section, the properties of films obtained using the viscous shear thinning inks in the presence of the gelifying agent and prepared using the reactor will be examined. We recall that these inks have optimal properties for film formation using screen-printing or doctor blading.

## 3.4.5 Properties of films

### 3.4.5.1 Structure of films obtained using T\_P10\_D5\_R

SEM images of T\_P10\_D5\_R films obtained using doctor blading on glass substrates, dried at 135°C and cooled at room temperature, are displayed in Figure 3.23. Homogeneous films with no big domains are obtained at large scales (a). At greater magnification, linear structures appear (b) which become even more pronounced at higher and higher magnifications (c,d). In image d, taken at the highest resolution one can distinguish structure reminiscent of those observed in Figure 3.21 and obtained in cryo SEM. Similar images are obtained for films dried at room temperature and then annealed at 135°C during 40 min and cooled down at room temperature. The lines can be attributed to DMDBS. Indeed, it has been shown that DBS forms crystalline fibers that are nucleating sites on which polymers can crystallise epitaxially.<sup>12</sup> A similar mechanism could apply for DMDBS.

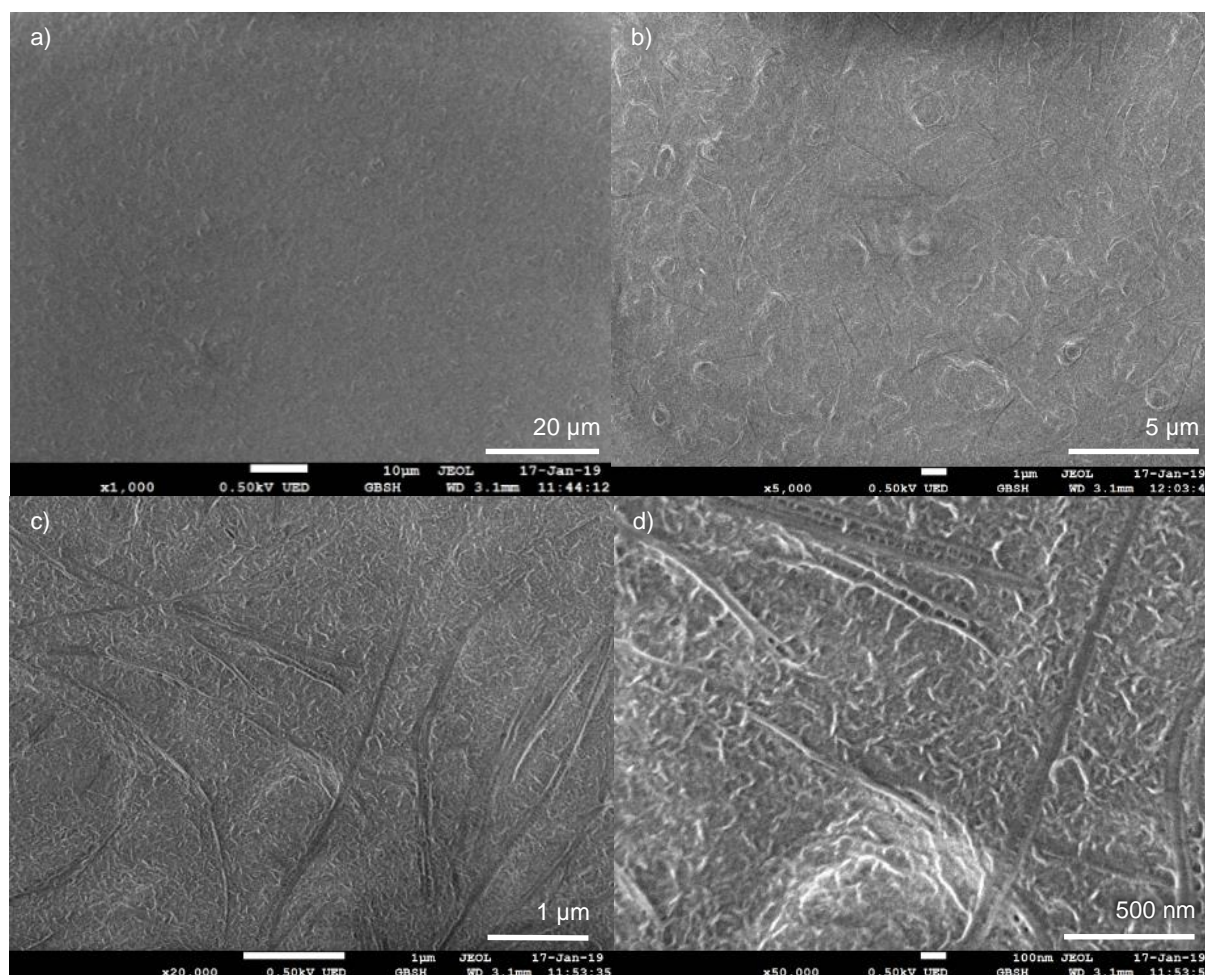


Figure 3.23: SEM image of dried film of the ink T\_P10\_D5\_R (spin coated on glass) dried at 135°C and cooled down at room temperature (x 5 000; x 20 000; and x 50 000)

To summarize, the ink T\_P10\_D5\_R has rheological properties which are suitable for screen-printing and doctor blading and allows for the formation of homogeneous P(VDF-TrFE) films.

### 3.4.5.2 Wettability of films

For processing purposes, it is important to measure the surface free energy of dried films. Measurements for P(VDF-TrFE) films are shown in Figure 3.24. Before annealing, the surface free energy is of  $27 \pm 6$  mN/m when the solvent used is TEP independently of the presence or not of the gelifying agent. After annealing, the surface free energy increases to  $30 \pm 2$  mN/m. For P(VDF-TrFE) in GBL, the surface free energy of dried films is the same before and after annealing ( $31 \pm 3$  mN/m). For all cases, the dispersive contribution to the free energy dominates over the polar contribution. In accordance with this observation, a contact angle between water drops and the films are around  $100^\circ$  before annealing, and  $95^\circ$  after annealing [Table 3.5] (a little lower in GBL). Such high contact angles can be problematic when depositing aqueous inks on these films. For example, dewetting problems are encountered when inkjet printing PEDOT aqueous solutions, to create a conducting film on top on PVDF films. To overcome this problem, UV-Ozone treatment as well as heating the substrate will be used for PEDOT layers printed by inkjet in the next chapter.

Ink	Contact angle of water drops [ $^\circ$ ]	
	Before annealing	After annealing
3D7T_P12_D5_R	$99.9 \pm 0.2$	$95.3 \pm 1.3$
T_P10_D5_GR	$97.7 \pm 0.5$	$92.5 \pm 2.1$
T_P15	$99.1 \pm 0.4$	$95.4 \pm 1$
G_P15	$91.1 \pm 2$	$81.4 \pm 0.7$

Table 3.5: Contact angle of water drops on P(VDF-TrFE) dried films obtained from different formulation: T\_15P, G\_15P, T\_P10\_D5\_R, 3D7T\_P12\_D5\_R.

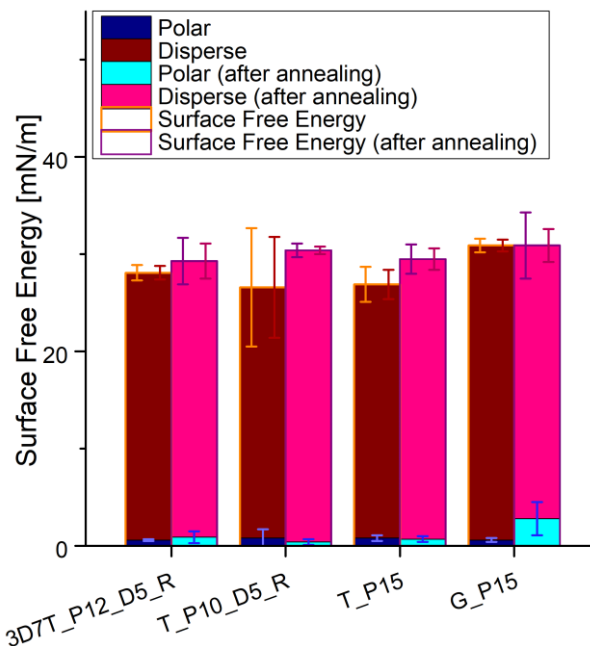


Figure 3.24: Surface free energy of films made from different solutions of P(VDF-TrFE): T\_15P, G\_15P, T\_P10\_D5\_R, and 3D7T\_P12\_D5\_R.

### 3.4.5.3 Crystallinity of films

DSC measurements were done on dried films using different formulations of P(VDF-TrFE) with DMDBS as gelifying agent.

Indeed, DMDBS is also known to be a nucleating agent: smaller crystals, in higher number, and with more homogeneous size should be obtained.

Figure 3.25 shows that the Differential Scanning Calorimetry (DSC) curves of films obtained with different formulations with DMDBS concentrations of 0, 0.1, 1 and 5 %<sub>wt/polymer</sub>. For the 1 or 5 %<sub>wt/polymer</sub> DMDBS, the melting peak becomes sharper compared to the smallest concentrations indicating that the size of the crystals has less dispersity. If annealing is performed for 30 min at 135°C, the Curie peak shifts to higher temperatures, but the shift is smaller for the 5 %<sub>wt</sub> DMDBS solution. It is possible that the crystals are of smaller size in this case as the nucleating agent may favor the appearance of numerous crystal nuclei, or because the annealing was done at temperature a little higher than the onset of the crystallization peak. The Curie peak is also broader. By adding 30 %<sub>vol</sub> of DMSO in the formulation, the peaks are similar as for TEP alone, but with a broader melting peak indicating more dispersity in crystal sizes.

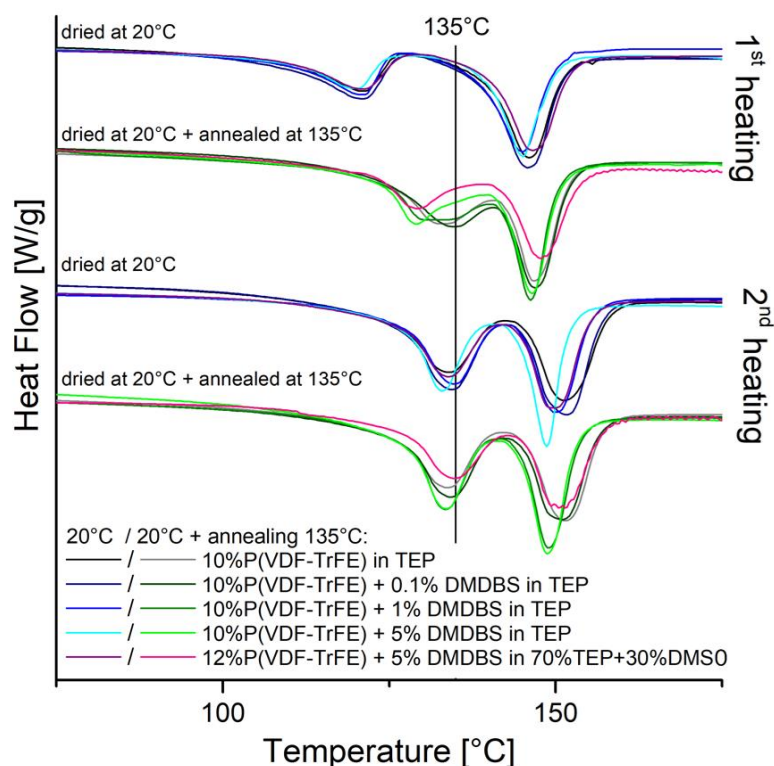


Figure 3.25: Differential Scanning Calorimetry of films of P(VDF-TrFE) obtained by drop casting different formulations of P(VDF-TrFE) (10%<sub>wt</sub> or 12%<sub>wt</sub>) in TEP (or 70 %<sub>vol</sub> TEP and 30 %<sub>vol</sub> DMSO) with DMDBS as gelifying agent (0.1, 1 or 5 %<sub>wt/polymer</sub>) and dried at 20°C, with or without annealing 30 min at 135°C.

A degree of crystallinity  $\Delta X_c$  was calculated using the enthalpy of the melting peak  $\Delta H_{melt}$ , which is the area of the peak divided by the heating rate ( $1^\circ\text{C}/3\text{s}$ ), with the relation  $\Delta X_c = \frac{\Delta H_{melt}}{\Delta H_\infty}$ . The melting enthalpy for a 100 % crystalline sample  $\Delta H_\infty$  was estimated at 86.92 J/g using the weighted average of  $H_{\infty PVDF}$  (1435 cal/mol from literature<sup>14</sup> equal to 93.76 J/g) and  $H_{\infty TrFE}$  (1300 cal/mol from literature<sup>14</sup> equal to 66.31 J/g). Finally, a degree of crystallinity between 20 and 38 % was found, but the difference between the samples is within the estimation error due to the error in the measurement of the weight of the sample, as well as the determination of the area under the melting peak.

To conclude, the differences in structure between the different formulations is small indicating that the use of a gelifying agent (with or without DMSO) does not drastically modify the properties of the films.

In next section, a more complex formulation will be studied using a mixture between a good and a bad solvent of P(VDF-TrFE). A phase separation is expected with consequences on the rheological behavior of the solutions.

## 3.5 P(VDF-TrFE) solutions in a mixture of a good and a bad solvent

The aim of this part is to formulate a shear-thinning ink of P(VDF-TrFE) without using a gelifying/nucleating agent, to obtain a film composed of polymer only. Indeed, impurities can lead to deterioration of the device during the polarization of the P(VDF-TrFE) films with high voltages and cause short-circuits. The use of a combination of a good and a bad solvent for the polymer may lead to phase separation and consequently give rise to interesting rheological behavior. A shear-thinning behavior may be expected. If this strategy succeeds, films composed of only P(VDF-TrFE) will be obtained after complete evaporation of the solvents.

### 3.5.1 Formulations of $x_B\text{B}/x_G\text{G}_P x_p$ inks

The good solvent of P(VDF-TrFE) used is  $\gamma$ -butyrolactone (GBL). It was combined with benzyl alcohol (BzOH), a bad solvent of the polymer. The solution studied consists of 15 %<sub>w</sub> of P(VDF-TrFE) which was first dissolved in GBL at 50 – 60°C (to speed up the solubilization) before different amounts of BzOH were added at the same temperature. These solutions were transparent. If, on the other hand, the components were mixed together at room temperature, the polymer stayed in powder form and did not dissolve, but after heating at 50 – 60°C, the solutions

became transparent. The solutions were then studied at lower temperatures to examine whether phase separation occurs and what its consequences are for the rheology of the phase separated mixture.

P(VDF-TrFE) inks	Visual observations
33B/67G_P15	Become opaque (white) during the first day
28B/72G_P15	
26B/74G_P15	
20B/80G_P15	Become slightly opaque (white) after one week
10B/90G_P15	Keep transparency after 1 year
5B/95G_P15	

*Table 3.6: Visual observation of solutions of 15 %<sub>wt</sub> P(VDF-TrFE) in GBL (G) and BzOH (B) after some days stored at 4-6°C.*

The transparent solutions were stored at 4 – 6°C several days [Table 3.6]: for concentrations higher or equal to 26 %<sub>vol</sub> of BzOH, the solutions acquire a white appearance and became opaque quickly. This is indicative of a phase separation and a possible formation of an emulsion. For 20 %<sub>vol</sub> of BzOH, a longer time was needed to become opaque, meaning that the solution is more stable at this temperature. For concentrations lower or equal to 10 %<sub>wt</sub>, the solutions stayed transparent, even after one year at 4 – 6°C, meaning that they are either stable or needed a lower temperature to phase separate.

Three solutions were studied in term of rheological behaviors: 33B/67G\_P15 with  $\frac{1}{3}$  of BzOH and 15 %<sub>wt</sub> of P(VDF-TrFE), and more stable ones, 25B/75G\_P15 and 25B/75G\_P12, with less BzOH or less polymer. We noted that the concentration of P(VDF-TrFE) has an impact on the stability of the ink: the more concentrated the solution, the faster the destabilisation.

### 3.5.2 Rheological behavior

The rheological properties of the first ink, 33B/67G\_P15, were measured just after formulation (the solution was still transparent) and after being stored three days at 20°C (the solution was white). The shear ramps were done at 30°C and the resulting viscosities are shown in Figure 3.26.

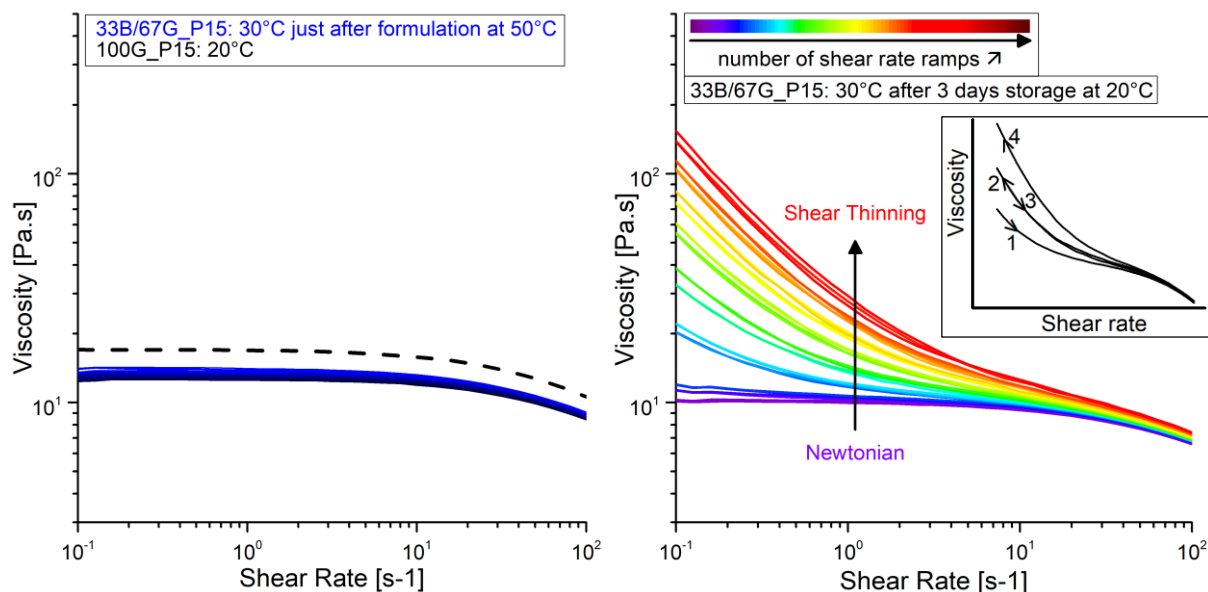


Figure 3.26: Rheological behavior of a solution of 15%<sub>wt</sub> P(VDF-TrFE) in 1/3 BzOH and 2/3 GBL measured with a shear rheometer (cone plate geometry: 50 mm diameter and 1° angle): viscosity versus shear rate obtained by applying multiple shear rate ramps (increasing and decreasing) at 30°C just after formulating the ink (left: 56 ramps) or after storage 3 days at 20°C (right: 30 ramps). The inset displays the non-reversibility of the cycles: the numbers and arrows indicate the number of the cycle and the direction of the ramp.

For the ink measured just after formulation, a stable Newtonian plateau was observed even after 56 shear ramps [Figure 3.26 (left)]. The rheological properties of the ink stored at 20°C, which has a white appearance, were difficult to measure at temperatures around 20°C and the ink is ejected from the rheometer upon application of shear. Most probably, these inks at such temperatures develop strong normal stresses and possibly shear thicken. In order to measure the rheological properties of these solutions a higher temperature of 30°C was used instead. Even at this temperature a complex behavior is observed. At the beginning, Newtonian behavior was observed (in purple), then after each cycle, the viscosity increases at all shears and shear thinning behavior emerges for a high number of cycles. The solution properties clearly evolve with the number of cycles and the viscosity increases by an order of magnitude at low shears. The cycles are actually not reversible. If the shear ramp is from low to high shear and back the cycle is not reversible. On the other hand, if the cycle is from high to low shear and back, the cycle is reversible [inset Figure 3.26 (right)]. We do not have a simple explanation for this behavior. The application of high shear rates to these solutions gives rise to a large viscosity increase. It is possible that shear modifies the structure of the phase separated solution or emulsion. Indeed, if the ink is stored at 20°C, it destabilises slowly, but if the ink is stirred in a reactor, the white color appears quickly.

Additional insight into the behavior of these solutions comes from measurements at different temperatures. A constant shear rate of 10 s<sup>-1</sup> was applied while the temperature was decreased in steps [Figure 3.27]. At a temperature of 30°C, the viscosity remains constant with

time. As the temperature was decreased to 29°C, the viscosity started increasing with time until the ink was ejected from the rheometer making the measurements unreliable.

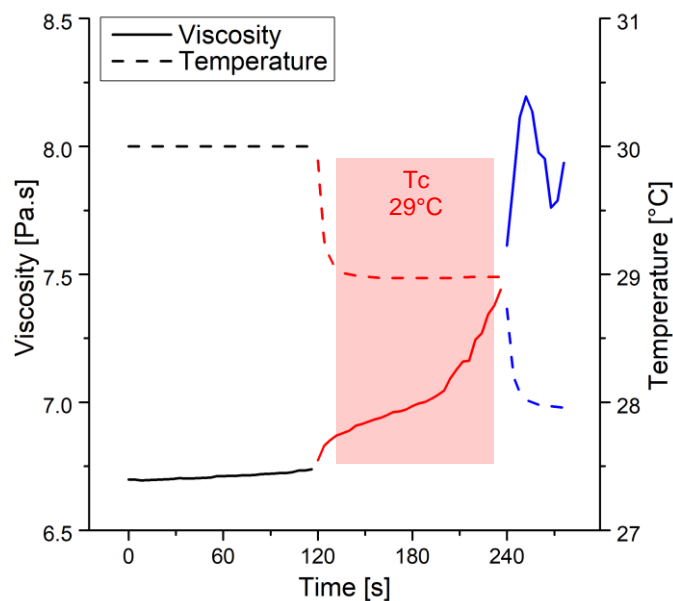


Figure 3.27: Rheological behavior of a solution of 15%wt P(VDF-TrFE) in 1/3 BzOH and 2/3 GBL measured with a shear rheometer (cone plate geometry: 50 mm diameter and 1° angle): viscosity and temperature versus time obtained by applying temperature steps at 10s<sup>-1</sup>. The solution is ejected from the rheometer right before 28°C.

At 30°C, the ink can be rendered shear thinning by using a number of shear cycles. For lower temperatures, the rheological properties are difficult to measure and the solutions are probably shear thickening. If we call  $T_w$  the temperature at which the viscosity starts to increase dramatically with time,  $T_w$  decreases with decreasing amounts of polymer and of BzOH. The  $T_w$  of two other formulations with less BzOH or less P(VDF-TrFE) were measured [see Appendix A.8]. We obtain  $T_w = 21 - 22^\circ\text{C}$  for 25B/75G\_P15, and  $T_w = 6 - 7^\circ\text{C}$  for 25B/75G\_P12. The difference is important between the two inks although there is only 3%wt of polymer difference. The diagram of Figure 3.28 summarizes these properties. The ink 25B/75G\_P15 has a working temperature close to the ambient temperature and could be suitable for screen printing.

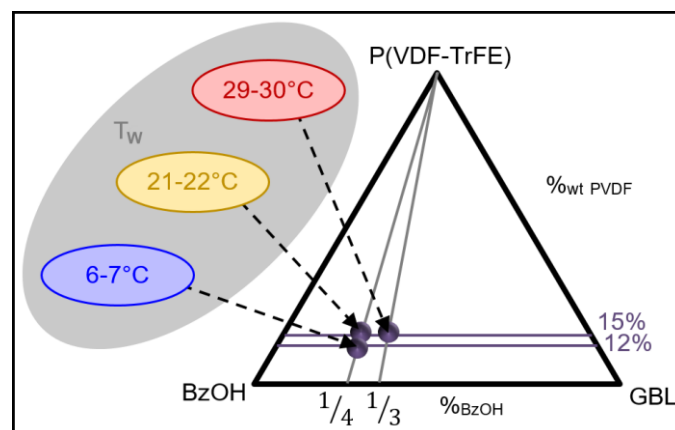


Figure 3.28: Phase diagram of the different P(VDF-TrFE) inks in a good and a bad solvent and corresponding working temperature  $T_w$ .

In the next part, the ink 33B/67G\_P15 will be studied in more details in term of structural properties to get more insight on the peculiar rheological properties of these solutions.

### 3.5.3 Structural study of 33B/67G\_P15 ink and 33B/67G solution

Scanning Electron Microscopy (SEM) was performed on 33B/67G\_P15 ink using cryogenic mode, and on dried drop-cast films.

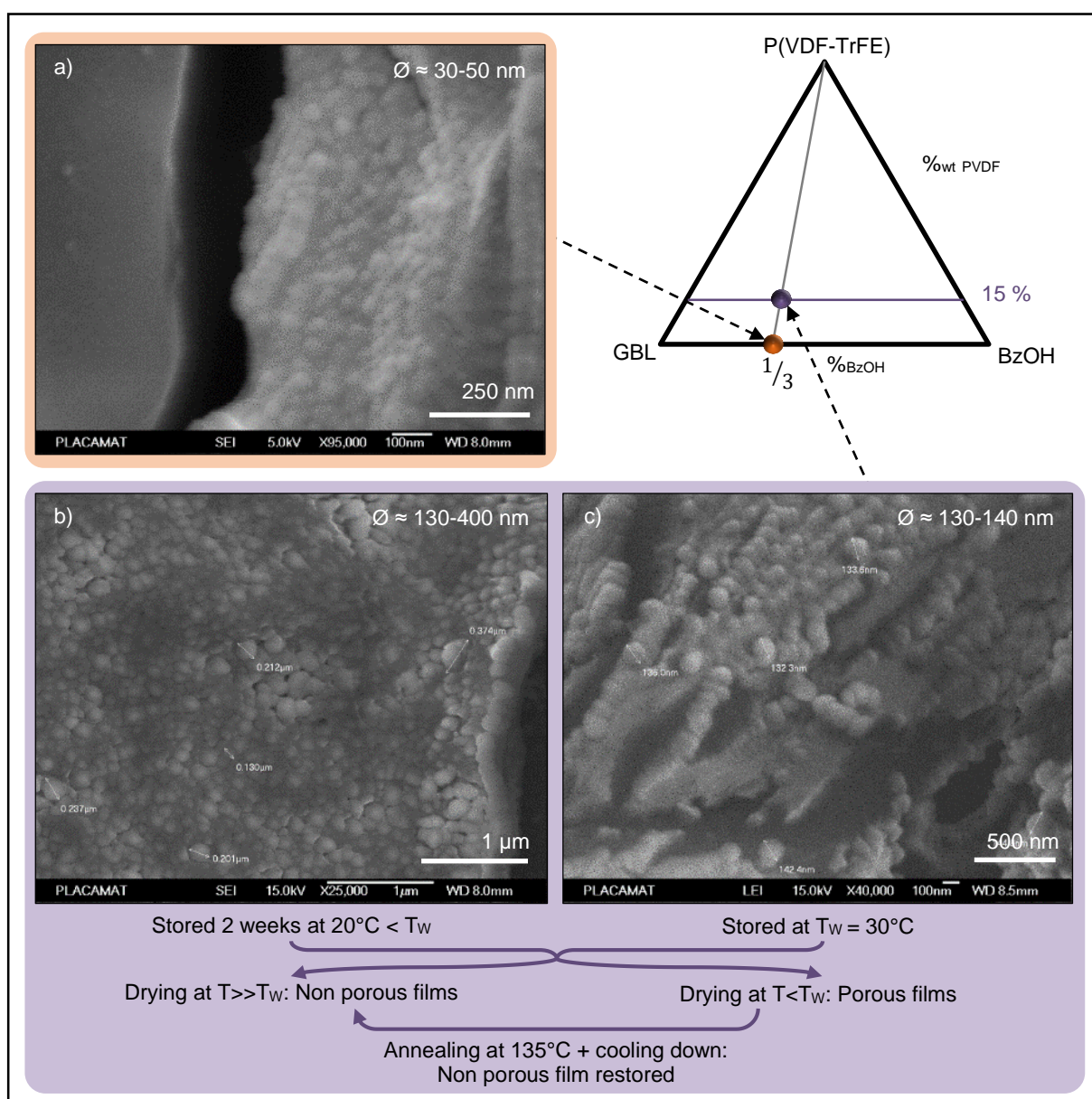


Figure 3.29: Phase diagram of P(VDF-TrFE) in GBL and BzOH and cryo-Scanning Electron Microscopy (cryo-SEM) pictures of solutions of a) 0 %wt or b) and c) 15 %wt P(VDF-TrFE) in 1/3 BzOH + 2/3 GBL (without sublimation and with metallisation).

Figure 3.29 displays SEM images of 33B/67G\_P15 inks, and of a mixture of the two solvents 33B/67G (= 1/3 BzOH + 2/3 GBL). The two solvents were supposed to be miscible: the solutions appear transparent. However, very small spheres of diameters between 30 and 50 nm appear in cryo-SEM [Figure 3.29 a)]. The solution has therefore the structure of a nano-emulsion. Its

rheological behavior is Newtonian with viscosities of few mPa.s. For 33B/67G\_P15 ink, a similar structure is observed with spherical particles of diameter comprised between 130 and 140 nm if the ink was stored at  $T_W = 30^\circ\text{C}$  [Figure 3.29 c)]. In the case where the ink was stored under the critical temperature, at  $20^\circ\text{C} < T_W$  for two weeks, the diameter of the spheres increases in size and shows more dispersity and is comprised between 130 and 400 nm [Figure 3.29 b)].

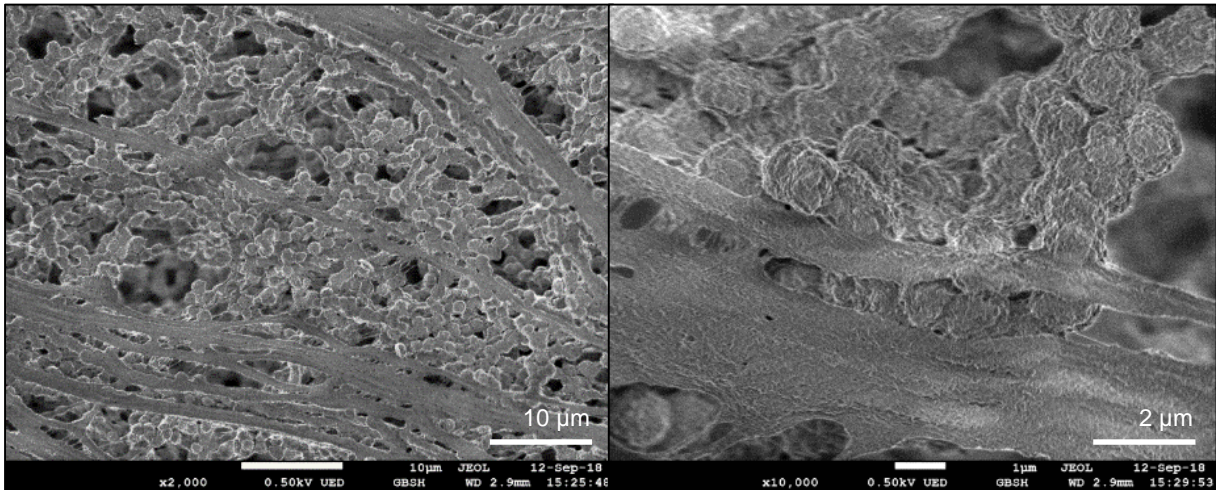


Figure 3.30: SEM images (without metallisation, GBSH mode) of film obtained by drop-casting a 33B/67G\_P15 ink on glass, drying two days at  $23^\circ\text{C}$ .

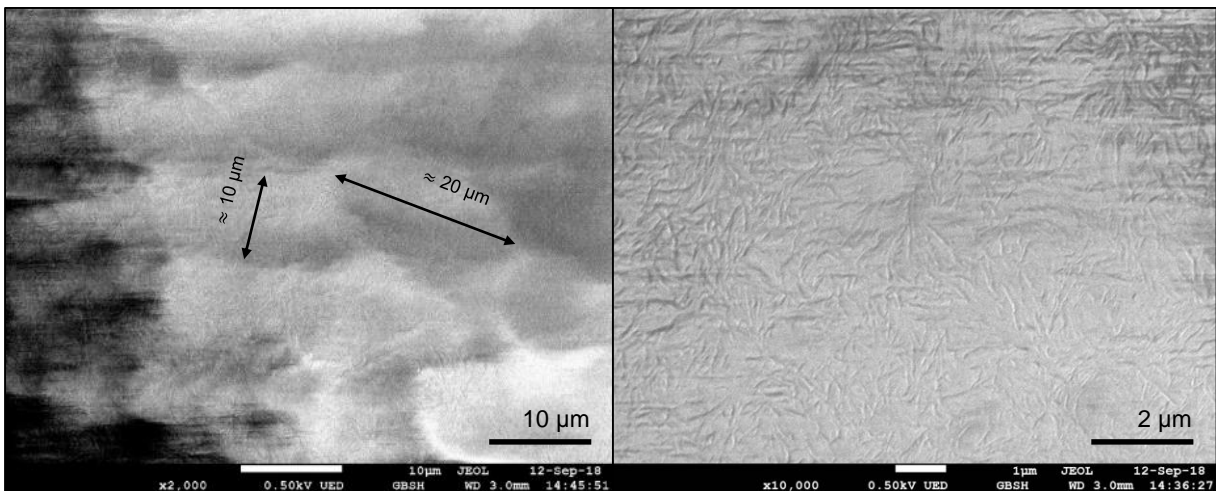


Figure 3.31: SEM images (without metallisation, GBSH mode) of film obtained by drop-casting a 33B/67G\_P15 ink on glass, drying at  $135^\circ\text{C}$  during 30 min and cooling down slowly at room temperature.

SEM images of drop cast films of this solution are shown in Figure 3.30 and Figure 3.31. The image of the films dried at  $23^\circ\text{C}$  show a porous like structure and the presence of spheres intercalated by linear domains, which are clearly visible at higher magnification. The size of the spheres is of order  $1\ \mu\text{m}$  in diameter; the lines have roughly similar widths.

If the drop-cast ink is dried at  $135^\circ\text{C}$  for 30 min and then cooled down progressively to room temperature, a more homogeneous film is obtained [Figure 3.31] with domains of sizes in the order of 10 – 20  $\mu\text{m}$ . At higher magnification, a homogeneous texture with line like structures is

observed. If the porous film dried at 23°C is further annealed at 135°C for 30 min and then cooled down, a structure similar to that of films dried directly at 130°C is recovered. Both porous and homogeneous structures can therefore be obtained with this ink depending on the drying conditions.

We think that the polymer migrates in the domains of the good solvent.

To conclude, P(VDF-TrFE) is soluble in mixtures of GBL (a good solvent for the polymer) and BzOH (a bad solvent) for the temperatures greater than 30°C and the solutions are transparent. These inks are unstable at lower temperatures and when subjected to shear. The critical temperature below which the solutions become unstable increases with the concentration of polymer or of BzOH. When the ink is sheared near the critical temperature  $T_w$ , its initial Newtonian behavior changes to a shear-thinning behavior with a large increase of the viscosity for low shears. This feature can then be used to prepare viscous solutions with shear thinning behavior, in a reactor, and the solution used at the appropriate temperature (which can be controlled and varied by changing the concentration of polymer or bad solvent) for processing and film making.

While the formulation remains complex with a precise protocol for producing shear thinning inks, an advantage of this formulation strategy is that the solution properties are reversible by heating the ink as it goes back to its initial state at high temperatures (transparent and Newtonian). Further, these inks provide the possibility to form microporous films of P(VDF-TrFE). These piezoelectric porous films are attracting much attention<sup>15</sup> and have applications in energy harvesting: they can for instance be used as separator membranes in lithium-ion battery.<sup>16-18</sup>

## 3.6 Conclusion

Two batches of P(VDF-TrFE) were studied. Both contained 79.4 %<sub>wt</sub> of VDF unit and 20.6 %<sub>wt</sub> of TrFE unit. Their weight average molar mass in equivalent PS is respectively 238 and 278 kDa (measured in THF). The critical concentration  $C^*$  was determined by a systematic rheological study as a function of the concentration: 18.7 %<sub>wt</sub> = 0.26 g/mL and 14.1 %<sub>wt</sub> = 0.19 g/mL were found for the two batches respectively. For all the concentrations, the elasticity of P(VDF-TrFE) solutions was lower than its viscous part, and the shear behavior was Newtonian. To modify this behavior and render it shear-thinning for screen-printing applications, two different ways were developed.

First, a gelifying agent was added in one or two good solvents of P(VDF-TrFE). In this case DMDBS was found to be an interesting gelifying agent. The solvents used are TEP, present in the commercial ink, and DMSO. Optimization of the proportions have shown that around 5 %<sub>wt/polymer</sub> DMDBS is needed in 10 – 12 %<sub>wt/total</sub> P(VDF-TrFE) to obtain an adequate shear thinning behavior with a sufficiently high viscosity. The elasticity of the ink also increases and becomes closer to its viscous part. After a proper stirring, the rheological behavior of the ink becomes stable. Cryo-SEM measurements have shown that P(VDF-TrFE) is in the shape of spheres of 40 – 50 nm diameter in TEP, and DMDBS organizes them in a fern like shape: parallel lines spaced by  $350 \pm 100$  nm with subdivision and the appearance of the polymer as small spheres when the sublimation is high enough. The shear thinning behavior is most probably due to the presence of these lines which can orient in the direction of the flow. DMSO can also be used to decrease the solubilization temperature of DMDBS (from 130 – 140°C in TEP to 60°C. The printed films are quite homogeneous with some lines and, as expected, no big crystal domains are visible because of DMDBS which acts as a nucleating agent. DSC measurements have shown that the impact on the size of the crystals for formulations with 0 to 5 %<sub>wt/polymer</sub> DMDBS is not so important.

The second kind of inks developed use a good and bad solvent of the polymer, both miscible, to obtain a segregation and a sort of nano-emulsion. GBL was used as a good solvent and BzOH as a bad solvent of P(VDF-TrFE). Cryo-SEM images has shown that contrary to expectations, GBL and BzOH were not fully miscible and form a nano-emulsion. Then the added polymer stays in the GBL domains and make them growth: that is the destabilisation of the ink. The addition of polymer to this mixture, induces a phase separation at low temperatures and the rheological properties of the phase separated mixture are highly dependent on the shear history of the sample. This dependence is important especially near a critical temperature (itself related to the concentration of the bad solvent and of the polymer). Subjecting the samples to repeated shear cycles renders them shear thinning with high viscosities at low shears. The inks prepared using shear under appropriate temperatures are well adapted to screen printing applications. The obtained films can be porous if dried at room temperature, or completely homogeneous with big domains if dried at 135°C or if the porous films are annealed at 135°C. The porous films can have applications in lithium-ion batteries as membrane separators.

## Bibliography

- (1) Heremans, P.; Gelinck, G. H.; Müller, R.; Baeg, K.-J.; Kim, D.-Y.; Noh, Y.-Y. Polymer and Organic Nonvolatile Memory Devices. *Chem. Mater.* **2011**, *23* (3), 341–358. <https://doi.org/10.1021/cm102006v>.
- (2) Abbott, S. *How to Be a Great Screen Printer*, Macdermid Autotype Limited.; HowTo eBook; 2008.
- (3) Spampinato, N.; Maiz, J.; Portale, G.; Maglione, M.; Hadziioannou, G.; Pavlopoulou, E. Enhancing the Ferroelectric Performance of P(VDF-Co-TrFE) through Modulation of Crystallinity and Polymorphism. *Polymer* **2018**, *149*, 66–72. <https://doi.org/10.1016/j.polymer.2018.06.072>.
- (4) Gregorio, R.; Botta, M. M. Effect of Crystallization Temperature on the Phase Transitions of P(VDF/TrFE) Copolymers. *J. Polym. Sci. Part B Polym. Phys.* **1998**, *36* (3), 403–414. [https://doi.org/10.1002/\(SICI\)1099-0488\(199802\)36:3<403::AID-POLB2>3.0.CO;2-S](https://doi.org/10.1002/(SICI)1099-0488(199802)36:3<403::AID-POLB2>3.0.CO;2-S).
- (5) Kim, K. J.; Kim, G. B.; Vanlencia, C. L.; Rabolt, J. F. Curie Transition, Ferroelectric Crystal Structure, and Ferroelectricity of a VDF/TrFE(75/25) Copolymer 1. The Effect of the Consecutive Annealing in the Ferroelectric State on Curie Transition and Ferroelectric Crystal Structure. *J. Polym. Sci. Part B Polym. Phys.* **1994**, *32* (15), 2435–2444. <https://doi.org/10.1002/polb.1994.090321501>.
- (6) Elias, H.-G. *Macromolecules. Volume 3, Physical Structures and Properties*; John Wiley & Sons, Ltd, 2014. <https://doi.org/10.1002/9783527627233.fmatter>.
- (7) Cho, J. W.; Song, H. Y.; Kim, S. Y. Thermoreversible Gelation of Poly(Vinylidene Fluoride) in  $\gamma$ -Butyrolactone Solution. *Polymer* **1993**, *34* (5), 1024–1027. [https://doi.org/10.1016/0032-3861\(93\)90224-X](https://doi.org/10.1016/0032-3861(93)90224-X).
- (8) Saha, D.; Bhattacharya, S. Hydrocolloids as Thickening and Gelling Agents in Food: A Critical Review. *J. Food Sci. Technol.* **2010**, *47*(6), 587–597. <https://doi.org/10.1007/s13197-010-0162-6>.
- (9) Fairgrieve, S. *Nucleating Agents*; iSmithers Rapra Publishing, 2007.
- (10) Treat, N. D.; Nekuda Malik, J. A.; Reid, O.; Yu, L.; Shuttle, C. G.; Rumbles, G.; Hawker, C. J.; Chabiny, M. L.; Smith, P.; Stingelin, N. Microstructure Formation in Molecular and Polymer Semiconductors Assisted by Nucleation Agents. *Nat. Mater.* **2013**, *12* (7), 628–633. <https://doi.org/10.1038/nmat3655>.
- (11) Masi, S.; Rizzo, A.; Munir, R.; Listorti, A.; Giuri, A.; Esposito Corcione, C.; Treat, N. D.; Gigli, G.; Amassian, A.; Stingelin, N.; et al. Organic Gelators as Growth Control Agents for Stable and Reproducible Hybrid Perovskite-Based Solar Cells. *Adv. Energy Mater.* **2017**, *7* (14), 1602600. <https://doi.org/10.1002/aenm.201602600>.
- (12) Thierry, A.; Fillon, B.; Straupé, C.; Lotz, B.; Wittmann, J. C. Polymer Nucleating Agents: Efficiency Scale and Impact of Physical Gelation. In *Solidification Processes in Polymers*; Jansson, J.-F., Gedde, U. W., Eds.; Progress in Colloid & Polymer Science; Steinkopff, 1992; pp 28–31.
- (13) Shen, H.; Niu, L.; Fan, K.; Li, J.; Guan, X.; Song, J. Application of Solubility Parameters in 1,3:2,4-Bis(3,4-Dimethylbenzylidene)Sorbitol Organogel in Binary Organic Mixtures. *Langmuir* **2014**, *30* (30), 9176–9182. <https://doi.org/10.1021/la5019532>.
- (14) Clements, J.; Davies, G. R.; Ward, I. M. A Broad-Line Nuclear Magnetic Resonance Study of a Vinylidene Fluoride/Trifluoroethylene Copolymer. *Polymer* **1992**, *33* (8), 1623–1629. [https://doi.org/10.1016/0032-3861\(92\)91058-A](https://doi.org/10.1016/0032-3861(92)91058-A).
- (15) Cardoso, V. F.; Lopes, A. C.; Botelho, G.; Lanceros-Méndez, S. Poly(Vinylidene Fluoride-Trifluoroethylene) Porous Films: Tailoring Microstructure and Physical Properties by Solvent Casting Strategies. *Soft Mater.* **2015**, *13* (4), 243–253. <https://doi.org/10.1080/1539445X.2015.1083444>.
- (16) Chen, D.; Chen, K.; Brown, K.; Hang, A.; Zhang, J. X. J. Liquid-Phase Tuning of Porous PVDF-TrFE Film on Flexible Substrate for Energy Harvesting. *Appl. Phys. Lett.* **2017**, *110* (15), 153902. <https://doi.org/10.1063/1.4980130>.

- 
- (17) Chen, D.; Zhang, J. X. J. Microporous Polyvinylidene Fluoride Film with Dense Surface Enables Efficient Piezoelectric Conversion. *Appl. Phys. Lett.* **2015**, *106* (19), 193901. <https://doi.org/10.1063/1.4921007>.
- (18) Costa, C. M.; Sencadas, V.; Rocha, J. G.; Silva, M. M.; Lanceros-Méndez, S. Evaluation of the Main Processing Parameters Influencing the Performance of Poly(Vinylidene Fluoride-trifluoroethylene) Lithium-Ion Battery Separators. *J. Solid State Electrochem.* **2013**, *17*(3), 861–870. <https://doi.org/10.1007/s10008-012-1928-8>.



# 4 Piezoelectric devices

4.1 Introduction.....	146
4.2 Materials & Methods .....	148
4.2.1 Materials .....	148
4.2.2 Devices fabrication .....	148
4.2.3 Characterization .....	149
4.3 Thermal evaporated metal electrodes & spin coated or doctor bladed P(VDF-TrFE) layer..	152
4.3.1 Device fabrication .....	152
4.3.2 Device characterization .....	153
4.4 Printed PEDOT:PSTFSI electrodes & doctor blading of P(VDF-TrFE) solutions.....	156
4.4.1 Device fabrication .....	156
4.4.2 Device characterization .....	158
4.5 Screen-printed and stencil-printed commercial PEDOT:PSS electrodes & new P(VDF-TrFE) formulations .....	159
4.5.1 Device fabrication .....	159
4.5.2 Device characterization .....	162
4.6 Conclusion .....	164

## 4.1 Introduction

Piezoelectric devices are composed of a piezoelectric layer sandwiched between two electrodes. The direct piezoelectric effect is the response of a piezoelectric material to a mechanical external stress: a strain is induced which generates an electrical potential proportional to the applied stress. Inversely, the reverse piezoelectric effect is the response of a piezoelectric material to an electric field: a mechanical deformation is induced.<sup>1</sup> The purpose of piezoelectric devices is then to obtain a displacement by applying a voltage (in the case of actuators, speakers, etc.), or to apply a displacement to create a voltage (in the case of a pressure sensor). Using P(VDF-TrFE) as a piezoelectric layer in the field of medical pressure sensors is a possibility which is considered by many studies.<sup>2</sup>

Piezoelectric catheters are medical devices used to measure and treat cardiovascular diseases such as arrhythmia. This disease consists of abnormal heartbeat (too fast, too slow, or irregular), and leads to stroke and cardiac arrest. To treat these fibrillations, catheters are used. They measure the heart beat and locate the tissues causing the abnormal electrical signal. The tissues are then burned, by radio-frequency heating or cryotherapy cooling, to restore normal heart beat: this is called cardiac ablation.<sup>3,4</sup> The challenge is to diagnose and treat the precise anatomic location of the arrhythmia.

In this context, a collaboration with the IHU (Institut Hospitalo-Universitaire) Liryc (L'Institut de Rythmologie et Modélisation Cardiaque) was established. The aim was to develop flexible pressure sensors, allowing the exact localisation and the measurement of the applied force on the inside of a 3D printed heart for laparoscopic training simulators. For that purpose, a matrix of pressure sensors was conceived. The devices should have electrodes to record the signal, and a piezoelectric layer. All the materials used should be easily processable. The 3D-printed heart has similar mechanical characteristics as the human heart and will be used by students to simulate surgery using catheters. Arrhythmia is detected when an abnormal output electrical signal is recorded when a pressure is applied by a catheter. The human body simulator as well as the 3D-printed heart and a schematic of a matrix of piezoelectric devices is presented in Figure 4.1: electrodes are represented with blue lines, one device being the intersection between two lines.

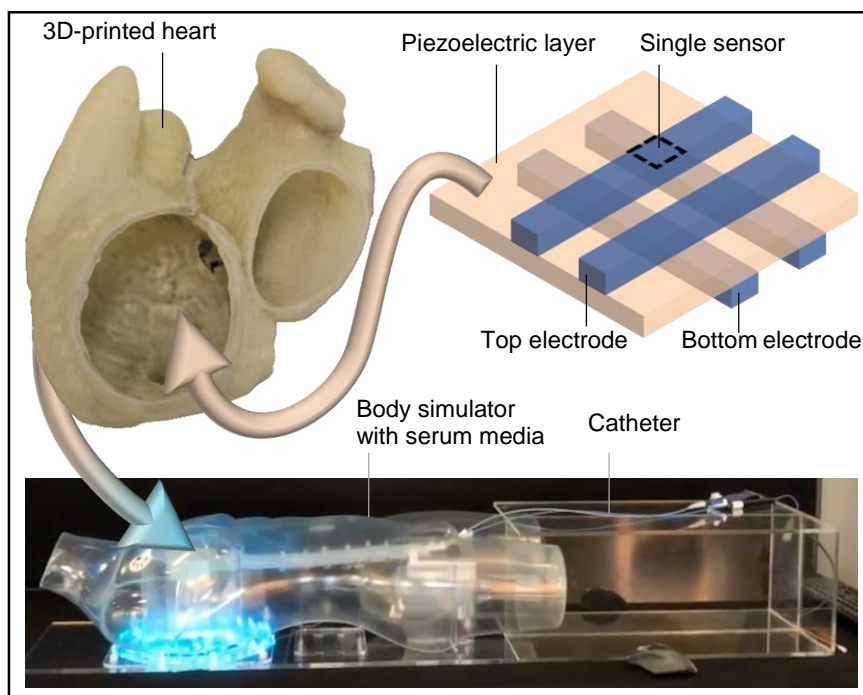


Figure 4.1: Human body simulator for laparoscopic training with 3D-printed heart and schematic of a matrix of piezoelectric devices to be deposited on the inner walls.

This chapter combined two goals: using the inks formulated in previous chapters to develop pressure sensors, as well as designing devices to be implemented in the 3D-printed heart in the framework of the collaborative project. Nicoletta Spampinato, Konstantinos Kallitsis, Gomes Correia and Lauriane Giraud from LCPO were part of the collaborative work as well as Rémi Dubois and Pierre Jais from Liryc. Nicoletta Spampinato and Konstantinos Kallitsis have developed more particularly the devices with metallic electrodes, while I developed the devices with PEDOT electrodes. The piezoelectric layer is in each case made from P(VDF-TrFE).

A previous attempt spraying directly the bottom electrode into the 3D-printed heart has shown that the polymer used for the heart was cracking due to the temperature used during the spray (110°C). This is why the various devices presented below will be prepared separately from the heart. The devices have to conform to the shape of the artificial heart as they will be fixed on the inner walls of this latter.

In this chapter, devices with metallic electrodes will be characterized as this is simpler to implement, then more flexible devices with organic PEDOT:PSTFSI electrodes will be introduced, and finally devices screen-printed with commercial PEDOT:PSS and different formulations of P(VDF-TrFE) will be discussed.

## 4.2 Materials & Methods

### 4.2.1 Materials

The materials used are: commercial PEDOT:PSS ink (Orgacon EL-P 5015 from Sigma Aldrich), commercial P(VDF-TrFE) ink (FC25 Ink P from Arkema), and formulated inks 1 %<sub>wt</sub> or 0.5 %<sub>wt</sub> PEDOT:PSTFSIK<sub>80 kDa</sub>, and P(VDF-TrFE) inks T\_P10\_D5\_R and 3D7T\_P12\_D5\_R from previous chapter, and 10 – 15 %<sub>wt</sub> P(VDF-TrFE)<sub>75/25</sub> (from Arkema) in Cyclopentanone (from Acros Organics). All PEDOT inks were formulated (even the commercial one), with 5 %<sub>vol</sub> DMSO or Ethylene Glycol (EG) and 0.04 %<sub>wt</sub> Zonyl FS-300 fluorosurfactant.

Polydimethylsiloxane (PDMS) (from Neyco: 10 %<sub>wt</sub> crosslinker added to 1 %<sub>wt</sub> PDMS), Kapton tape (poly(4,4'-oxydiphenylene-pyromellitimide) tape) and polyethylene terephthalate (PET) (from DuPont Teijin Films: 125 and 175 μm) were used as substrates.

Carbon tape was used to create better contact between the tips and the PEDOT electrodes during the polarisation.

### 4.2.2 Devices fabrication

Different types of devices were made either using a substrate or using free standing films of the piezoelectric polymer. Metallic or organic electrodes were then introduced using various types of deposition processes. All the created and characterized devices are listed in Table 4.1.

	Electrodes		Piezoelectric layer		Substrate	Section
	Material	Process	Material	Process		
Metallic	Au (+Cr)	Thermal evaporation	10 – 15 % <sub>wt</sub> P(VDF-TrFE) <sub>75/25</sub> in Cyclopentanone	Doctor blading, Drop casting or Spin coating	- Kapton tape - PDMS (+ free standing film*) - free standing film*	4.4
						4.5
Organic	0.5 % <sub>wt</sub> PEDOT:PSTFSIK	Spray			- PET - PDMS	4.5
	1 % <sub>wt</sub> PEDOT:PSTFSIK	Doctor Blade				
	0.5 % <sub>wt</sub> PEDOT:PSTFSIK or PEDOT:PSS <sub>PH 1000</sub>	Inkjet				
PEDOT:PSS <sub>EL-P 5015</sub>	Screen-printing		FC25 Ink P	Screen-printing	- PDMS - PET	4.6
			T_P10_D5_R			
			3D7T_P12_D5_R			

Table 4.1: Summary of the devices created and characterized. (\* free standing film of P(VDF-TrFE))

The metal electrodes were evaporated in inert atmosphere at 10<sup>-6</sup> mbar with a PLASSYS ME400B evaporator (Chrome: 10 nm, Gold: 200 or 300 nm). The organic electrodes and the piezoelectric layer were deposited using different printing methods: a A4809 Aztek airbrush with a 1.02 mm nozzle (for spray coating), an Erichsen Doctor Blade (air gaps 150 μm and 10 mm/s

speed), a single nozzle Microfab Jetlab4 inkjet printer with a MJ-ATP-01-050 piezoelectric nozzle (the optimized parameters of the printer were the following: frequency: 600 Hz, first rise time: 15  $\mu$ s, dwell time: 15  $\mu$ s, fall time: 20  $\mu$ s, echo time: 10  $\mu$ s, second rise time: 10  $\mu$ s, dwell voltage: 55 V, echo voltage: 0 or 10 V), and an EKRA X5 screen-printer (pressure: 120 N, snap off: 1 mm, speed: 180 or 300 mm/s for electrodes with respective screens 150 – 30 and 200 – 27; and 100 or 50 mm/s for P(VDF-TrFE) with screen 90 – 48).

All the devices, with metal and organic electrodes, were annealed at 135°C (value taken from the literature<sup>5</sup>) (or 129°C for the formulations T\_P10\_D5\_R and 3D7T\_P12\_D5\_R, that is the onset of the melting peak measured in Chapter 3) during 30 min and cooled down slowly at room temperature before being characterized.

To encapsulate the devices, a PDMS layer can be added at the top of the devices.

### 4.2.3 Characterization

A proof of concept of a piezoelectric device with a thick free standing film of P(VDF-TrFE) obtained by drop casting, and aluminum foil used as electrodes (very large area of 16 cm<sup>2</sup>) is presented in Figure 4.2. By applying a pressure on the device, an output voltage was recorded with an oscilloscope. The signal is generated during the displacement and not when pressure is held constant. Two peaks appear: one when the device is pressed, and one when the pressure is released.

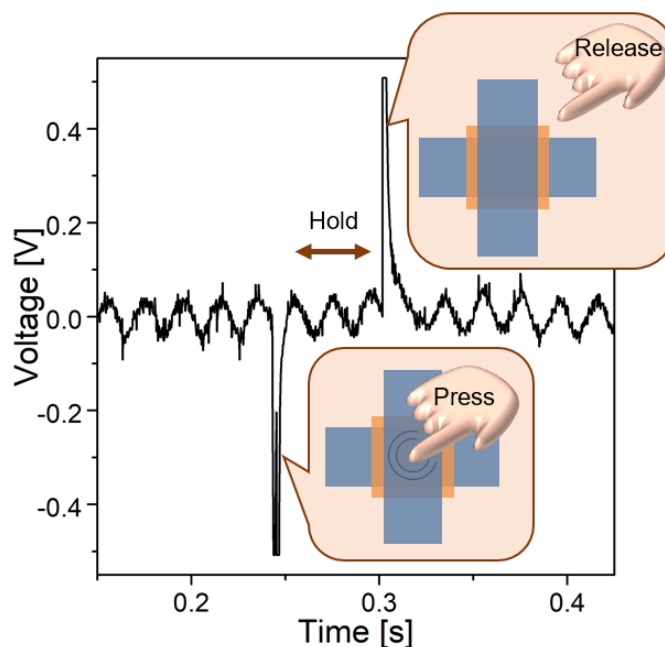


Figure 4.2: Electric response to a pressure applied to a piezoelectric device

However, for thin films, the signal generated during the displacement is in the noise level of the measurement. Polarization of the piezoelectric layer is then very important and increases the output voltage as shown in Figure 4.3.

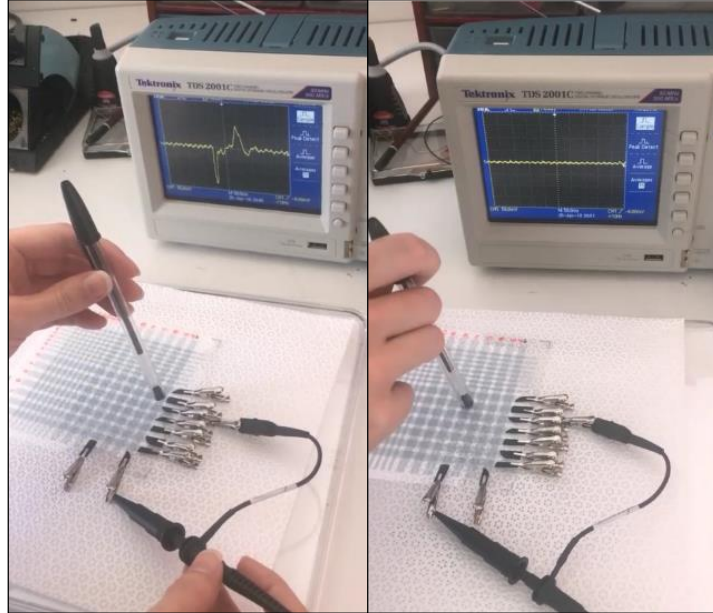


Figure 4.3: Electric response to a pressure for polarized devices (left) and non-polarized devices (right) using a 10  $\mu\text{m}$  thick P(VDF-TrFE) layer.

To polarize the obtained devices, a aixACCT Systems TF Analyzer 2000E was used. A continuous sinusoidal voltage was applied at different frequencies (usually 1 Hz) using increasing voltage steps until the electric field  $E$  reached 100 MV/m (or before in the case the device breaks).

The electric field  $E$  is obtained by dividing the applied voltage  $V$  by the thickness  $t$  of the piezoelectric layer:  $E = \frac{V}{t}$ . The electrical displacement  $D$  is then obtained by integrating the output current (which is done directly in the aixPlover30 software):  $D = \epsilon_0 E + P$  where  $P = \epsilon_0(\epsilon_r - 1)E$  is the polarization,  $\epsilon_0$  is the vacuum permittivity, and  $\epsilon_r$  is the relative permittivity (or dielectric constant).<sup>6</sup> The polarization is then proportional to the displacement with a constant factor  $\frac{\epsilon_r - 1}{\epsilon_r}$ . In this chapter, the devices will be characterized by the displacement hysteresis loop as a function of the electric field.

These loops have several characteristic features. The saturated displacement  $D_{\text{sat}}$  (or saturated polarisation  $P_{\text{sat}}$ ) is the maximum displacement (or polarization) reached for a certain field. The remanent displacement  $D_r$  (or remanent polarization  $P_r$ ) is the displacement (or polarisation) that remains after switching down the field. The coercive field  $E_c$  is the field required to suppress the remanent polarization [Figure 4.4]. In the plots of intensity versus field, two maxima appear at  $\pm E_c$ . These maxima correspond to the displacement of charges which occurs upon the change of sign of the polarization.<sup>7</sup>

In the case of a pressure sensor, the piezoelectric polymer is used as a capacitor. The aim is then to have the highest output voltage for the smallest applied strain. Efficient pressure sensors are then obtained when the difference between  $P_r$  and  $P_{sat}$  is small. Efficient actuators are obtained when the slope near  $E_c$  is very high.

An example of a measured ferroelectric hysteresis loop and the corresponding switching current peaks is displayed in Figure 4.4, with a schematic of the polarization and charge accumulation for different applied fields.

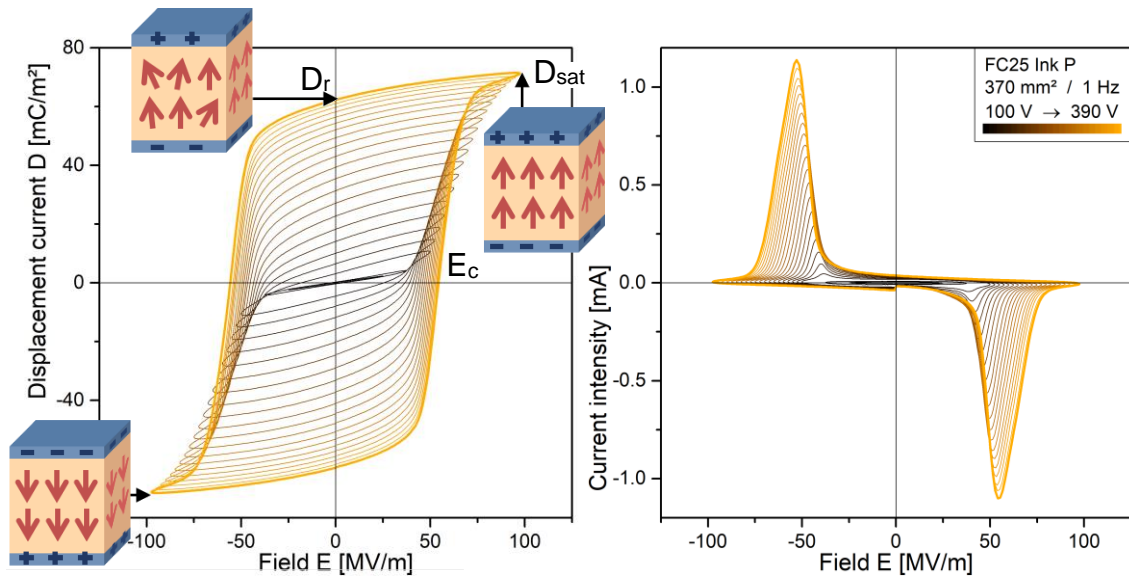


Figure 4.4: Displacement and intensity of the output current versus field measured on a 368 mm<sup>2</sup> / 4 μm thick device stencil-printed with commercial inks: PEDOT:PSS EPL5015 for electrodes and P(VDF-TrFE) FC25 Ink P for piezoelectric layer. The polarization and charge accumulation are schematized for different applied field.

Figure 4.5 shows the response when a short circuit occurs between the top and the bottom electrodes for sinusoidal and triangular signals: the sinusoidal signal will be used for the rest of the experiments. A short circuit will then be seen as a circle instead of a sharp hysteresis loop in the displacement curve, and no peaks in the intensity curve.

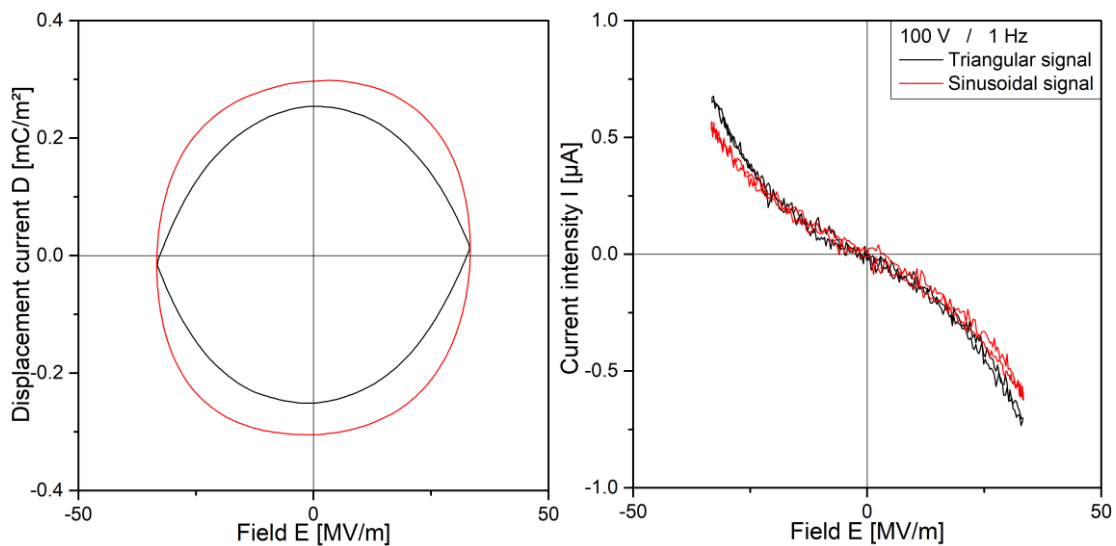


Figure 4.5: Short-circuit of one device measured with triangular or sinusoidal signals at 100 V and 1 Hz

## 4.3 Thermal evaporated metal electrodes & spin coated or doctor bladed P(VDF-TrFE) layer

### 4.3.1 Device fabrication

First, attempts with metallic electrodes were carried out. Thermal evaporation of gold was performed on Kapton tape, free standing films of P(VDF-TrFE), or on PDMS. In the case of Kapton tape as substrate, the P(VDF-TrFE) layer was spin coated from a solution at 10 %<sub>wt</sub>. The free standing film of P(VDF-TrFE) used as substrate was deposited by doctor blade from a 15 %<sub>wt</sub> solution on a glass substrate heated at 60°C, and dried 20 min at 60°C [Figure 4.6]: the obtained films in this condition have a thickness close to 15 μm. The film is then peeled off the glass substrate to obtain a free standing film. Last, an encapsulation was tried: the electrodes were evaporated on top of two PDMS substrates, and a thick free standing film of P(VDF-TrFE) obtained by drop casting was sandwiched between the two electrodes. The purpose of increasing the thickness of the film was to improve the output signal, and the evaporation of the electrodes onto PDMS was to avoid the use of high temperatures to the P(VDF-TrFE) layer during the thermal evaporation. The obtained devices are displayed in Figure 4.7.

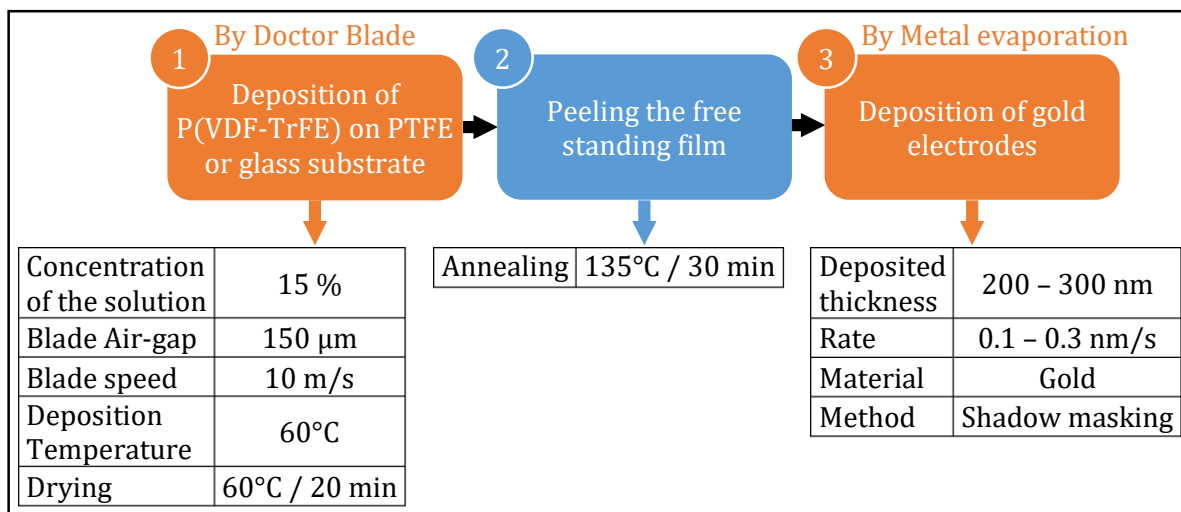


Figure 4.6: Processes parameters for metal electrodes on top of free standing film of P(VDF-TrFE)

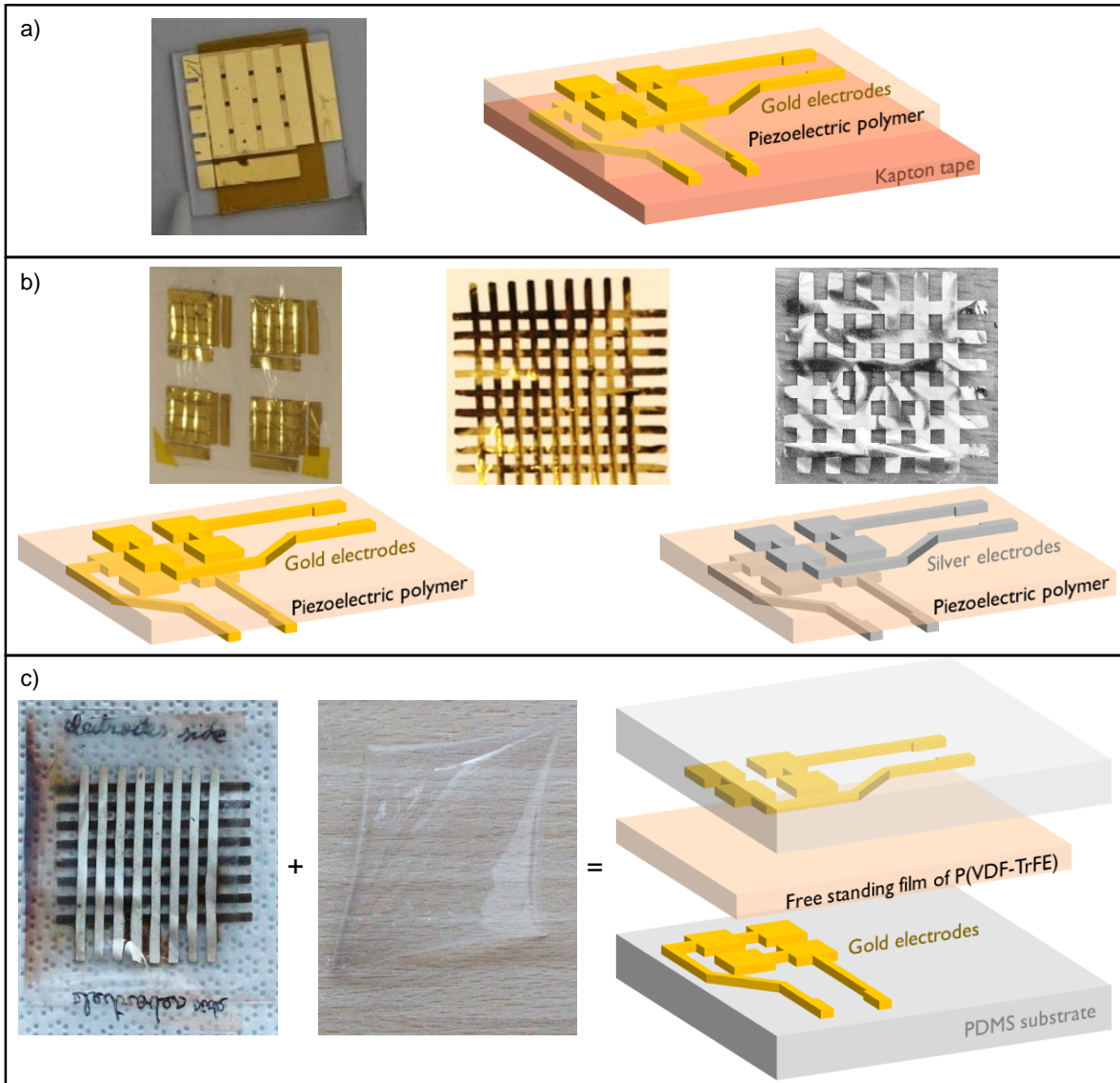


Figure 4.7: Photo and schematic of the devices with metal electrodes: a) using Kapton tape as substrate, b) using a free standing film of P(VDF-TrFE) as substrate, c) using PDMS as substrate and a free standing film of P(VDF-TrFE).

### 4.3.2 Device characterization

In this part the devices with metallic electrodes and commercial P(VDF-TrFE) will be polarized. First the device with gold electrodes on Kapton tape [Figure 4.8], and then the one with gold electrodes on free standing P(VDF-TrFE) films [Figure 4.9].

For the device on Kapton tape, the hysteresis has the shape of rounded rectangle and the intensity curve is tilted from the horizontal [Figure 4.8]. That means the device is very leaky and a short-circuit occurs.

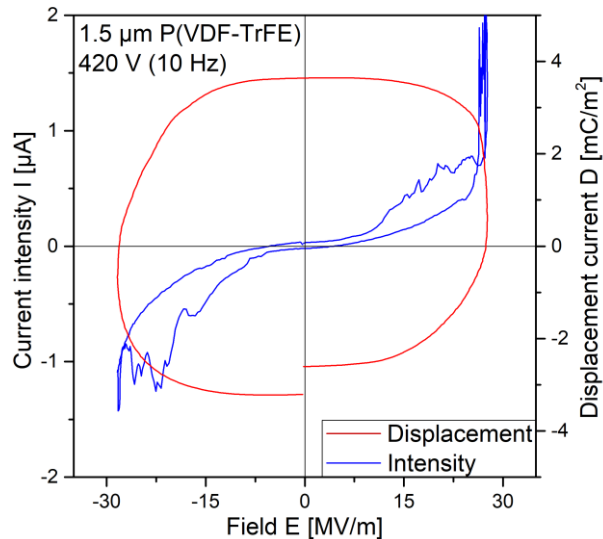


Figure 4.8: Current intensity and displacement versus field of devices with gold electrodes, Kapton tape as substrate, and spin coated P(VDF-TrFE) layer.

In the case of gold electrodes on top of free standing film of P(VDF-TrFE), the device is more flexible, and a hysteresis loop can be recorded. A higher displacement (and so polarisation) as well as a sharper hysteresis loop are obtained when the temperature during the thermal evaporation of the electrodes is controlled to be under the annealing temperature [Figure 4.9].

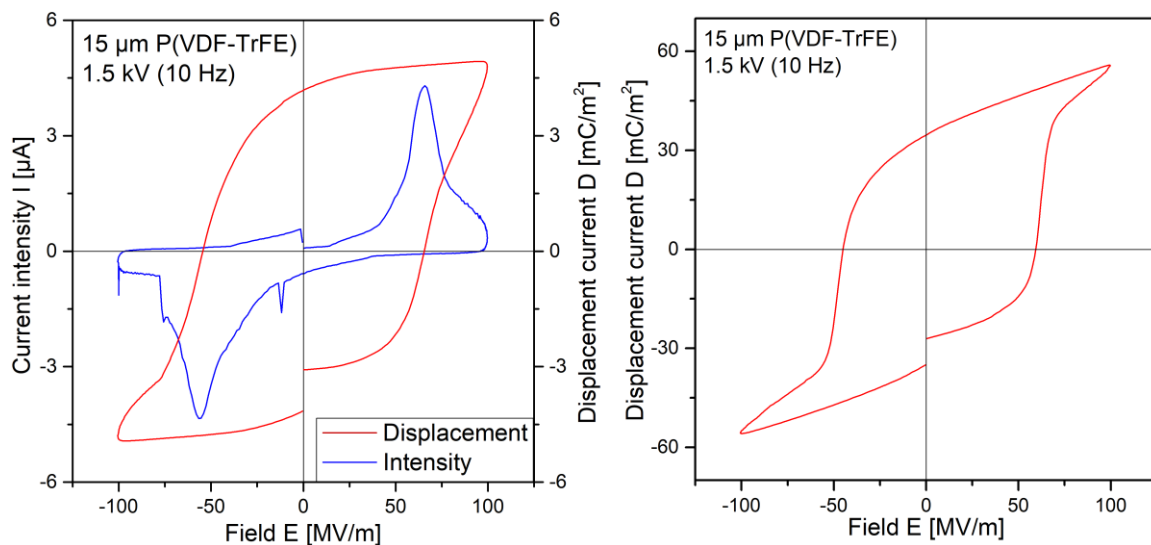
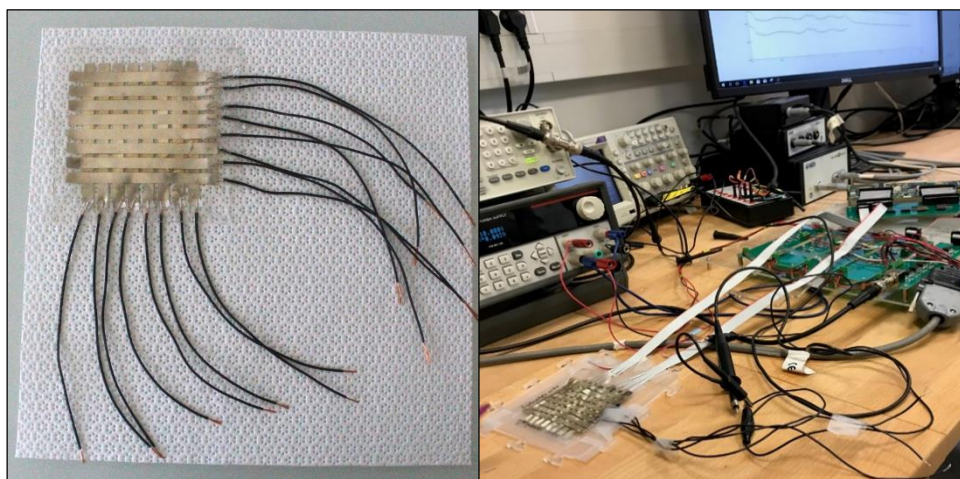


Figure 4.9: Current intensity and displacement versus field of devices with gold electrodes on free standing P(VDF-TrFE) film: non optimized (with 300 nm of gold and uncontrolled temperature) and optimized (with 200 nm of gold and controlled temperature under 135°C).

The deposition process of the electrodes is then very important. The melting of the P(VDF-TrFE) has to be avoided.

However, the output voltage of the devices on top of free standing films of P(VDF-TrFE), measured with an oscilloscope, was too low and in the range of the electrical noise of the instrument.

Therefore, another type of device with metallic electrodes was made: a thick drop casted P(VDF-TrFE) film was embedded between two PDMS substrates on top of which the electrodes were evaporated. Copper wires were attached at the extremity of the electrodes with silver paste before finishing the encapsulation with PDMS. These devices had good output voltage signal (albeit not recorded by us prior to use). In the Liryc institute, the devices were connected to an electrical grid which enables the measurement of the output voltages of multiple devices simultaneously [Figure 4.10]. However, a similar output voltage was measured for different devices in the matrix when only one was pressed. It was attributed to the grid design.



*Figure 4.10: Encapsulated device (left) and setup used by the team of the Liryc centre to measure the output current of multiple devices at the same time in response to an external pressure (right).*

These devices, although showed a good response, are not flexible enough and the bending of the devices caused cracking and damage of the electrodes. In the next section we will examine the use of organic electrodes.

## 4.4 Printed PEDOT:PSTFSI electrodes & doctor blading of P(VDF-TrFE) solutions

### 4.4.1 Device fabrication

Attempts with doctor bladed P(VDF-TrFE) layers and PEDOT:PSTFSI electrodes were carried out using three different deposition processes: spray coating, doctor blading and inkjet printing.

For the spray coating, a mask made of PET was deposited on top of the PET substrate and 0.5 %<sub>wt</sub> PEDOT:PSTFSI<sub>80 kDa</sub> with 5 %<sub>wt</sub> DMSO was sprayed. The substrate was heated at 120°C during the deposition to enhance evaporation of the solvent. The P(VDF-TrFE) layer was then deposited by doctor blade and the top electrode sprayed in the same way as the bottom electrode. Unfortunately, a short circuit was found between the top and bottom electrodes. It was attributed to the DMSO from the PEDOT ink formulation as the P(VDF-TrFE) is soluble in DMSO. For the rest of the depositions, the formulation will use EG as additive instead of DMSO. The PEDOT electrodes were too rough due to the spray coating method. That is why other techniques were then used, and the substrate was changed for PDMS to be more flexible and so easily adaptable to the 3D-printed heart.

The ink, 1 %<sub>wt</sub> PEDOT:PSTFSI<sub>80 kDa</sub> and 5 %<sub>wt</sub> EG, was deposited with a doctor blade on a PDMS substrate, using a mask made of PET to shape the electrodes. Despite the good adherence between the 125 μm PET mask and the PDMS substrate (due to the stickiness of the PDMS), some PEDOT flowed under the mask making short circuits between the different bottom electrodes. Heating the substrate during the printing at 120°C gives the same result but with higher resistivity between the electrodes (from 1 to 300 kΩ/□). P(VDF-TrFE) was deposited by doctor blade as for the free standing films previously described. For the top electrodes, the use of the PET mask was not possible: during the removal of the mask, a delamination between the bottom electrode and the P(VDF-TrFE) layer occurs due to better adhesion between PEDOT and PDMS than between PEDOT and P(VDF-TrFE). This technique was therefore abandoned and inkjet printing was pursued for the top and bottom electrodes. Inkjet printing does not need a mask to shape the electrodes.

Inkjet printing was used with 0.5 %<sub>wt</sub> PEDOT:PSTFSI<sub>80 kDa</sub> with 5 %<sub>wt</sub> EG and 0.04 %<sub>wt</sub> surfactant. Before printing the 2 mm width lines, the ink was sonicated 5 min and filtrated with a 0.45 μm PTFE filter. To improve adhesion of PEDOT, a UV-Ozone treatment was performed during at least 30 min for PDMS and during 10 min for P(VDF-TrFE) [See Appendix A.4 for details on the wettability of PEDOT films]. The substrate was heated at 50°C for the bottom electrode, and 60°C

for the top electrode to improve adhesion even further. The printing resolution which has given the best results is 400 dpi. The PEDOT ink was dried 5 min at 120°C, and the P(VDF-TrFE) layer was deposited by doctor blade [Figure 4.11].

	1 By Doctor Blade Deposition of PDMS on aluminum plate	2 By Inkjet Deposition of the bottom PEDOT electrode	3 By Doctor Blade Deposition of piezoelectric layer	4 By Inkjet Deposition of the top PEDOT electrode
Deposition temperature	50°C	50°C	60°C	60°C
Drying	100°C / 1h	120°C / 5 min	60°C / 20 min	120°C / 5 min
Preparation of the substrate	UV-ozone treatment	35 min	-	10 min
	Pre-heating	50°C / 5 min	60°C / 5 min	60°C / 5 min

Figure 4.11: Processes parameters for inkjet printed PEDOT electrodes

For the PDMS substrate, if it was deposited on a flexible aluminum plate, the PDMS layer can be peeled off without too much difficulty. On the other hand, if the PDMS was deposited on a rigid aluminum plate, the PDMS layer adhered strongly and was difficult to peel off. In this case, the electrodes and the P(VDF-TrFE) film can actually be peeled off the PDMS layer and obtain free standing films with embedded electrodes.

The organic printed devices obtained by spray coating, doctor blade or inkjet printing are displayed in Figure 4.12.

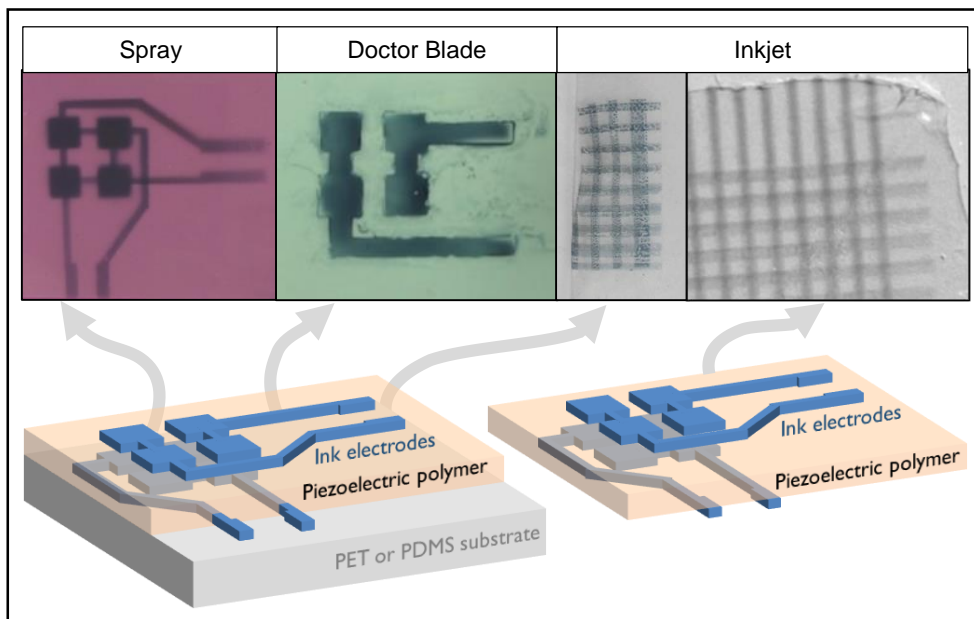


Figure 4.12: Photo and schematic of the devices with organic electrodes deposited by spray, doctor blade and inkjet printing.

### 4.4.2 Device characterization

The spray coated or doctor bladed devices were completely leaky and no further characterization was possible. The hysteresis loops of the devices obtained by inkjet printing PEDOT:PSTFSI electrodes on PDMS substrate and on free standing films of P(VDF-TrFE) are presented respectively in Figure 4.13 and Figure 4.14.

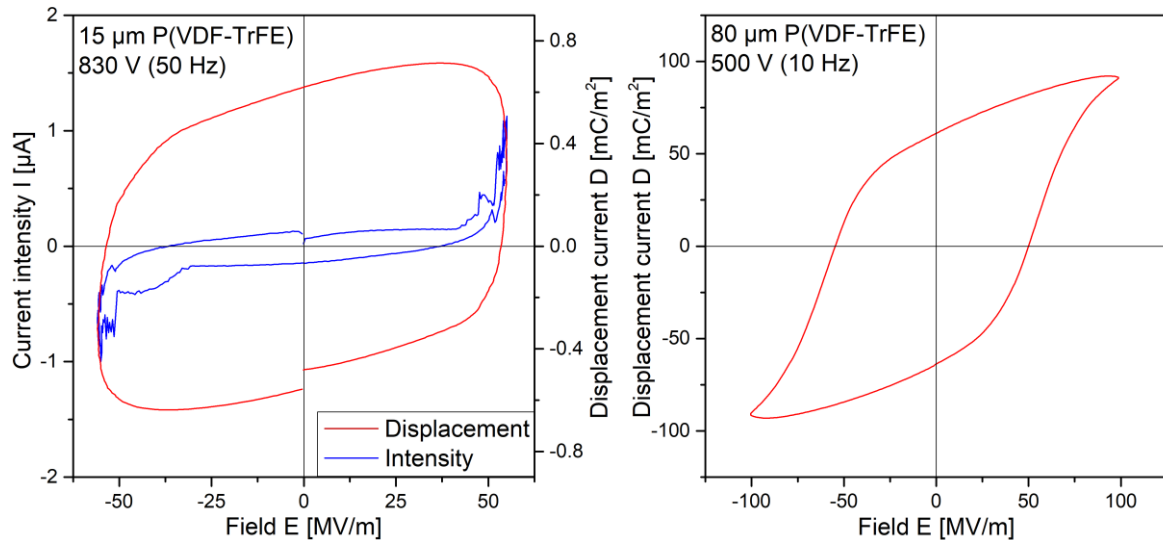


Figure 4.13: Current intensity and displacement versus field of devices obtained by inkjet printing PEDOT:PSTFSI electrodes, with PDMS substrate, and doctor bladed (left) or drop casted (right) P(VDF-TrFE): respectively 15 μm and 80 μm thick.

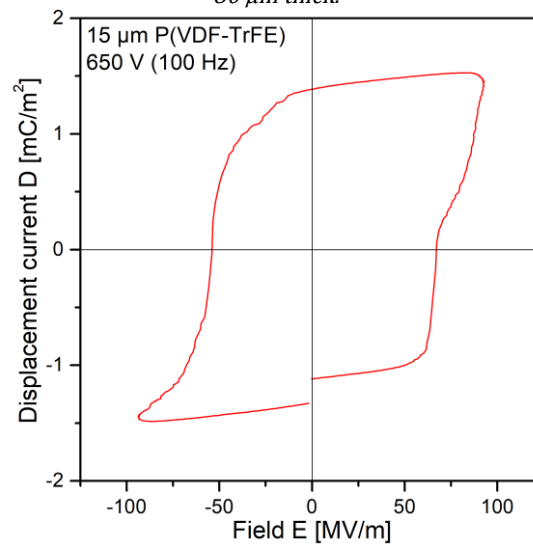


Figure 4.14: Displacement versus field of devices obtained by inkjet printing PEDOT:PSTFSI electrodes on top of free standing P(VDF-TrFE) film.

Because of the roughness of the PEDOT layer, a 15 μm layer of P(VDF-TrFE) was not sufficient to have an efficient device: the rounded shape of the hysteresis loop shows short-circuits in the device. However, increasing the thickness of the piezoelectric layer to 80 μm reduced the short-circuits as seen with the sharper hysteresis loop. The free standing inkjet printed device shows also a nice hysteresis loop. The displacement is related to the thickness of the piezoelectric

layer. Indeed, for a five times thicker layer ( $80\ \mu\text{m}$  instead of  $15\ \mu\text{m}$ ), the displacement is 50 times higher ( $D_{\text{sat}}$ : 92.1 versus 1.5 /  $D_r$ : 61 versus 1.4). The thickness of the device is then very important.

To be able to compare the different formulations of P(VDF-TrFE) developed in Chapter 2, devices were then printed via screen-printing using commercial PEDOT:PSS as electrodes. This will be described in the next section.

## 4.5 Screen-printed and stencil-printed commercial PEDOT:PSS electrodes & new P(VDF-TrFE) formulations

### 4.5.1 Device fabrication

Two different geometries were considered: A) an array of 15 by 15 devices of three different areas ( $25$ ,  $10$  and  $4\ \text{mm}^2$ ), and B) an array of 2 by 3 devices of two types of areas ( $270$  and  $370\ \text{mm}^2$ ) [Figure 4.15].

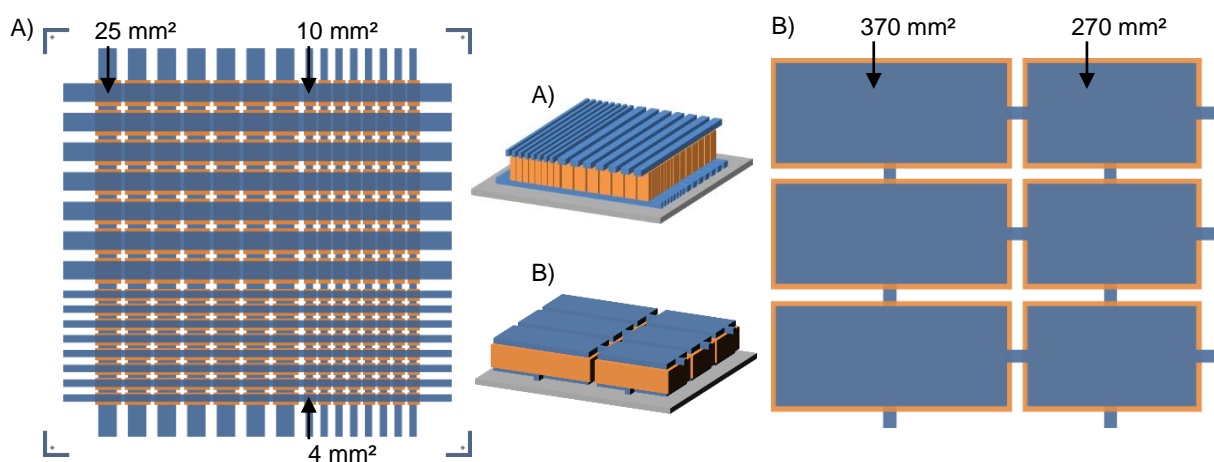


Figure 4.15: Geometry of the devices using A) screen-printing, and B) stencil-printing for the P(VDF-TrFE) layer. In blue the electrodes and in orange the P(VDF-TrFE).

The mask used for the electrodes for geometry A is composed of 2 and 5 mm width lines. These electrodes were screen-printed. The piezoelectric polymer was screen-printed or stencil printed using a mask composed of rectangles corresponding to the area at the intersection of the electrodes. Note here that the P(VDF-TrFE) is not complete but consist of an array of small rectangles separated from each other to avoid a global response of the piezoelectric material and increase the flexibility of the matrix.

In geometry B, the electrodes were screen-printed over six large areas. The P(VDF-TrFE) film was stencil-printed between the two electrodes. Stencil printing was used because one of the P(VDF-TrFE) formulations we wanted to test dissolves the screen-printing mask. In the case of stencil printing, the screen is a metallic mask without mesh, and the squeegee used is a metallic blade.

The electrodes were always printed via screen-printing with PEDOT:PSS EL-P 5015 ink and dried 5 min at 110°C. For the piezoelectric layer, screen-printing was performed with FC25 ink P, T\_P10\_D5\_R and 3D7T\_P12\_D5\_R inks. A speed of 100 mm/s or 50 mm/s was used; the speed is generally reduced to avoid the formation of bubbles during the printing. In the case of the last ink (3D7T\_P12\_D5\_R), the concentration of DMSO in the formulation was too high and dissolved the mask of the screen. To be able to compare it with commercial ink (FC25 ink P), stencil printing was used.

To increase the thickness of the screen-printed P(VDF-TrFE) layer ( $\approx 1 - 2 \mu\text{m}$ ), multiple layers were printed (with drying at 110°C between each layer from 5 min to 1 h).

All of the devices used PET as a substrate. A few devices used PDMS, but the electrical resistance of the electrodes was very high. It is possible that the poor wettability of the PEDOT solutions on PDMS makes for less homogeneous films.

The organic screen-printed devices obtained are displayed in Figure 4.16 and the characteristics of the different devices is given in Table 4.2.

Ink	Printing method	Number of P(VDF-TrFE) layers	Drying duration at 110°C	Squeegee speed
FC25 ink P	Screen-printing	5	5 min	100 mm/s
T_P10_D5_R		2	1 h	50 mm/s
FC25 ink P	Stencil-printing	1	10 min	100 mm/s
T_P10_D5_R				
3D7T_P12_D5_R				

*Table 4.2: Printing parameters for the piezoelectric layer in screen-printing or stencil printing.*

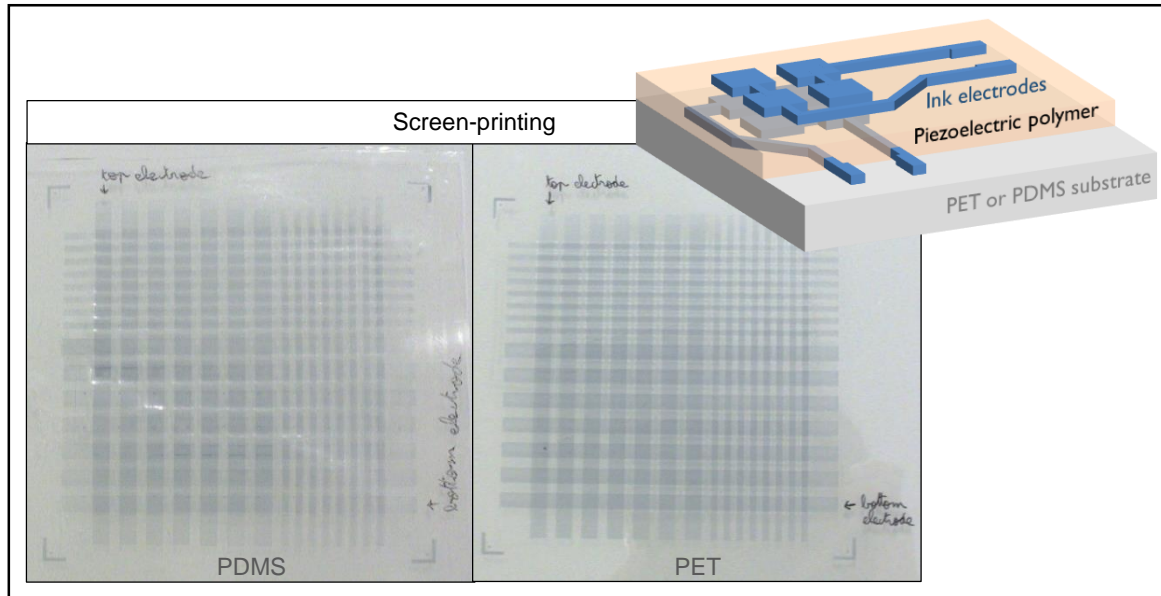


Figure 4.16: Photos and schematic of the devices with organic electrodes and P(VDF-TrFE) deposited by screen-printing.

Figure 4.17 displays a 3D schematic of the printed patterns and a microscope picture. When 1 h is used to dry the P(VDF-TrFE) layers, homogeneous films of the different layers are obtained as shown by microscopy images [Figure 4.17].

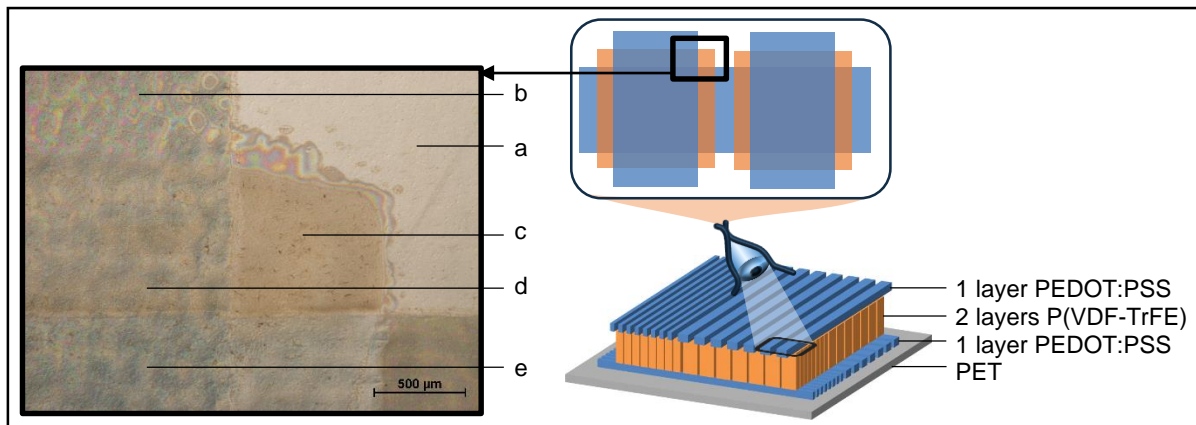


Figure 4.17: Schematic of a piezoelectric device: 1 layer of PEDOT:PSS<sub>EL-P5015</sub> deposited by screen-printing, 2 layers of T\_P10\_D5\_R, and 1 layer of PEDOT:PSS<sub>EL-P5015</sub> deposited by screen-printing. Drying between the T\_P10\_D5\_R layers during 1 h at 110°C. Microscope image at the intersection of the layers. Picture's caption: a) PET; b) PEDOT:PSS on PET; c) P(VDF-TrFE) on PET; d) P(VDF-TrFE) on PEDOT:PSS on PET; e) PEDOT:PSS on P(VDF-TrFE) on PEDOT:PSS on PET.

If the P(VDF-TrFE) layers are dried 5 min only, the layers of PEDOT:PSS or P(VDF-TrFE) on top of PET are quite homogenous. The region where P(VDF-TrFE) covers the PEDOT:PSS film shows several folds and possibly wrinkles. Since the PEDOT:PSS film is thicker and more visible under the microscope, we believe that these folds and wrinkles are actually on the PEDOT:PSS film. The P(VDF-TrFE) then inherits these folds and wrinkles as shown in the profile of the thickness [Figure 4.18].

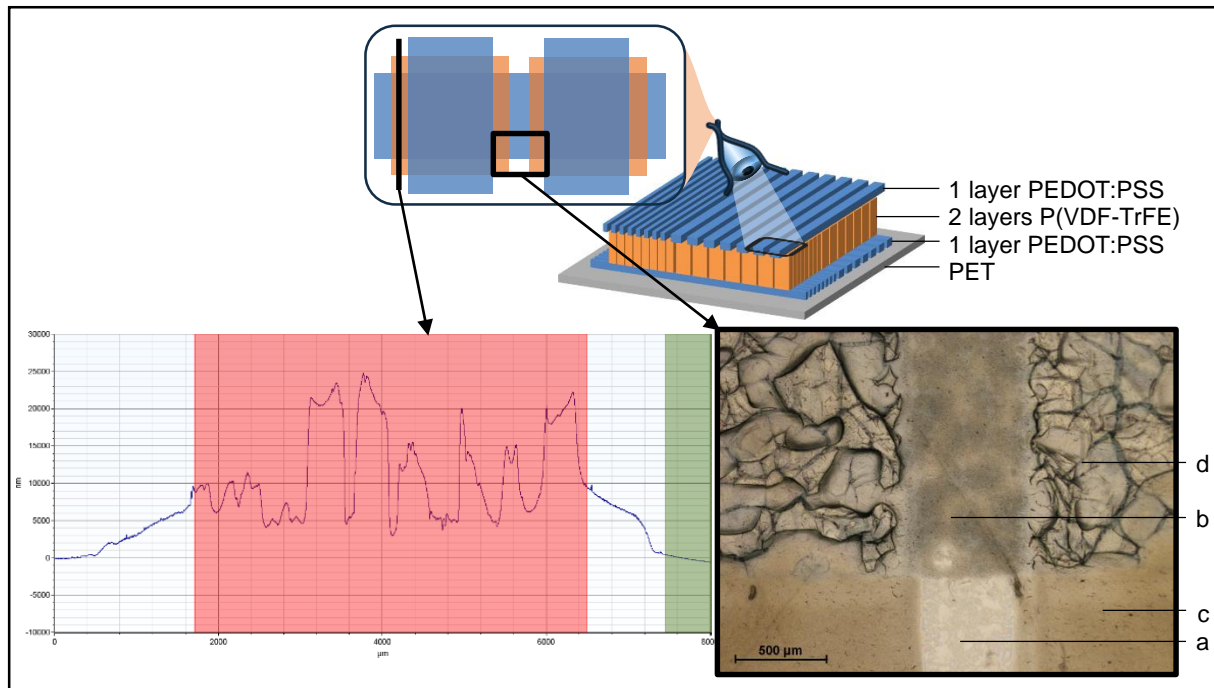


Figure 4.18: Schematic of a piezoelectric device: 1 layer of PEDOT:PSS<sub>EL-P 5015</sub> deposited by screen-printing, and 2 layers of T\_P10\_D5\_R. Drying between the layers during 5 min at 110°C. Profile and microscope images at the intersection of the layers. Picture's caption: a) PET; b) PEDOT:PSS on PET; c) P(VDF-TrFE) on PET; d) P(VDF-TrFE) on PEDOT:PSS on PET.

When 1 h is used to dry the P(VDF-TrFE) layers, wrinkling problems clearly disappear. The stress generated during the drying process when the layer of P(VDF-TrFE) is not well dried could cause such folding. It is then very important to dry the layers completely. In fact, a drying time of 1 h was more than enough: doctor blading trials have shown that 10 – 20 min are enough.

## 4.5.2 Device characterization

In this section we will present the electrical characteristics of the different devices.

As mentioned previously, the adhesion of the PEDOT layer on PDMS was not optimal and the resistance of the electrodes was high compared to PET. Further, the roughness of the PEDOT electrode was high. The devices on PDMS were leakier than on PET and only the devices on PET were sent to the Lyric institute for further characterization. Figure 4.19 shows a comparison between PDMS and PET based devices. It is clearly seen that the PDMS devices show a hysteresis loops with a rounded shape, that is characteristic of leakage, while the PET devices show sharper hysteresis loops and clearly defined current peaks contrary to the PDMS devices. The PET devices are more optimal than the devices on PDMS.

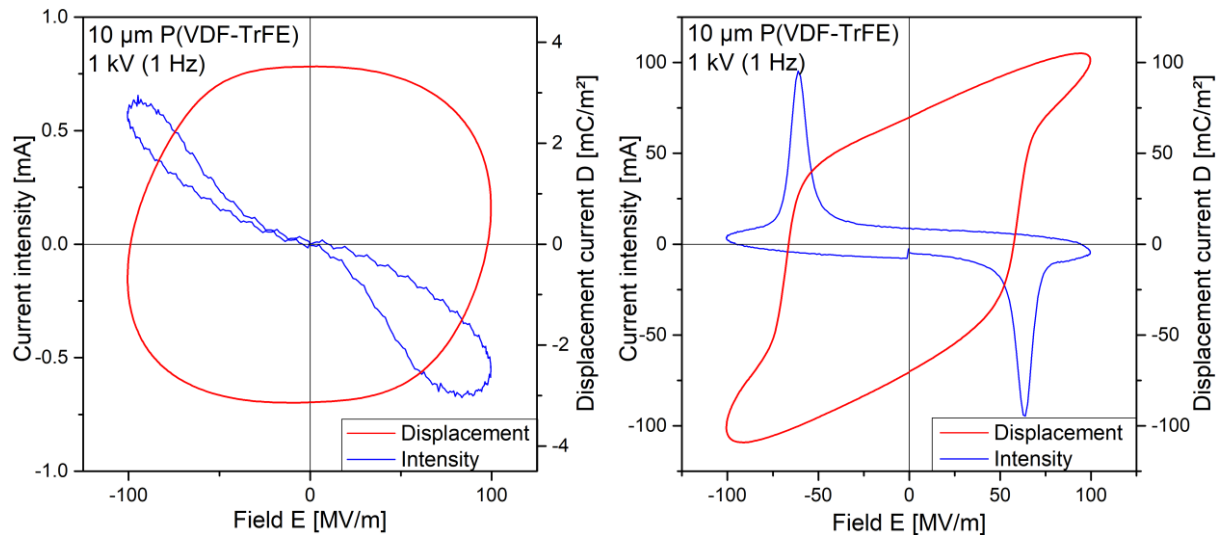


Figure 4.19: Current intensity and displacement versus field of devices obtained by screen-printing commercial PEDOT:PSS EL-P 5015 and commercial P(VDF-TrFE) FC25 Ink P on PDMS (left) and PET (right) substrates.

Figure 4.20 displays the displacement versus field of the devices on PET using stencil printed T\_P10\_D5\_R, 3D7T\_P12\_D5\_R and FC25 Ink P inks. These devices clearly show sharp hysteresis loops. The home-made formulated inks show behavior very close to the commercial ink. This figure also shows the characterisation of the device with one home made ink using different field intensities. The current peaks are well defined and the behavior is again similar to the commercial ink (see Figure 4.4 for comparison).

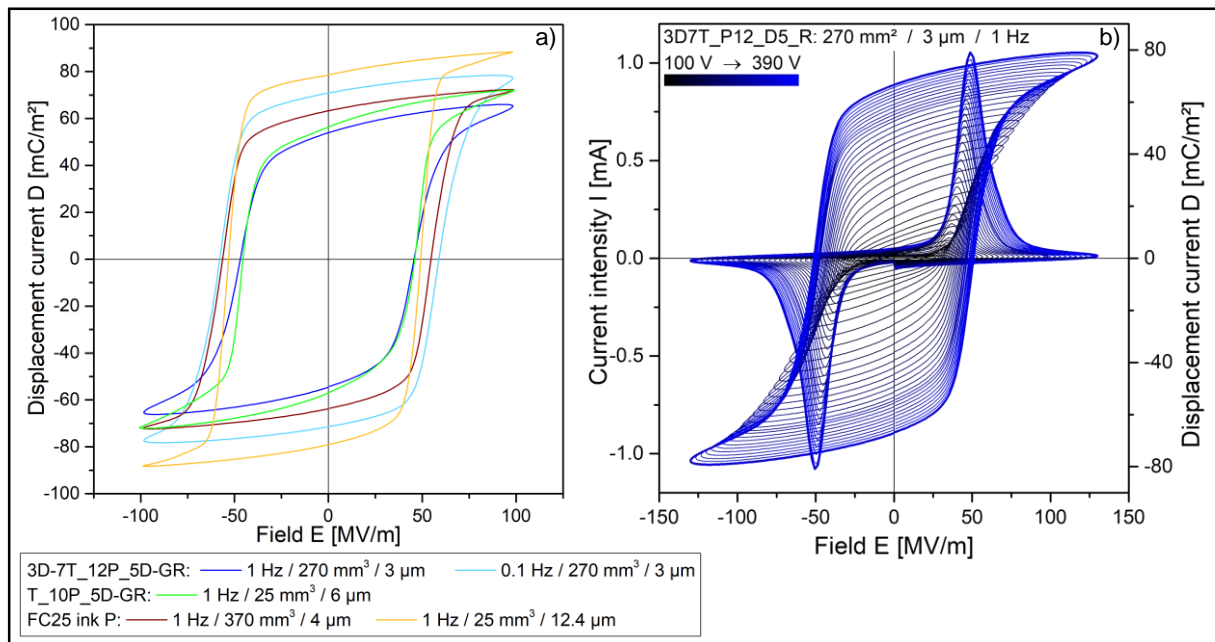


Figure 4.20: a) Displacement versus field of devices obtained by screen-printing electrodes (PEDOT:PSS EL-P 5015) on PET and stencil-printing different formulations of P(VDF-TrFE). b) Details of the polarization process (with increasing voltage steps) of the devices using 3D7T\_P12\_D5\_R to print the piezoelectric layer.

Table 4.3 gathers information for the different devices as well as the electrical characteristics extracted from Figure 4.19 and Figure 4.20 (the remanent and saturated displacement, and the coerced field for an amplitude of 100 MV/m).

N°	Ink	Process	Frequency [Hz]	Area [mm <sup>2</sup> ]	Thickness [μm]	D <sub>r</sub> [mC/m <sup>2</sup> ]	D <sub>sat</sub> [mC/m <sup>2</sup> ]	E <sub>c</sub> [MV/m]
1	FC25 inkP	Screen	1	25	10	70	105	57.5
2		Stencil		380	4	63	72	54.7
3				25	12.4	79	88	49.1
4	T_P10_D5_R		25	6	56	72	46.0	
5	3D7T_D12_D5_R	Stencil	0.1	270	3	54	66	45.6
6				270	3	71	78	58.8

Table 4.3: remanent and saturated displacement and the coerced field of devices obtained by screen- and stencil printing for the curves obtained with a maximum field at 100 MV/m.

The coerced field is in the same range for all the devices (45 – 59 MV/m). The saturated and the remanent displacements are close to each other and are comparable for all stencil-printed devices. The screen-printed device with the commercial ink, shows a similar behavior as the stencil-printed one. In summary, the home-made T\_P10\_D5\_R and 3D7T\_D12\_D5\_R inks have comparable characteristics as the commercial ink when stencil printed.

## 4.6 Conclusion

In this chapter, pressure sensors were developed with the aim of embedding them into a 3D printed heart for cardiac surgery training. Two main types of pressure sensors were studied: with metallic or organic electrodes. Even if good electronic properties were found for the devices with metallic electrodes, they were not flexible enough to be implemented into the heart. For the “all organic” devices, the formulation of PEDOT inks has to avoid the use of DMSO. Indeed, this is also a solvent of P(VDF-TrFE) and that leads to leakage between the top and bottom electrodes. The use of spray or doctor blade for the electrodes has resulted in leakage due to high roughness in the first case, and to bad adhesion between the mask and the substrate in the second case. Inkjet printed (using PEDOT:PSTFSI) or screen-printed (using PEDOT:PSS) devices have shown good electronic properties. The optimisation of the process to obtain smooth surfaces with less defects was very important to improve those properties. PDMS substrate is preferred to PET for its conformability to the 3D printed heart, however, the adhesion between PEDOT and PET is better. That is why PET was chosen to compare the different P(VDF-TrFE) formulations. However, pre-layers on top of PDMS substrate could be developed to resolve this problem.

The formulations T\_P10\_D5\_R and 3D7T\_P12\_D5\_R were used to make devices and compared to devices made with the commercial ink FC25 Ink P. The devices using both formulations have properties very similar to those made with the commercial ink, with sharp hysteresis loops and well defined current peaks, making them ideal for use as sensors.

In conclusion, our home-made formulations seem promising in the fabrication of piezoelectric devices by screen- or stencil-printing methods. Further investigation in terms of crystallinity could be interesting to determine the structural cause of the differences between the devices.

## Bibliography

- (1) Ferry, J. D. *Viscoelastic Properties of Polymers*; Wiley: New York, 1980.
- (2) Sharma, T.; Je, S. S.; Gill, B.; Zhang, X. Patterning Piezoelectric Thin Film PVDF-TrFE Based Pressure Sensor for Catheter Application. *Sens. Actuators Phys.* **2012**, *177*, 87-92. <https://doi.org/10.1016/j.sna.2011.08.019>.
- (3) Kang, S.-J.; Pak, J. J. A Review: Flexible, Stretchable Multifunctional Sensors and Actuators for Heart Arrhythmia Therapy. *Micro Nano Syst. Lett.* **2017**, *5* (1), 22. <https://doi.org/10.1186/s40486-017-0055-9>.
- (4) Langberg, J. J.; Franklin, J. O.; Landzberg, J. S.; Herre, J. M.; Kee, L.; Chin, M. C.; Bharati, S.; Lev, M.; Himelman, R. B.; Schiller, N. B.; et al. The Echo-Transponder Electrode Catheter: A New Method for Mapping the Left Ventricle. *J. Am. Coll. Cardiol.* **1988**, *12* (1), 218-223. [https://doi.org/10.1016/0735-1097\(88\)90377-4](https://doi.org/10.1016/0735-1097(88)90377-4).
- (5) Spampinato, N.; Maiz, J.; Portale, G.; Maglione, M.; Hadziioannou, G.; Pavlopoulou, E. Enhancing the Ferroelectric Performance of P(VDF-Co-TrFE) through Modulation of Crystallinity and Polymorphism. *Polymer* **2018**, *149*, 66-72. <https://doi.org/10.1016/j.polymer.2018.06.072>.
- (6) Soulestin, T.; Ladmiral, V.; Dos Santos, F. D.; Améduri, B. Vinylidene Fluoride- and Trifluoroethylene-Containing Fluorinated Electroactive Copolymers. How Does Chemistry Impact Properties? *Prog. Polym. Sci.* **2017**, *72*, 16-60. <https://doi.org/10.1016/j.progpolymsci.2017.04.004>.
- (7) Spampinato, N. Ferroelectric Polymers for Organic Electronic Applications. thesis, Bordeaux, 2018.

# General conclusion and perspectives

In this work, the properties of PEDOT:PSTFSI and P(VDF-TrFE) inks, two polymeric solutions were explored. Various formulations were needed to tune the rheological behaviors of these inks to allow their deposition using different printing techniques. Pressure sensors were then designed and fabricated to demonstrate the application of these organic functional inks in organic devices.

In the case of the PEDOT:PSTFSI inks, the monomer STFSI and the polyanion PSTFSI were synthesized. Structural studies by DLS, liquid AFM and cryo-SEM of the complex PEDOT:PSTFSI have shown that the polymers form a network in water. The dimensions of the polyanion that forms the network are in the range of few nanometers width and half micrometer long. The conductive polymer, PEDOT, forms small nano-objects of 5 – 15 nm along the polyanion. A systematic study of the rheological behaviors as a function of the concentration of PEDOT:PSTFSI solution has shown that the ink has a Newtonian behavior at low concentrations, and becomes shear thinning with gel properties at higher concentrations. The processability of these inks is controlled by their viscosity and rheological properties and can be tuned by simply varying the concentration of the complex or the molar mass of the polyanion. Surfactant was added in the formulation to decrease the surface tension of the inks and make them compatible with low surface energy substrates. High boiling point solvents such as dimethyl sulfoxide (DMSO) or ethylene glycol (EG) were also used to increase the conductivity and the water resistance of the dried films.

Four different deposition processes were then used with PEDOT:PSTFSI inks: doctor blade, inkjet, screen-printing, and a soft blade deposition process. Homogeneous films were obtained by doctor blading and inkjet printing of PEDOT:PSTFSI solutions, concentrated respectively at 1 %<sub>wt</sub> and 0.5 %<sub>wt</sub>. The measured transmittance (72 – 93 %), the roughness and the conductivity (230 – 380 S/cm) are similar to those obtained with the commercial PEDOT:PSS ink with the same formulation. Promising figures of merit up to 31 were reached, which is close to the minimum used in industry for transparent electrodes.

For the screen-printing deposition, inhomogeneous films were obtained. This is mostly due to capillary interactions between the ink and the screen. A systematic study using different screens and different surfactants should be performed to obtain a better formulation of PEDOT:PSTFSI for screen-printing. For the soft blade deposition, lines of PEDOT were obtained by adding a high neutral polymer to increase the extensional properties of the ink. The deposition was done on silanized glass, on PET, and on evaporated gold treated with octane-thiol. The well-

defined lines have a thickness close to 700 nm and a width near 20 – 25 nm. Conductive AFM has shown that the lines are conductive and polymers are aligned in the direction of the deposition. A more systematic study on the conductivity of PEDOT lines should be performed using different types of conductive AFM tips to better measure and understand the conductivity of the lines.

For the P(VDF-TrFE) inks, two batches of polymers were studied, containing 79.4 %<sub>w</sub> of VDF units and 20.6 %<sub>w</sub> of TrFE units, with respective average molar masses of 238 and 278 kDa. A systematic study of the concentration dependence of the rheological behavior has shown that P(VDF-TrFE) in gamma-butyrolactone (GBL) is Newtonian for all concentrations at low shear, and becomes slightly shear-thinning at very high concentrations and shear rates. To modify this behavior and make the solutions shear-thinning for screen-printing applications, two different ways were developed.

First, a gelifying agent, 1,3:2,4-bis(3,4-dimethylbenzylidene) sorbitol (DMDBS), was added in one or two good solvents of P(VDF-TrFE): triethylphosphate (TEP), present in the commercial ink, and DMSO. The addition of this agent allowed to obtain an adequate shear thinning behavior with a sufficiently high viscosity and elasticity. To understand the modification of the rheological behavior of the ink by adding the gelifying agent, a structural study was done using Cryo-SEM measurements. The drawback of this formulation is that it required high temperatures, 130 – 140°C, to dissolve the gelifying agent in the solvent. To reduce this temperature, DMDBS can be dissolved beforehand at 60°C in DMSO, which is a good solvent of DMDBS. The same shear thinning behavior is obtained for inks using 30 %<sub>vol</sub> DMSO and 70 %<sub>vol</sub> TEP. However, this high amount of DMSO in the formulation is not compatible with the screen-printing mask tested, as the latter was dissolved by this formulation. A study on the various screen-printing masks and their compatibility with DMSO should be performed as well as a study using other gelifying agents compatible with solvents of P(VDF-TrFE) and which can be dissolved at low temperatures. Nevertheless, it was possible to print these two inks using doctor blade, a screen in the case of the formulation without DMSO, and a stencil for the formulation with DMSO. The obtained films were quite homogeneous. Further characterization of these films showed that the gelifying agent does not affect crystal sizes. The use of the gelifying agent is then promising to formulate P(VDF-TrFE) screen-printing inks for piezoelectric layer deposition.

The second kind of P(VDF-TrFE) inks was formulated using a good solvent of the polymer, GBL, and a bad solvent, benzyl alcohol. A nano-emulsion is formed by the two solvents, and the addition of P(VDF-TrFE) makes the GBL domains grow. At room temperature, the rheological behavior of the ink is highly dependent on its shear history, especially near a critical temperature, itself related to the concentration of the bad solvent and of the polymer. The Newtonian inks can

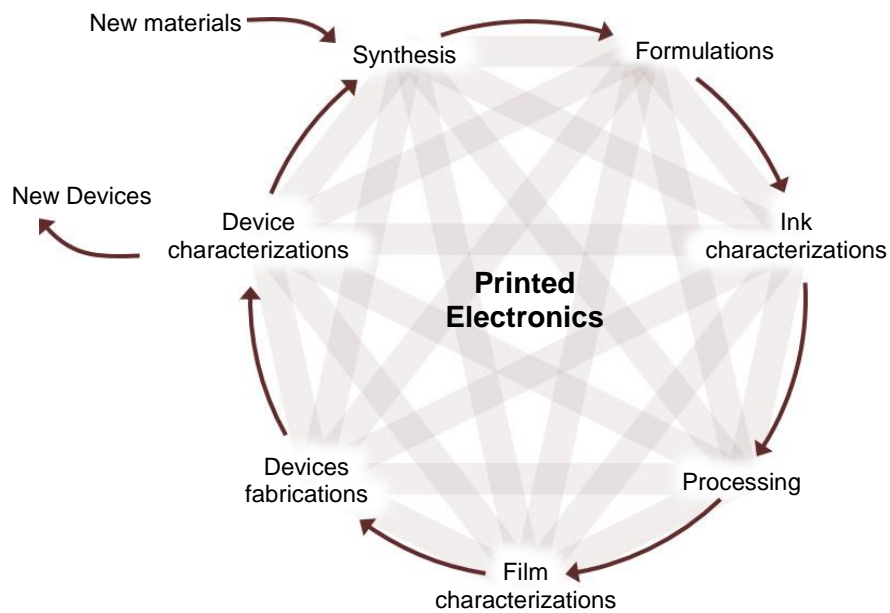
become shear-thinning, with high viscosities at low shears, when repeated shear cycles are applied. A precise protocol has to be used to prepare inks using appropriate temperatures to be adapted to the screen-printing technique. The obtained films can be either porous if dried at room temperature, or dense and homogeneous if dried at high temperature (135°C). The porous films can be rendered homogeneous by annealing. The porous films could be used as membrane separators in lithium-ion batteries.

Finally, pressure sensors using the previous inks were made by encapsulating a P(VDF-TrFE) layer between two electrodes (made of either PEDOT inks or metal evaporation): on PDMS substrates, using free standing films of P(VDF-TrFE) to be embedded into a 3D-printed heart for cardiac surgery training, and on PET to compare the different home-made P(VDF-TrFE) formulations. While PDMS has the correct flexibility to make flexible devices, the wettability and the adhesion of the PEDOT inks on this substrate was not optimal. Pre-layers on top of PDMS substrates could be developed to increase the wettability and adhesion of PEDOT aqueous solutions. Devices with metallic electrodes have shown good electric properties, but were not flexible enough to be integrated into the 3D-printed heart. PEDOT inks used to print the electrodes have to be formulated preferably with EG than DMSO. Indeed, the use of DMSO, which is also a good solvent of P(VDF-TrFE), has led to short-circuits when P(VDF-TrFE) films were sandwiched between PEDOT electrodes. Spraying or doctor blading using a mask have resulted respectively in leakage between the bottom and top PEDOT electrodes, due to high roughness, or between the bottom electrodes of the different devices, due to bad adhesion between the mask and the substrate.

However, good electronic properties were obtained by inkjet printing PEDOT:PSTFSI and doctor blading P(VDF-TrFE) solutions, or by screen-printing commercial PEDOT:PSS and screen- or stencil-printing home-made P(VDF-TrFE) formulations. An important process optimisation was therefore necessary to obtain smooth surfaces with less defects and thus improve the device properties. The devices using stencil-printed P(VDF-TrFE) inks with DMSO or the commercial screen-printing ink have shown similar properties: sharp polarization hysteresis loops and well defined current peaks. These devices can be used in pressure sensor applications. Further investigation in terms of crystallinity should be performed to better understand the differences between the devices.

In conclusion, it has been shown that the studied PEDOT:PSTFSI and P(VDF-TrFE) inks can be formulated adequately to be deposited using various printing technologies in order to make functional pressure sensors. Additional work is needed to optimize such devices.

As general perspectives, PEDOT inks could be chemically modified to make them sensitive to biological molecules, such as glucose, for organic electrochemical transistor applications, while keeping their easy processability using various printing techniques. Both P(VDF-TrFE) and PEDOT inks could be developed to become crosslinkable, which would reduce leakage issue in devices. More generally, the methodology used, going from the synthesis to the characterisation of the materials, to the deposition and the characterisation of the devices, could be applied to other materials for other applications to contribute to the development of printed electronics.



# Appendices

A.1	Size-exclusion chromatography of PSTFSIK.....	172
A.2	Extensional rheology of a PEDOT:PSTFSI solution: similar behavior to shear rheology.....	173
A.3	Energy Dispersive X-ray spectrometry of PEDOT:PSTFSI films on glass substrate.....	175
A.4	Wetting surface properties of PEDOT:PSS and PEDOT:PSTFSI films.....	176
A.5	Size-exclusion chromatography in DMF or THF of P(VDF-TrFE).....	178
A.6	Rheological measurements of P(VDF-TrFE) solutions at different concentrations (batch FC20 62-053).....	179
A.7	Temperature dependence of P(VDF-TrFE) solution in GBL.....	180
A.8	Critical temperature $T_w$ of 25B/75G_P15 and 25B/75G_P12.....	181

## A.1 Size-exclusion chromatography of PSTFSIK

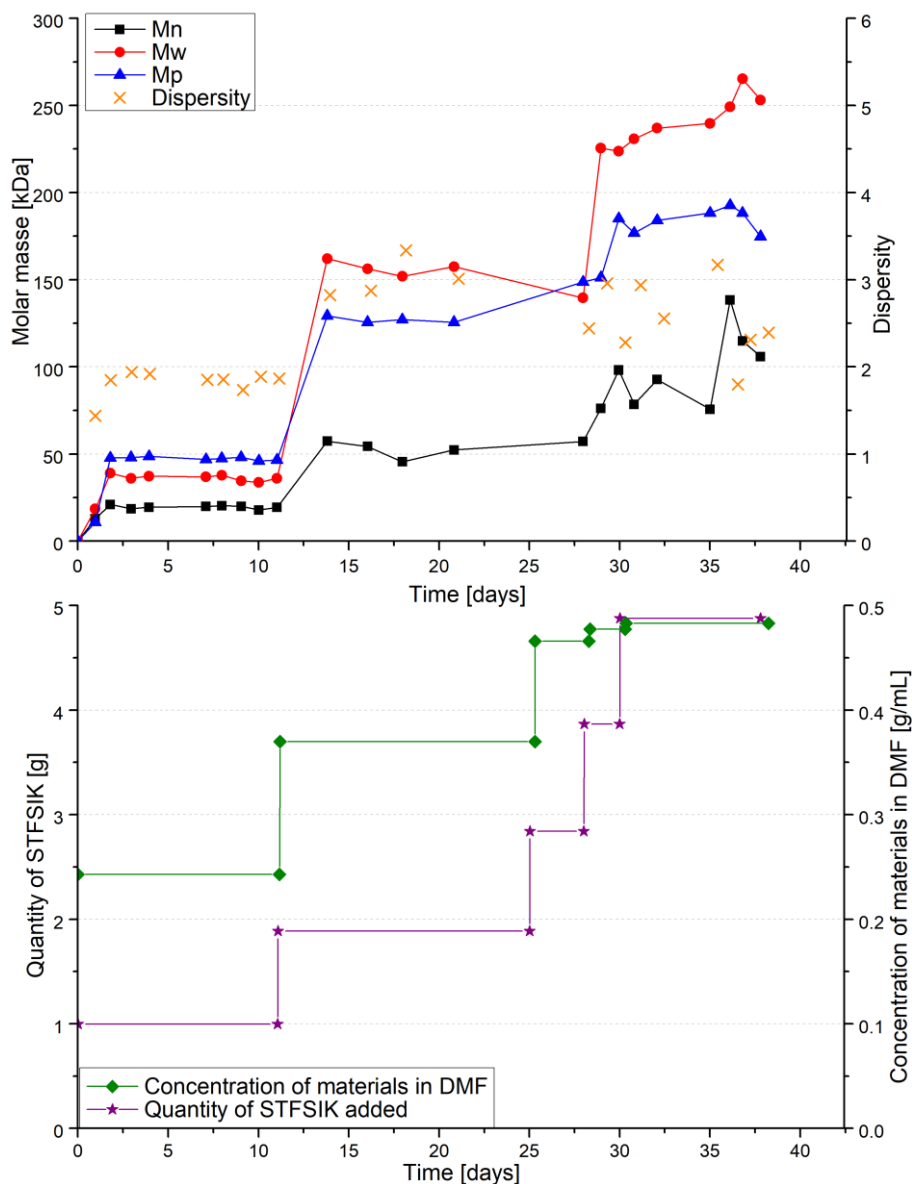


Figure A.1-1: Evolution of the molar mass of  $PSTFSIK_{250\text{ kDa}}$  during its synthesis, in function of time, STFSIK added, and concentration of the materials in DMF (without flow marker) in equivalent PS.

Polyanion	$M_p$	$M_n$	$M_w$	Dispersity	With or without flow marker
$PSTFSIK_{250\text{ kDa}}$	197	94	<b>249</b>	2.7	without
	237	114	<b>277</b>	2.4	with toluene
$PSTFSIK_{90\text{ kDa}}$	93	45	<b>89</b>	2.0	with toluene
$PSTFSIK_{80\text{ kDa}}$	82	43	<b>78</b>	1.8	with toluene

Table A.1-1: Molar masses of three polyanions designated as  $PSTFSIK_{80\text{ kDa}}$ ,  $PSTFSIK_{90\text{ kDa}}$  and  $PSTFSIK_{250\text{ kDa}}$  obtained after precipitation by SEC in DMF + LiBr in equivalent PS.

## A.2 Extensional rheology of a PEDOT:PSTFSI solution: similar behavior to shear rheology

The extensional viscosity  $\eta_{ext}$  of PEDOT:PSTFSI<sub>90 kDa</sub> (0.96 %wt) was calculated with the relation for viscous liquids<sup>1</sup>:  $\eta = \frac{2^{n-1}n^n\varphi_0(n)\gamma}{dR_{min}/dt}$  where  $R_{min}$  is the smaller radius of the neck of the drop [Figure A.2-1],  $\gamma$  is the surface tension of the fluid,  $\varphi_0(n)$  depends only on the shear thinning flow behavior index  $n$  (determined at 0.38 in shear measurements [Figure A.2-2]).

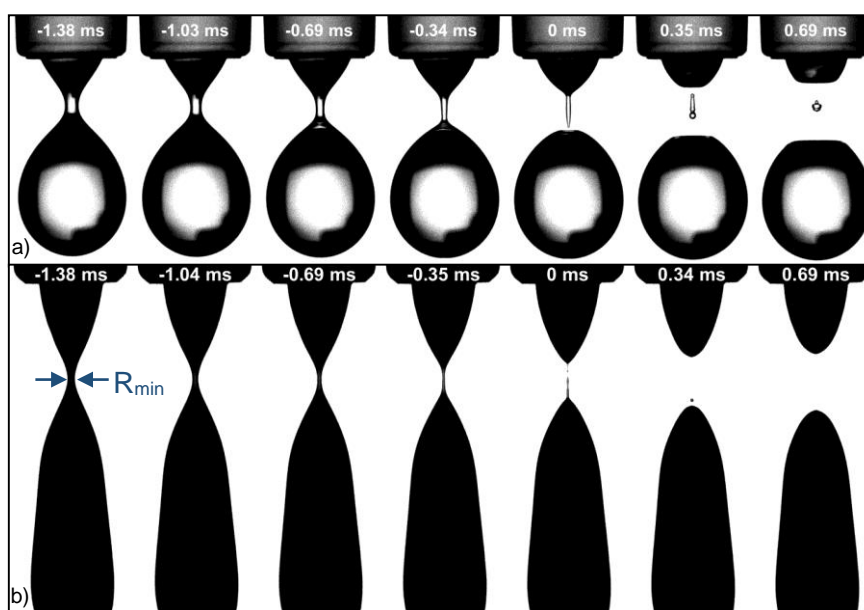


Figure A.2-1: Detaching drops from a needle of: a) pure water and b) 0.96 %wt of PEDOT:PSTFSI<sub>90 kDa</sub> in water.

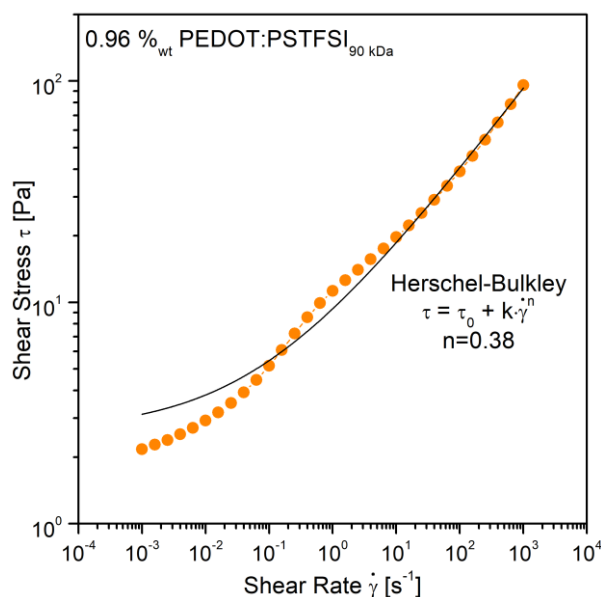


Figure A.2-2: Shear stress versus shear rate of 0.96 %wt of PEDOT:PSTFSI<sub>90 kDa</sub> ink measured with a shear rheometer (cone plate geometry: 50 mm diameter and 1° angle) at 18°C.

<sup>1</sup> Louvet, N.; Bonn, D.; Kellay, H. Nonuniversality in the Pinch-Off of Yield Stress Fluids: Role of Nonlocal Rheology. *Phys. Rev. Lett.* **2014**, *113* (21), 218302. <https://doi.org/10.1103/PhysRevLett.113.218302>.

$R_{\min}$  can be fitted considering that  $R_{\min}^{1/n}$  is linear in time [Figure A.2-3]. The extensional rate is then calculated with the relation  $\dot{\epsilon} = \frac{2}{R_{\min}} \frac{dR_{\min}}{dt}$ .

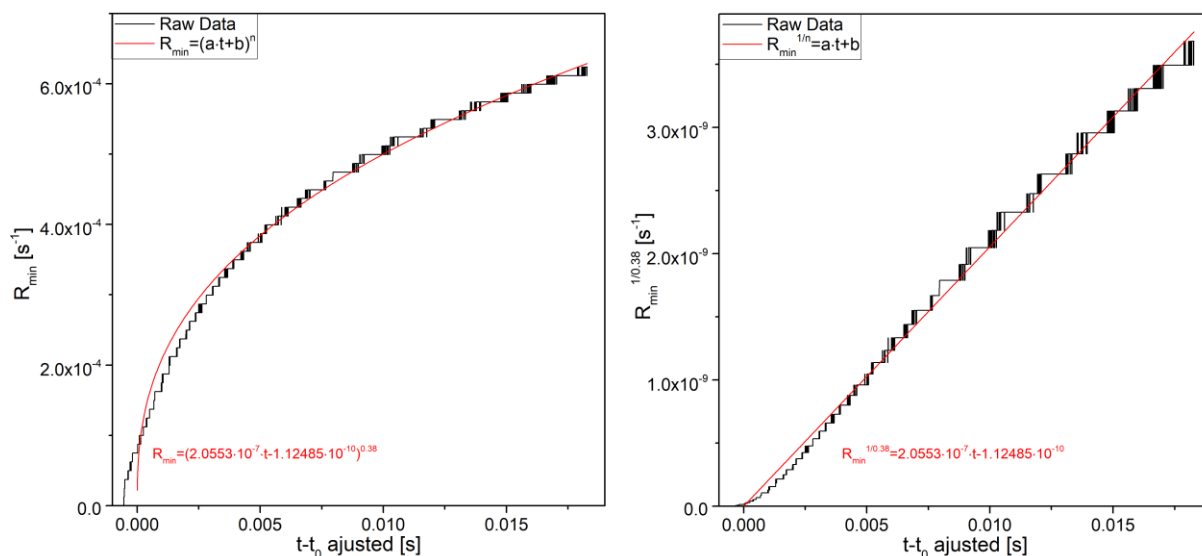


Figure A.2-3: Smaller radius  $R_{\min}$  of the neck of the drop of 0.96 %wt of PEDOT:PSTFSI<sub>90 kDA</sub> ink at 18°C versus time and  $R_{\min}^{1/n}$  ( $n=0.38$ ).

If we assume that the surface tension of the solution is 55 mN/m [See 2.3.5], we obtain an extensional viscosity with an identical extensional/shear thinning behavior than the shear viscosity [Figure A.2-4]. The small shift in viscosity is due to the yield in the solution.<sup>2</sup>

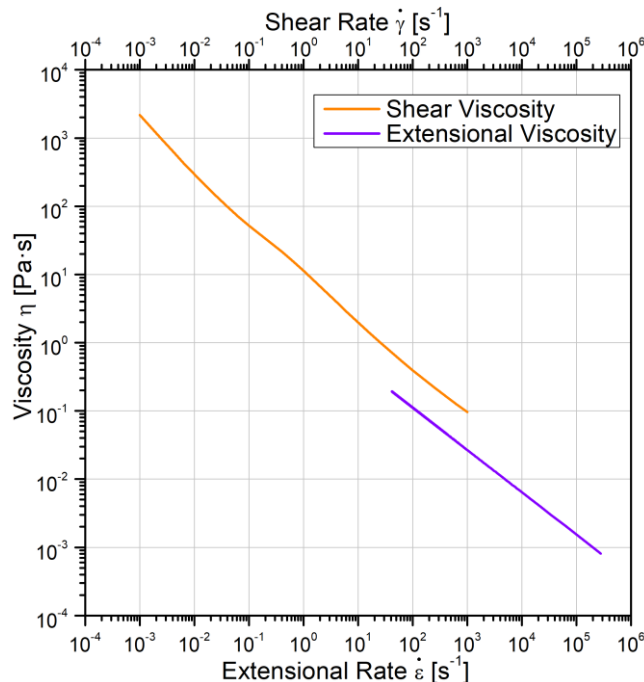


Figure A.2-4: Shear and extensional viscosity of 0.96 %wt of PEDOT:PSTFSI<sub>90 kDA</sub> ink at 18°C.

<sup>2</sup> Louvet, N.; Bonn, D.; Kellay, H. Nonuniversality in the Pinch-Off of Yield Stress Fluids: Role of Nonlocal Rheology. *Phys. Rev. Lett.* **2014**, *113* (21), 218302. <https://doi.org/10.1103/PhysRevLett.113.218302>.

### A.3 Energy Dispersive X-ray spectrometry of PEDOT:PSTFSI films on glass substrate

The SEM image of films deposited by inkjet printing has shown shiny points. First we suspected nanoparticles (used for other formulations using the same ultrasonic probe). Energy Dispersive X-ray spectrometry (EDX) was performed [Figure A.3-1] and didn't show any difference between films deposited by both depositions techniques. In fact, glass atoms were also measured. The explanation of the white points finally comes from the SEM technic itself: the electrons can penetrate the sample, and this penetration depends on the compound:  $r = \frac{2.76 \times 10^{-2} A E_0^{1.67}}{\rho Z^{0.89}}$  where  $A$  is the average atomic weight (g/mol),  $E_0$  is the accelerating voltage (keV),  $Z$  is the average atomic number, and  $\rho$  the density (g/cm<sup>3</sup>).<sup>3</sup> For atoms of C, S, O, F or N, at 0.5 keV, the penetration depth of the electron is then in the order of 10 – 30 nm. The thicknesses of the observed films were  $230 \pm 30$  nm (inkjet) and  $510 \pm 80$  nm (doctor blade), and so the contribution of the substrate was more visible in the case of thinner films. The points come then from the glass substrate itself.

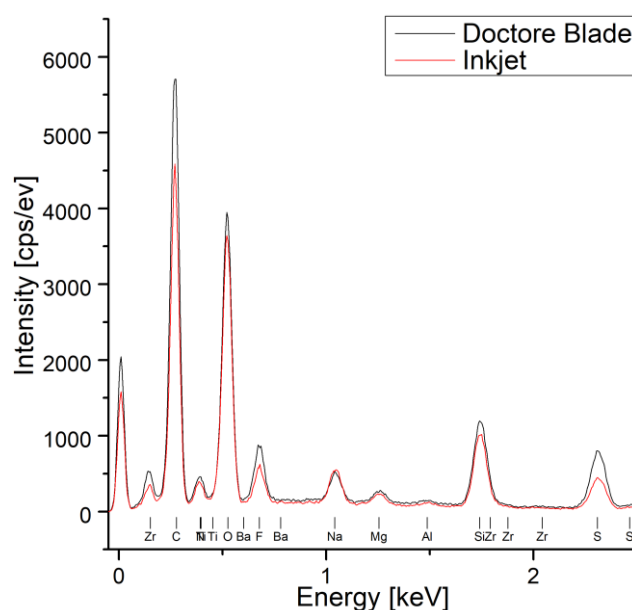


Figure A.3-1: Energy Dispersive X-ray spectrometry (EDX) of PEDOT:PSTFSI<sub>80 kDa</sub> films deposited by doctor blade or inkjet.

<sup>3</sup> Kanaya, K.; Okayama, S. Penetration and Energy-Loss Theory of Electrons in Solid Targets. *J. Phys. Appl. Phys.* **1972**, *5* (1), 43–58. <https://doi.org/10.1088/0022-3727/5/1/308>.

## A.4 Wetting surface properties of PEDOT:PSS and PEDOT:PSTFSI films

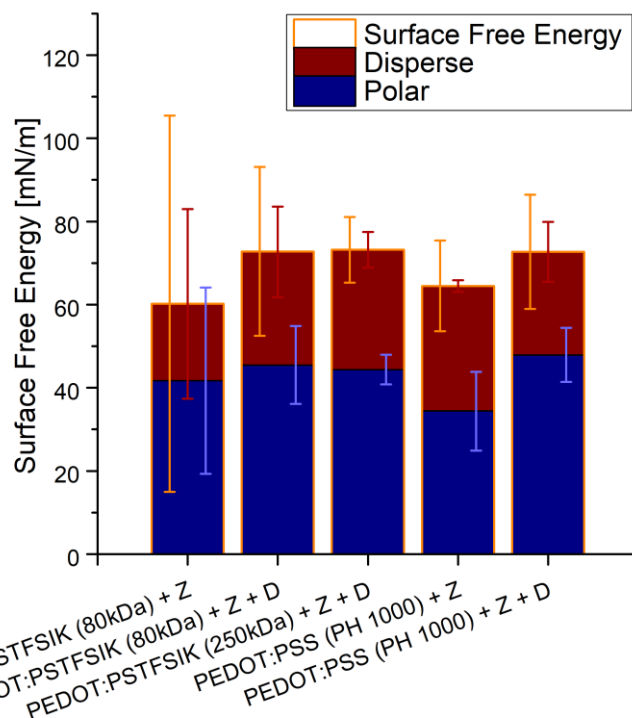


Figure A.4-1: Surface free energy of films made from different solutions of PEDOT:PSTFSI (80 and 250 kDa) and PEDOT:PSS (PH 1000) with and without Zonyl fluoro-surfactant (Z) / DMSO (D).

The surface free energy of PEDOT films (PEDOT:PSTFSI<sub>80 kDa</sub>, PEDOT:PSTFSI<sub>250 kDa</sub>, and PEDOT:PSS<sub>PH 1000</sub>) is  $73 \pm 20$  mN/m [Figure A.4-1] for films obtained with solutions using DMSO, which result in a contact angle between water drops and the film of about  $90^\circ$  just after deposition [Figure A.4-2, a)]. By waiting, the water spreads onto the film and the contact angle becomes  $5 \pm 1^\circ$  after 1 min [Figure A.4-2, d)]. For PEDOT films without DMSO, water start to spread onto the film and at a certain point it infiltrates the film and make it break and fold on itself (the water goes under the film) as shown in Figure A.4-2, c) and d). The resulting folding of the PEDOT layer after drying of the drops is displayed in Figure A.4-3. It could be explained by a better segregation between the PEDOT and the polyanion for films obtained with PEDOT:polyanion solutions containing DMSO. Indeed, PEDOT is insoluble in water and so the film become more resistant to

the water drop. That is in accord with the literature explaining the increase of conductivity of PEDOT films with DMSO by this segregation during the drying.<sup>4,5</sup>

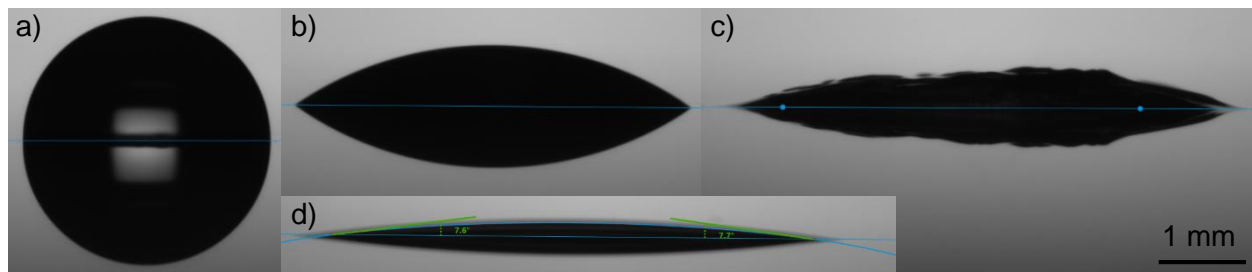


Figure A.4-2: Water drop on PEDOT:PSTFSI<sub>80 kDa</sub> + Zonyl fluoro-surfactant dried film: a) just after deposition (with or without DMSO), b) before dissolving of the film (without DMSO), c) during dissolving of the film (without DMSO), d) after one minute (with DMSO)

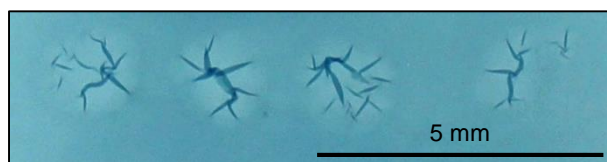


Figure A.4-3: Picture of a PEDOT:PSTFSI film on top of which four drops of water were deposited and left to dry at room temperature. The PEDOT:PSTFSI formulation used to deposit the film didn't contain a high boiling point solvent (DMSO or EG). The same picture is obtained for PEDOT:PSS films without DMSO or EG.

The surface free energy of PEDOT films is not only composed by a polar part as expected for films from aqueous inks. The dispersive part should come from the PEDOT contribution, and the polar part from the polyanion.

<sup>4</sup> Shi, H.; Liu, C.; Jiang, Q.; Xu, J. Effective Approaches to Improve the Electrical Conductivity of PEDOT:PSS: A Review. *Adv. Electron. Mater.* **2015**, *1* (4), n/a-n/a. <https://doi.org/10.1002/aelm.201500017>.

<sup>5</sup> Palumbiny, C. M.; Heller, C.; Schaffer, C. J.; Körstgens, V.; Santoro, G.; Roth, S. V.; Müller-Buschbaum, P. Molecular Reorientation and Structural Changes in Cosolvent-Treated Highly Conductive PEDOT:PSS Electrodes for Flexible Indium Tin Oxide-Free Organic Electronics. *J. Phys. Chem. C* **2014**, *118* (25), 13598–13606. <https://doi.org/10.1021/jp501540y>.

## A.5 Size-exclusion chromatography in DMF or THF of P(VDF-TrFE)

P(VDF-TrFE) batch		FC20 62-053		FC20 62-054		Solvent
Calibration		eq. PS	eq. PMMA	eq. PS	eq. PMMA	
SEC	$M_p$ [kDa]	228	-	248	-	DMF
		255	283	317	401	THF
	$M_n$ [kDa]	161	-	138	-	DMF
		121	152	135	102	THF
	$M_w$ [kDa]	503	-	504	-	DMF
		238	312	278	376	THF
Dispersity	3.1	-	3.6	-	DMF	
	2.0	2.1	2.1	3.7	THF	
MFI ( $M_w$ calculated (DMSO / eq. PMMA) [kDa])		-	7.9 (512)	-	3.25 (640)	DMSO

Table A.5-1: Size-exclusion chromatography in DMF (+LiBr) in orange, and in THF in blue, in equivalent PS or PMMA, and corresponding Melting Flow Index (given by Piezotech) for two batches of P(VDF-TrFE) ( $M_p$ : Peak molecular weight;  $M_n$ : Number-average molecular weight;  $M_w$ : Weight-average molecular weight, Dispersity= $M_w/M_n$ , MFI: Melt flow index).

The molar mass in weight in equivalent PS determined in DMF (503 – 504 kDa) is higher than in THF (238 – 278 kDa) with similar molar masses in number (121 – 161 kDa), which result in a higher dispersity (3.1 – 3.6 in DMF and 2.0 – 2.1 in THF). That can be explained by the fact that some polymer sticks to the column in DMF [Figure A.5-1] and result in misleading values.

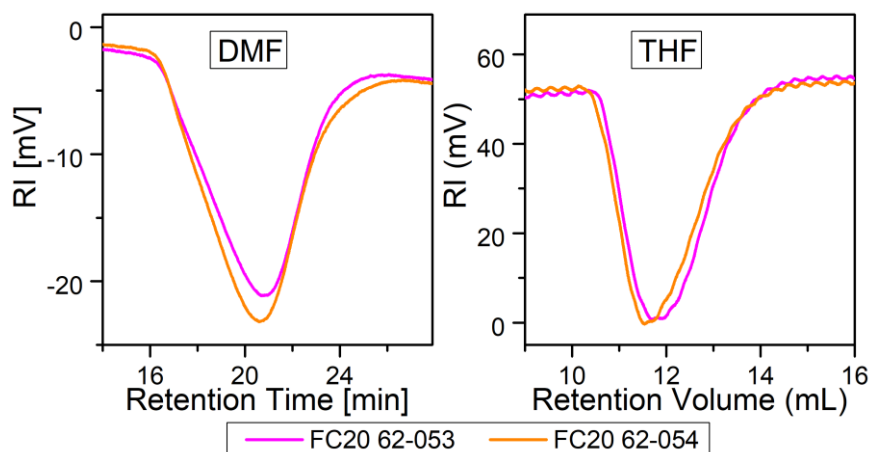


Figure A.5-1: Raw signal of size-exclusion chromatography in DMF (+LiBr) and in THF, for two batches of P(VDF-TrFE)

## A.6 Rheological measurements of P(VDF-TrFE) solutions at different concentrations (batch FC20 62-053)

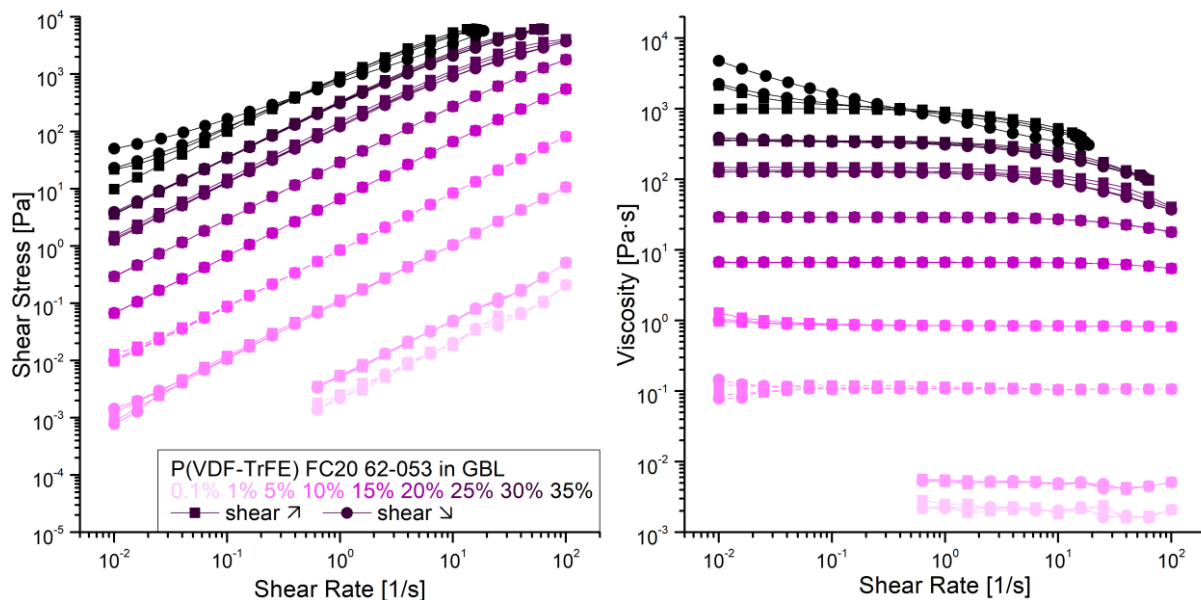


Figure A.6-1: Rheological behavior of P(VDF-TrFE) (batch FC20 62-053) in GBL at different concentration (0.1, 1, 5, 10, 15, 20, 25, 30 and 35 %wt), measured with a shear rheometer (cone plate geometry: 50 mm diameter and  $1^\circ$  angle): viscosity versus shear rate and shear stress versus shear rate, obtained by applying shear rate ramps at  $20^\circ\text{C}$ .

## A.7 Temperature dependence of P(VDF-TrFE) solution in GBL

Temperature dependency of the viscosity of a solution concentrated at 12 %<sub>wt</sub> in GBL was measured on a large range: no drastic change in the slope of the curve Figure A.7-1 occurs and so we expect that the state of P(VDF-TrFE) doesn't change on all the temperature range measured.

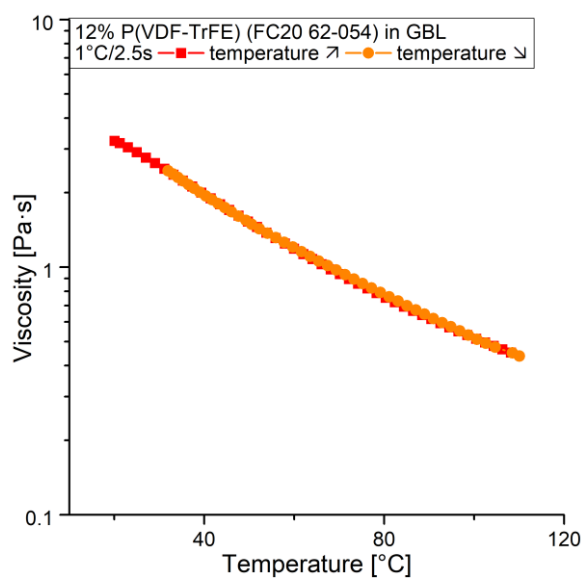


Figure A.7-1: Rheological behavior of 12 %<sub>wt</sub> P(VDF-TrFE) (batch FC20 62-054) in GBL, measured with a shear rheometer (cone plate geometry: 50 mm diameter and 1° angle): viscosity versus temperature at 10 s<sup>-1</sup>.

## A.8 Critical temperature $T_W$ of 25B/75G\_P15 and 25B/75G\_P12

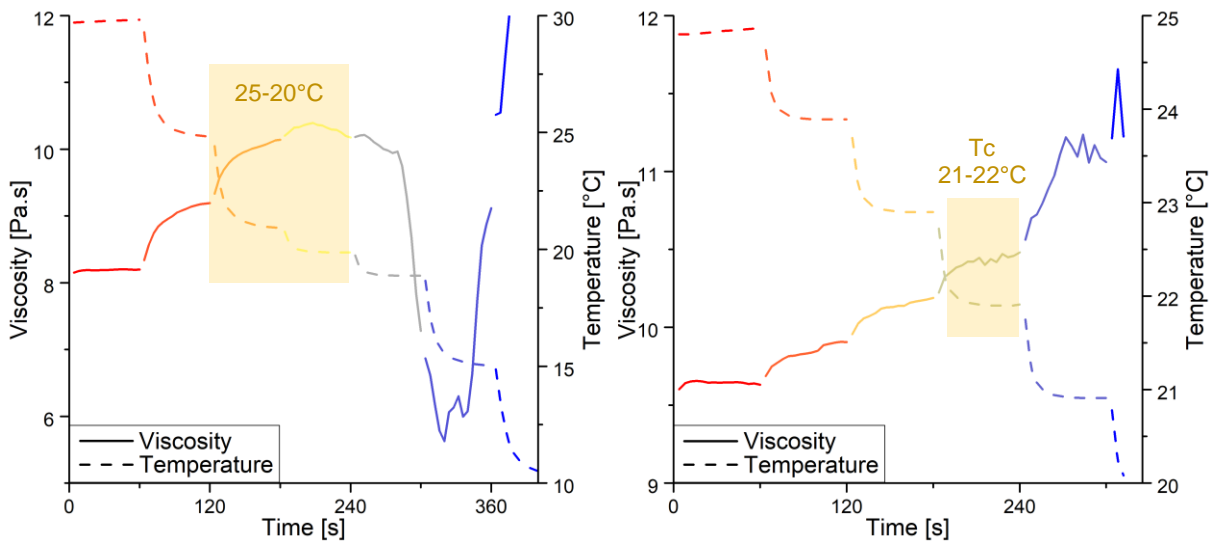


Figure A.8-1: Rheological behavior of a solution of 15 %<sub>wt</sub> P(VDF-TrFE) in 1/4 BzOH and 3/4 GBL measured with a shear rheometer (cone plate geometry: 50 mm diameter and 1° angle): viscosity and temperature versus time obtained by applying temperature stages at 10 s<sup>-1</sup>.  $T_W = 21 - 22^\circ\text{C}$ .

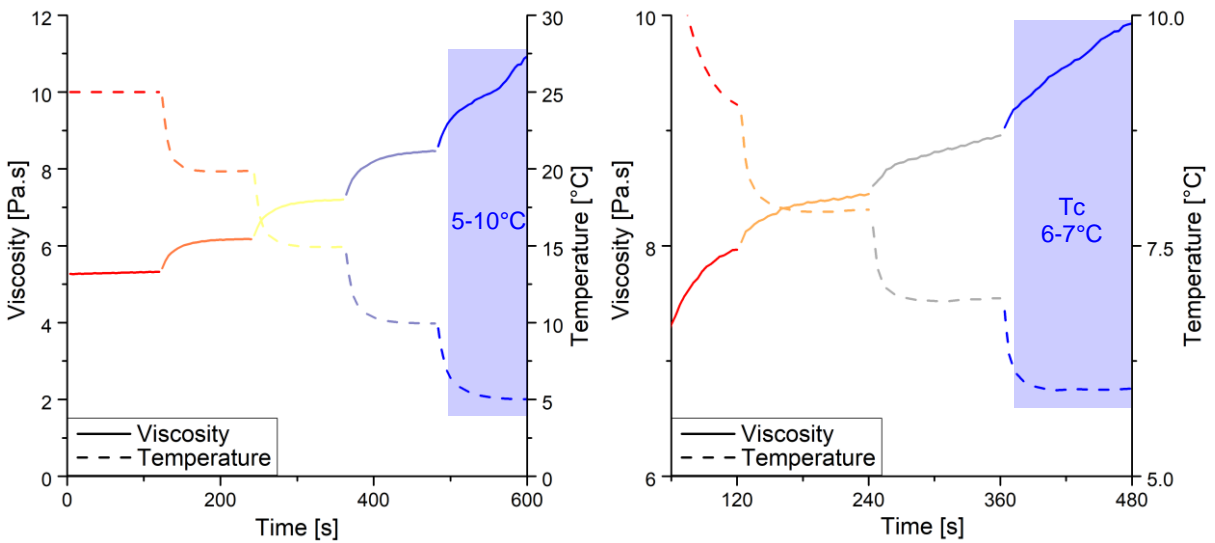


Figure A.8-2: Rheological behavior of a solution of 12%<sub>wt</sub> P(VDF-TrFE) in 1/4 BzOH and 3/4 GBL measured with a shear rheometer (cone plate geometry: 50 mm diameter and 1° angle): viscosity and temperature versus time obtained by applying temperature stages at 10 s<sup>-1</sup>.  $T_W = 6 - 7^\circ\text{C}$





**Titre :** Encres Polymères pour l'Électronique Imprimée : Synthèse, Formulation et Impression

**Résumé :** Dans ce travail, deux encres fonctionnelles pour l'électronique imprimée ont été étudiées. La première est composée d'un polymère semi-conducteur, le poly(3,4-éthylène dioxythiophène) (PEDOT), qui forme un complexe avec un polyanion isolant, le poly(4-styrène trifluorométhyl (bissulfonylimide)) (PSTFSI). Celui-ci stabilise le PEDOT dans l'eau. La deuxième encre contient un polymère piézoélectrique, le poly(fluorure de vinylidène-co-trifluoroéthylène) (P(VDF-TrFE)), dans des solvants organiques. Les propriétés rhéologiques, capillaires et de mouillage de ces encres doivent être ajustées par formulation pour les rendre imprimables par divers procédés d'impression. Les encres PEDOT ont été formulées pour l'impression jet d'encre, la sérigraphie, le dépôt avec une racle rigide (doctor blade) ou le dépôt de lignes avec une lame souple. Il a été montré qu'aucun additif n'est nécessaire pour modifier les propriétés rhéologiques de ces encres : un simple ajustement de la concentration en polymère leur permet de passer d'un comportement Newtonien à rhéofluidifiant avec des propriétés de gel. En revanche, divers additifs ont été ajoutés pour améliorer les propriétés de mouillage, d'élasticité des encres, et de conductivité des films une fois ceux-ci séchés. Les encres P(VDF-TrFE) ont été formulées pour la sérigraphie. Leur comportement newtonien a été rendu rhéofluidifiant en utilisant soit un agent gélifiant, qui modifie l'agencement du polymère en solution, soit un mélange d'un bon et d'un mauvais solvant du polymère, qui résulte en une micro-émulsion. Une fois les propriétés des films séchés étudiées, les deux types d'encres ont été employées pour créer des capteurs de pression fonctionnels.

**Mots clefs :** Polymère, Formulation, Synthèse, Dépôt, Encre Conductrice, PEDOT:polyanion, Encre Ferroélectrique, P(VDF-TrFE)

---

**Title:** Polymer Electronic Inks: Synthesis, Formulation and Processing

**Abstract:** In this work, two organic functional inks for printed electronic were studied. The first is composed of a semi-conducting polymer, poly(3,4-ethylene dioxythiophene) (PEDOT), in complex with an insulating polyanion, poly(4-styrene trifluoromethyl (bissulfonylimide)) (PSTFSI), which stabilizes PEDOT in water. The second ink contains the piezoelectric polymer poly(vinylidene fluoride-co-trifluoroethylene) (P(VDF-TrFE)) in organic solvents. To be processable using a wide range of deposition processes, the rheological behaviors, wettability and capillary properties of these inks have to be adjusted. For that purpose, both types of inks were formulated. PEDOT inks were formulated for inkjet printing, screen-printing, doctor blading, and for a deposition of lines using a soft blade. No additive is necessary to modify the rheological properties of these inks: by simply tuning the concentration in polymer, their behavior go from Newtonian to shear-thinning with gel properties. Further formulations to improve the wettability, the elasticity of the inks, and the conductivity of dried films were performed. P(VDF-TrFE) inks were formulated for screen-printing using a gelifying agent, which modify the organization of the polymer in solution, or a mixture of a good and a bad solvent, which gives rise to a micro-emulsion. The Newtonian inks thereby become shear-thinning. Once the properties of the dried films were studied, both types of polymeric inks were used to create functional pressure sensors.

**Keywords:** Polymer, Formulation, Synthesis, Processing, Conductive Ink, PEDOT:polyanion, Ferroelectric Ink, P(VDF-TrFE)

---

### Unités de recherche

Laboratoire de Chimie des Polymères Organiques (LCPO), UMR 5629,  
bâtiment B8, Allée Geoffroy Saint Hilaire, 33615 Pessac, France

Laboratoire Ondes et Matière d'Aquitaine (LOMA), UMR 5798  
bâtiment A4N, 351 Cours de la Libération, 33400 Talence, France